**US Army Corps
Of Engineers**

Earthquake Design and Evaluation of Concrete Hydraulic Structures

ENGINEER MANUAL

Engineering and Design
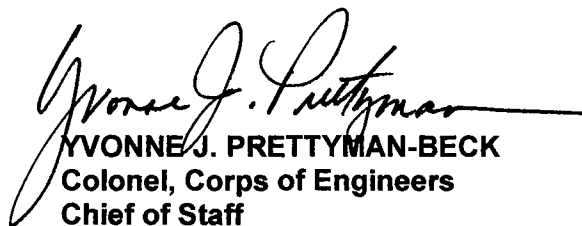## EARTHQUAKE DESIGN AND EVALUATION OF
CONCRETE HYDRAULIC STRUCTURES

1. Purpose. This manual provides guidance for performance-based design and evaluation of concrete hydraulic structures (CHS). It introduces procedures that show how to design or evaluate a hydraulic structure to have a predictable performance for specified levels of seismic hazard. Traditional design and evaluation procedures may still be used for feasibility and screening purposes. However, for critical facilities, they should be followed by the procedures of this manual to prevent sudden collapse even thought the structure may suffer severe damage, to limit damage to a repairable level, or to maintain functionality immediately after the earthquake.

2. Applicability. This manual applies to all USACE commands having responsibilities for civil works projects.

3. Distribution. This manual is approved for public release. Distribution is unlimited.

4. Discussion. This manual covers requirements for the seismic design and evaluation of plain and reinforced concrete hydraulic structures. The types of concrete hydraulic structures addressed in this manual include dams, U- and W-frame locks, gravity walls, and intake/outlet towers. The guidelines are also applicable to spillways, outlet works, hydroelectric power plants, and pumping plants. The structures may be founded on rock, soil, or pile foundations and may or may not have backfill soil.

FOR THE COMMANDER:

YVONNE J. PRETTYMAN-BECK
Colonel, Corps of Engineers
Chief of Staff

DEPARTMENT OF THE ARMY
U. S. Army Corps of Engineers

CECW-CE   Washington D. C. 20314-100

Manual
No. 1110-2-6053

Engineering and Design

EARTHQUAKE DESIGN AND EVALUATION OF
CONCRETE HYDRAULIC STRUCTURES
Table of Contents

Chapter 5
Concrete Properties and Capacities   Page

Chapter 6
Analysis Procedures and Evaluation of Results   Page

Chapter 1
Introduction

1-1. Purpose

This manual provides guidance for performance-based design and evaluation of concrete hydraulic structures (CHS). It introduces procedures that show how to design or evaluate a hydraulic structure to have a predictable performance for specified levels of seismic hazard. Traditional design and evaluation procedures may still be used for feasibility and screening purposes. However, for critical facilities, they should be followed by the procedures of this manual to prevent sudden collapse even though the structure may suffer severe damage, to limit damage to a repairable level, or to maintain functionality immediately after the earthquake.

1-2. Applicability

This manual applies to all USACE commands having responsibilities for civil works projects.

1-3. References

Required and related publications are listed in Appendix A.

1-4. Distribution Statement

This manual is approved for public release with unlimited distribution.

1-5. Mandatory Requirements

Engineers performing seismic design and evaluation of concrete hydraulic structures are required to satisfy specific mandatory requirements. The purpose of mandatory requirements is to assure that the structure meets minimum safety and performance objectives. Mandatory requirements usually pertain to critical elements of the design and evaluation, such as loads and load combinations, to analytical procedures used to determine force and displacement demands, and to methods used to determine member strength and displacement capacities. Mandatory requirements pertaining to the guidance contained in a particular chapter are summarized at the end of that chapter. No mandatory requirements are identified in the appendices. Instead, any mandatory requirements pertaining to information contained in the appendices is cited in chapters that reference those appendices. Where other Corps guidance documents are referenced, the engineer must review each document to determine which of its mandatory requirements are applicable to the design or/ evaluation of the project. Engineers performing the independent technical review must ensure that the designers and/or analysts have satisfied all mandatory requirements.

1-6. Scope

This manual covers requirements for the seismic design and evaluation of plain and reinforced concrete hydraulic structures. The types of concrete hydraulic structures addressed in this manual include dams, U- and W-frame locks, gravity walls, and intake/outlet towers. The guidelines are also applicable to spillways, outlet works, hydroelectric power plants, and pumping plants. The structures may be founded on rock, soil, or pile foundations and may or may not have backfill soil.

Chapter 2
Design Criteria

2-1. Design Earthquakes

a. General. Earthquake ground motions for the design and evaluation of Corps CHS are the Operating Basis Earthquake (OBE) and the Maximum Design Earthquake (MDE) ground motions. Seismic forces associated with the OBE are considered unusual loads. Those associated with the MDE are considered extreme loads. Earthquake loads are to be combined with other loads that are expected to be present during routine operations.

b. Operating Basis Earthquake. The OBE is a level of ground motion that is reasonably expected to occur within the service life of the project, that is, with a 50-percent probability of exceedance during the service life. (This corresponds to a return period of 144 years for a project with a service life of 100 years).

c. Maximum Design Earthquake. The MDE is the maximum level of ground motion for which a structure is designed or evaluated. As a minimum, for other than critical structures, the MDE ground motion has a 10 percent chance of being exceeded in a 100-year period, (or a 1000-year return period). For critical structures, the MDE ground motion is the same as the maximum credible earthquake (MCE) ground motion. Critical structures, by ER 1110-2-1806 definition, are structures that are part of a high hazard project and whose failure will result in loss of life. The MCE is defined as the largest earthquake that can reasonably be expected to occur on a specific source, based on seismological and geological evidence.

2-2. Performance Levels

a. General. Various performance levels are considered when evaluating the response of CHS to earthquake ground motions. The performance levels commonly used are serviceability performance, damage control performance, and collapse prevention performance.

b. Serviceability performance. The structure is expected to be serviceable and operable immediately following earthquakes producing ground motions up to the OBE level.

c. Damage control performance. Certain elements of the structure can deform beyond their elastic limits (non-linear behavior) if non-linear displacement demands are low and load resistance is not diminished when the structure is subjected to extreme earthquake events. Damage may be significant, but it is generally concentrated in discrete locations where yielding and/or cracking occur. The designer should identify all potential damage regions, and be satisfied that the structure is capable of resisting static loads and if necessary can be repaired to stop further damage by non-earthquake loads. Except for unlikely MCE events, it is desirable to prevent damage from occurring in substructure elements, such as piling and drilled piers, and other inaccessible structural elements.

d. Collapse prevention performance. Collapse prevention performance requires that the structure not collapse regardless of the level of damage. Damage may be unrepairable. Ductility demands can be greater than those associated with the damage control performance. If the structure does not collapse when subjected to extreme earthquake events, resistance can be expected to decrease with increasing displacements. Collapse prevention performance should only be permitted for unlikely MCE events. Collapse prevention analysis requires a Nonlinear Static Procedure (NSP) or Nonlinear Dynamic Procedure (NDP) in accordance with the guidance in Chapter 6.

2-3. Performance Goals

a. General. Both strength and serviceability must be considered in the design of structures. For plain concrete structures, the consequences of inadequate strength can be failure by shear, flexure, tension, or compression. The same consequences exist for reinforced concrete structures except that additional failure mechanisms such as bond failure and buckling and tensile failure of reinforcing steel are also possible. Lack of adequate strength can result in loss of life and severe economic loss. Structures must also be serviceable under sustained and frequent loads. Serviceability for usual static load conditions is a matter of limiting structural displacements. For unusual earthquake loading (i.e. OBE), the serviceability requirement is to assure the project will function without interruption, with little or no damage. For new structures, the additional cost of designing for linear elastic performance during OBE events is usually low. However, the cost of strengthening an existing structure to obtain the same performance objective may be high. The cost of seismic strengthening of an existing structure for serviceability purposes must be weighed against the cost of repairing the structure after it has experienced an OBE event. The performance goals for concrete hydraulic structures are demonstrated using idealized force displacement curves (Figures 2-1 through 2-3) representing ductile, limited-ductile, and brittle failure behavior. Using procedures described in Chapters 5 and 6, a capacity curve is constructed. With this curve serviceability, damage control, and collapse prevention performance regions are identified. To properly assess the performance of complex structures it is necessary to understand the loading history, the changes in system stiffness and damping as yielding and cracking occur, the redistribution of resisting loads, and the path the structure follows from the initial elastic state to a collapse prevention limit state. This is done using nonlinear static analysis and/or nonlinear dynamic analysis if sufficient information is known about the nonlinear properties of the system. For most structures, a combination of engineering analysis and judgment must be used to determine if performance objectives have been met.

b. Ductile behavior. Ductile behavior is illustrated in Figure 2-1. It is characterized by an elastic range (Point 0 to Point 1 on the curve), followed by a plastic range (Points 1 to 3) that may include strain hardening or softening (Points 1 to 2), and a strength degradation range (Points 2 to 3) in which some residual strength may still be available before collapse occurs. Building frame systems designed according to FEMA or ACI provisions exhibit this type of behavior in flexure. Shear and bond mechanisms, however, exhibit limited-ductile or brittle behavior and therefore these failure modes must be suppressed if overall ductile behavior as illustrated by Figure 2-1 is to be achieved. When subjected to MDE ground motion demands, ductile structures should have sufficient strength to assure performance will remain within the strain hardening region (Points 1 to 2), an inelastic region where strength increases with an increase in strain. In addition, in case of OBE ground motion demands, all elements of the structure should perform within the linear elastic range (Points 0 to 1). Designers of new reinforced concrete structures should establish a hierarchy in the formation of failure mechanisms by allowing flexural yielding to occur while at the same time suppressing shear, and other brittle or limited-ductile failure mechanisms. Such a design produces ductile behavior. Reinforced concrete structures designed by older codes do not provide the quantity of reinforcement (flexural and confinement), or the proper details needed to assure ductile behavior. For those structures, it is necessary to evaluate all three types of brittle, limited-ductile, and ductile failure mechanisms in order to determine which mode of behavior can be expected.

c. Limited-ductile behavior. Limited-ductile behavior (Figure 2-2) is characterized by an elastic range and limited plastic range that may include strain hardening or softening, followed by a complete loss of strength. Plain concrete structures and lightly reinforced concrete struc-

tures such as intake/outlet towers (structures with cracking moment capacities equal or greater than nominal strength) generally exhibit this type of behavior in flexure, although the plastic range may be limited. It should be recognized that some residual capacity, as indicated in Figure 2-2, may still exist in concrete gravity dams and in other plain and lightly reinforced concrete structures. This residual capacity occurs due to dead load effects that contribute to shear-friction resistance and to overturning resistance. This residual capacity exists even though cracks have propagated through the structure, or in the case of reinforced concrete structures, even though the principal reinforcing steel has fractured. Limited ductile structures when subjected to MDE ground motion demands should also have sufficient strength to assure performance will be within the inelastic region where strength increases with an increase in strain (strain hardening region). All elements of the structure when subjected to OBE ground motion demands should perform within the linear elastic range.

d. Brittle behavior. An elastic range of behavior, followed by a rapid and complete loss of strength, characterizes brittle, or non-ductile, behavior. Certain failures such as reinforcing steel buckling failures, reinforcing steel splice failures and anchorage failures exhibit this type of behavior under earthquake loading conditions. Sudden failure occurs because the concrete is not adequately confined to prevent spalling which in turn leads to a rapid loss of bond strength, and to buckling of the reinforcing steel. Brittle failure mechanisms should be avoided for the OBE and MDE. In other words the behavior controlled by such mechanisms should remain within the elastic range.
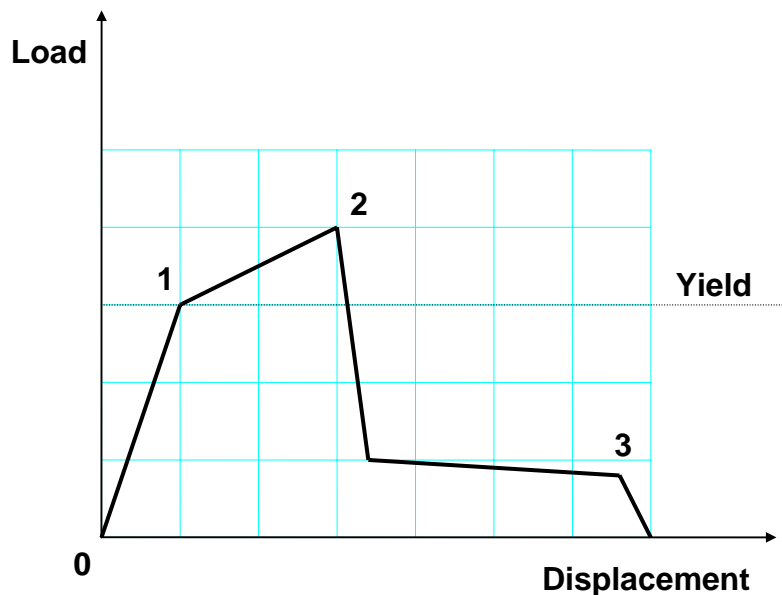
Figure 2-1. Ductile Behavior Curve (From FEMA 273)
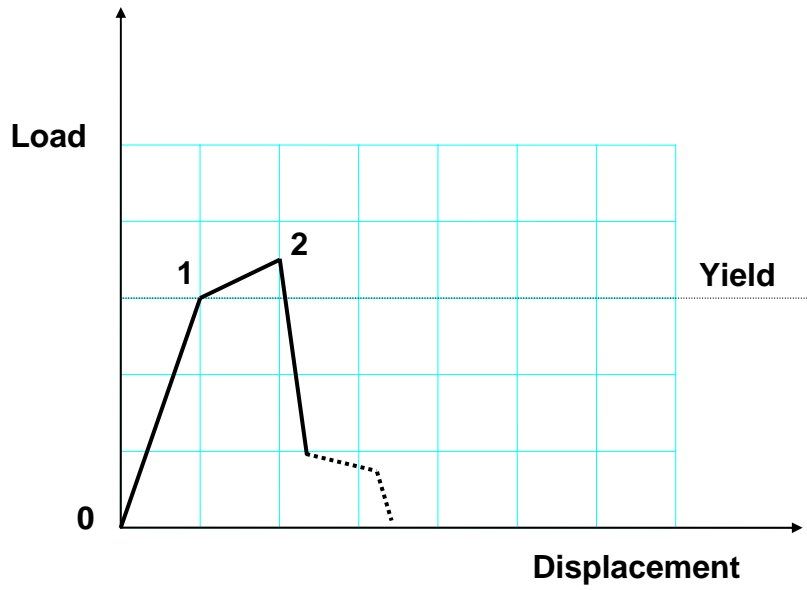
Figure 2-2. Limited-ductile Behavior Curve (consistent with FEMA 273)
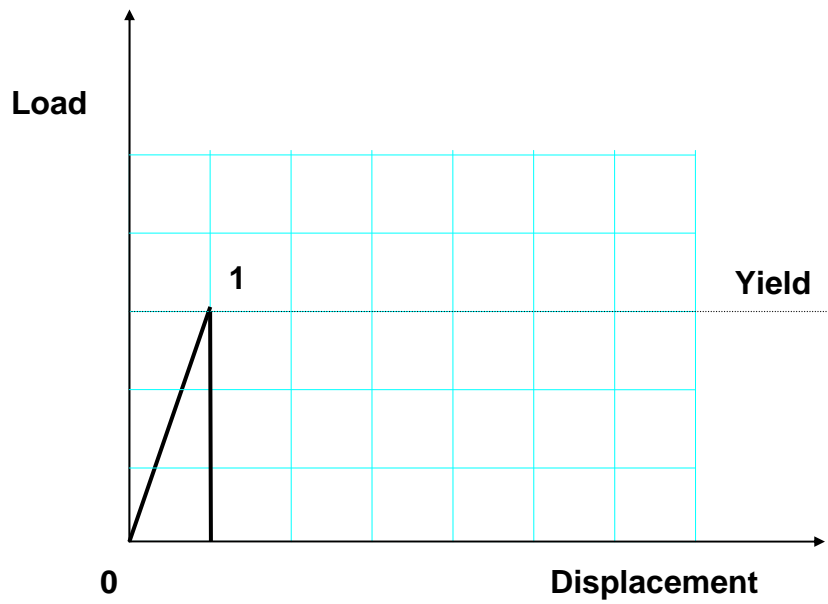
Figure 2-3. Brittle Behavior Curve (From FEMA 273)

2-4. Design Requirements

a. Strength design. Strength design for CHS subjected to earthquake ground motions is achieved by reducing the probability of structure collapse to an acceptable level. This is accomplished by selecting an appropriate design basis earthquake event to be used in combination with specific design and evaluation procedures that assure the structure will perform as intended. Seismic design and evaluation is most often based on linear-elastic response-spectrum or time-history analysis procedures, although nonlinear analysis procedures can be used for evaluation of certain nonlinear mechanisms. The design basis earthquake event used for strength evaluation of CHS is the Maximum Design Earthquake (MDE).

b. Serviceability design. Serviceability design for CHS subjected to earthquake ground motions is achieved by reducing the possibility of structure damage to a negligible level. As for strength performance, this is accomplished by selecting an appropriate design basis earthquake event to be used in combination with appropriate design and evaluation procedures. Evaluation is based on linear-elastic response spectrum analysis or time history analysis procedures. The design basis earthquake event used for serviceability evaluation of CHS is the Operating Basis Earthquake (OBE).

c. Loading combinations. The following loading combinations establish the ultimate strength and serviceability requirements for the design and evaluation of both plain and reinforced concrete hydraulic structures. The loading combinations represent the total demand (dead load + live load + earthquake) for which the structure must be designed or evaluated.

(1) *Earthquake strength design loading combination.* The following strength design loading combination shall be used to determine the total static plus earthquake demand on concrete hydraulic structures for Maximum Design Earthquake (MDE) conditions:

$$Q_{DC} = Q_D + Q_L + Q_{MDE} \qquad\qquad (2\text{-}1)$$

where;

Q_{DC} = Combined action due to dead, live, and maximum design earthquake loads for use in evaluating damage control performance

Q_D = Dead load effect

Q_L = Live load effect + uplift

Q_{MDE} = Earthquake load effect from MDE ground motions including hydrodynamic and dynamic soil pressure effects

The live load effect is the structure response to live loads such as hydrostatic, earth pressure, silt, and temperature loads. Live loads to be considered are those that are likely to be present during the design earthquake event. The earthquake load effect is the response of an elastic structure to design earthquake ground motions. The earthquake load may involve multi-component ground motions with each component multiplied by +1 and -1 to account for the most unfavorable earthquake direction.

(2) *Serviceability loading combination.* The following serviceability design loading combination shall be used to determine the total earthquake demand on concrete hydraulic structures for Operating Basis Earthquake (OBE) conditions:

$$Q_S = Q_D + Q_L + Q_{OBE} \qquad\qquad (2\text{-}2)$$

where;

Q_S =   Combined action due to dead, live, and OBE loads for use in evaluating serviceability performance

Q_D =   Dead load effect

Q_L =   Live load effect + Uplift

Q_{OBE} =   Earthquake load effect from OBE ground motions including hydrodynamic and dynamic soil pressure effects

Live loads to be considered are those that are likely to be present during the OBE earthquake event.

2-5. Performance Evaluation

a. Plain Concrete Structures

(1) *General.* Although resistance to compressive and shear stresses are evaluated, the safety and serviceability of large plain concrete structures is usually controlled by the tensile behavior and cracking of the concrete. The actual response of massive concrete structures to earthquake ground motions is very complex. Loading histories and rapid seismic strain rates have an important influence on structural performance. The ultimate tensile strength of concrete is especially sensitive to strain rate. Most often, a concrete gravity dam or arch dam is evaluated based on the linear-elastic finite-element method (FEM) of analysis. The resulting stress demands from the FEM combined with engineering judgment and past experience are used to assess the performance. The assessment process requires knowledge on how the tensile strength might vary with loading history, strain rates, and construction methods (especially with respect to construction and contraction joints), and on how cracking might propagate as a result of repeated excursions beyond the tensile strength. The assessment is facilitated by using the stress demand-capacity ratios in conjunction with spatial extent of overstressed regions and cumulative duration of excursions beyond the tensile strength of the concrete. The demand-capacity ratios are obtained from division of computed stress demands by the static tensile strength of the concrete.

(2) *Response to internal force or displacement controlled actions*

(a) The response of a gravity dam to earthquake ground motions is illustrated in Figure 2-4. For earthquake motion cycles in the upstream direction, the potential cracking usually occurs at the heel of the dam at the maximum expected water levels. For earthquake motion cycles in the downstream direction, the potential cracking usually occurs at the slope discontinuity under the minimum expected water level conditions and near the toe of the dam. As earthquake motion cycles swing toward the upstream direction, the potential cracking shifts to the upper part and the base of the dam. In general, the tensile stress-strain results from linear elastic FEM are used to determine if the structure meets established project performance requirements. Performance under OBE loading conditions should be in the linear elastic range (Serviceability Performance) as illustrated on the tensile stress-strain diagram of Figure 2-5.

**High Tensile
Stress Regions**

Ground Motion
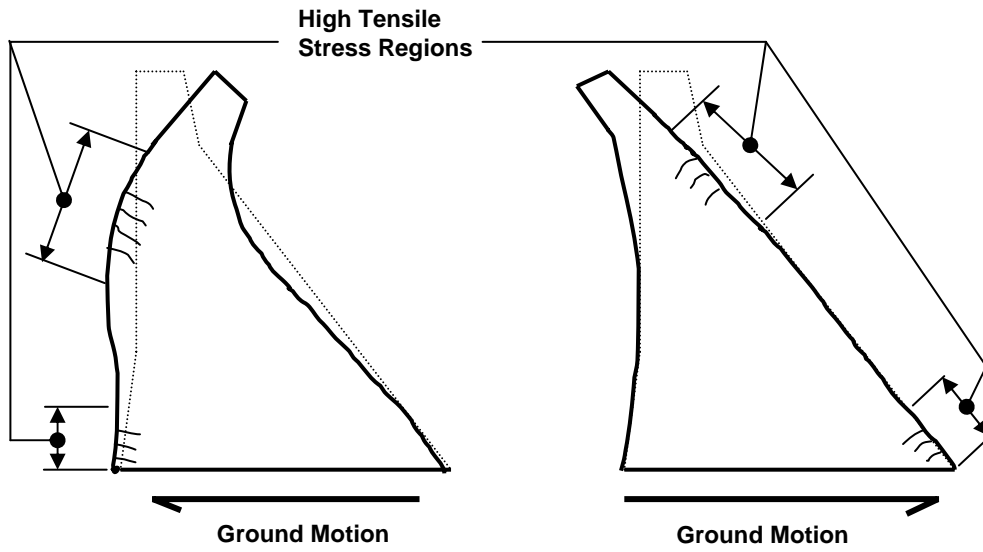
Ground Motion

Figure 2-4. Gravity Dam Subjected to Earthquake Ground Motions

Serviceability Performance
(Linear Elastic Range)

Damage Control Performance
(Nonlinear strain hardening range

Collapse Prevention
Nonlinear strain softening range

Tensile
Stress

Tensile Strength
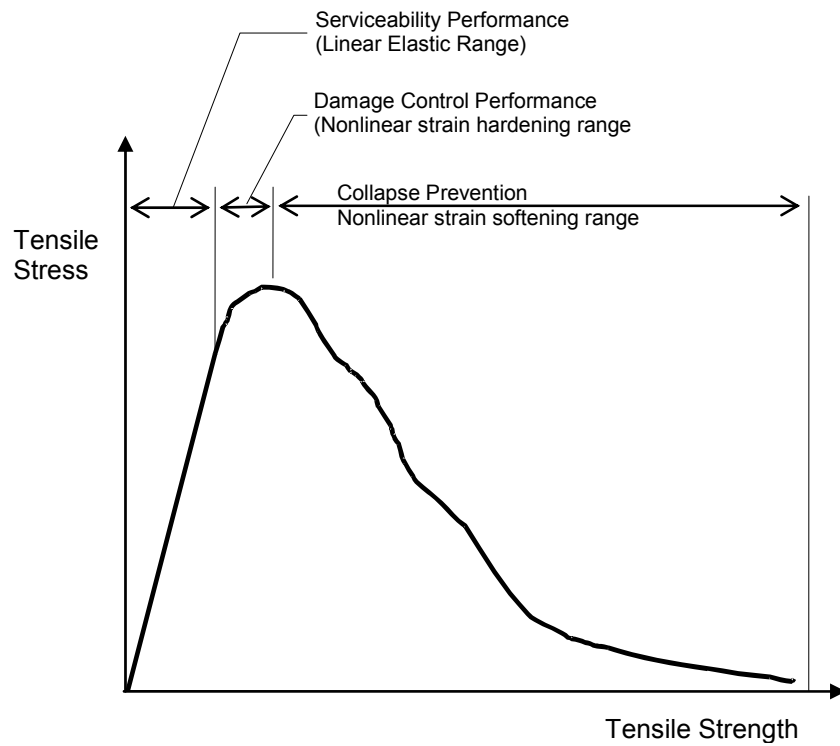
Figure 2-5. Stress – Strain Relationship for Plain Concrete Structures

Performance under MDE loading conditions should be within the non-linear strain hardening range (Damage Control). The strain softening range provides reserve capacity against collapse and represents the concrete capacity to absorb additional energy demands from earthquake ground motions. Additional information on the tensile capacity of plain concrete structures can be found in Chapter 5.

(b) The response of an arch dam to earthquake ground motion is shown in Figure 2-6. Arch dams are generally built as independent cantilever monoliths separated by vertical contraction joints. Since contraction joints can only transfer limited tensile stresses in the horizontal arch direction, the joints can be expected to open and close repeatedly as the dam vibrates in response to severe earthquake ground motion. The contraction joint opening releases tensile arch stresses but increases compressive stresses and vertical cantilever stresses by transferring forces to the cantilevers. The increased compressive stresses could lead to concrete crushing, especially due to impact of joint closing. The increased vertical cantilever stresses could exceed tensile strength of the lift lines (or horizontal joints); in which case tensile cracking is likely to occur along the horizontal lift lines. High tensile stresses also develop along the dam-foundation interface and could cause cracking along the dam-foundation contact or could be absorbed by minor displacements of the jointed foundation rock.
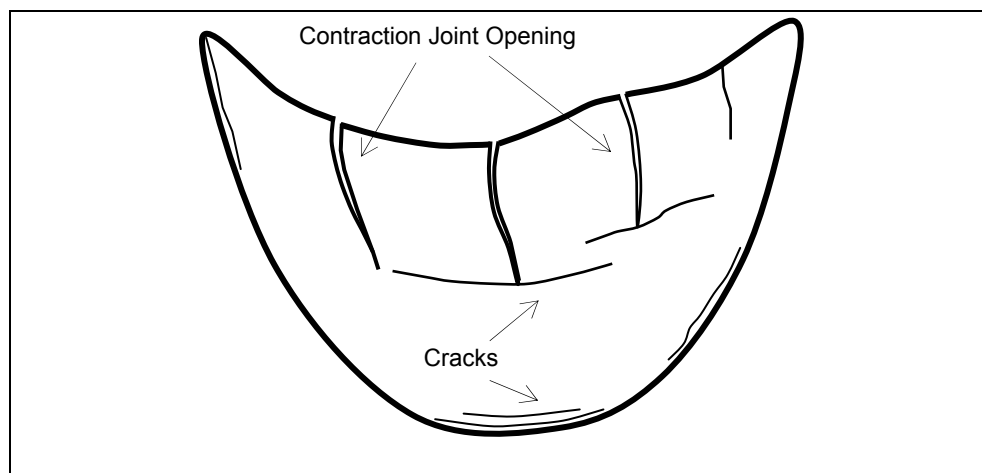
Figure 2-6. Response of Arch Dams to Major Earthquakes

(3) *Response to stability controlled actions.* Once cracking has propagated through the structure along potential failure planes, or along joints where the tensile strength can be substantially less than that of the parent concrete, the structural stability against sliding or rotation should be considered. Rotational failures of a massive concrete hydraulic structure are highly unlikely due to wedging action that limits the rotation. Note that rotational stability assessed based on a 2D analysis ignores additional resistance that might exist due to 3D effects. Even in a straight gravity dam, especially if built in a narrow valley, each monolith can draw resistance from adjacent blocks to remain stable. Evaluation of this mode of failure is discussed in following paragraphs of this Chapter and in Chapter 7. Sliding due to shear failure can occur, leading to unacceptable permanent displacements. The sliding displacements should be evaluated whenever the shear demands along potential failure planes exceed the sliding resistance (shear-friction capacity). An estimate of the permanent displacement can be made using the upper bound sliding displacement methods described in Chapters 4 and 7. Non-linear analysis methods are also available for determining the permanent displacement (Fronteddu et al., 1998; Chavez and Fenves, 1993).

(a) For gravity dams, the sliding may occur along the construction joints, cracked sections within the dam, dam-foundation interface, weak planes within the foundation, or any combination of these. As long as the permanent displacements at construction joint surfaces are within acceptable limits, the sliding response that occurs at joint locations can actually reduce permanent displacements at the dam-foundation interface, and in the case of arch dams can reduce the potential for block shear failure. The sliding response of a gravity dam to earthquake ground motions with joints as strong as the parent concrete may take place at the dam-foundation interface or along weak planes within the foundation. As illustrated in Figure 2-7 (adapted from Fronteddu, Leger, and Tinawi, 1998), the weaker joint condition can cause sliding in the body of the dam thereby reducing the displacement demands at the base of the dam. A rocking response can also have beneficial effects provided such a response does not lead to a rotational stability failure.
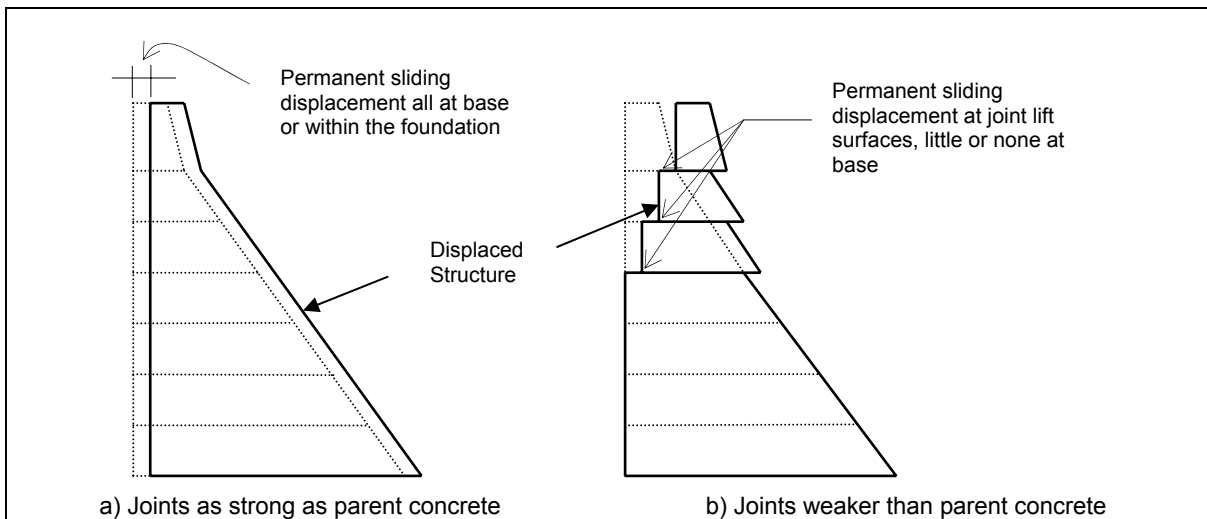
Figure 2-7. Dam Permanent Sliding Displacements

(b) In arch dams, potentially opened contraction joints and cracked lift lines may subdivide the monolithic arch structure into partially free cantilever blocks, capable of transmitting only compressive or frictional forces. In this situation, any failure mode of the arch structure would more likely involve sliding stability of the partially free cantilevers. For small and moderate joint openings, the partially free cantilever blocks, bounded by opened joints, may remain stable through interlocking (wedging) with adjacent blocks. The extent of interlocking depends on the depth and type of shear keys and the amount of joint opening. If potentially dangerous blocks can be shown to be incapable of moving because of friction, tapering, gravity, or orientation consideration, their stability is of no concern. A shear key of rectangular shape would permit only normal opening, but no sliding. Triangular or trapezoidal shear keys allow both opening and some sliding. Hence, the depth of the shear keys controls the maximum amount of joint opening for which adjacent blocks would remain interlocked; deeper shear keys permit larger joint openings. When the partially free cantilevers are treated as rigid blocks, the maximum joint opening with active interlocking can be estimated from rigid block geometry. Therefore, for nonlinear response behavior, the magnitude of compressive stresses, the extent of joint opening or cracking, and the amplitude of non-recoverable movements of concrete blocks bounded by failed joints will control the overall stability of the dam, rather than the magnitude of calculated tensile stresses.

b. Reinforced Concrete Structures

(1) *General.* Under major earthquakes, reinforced concrete structures perform satisfactorily if they are detailed to provide adequate ductility and designed to possess sufficient strength to prevent shear failure. Most existing reinforced concrete hydraulic structures do not conform to modern code detailing and strength requirements, but since they are massive, they may still perform adequately during major earthquakes. Although large diameter steel reinforcing bars are used in construction of these structures, the ratio of the steel area to concrete area is small. They are therefore, classified as lightly reinforced concrete structures, for which the cracking moment capacity is greater than the nominal strength. Code provisions applicable to buildings and bridges may not be directly applicable to lightly reinforced hydraulic structures because of significant differences in reinforcement ratio and axial load ratio. Issues specific to the perform-ance of lightly reinforced concrete structures are presented in Chapter 5. General issues and potential modes of failure that must be examined in seismic response evaluation of reinforced concrete hydraulic structures are discussed below. Failures can occur when:

- Flexural displacement demands exceed flexural displacement capacity
- Shear demands exceed shear (diagonal tension) capacity
- Shear demands exceed sliding shear capacity
- Moment demands exceed overturning capacity (rocking)

Figure 2-8 illustrates types of responses that can lead to one of the above failures.

(2) *Response to internal forces or displacement controlled actions*

(a) *Flexural response.* The flexural response illustrated in Figure 2-8b can lead to a flexural failure if rotation demands in plastic hinge regions (where yielding occurs) exceed the rotational capacity of reinforced concrete. Rotational capacity is a function of curvature capacity and plas-tic hinge length. In lightly reinforced concrete structures, the curvature capacity is often limited by the ultimate strain capacity of the reinforcing steel. For members with high reinforcement ratios and large axial loads, the curvature capacity will be limited by the compressive strain ca-pacity of the concrete. Low reinforcement ratios limit plastic hinge length and thus flexural rota-tion capacity. The capacity of bar anchorage lengths and lap splices must be evaluated as part of a flexural response analysis to assure that bond and splice failures, which could limit flexural ductility, do not occur. There is a potential for splice failure under repeated cycles of inelastic rotation where lap splicing occurs in plastic hinge regions, or where lap splices are not suitably confined by transverse reinforcement.

(b) *Shear (diagonal tension).* A shear (diagonal tension) response is illustrated in Figure 2-8c. Since shear failure is a brittle sudden failure, energy dissipation as a result of yielding should take place through a flexural response rather than a shear response. To assure this, it is desirable to provide shear capacity equal to the shear demands the structure would experience if it remained elastic. As a minimum, the shear capacity of the structure should be greater than the shear forces associated with the development of the member flexural capacity, with consid-eration of possible flexural over-capacity due to strain hardening of the reinforcing steel. The shear capacity of reinforced concrete members includes contributions from the concrete due to aggregate interlock, from the transverse steel reinforcement due to truss action, and from axial load due to arching action. For typical lightly reinforced concrete hydraulic structures, the major contribution to shear capacity comes from the aggregate interlock. The shear capacity dimin-ishes as the flexural ductility demand in the plastic hinge region increases. Shear capacity and its sensitivity to flexural ductility demand are described in Chapter 5.
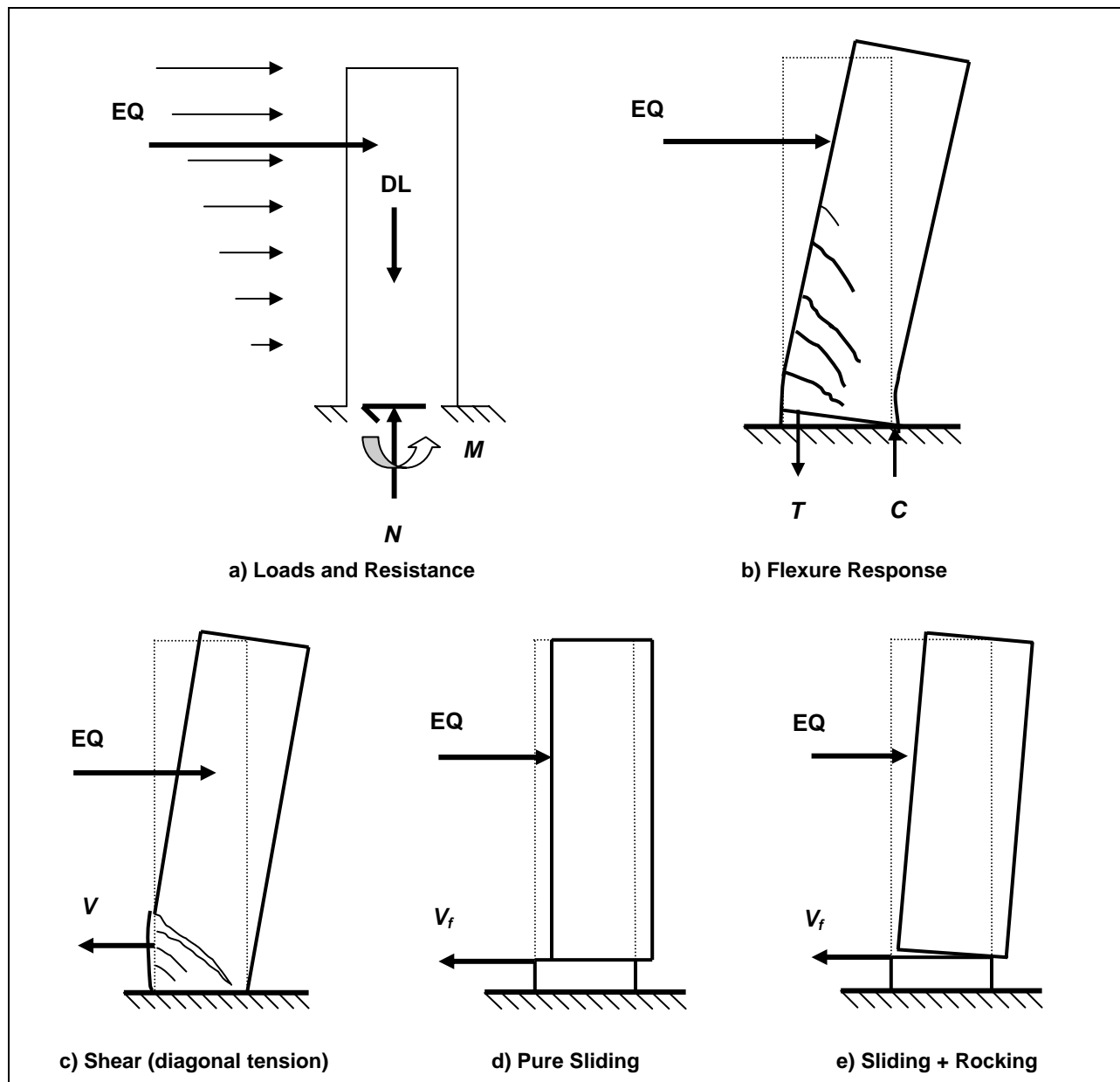
Figure 2-8. Response of a Free Standing Intake Tower to Earthquake Ground Motions

(c) *Sliding shear response.* Figure 2-8d illustrates a sliding shear response. This may occur in the upper part of the tower as well as at its base if the overturning moment is not large enough to cause rocking. When evaluating a sliding shear response within the structure, the capacity of the structure to resist shear will be based on shear-friction concepts ($V_f = N \tan\phi$) with the normal force (N) having contributions from the longitudinal reinforcing steel and axial dead load.

(d) *Sliding plus rocking response.* Figure 2-8e illustrates a sliding plus rocking response. A pure sliding shear may not occur at the structure-foundation interface due to earthquake load

distribution that could produce large overturning moment. In this situation a pure rocking or combined rocking plus sliding seems more plausible.

(3) *Response to stability controlled actions*

(a) *General.* Lightly reinforced concrete structures are most vulnerable to failure by fracturing of the flexural reinforcing steel. Once the flexural reinforcing steel fractures, the seismic evaluation becomes one of determining if the residual capacity of the cracked structure with ruptured reinforcing steel is adequate to prevent a failure by sliding instability, or by rotational instability. For sliding, the residual capacity is the shear-friction resistance of the concrete with no consideration given to the shear-friction resistance provided by the reinforcing steel. For rotation, the residual capacity or stabilizing moment is that provided by the moment resisting couple formed between the axial load and the concrete compressive stress zone formed at the extremity of the concrete section (Figure 2-9).

(b) *Sliding stability.* The sliding response will be as illustrated in Figure 2-8d. The capacity to resist sliding will be based on shear-friction principles except that the shear-friction contribution from reinforcing steel crossing the failure plane will be ignored. In cases where the sliding shear demand exceeds the sliding resistance (shear-friction capacity), an estimate of the permanent displacement can be made using the upper bound sliding displacement method described in Chapters 4 and 7. Non-linear analysis methods are also available for determining the permanent displacement that might occur as the result of the fracturing of the flexural reinforcing steel (Fronteddu, Leger, and Tinawi, 1998).

(c) *Rotational stability.* Once a tower has suffered a through crack at its base due to high seismic moments, it could undergo rocking response if the moment demands exceed the restoring or resisting moment of Equation 2-3. For the purpose of rocking response, the tower may be considered a rigid block. Depending on the magnitude and form of the ground motion, the tower may translate with the ground, slide, rock, or slide and rock. Assuming that the angle of friction is so large that sliding will not occur, the tower initially rotates in one direction, and, if it does not overturn, it will then rotate in the opposite direction, and so on until it stops. There are fundamental differences between the oscillatory response of a single-degree-of-freedom (SDOF) oscillator and the rocking response of a slender rigid block (Makris and Kostantinidis, 2001). Rocking structures cannot be replaced by "equivalent" SDOF oscillators. The rocking response of structures should be evaluated by solving equations that govern the rocking motion, as described in Chapter 7. The quantities of interest for a rocking block are its rotation, θ, and its angular velocity $\dot{\theta}$. Similar to the response spectra of SDOF oscillators, rocking response spectra which are plots of the maximum rotation and angular velocity vs. the frequency parameter of geometrically similar blocks can be produced for rocking response. The rocking response spectra can then be used directly to obtain the maximum uplift or rotation of the block for a given ground motion. A comparison of the estimated maximum rotation with the slenderness ratio (i.e. α in Figure 7-5) of the block will indicate whether the block will overturn in accordance with the procedure described in Chapter 7.

(d) *Toe crushing.* In rocking mode the entire weight of the tower is exerted on a small region called the toe of the tower. The resulting compressive stresses in the toe region could be high enough to either crush the concrete or the foundation rock below. In either case this has the effect of reducing the moment lever arm from (h/a) to (h-a)/2, as illustrated in Figure 2-9. Should this happen the stabilizing or resisting moment (M_r) discussed in paragraph 2-5b(3)(c) should be computed as follows:

$$M_r = P\left(\frac{h-a}{2}\right) \tag{2-3}$$

Where:

P = Axial load.

h = Dimension of the section in the direction of the earthquake load.

$$a = \frac{P}{0.85 f_{ca}'(b)} \tag{2-4}$$

The response to the forces causing seismic rotational instability is shown in Figure 2-9. In Equation (2-4), f_{ca}' is the best estimate of concrete compressive strength at the base of the structure.
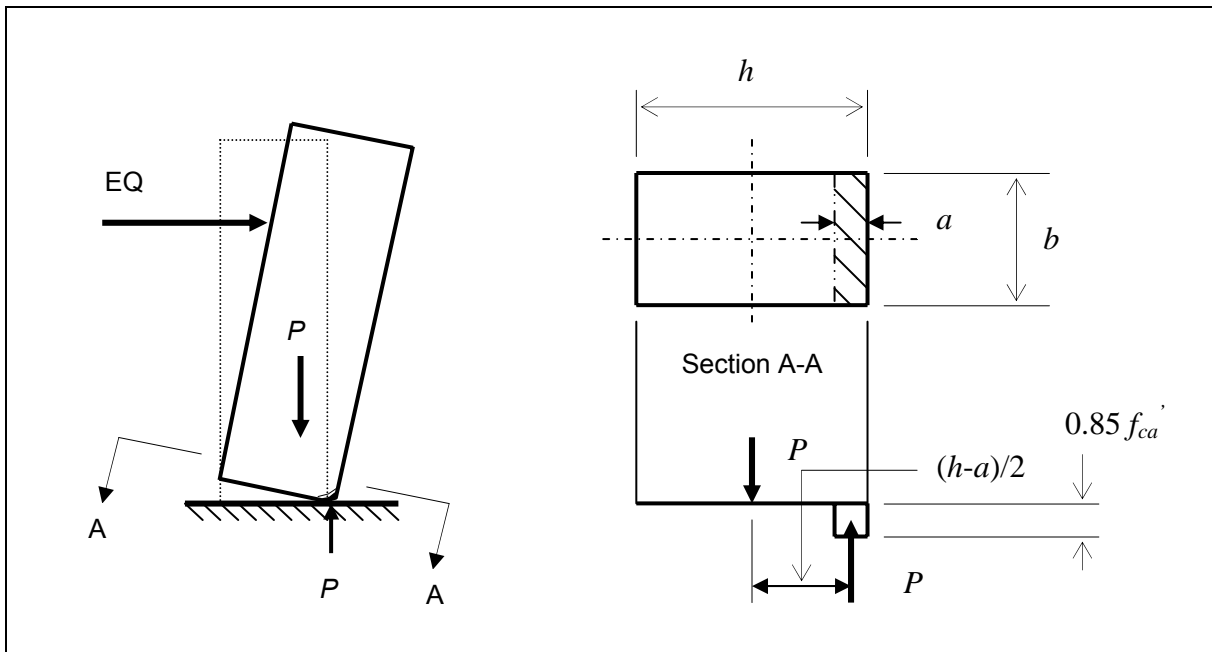
Figure 2-9. Toe Crushing Response of a Free Standing Intake Tower

(4) *Performance evaluation -- DCR allowable values*

(a) Demand to capacity ratios (DCR) are used to evaluate the seismic performance of reinforced concrete structures. Depending on whether the response is a force controlled action (shear) or a displacement controlled action (flexure), demands and capacities will be expressed in terms of forces, displacement ductility ratios, or displacements. Capacities are determined in accordance with procedures described in Chapter 5. The various methods of analysis used to determine demands are covered in Chapter 6. The most common method is the Linear Dynamic Procedure (LDP) in which seismic demands are computed by response-spectrum or time-history analysis methods. Under the Linear Dynamic Procedure, performance goals are met when all DCR ratios are less than or equal to allowable values established in Chapter 6.

(b) In addition to the DCR method, flexural response or displacement-controlled actions can be evaluated using a displacement-based approach where displacement capacities are compared to displacement demands. The moment-curvature diagram in Figure 2-10 illustrates the flexural performance requirements for reinforced concrete structures. Under OBE loading conditions the structure should respond within the serviceable performance range and under MDE within the damage control range. Reserve capacity against collapse is provided in part by reserve energy capacity contained in the strain softening range. Performance under shear and other brittle failure mechanisms is evaluated using DCR procedure in accordance with Paragraph 2-5b(4). The shear capacity needed for this evaluation is obtained as described in Chapter 5.
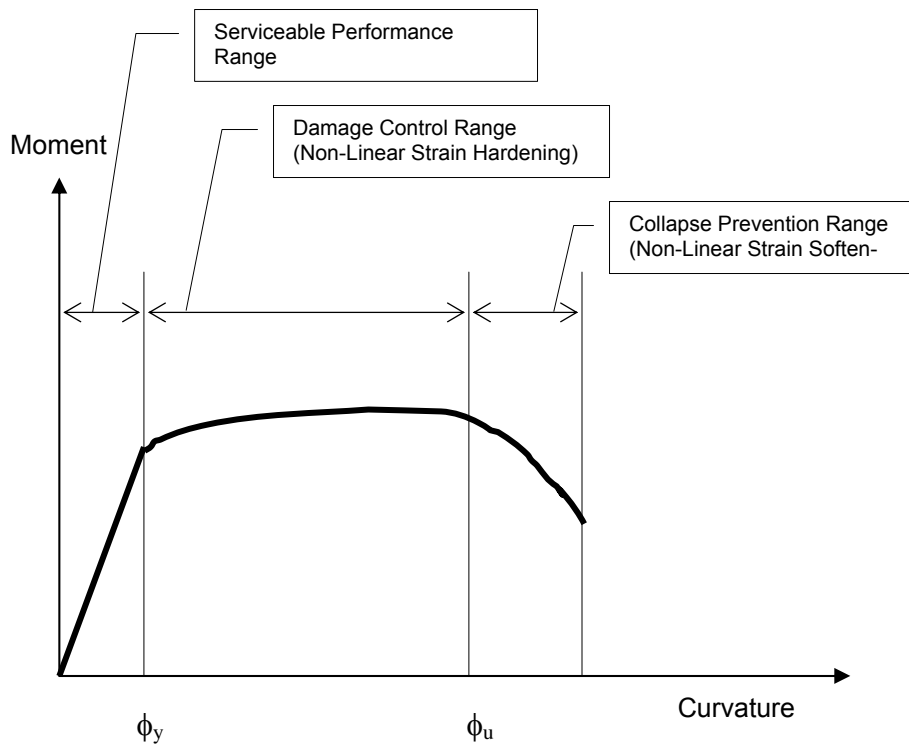
Figure 2-10. Moment-Curvature Diagram for Reinforced Concrete

2-6. Mandatory Requirements

a. Earthquake loading combinations for strength and serviceability of concrete hydraulic structures shall be in accordance with Equations 2-1 and 2-2.

b. Performance-based evaluation of CHS structures shall follow the methodology and goals established in Paragraph 2-5.

Chapter 3
Estimating Earthquake Ground Motion Demands

3-1. Specification of Earthquake Ground Motions

a. General. The earthquake ground motions for design and evaluation of CHS are generally characterized in terms of response spectra and acceleration time histories. Information on response spectra can be found in EM1110-2-6050, "Response Spectra and Seismic Analysis for Concrete Hydraulic Structures." Information on earthquake acceleration time histories and time history analysis can be found in EM 1110-2-6051, "Time History Analysis for Concrete Hydraulic Structures." ER 1110-2-1806, "Earthquake Design and Evaluation for Civil Works Projects," provides guidance and direction for the seismic design and evaluation of all civil works projects.

b. Using response spectra for earthquake design and analysis. Acceleration response spectra represent the peak acceleration response of a number of single-degree-of-freedom (SDOF) oscillators to particular earthquake ground motions. Information on response spectra can be found in Technical Report ITL-92-4 (Ebeling 1992) and EM1110-2-6050. Earthquake response spectra can be site specific or standard (non-site specific). Standard response spectra are based on spectral shapes developed for recorded ground motions with similar subsurface characteristics. The standard spectral shapes are defined with respect to effective peak ground accelerations or spectral accelerations taken from the national seismic hazard maps. Although a response spectrum represents the maximum response of SDOF systems, the response of multi-degree of freedom systems (MDOF) can also be obtained from the response spectrum by applying the mode-superposition technique. According to this technique the linear earthquake response of a MDOF system can be obtained by combining responses of several SDOF systems, each of which represents a mode of vibration of the MDOF system. The dynamics of MDOF systems are described in Technical Report ITL-94-4 (French et al. 1994) and EM 1110-2-6050.

c. Standard response spectra. Guidance is provided in Appendix B for constructing standard acceleration response spectra based on the most recent national seismic hazard data. Appendix B provides a procedure for developing standard acceleration response spectra and effective peak ground accelerations for use in the seismic design and evaluation of structural features of USACE projects as required by ER 1110-2-1806. Standard response spectra are based on a general characteristic shape that is defined in terms of effective peak accelerations or spectral accelerations. The effective peak ground acceleration is obtained from division of the spectral ordinate (for a 5%-damped spectrum) at period of 0.2 seconds by a standard value of 2.5. Examples of standard response spectra and determination of effective peak ground accelerations are given in Appendix C. The standard response spectra can be used as a starting point for developing conceptual designs and performing evaluations, determining if the earthquake loading controls the design, and establishing the need for more refined analysis and the impact the earthquake loading might have on construction cots.

d. Site-specific response spectra. Earthquake ground motions are dependent on source characteristics, source-to-site transmission path properties, and site conditions. The source characteristics include stress conditions, source depth, size of rupture area, amount of rupture displacement, rise time, style of faulting, and rupture directivity. The transmission path properties include the crustal structure and shear-wave velocity and damping characteristics of the crustal rock. The site conditions include the rock properties beneath the site to depths up to 2 km, the local soil conditions at the site up to a hundred meters or more in depth, and the

topography of the site. All these factors are considered in detail in a site-specific ground motion study, rather than in a general fashion as occur in the standard response spectra methodology. Also, due to regional differences in some of the factors affecting earthquake ground motions, different attenuation relationships exist. There are two basic approaches to developing site-specific response spectra: deterministic and probabilistic. In the deterministic approach, typically one or more earthquakes are specified by magnitude and location with respect to a site. Usually, the earthquake is taken as the Maximum Credible Earthquake (MCE), and assumed to occur on the portion of the source closest to the site. The site ground motions are then estimated deterministically, given the magnitude and source-to-site distance. In the probabilistic approach, site ground motions are estimated for selected values of probability of ground motion exceedance in a design time period or for selected values of the annual frequency or return period of ground motion exceedance. A probabilistic ground motion assessment incorporates the frequency of occurrence of earthquakes of different magnitudes on the various seismic sources, the uncertainty of the earthquake locations on the various sources, and the ground motion attenuation including its uncertainty. Guidance for developing site-specific response spectra and for using both the deterministic approach and the probabilistic approach can be found in EM 1100-2-6050.

e. Acceleration Time Histories. EM 1110-2-6051 describes the procedures for developing site-specific acceleration time-histories of ground motion for dynamic analysis of hydraulic structures. The overall objective is to develop a set (or sets) of time-histories that are representative of site ground motions that may be expected for the design earthquake(s) and that are appropriate for the types of analyses planned for specific structures. The following steps are included in this process:

(1) Initially selecting recorded time-histories that are reasonably consistent with the tectonic environment of the site; design earthquake (magnitude, source-to-site distance, type of faulting); local site conditions; and design ground motion characteristics (response spectral content, duration of strong shaking, and special characteristics, e.g. near-source characteristics). If sufficient recorded motions are not available, simulated recorded time-histories can be developed using ground motion modeling methods.

(2) Modifying time-histories selected in (1) above to develop the final set(s) to be used in dynamic analysis. Two approaches that can be used in this process are simple scaling of time-histories (by constant factors) so that a set of time-histories has spectral values that, on average, are at the approximate level of the design response spectrum; and spectrum matching, which involves modifying the frequency content of a given time-history so that its response spectrum is a close match to the design response spectrum.

(3) Further modifying the time-histories for site response effects, if the site is a soil site and the time-histories have been developed for outcropping rock conditions.

(4) Further modifying the time-histories for spatial variations of ground motion, if it is desired to incorporate effects of wave passage and incoherence in the ground motions that would arrive beneath a very large or long structure.

f. Selection of records for deterministically defined and probabilistically defined earthquakes. Application of the above guidelines is straightforward when design earthquakes are expressed deterministically, i.e., in terms of magnitude, faulting type, and source-to-site distance. However, the application of the guidelines is less straightforward when the design earthquake ground motions (typically the response spectrum) are derived from a probabilistic ground motion

analysis (often termed a probabilistic seismic hazard analysis or PSHA). From this type of analysis, which is described in detail in EM 1110-2-6050, the design response spectrum for a certain selected probability of exceedance in a design time period (or, equivalently, for a design return period) reflects the contribution of different earthquake magnitudes and distances to the probabilities of exceedance. Therefore, when the design response spectrum is probabilistically based, the PSHA should be deaggregated to define the relative contributions of different magnitudes and distances to the ground motion hazard. Furthermore, the de-aggregation should be done for probability values or return periods that correspond to those of the design earthquake and for response spectral periods of vibration of significance for seismic structural response because the relative contributions of different magnitudes and distances may vary significantly with return period and period of vibration. The dominant magnitude and distance is then considered as representative in selecting time histories and defining strong motion duration.

3-2. Multi-Directional Effects

a. General. Two-dimensional structures are generally analyzed for one or two components of the earthquake ground motion (horizontal only, or horizontal + vertical). The ground motions may be defined as multi-component response spectra or acceleration time histories. Some three-dimensional structures such as navigation locks and straight gravity dams can be idealized as two-dimensional structures. While others such as arch dams must be evaluated using three-dimensional models requiring three components of ground motion (two horizontal + vertical). In certain cases, such as freestanding intake/outlet towers, the vertical component of earthquake ground motion may be ignored if it contributes very little to the total response. Structures must be capable of resisting maximum earthquake ground motions occurring in any direction. In response spectrum analysis, the secondary component of horizontal ground motion is usually set equal to the primary component. This is somewhat conservative but eliminates the need to determine the ground motion direction of attack that produces the greatest demand to capacity response (DCR). However, in time history analysis it may be necessary to apply horizontal components in either horizontal direction in order to obtain the largest response in accordance with Paragraph *e* below. The orthogonal components of earthquake ground motion are commonly applied along the principal axes of the structure. In time history analysis the total response due to all components of the ground motion are obtained by algebraic summation of responses due to each individual component. In response-spectrum analysis the total response due to multiple earthquake components are estimated as described in the following paragraphs.

b. Percentage combination method. In a response-spectrum analysis, the percentage combination method can be used to account approximately for the simultaneous occurrence of earthquake forces in two perpendicular horizontal directions. For rectangular structures with clearly defined principal directions, this method yields approximately the same results as the SRSS method described in Paragraph 3-2*c* below. However, for non-rectangular and complex three-dimensional structures the percentage method can under estimate structural responses. The percentage combination is accomplished by considering two separate load cases for both the OBE and MDE. Illustrating for the MDE loading combination, Equation 2-1, the two load cases would be as follows:

Load Case 1:

$$Q_{DC} = Q_D + Q_L \pm Q_{MDE(X1)} \pm \alpha Q_{MDE(X2)} \qquad (3-1)$$

Load Case 2:

$$Q_{DC} = Q_D + Q_L \pm \alpha \, Q_{MDE(X1)} \pm Q_{MDE(X2)} \qquad (3\text{-}2)$$

Generally α is assumed to be 0.30 for rectangular structures, and 0.40 for circular structures.

Q_{DC} = peak value of any response quantity (forces, shears, moments, stresses, or displacements) due to the effects of dead load, live load, and the MDE

$Q_{MDE(X1)}$ = effects resulting from the X_1 component of the MDE ground motion occurring in the direction of the 1st principal axis of the structure.

$Q_{MDE(X2)}$ = effects resulting from the X_2 component of the MDE ground motion occurring in the direction of the 2nd principal axis of the structure.

c. Square Root of the Sum of the Squares Method (SRSS). A better way to combine structural responses for the multi-component earthquake response spectra is the use of the SRSS method. This method is applicable to rectangular and complex three-dimensional structures. For any response quantity of interest, e.g. moment or shear at a particular location, the results from the separate application of each component of ground motion are combined by the square root of the sum of the squares to obtain the total response. Note that since response-spectrum stresses, forces, or moments have no sign, the combination should consider response-spectrum quantities to be either positive or negative. Illustrating for the MDE loading combination, Equation 2-1, the SRSS demand would be as follows:

$$Q_{DC} = Q_D + Q_L \pm \left[(Q_{MDE(X1)})^2 + (Q_{MDE(X2)})^2 + (Q_{MDE(Z)})^2 \right]^{1/2} \qquad (3\text{-}3)$$

d. Critical Direction of Ground Motion. The directions of ground motion incidence are usually assumed along the fixed structural reference axes. Considering that the ground motion can act along any horizontal direction, there could be a different direction of seismic incidence that would lead to an increase of structural dynamic response. The maximum structural response associated to the most critical directions of ground motions has been examined in several publications (Wilson and Button 1982, Smedy and Der Kiureghian 1985, Wilson et al. 1995, Lopes and Torres 1997, and Lopez et al. 2000). These investigations indicate that the critical direction of the horizontal ground motion components yielding the maximum structural response depends on the two horizontal spectra and also on the structural response parameters but not on the vertical spectrum. For the special case of identical spectra along the two horizontal directions, the structural response does not vary with the angle of incidence, i.e. any direction is a critical direction. The response value for this special case is the upper bound to all possible structural responses due to any combination of spectral ratios and angle of incidence. A conservative approach is therefore to analyze the structure with the same horizontal spectrum applied simultaneously along the two horizontal structural reference directions, and the vertical spectrum.

e. Load combination cases for time history analysis. 3D time-history analysis of CHS with response in the damage control range should be evaluated for three or more sets of three-component earthquake ground motions plus the effects of usual static loads. For each set of three-component earthquake ground motions the static loads and earthquake ground motion components should be combined in accordance with Table 3-1. In general, a complete

permutation of all three components with positive and negative signs may be required to obtain the most critical directions that would cause the largest structural response (EM 1110-2-6051). 2D time-history analysis of CHS with response in the damage control range is conducted in a similar fashion requiring three or more sets of two-component acceleration time-history records, except that for two-component excitation a total of 4 permutations will be required.

Table 3-1
Load Combination Cases for Combining Static and Dynamic Stresses for Three-component Excitation

| Case | Seismic Loads | | | Static Loads |
	Horizontal (H1)	Vertical (V)	Horizontal (H2)	
1[1]	+	+	+	+
2	+	+	-	+
3	+	-	+	+
4	+	-	-	+
5	-	+	+	+
6	-	+	-	+
7	-	-	+	+
8	-	-	-	+

Note: The (+) and (-) signs indicate the loads are multiplied by +1 (zero phase) or -1 (180 phase) to account for the most unfavorable earthquake direction.
[1] Case-1: Static + H1 + V + H2

3-3. Earthquake Demands on Inelastic Systems

a. General. The inelastic response of a structure to earthquake ground motion is different than the elastic response. The difference occurs because the vibration characteristics of the structure change as the structure yields. The predominant change is a shift in the fundamental period of vibration. In most cases, a reduction in earthquake demand occurs as the period of the structure lengthens. In Figure 3-1, a capacity spectrum is used to illustrate the inertia force reduction (or spectral acceleration reduction) that occurs when a structure yields. In Figure 3-1, earthquake demands for an elastic system, as represented by a response spectrum, are reconciled with the elasto-plastic load/displacement characteristics for a ductile structure. Point "*A*" represents the earthquake demand assuming the structure remains elastic with the line "*O-A*" representing the linear elastic response. Point "*B*" represents the earthquake demands for elasto-plastic behavior with the line "*O-B-C*" representing the load/displacement characteristics of the elasto-plastic system. As can be seen, the earthquake force demand on the elasto-plastic system is substantially less than that of the elastic system. It should also be recognized that as a structure yields, damping increases significantly, thus leading to further reduction of earthquake demands. However, if the fundamental period of the structure falls in the ascending portion of the response spectrum, a shift in period may actually increase earthquake demands. This condition is likely to occur for stiff structures founded on soft soils, but can also occur for stiff structures founded on rock. In such cases, the structure should be designed to remain elastic.

b. Inelastic displacement demands. Knowing displacements in yielding structures, the level of damage or yielding can be controlled by limiting displacements to predetermined values for a specified level of earthquake shaking. Simple techniques have been developed for estimating inelastic displacements from elastic displacements. Structures with a period of vibration between zero and 0.75 T_0, where T_0 is characteristic ground motion period (period corresponding to the peak acceleration response), exhibit an equal acceleration response which offers no benefit from yielding. Structures with periods of vibration greater than 0.75 T_0, however, will benefit from structure displacement ductility. The inelastic response of structures

with fundamental periods of vibrations between 0.75 T_0 and 1.5 T_0, can be estimated using equal energy principles. The inelastic response of structures with fundamental periods of vibration greater than 1.5 T_0, can be estimated using equal displacement principles.

(1) Equal acceleration response. Rigid structures, with a period of vibration (T) equal or less than 0.04 sec (or between 0 and 0.75 T_0), will exhibit an equal acceleration response. In this case, force or acceleration is conserved regardless of any ductile properties attributed to the structure. Structures exhibiting an equal force or acceleration response should therefore be designed to remain elastic.
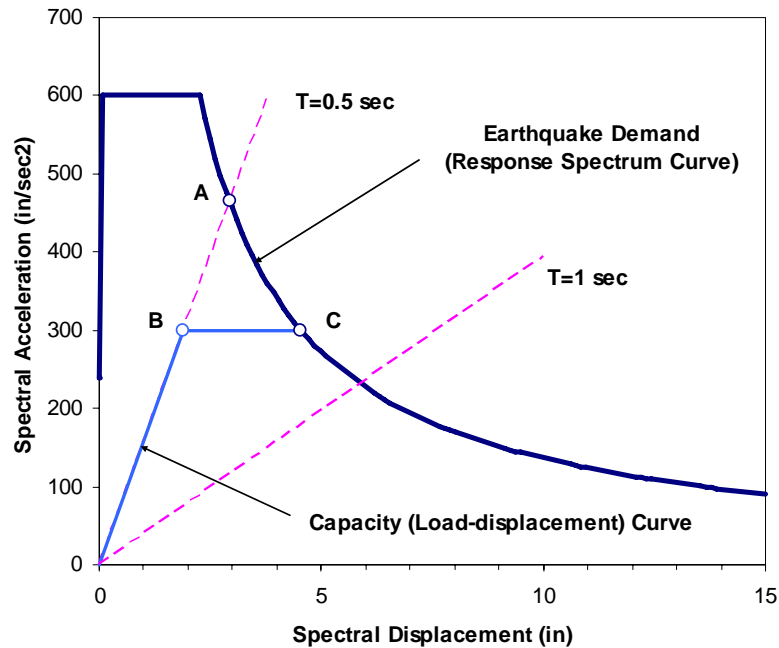
Figure 3-1. Earthquake Demands on Inelastic Structures

(2) Equal energy response. Structures with fundamental periods of vibration between 0.75 T_0 and 1.5 T_0 will exhibit an equal energy response. The characteristic ground motion period (T_0) generally varies between 0.2 seconds and 0.7 seconds depending on site conditions, with firm sites having shorter characteristic periods than soft sites. The structure must have sufficient displacement ductility to provide the reserve inelastic energy capacity needed to resist earthquake ground motion demands. The equal energy response concept is presented in Figure 3-2. For a given displacement ductility (μ_δ), the inelastic (yield) capacity (F_Y) must be sufficient to produce an equal energy response. Equating the energy for a linear elastic response to that for an inelastic response (hatched area under the nonlinear portion of the load displacement curve equal to the hatched area under the linear elastic curve), it can be determined that the yield capacity of the structure must be equal to or greater than the capacity required of the structure if it were to remain elastic (F_E) divided by $\sqrt{2\mu_\delta - 1}$, or:

$$F_Y \geq \frac{F_E}{\sqrt{2\mu_\delta - 1}} \qquad (3-4)$$
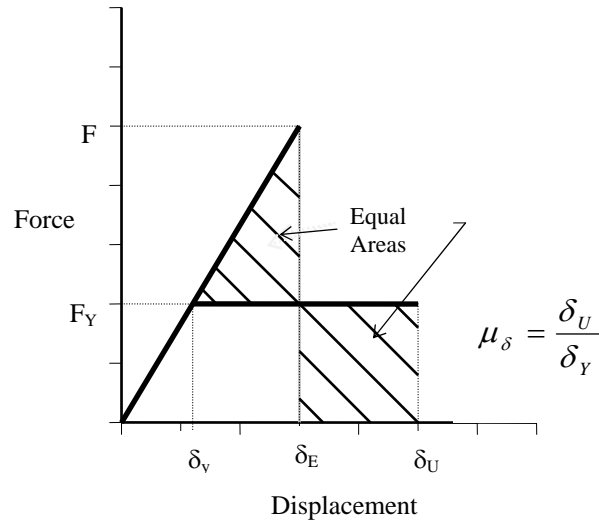
Figure 3-2. Equal Energy Response

(3) Equal displacement response. Structures with fundamental periods of vibration greater than 1.5 T_0 will exhibit an equal displacement response. An equal displacement response means that to perform as intended, the displacement ductility capacity must be sufficient to provide a structure displacement capacity equal to, or greater than, the peak displacement the structure will experience during the design earthquake. The equal displacement response concept is presented in Figure 3-3. From Figure 3-3 it can be determined that the yield capacity of the structure must be equal to or greater than the capacity required of the structure if it were to remain elastic (F_E) divided by μ_δ, or:

$$F_Y \geq \frac{F_E}{\mu_\delta}$$

(3-5)
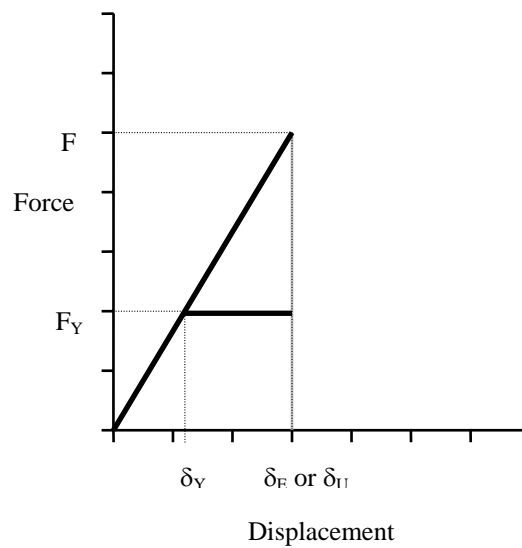
Figure 3-3. Equal Displacement Response

(4) General relationship between required yield strength (F$_Y$) and elastic demand (F$_E$). A general relationship has been developed (Paulay and Priestley, 1992) for relating required yield strength to elastic demand. This relationship provides a smooth transition from an equal acceleration response ($\frac{F_E}{F_Y} = 1$ regardless of μ_δ) at T = 0, through the equal energy approximation ($\frac{F_E}{F_Y} = \sqrt{2\mu_\delta - 1}$) at about T = 0.75 T_0, to the equal displacement approximation ($\frac{F_E}{F_Y} = \mu_\delta$) for $T \geq 1.5\ T_0$. The relationship for the smooth transition is:

$$\frac{F_E}{F_Y} = 1 + \frac{(\mu_\delta - 1)T}{1.5T_0} \geq \mu_\delta \qquad (3\text{-}6)$$

Using Equation 3-6; for a known level of displacement ductility (μ_δ) and a given elastic earthquake demand (F$_E$), the required yield capacity of a structural component (F$_Y$) can be determined.

3-4. Mandatory Requirements

a. Standard spectra. Standard spectra used in the preliminary design and evaluation of Corps hydraulic structures shall be developed in accordance with the procedures described in Appendix B.

b. Site-specific spectra. Site-specific spectra used in the preliminary design and evaluation of Corps hydraulic structures shall be developed in accordance with the procedures described in EM 1110-2-6050.

c. Acceleration time histories. Acceleration time histories for dynamic analysis of CHS shall be selected and developed in accordance with EM 1110-2-6051.

d. Multi-directional effects. Multi-directional effects shall be considered when designing or evaluating concrete hydraulic structures for earthquake ground motions. General information on multi-directional effects can be found in Paragraph 3-2.

Chapter 4
Methods of Seismic Analysis and Structural Modeling

4-1. Progressive Analysis Methodology

The evaluation of structures for earthquake ground motions should be performed in phases in order of increasing complexity progressing from simple equivalent lateral force methods, to linear elastic response-spectrum and time-history analysis, to nonlinear methods, if necessary. The following paragraphs describe the various analytical methods used to assess earthquake ground motion effects beginning with the simplest method and progressing to the more complex methods. In each analysis procedure idealized models of structures are used to estimate the dynamic response of structures to earthquakes.

4-2. Methods of Analysis

   a. Seismic coefficient method. Seismic coefficient method has traditionally been used to evaluate seismic stability of structures. According to ER 1110-2-1806 this method may still be used in the preliminary design and stability analyses. In the seismic coefficient method, earthquake forces are treated simply as static forces and are combined with the hydrostatic pressures, uplift, backfill soil pressures, and gravity loads. The analysis is primarily concerned with the rotational and sliding stability of the structure treated as a rigid body. The inertia forces acting on the structure are computed as the product of the structural mass, added-mass of water, and the effects of dynamic soil pressures, times a seismic coefficient. The magnitude of the seismic coefficient is often taken as a fraction of the peak ground acceleration expressed as a decimal fraction of the acceleration of gravity. In representing the effects of ground motion by static lateral forces, the seismic coefficient method neither accounts for the dynamic characteristics of the structure-water-soil system nor for the characteristics of the ground motion. The method however can give reasonable results when the structure primarily acts as a rigid body, such as sliding response of a gravity dam depicted in Figure 4-1. As the most probable sliding response, this failure mechanism is commonly used to determine a factor of safety against sliding. Note that prior to the sliding evaluation the dam should be analyzed as a flexible structure to determine stresses and the extent of cracking that might lead to such a sliding failure, as shown in Figure 2-4. Another instance where the structure may be analyzed as a rigid body is the case where the massive concrete structure is supported on a flexible foundation, such as the pile founded navigation lock monolith shown in Figure 4-2. In this case, accelerations will be nearly uniform from the base to top of the monolith, if the piles are relatively flexible with respect to the structure. This is similar to the response of base isolated stiff buildings. Under this condition the seismic coefficient method may be used for the preliminary design and evaluation of the lock system. The method, however, should be used with caution if the interaction between the structure and soil-pile foundation is significant. The seismic coefficient method is part of the Linear Static Procedure (LSP) described in Chapter 6.

   b. Equivalent lateral force method. The equivalent lateral force method (ELF) is commonly used for the seismic design of buildings. Assuming that the structure response is predominantly in the first mode, similar procedures have also been developed for preliminary seismic analysis of gravity dams (Fenves and Chopra, 1986) and intake towers (EM 1110-2-2400) using standard mode shapes and periods. In such cases, the first mode of vibration could contribute as much as 80-percent or more to the total seismic response of the structure. Therefore, the period and general deflected shape of the first mode are sufficient for estimating inertia forces or equivalent lateral loads needed for the seismic design or evaluation. The ELF Method is illustrated in Figure 4-3. The steps in the analysis are described as follows:

F_h = Seismic inertia load
F_{hd} = Hydrodynamic load
F_{hs} = Hydrostatic load
F_u = Uplift load
W = Structure weight

Displaced Structure

$F_h = W \times (SeismicCoefficient)$

Dam acting as rigid body

F_{hd}

F_{hs}

Ground Motion

F_U
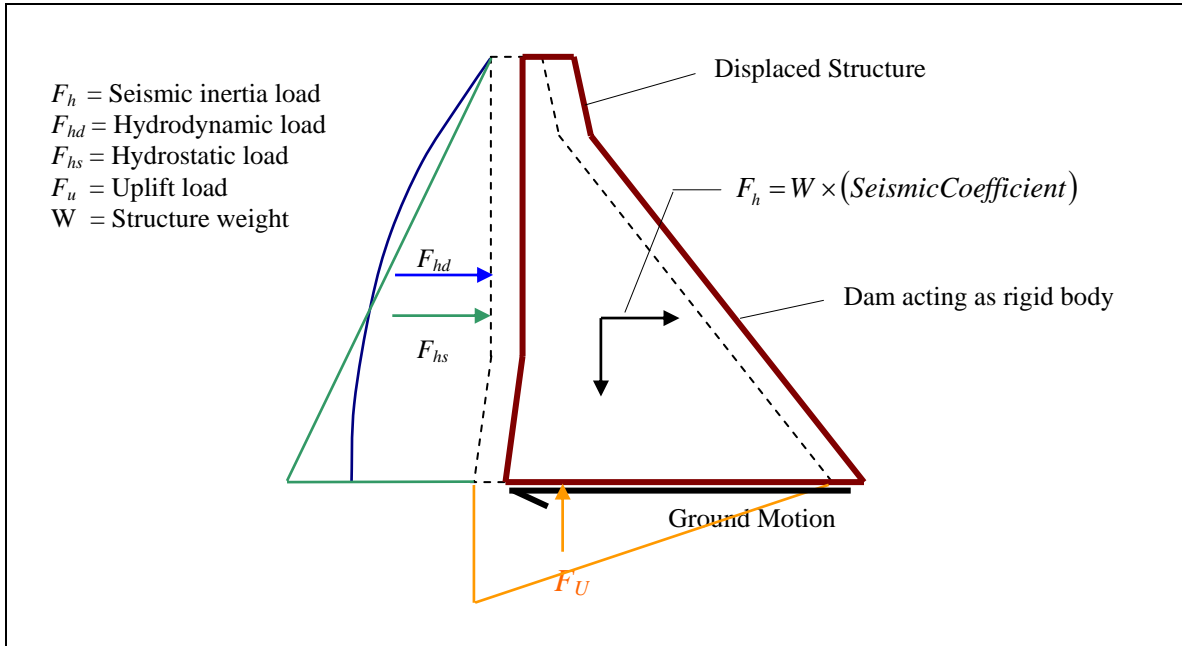
Figure 4-1. Gravity Dam Sliding on Foundation

Displaced
Structure

Ground Motion
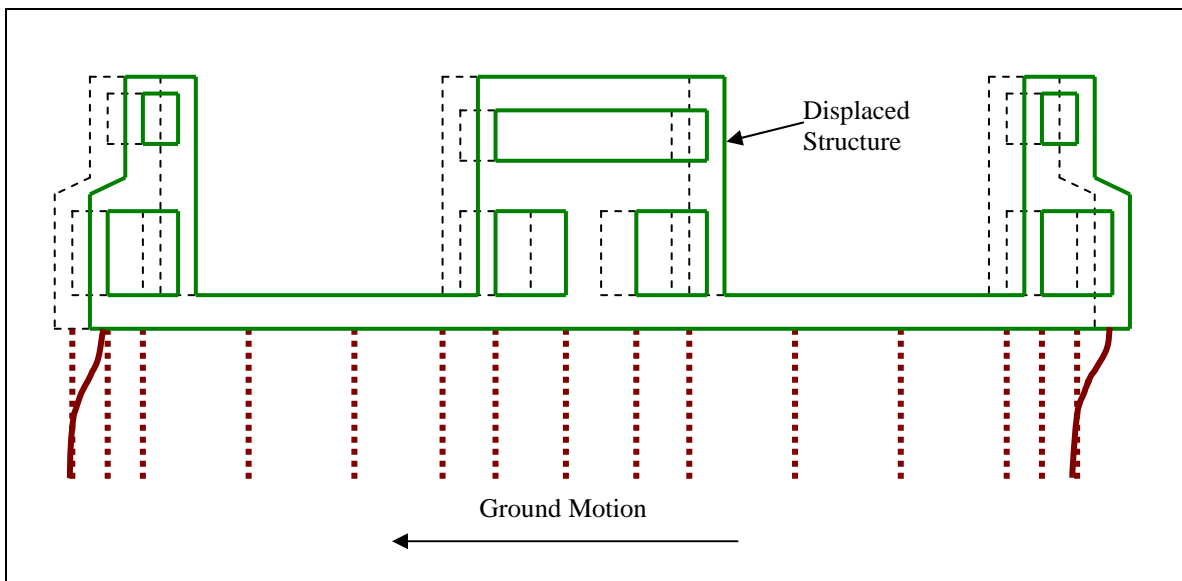
Figure 4-2. Navigation Lock on Flexible Pile Foundation

(1) The first step as illustrated in Figure 4-3a is to estimate the period of vibration of the first mode. This can be done using a general formula developed for the particular structure under consideration based on what is known about the stiffness of the structure-foundation system (*K*) and the total system mass (M = structure mass + added hydrodynamic mass + backfill.) The formula will be of the general form shown in Figure 4-3a.

(2) The second step is to determine the spectral acceleration (S_A) for an equivalent single-degree-of-freedom system. This can be done using the period of vibration determined in Step 1 in combination with a standard or site-specific acceleration response spectrum. This step is illustrated in Figure 4-3b. In some cases, as for buildings, the spectral acceleration will be represented by a standard spectrum in equation form as part of a base shear formula. The base shear formula will also account for the base shear participation factor described in the following step.

(3) Once the spectral acceleration (S_A) has been determined, the total inertial force on the structure due to the design ground motions (represented by the design response spectrum shown in Figure 4-3b) can be estimated using Equation (4-3) in Figure 4-3b. The spectral acceleration and the total mass being known, the base shear participation (α) can be estimated from the structure deflected shape and mass distribution.

(4) The analytical model of the structure is represented by a series of lumped masses as shown in Figure 4-3d. The total inertial force (base shear) is then distributed along the height of the structure at location of each lumped mass. The magnitude of each inertial force is obtained from the product of the mass participation factor (PF), times the lumped mass (w/g), times the spectral acceleration (S_A), times the value of the mode shape (ϕ_Z) at the lumped mass location, or:

$$F_Z = PF \left[\frac{w_Z}{g} \right] S_A (\phi_Z) \tag{4-1}$$

The first-mode mass participation factor (PF) is the same for each lumped mass location (Z) and can be determined based on the mass distribution and deflected shape. The mode shape value (ϕ_Z) will either be provided in the ELF Method, or will be incorporated in a base shear distribution formula as done for buildings. Once all the inertial forces have been determined, the analysis can proceed in the same fashion as any static analysis.

Because the dynamic characteristics of the structure are considered when determining earthquake demands and distributing inertia forces to the structural system, the ELF method is an excellent static force method. ELF methods in some cases, as for the evaluation of dams and intake towers, have the capability of including higher mode effects. The ELF method is part of the Linear Static Procedure (LSP) described in Chapter 6.

Ground Mc

$$T = 2\pi\sqrt{\frac{M}{K}} \qquad (4\text{-}2)$$

a) Step 1 – Determine Fundamental Period of Vibration (*T*)

Spectral
Acceleration

Acceleration
Response
Spectrum

S_A

Period

T

$$V_{Base} = \alpha(S_A)\frac{W}{g} \qquad (4\text{-}3)$$

b) Steps 2 & 3 –Determine Spectral Acceleration S_A at Period *T* and then Total Inertia Force

$$F_Z = PF\left[\frac{w_7}{g}\right]S_A(\phi_7)$$

$\frac{w_7}{g}$

7

4

Fundamental
Mode Shape

1

c) Step 4 -- Distribute Total Inertia Force along the Height In Accordance with
Fundamental Mode Shape

Figure 4-3. Illustration of Equivalent Lateral Force Method

c. Response spectrum – modal analysis procedure. The response spectrum–modal analysis procedure is similar to that described above for the ELF method, except that it is the most basic and truly dynamic method of analysis. In this method, the peak responses of linear elastic structures to earthquake ground motions characterized by response spectra are determined. The number of modes required varies for each analysis however; all modes with significant contribution to the total response of the structure should be included. Usually the numbers of modes are adequate if the total mass participation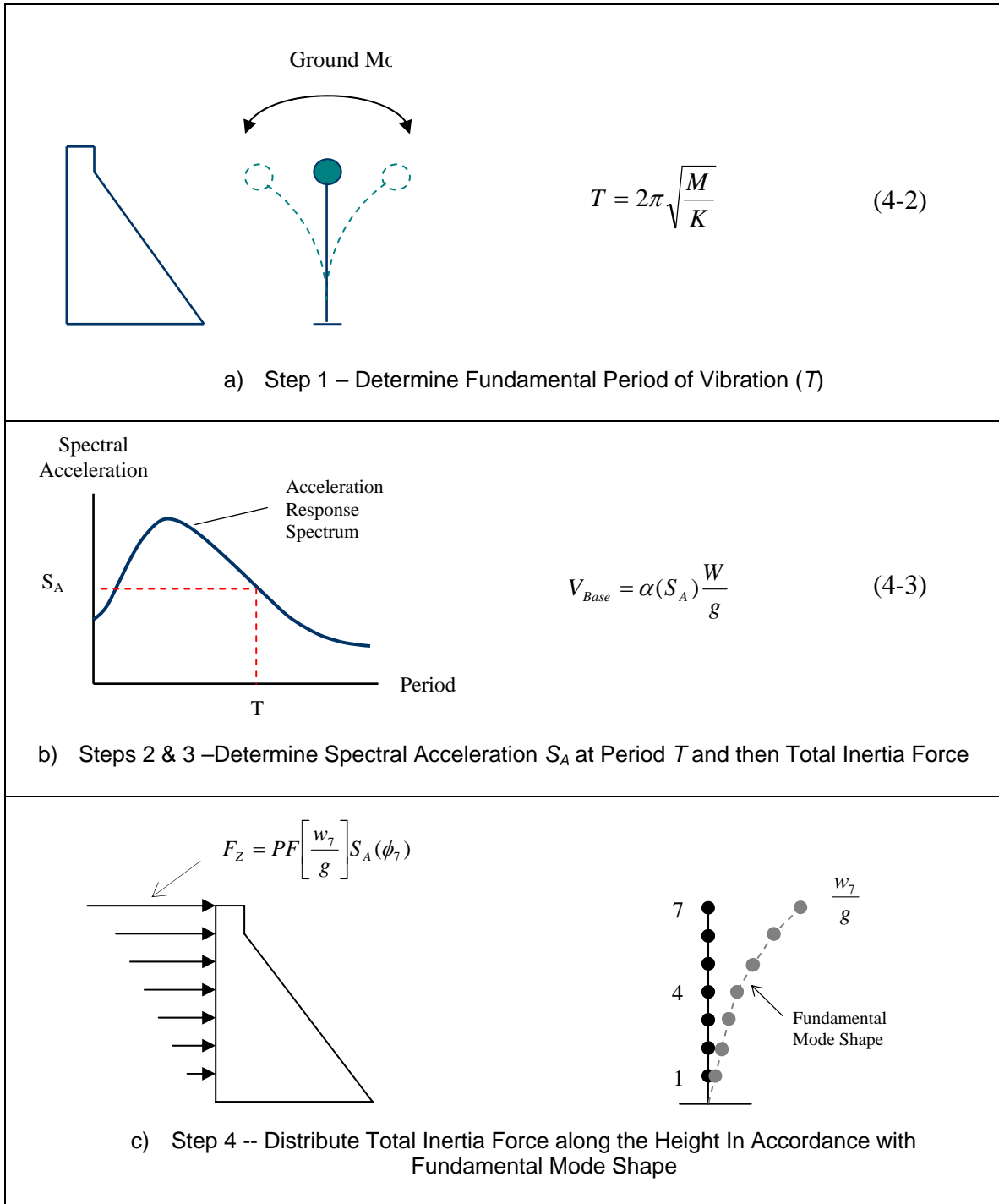 of the modes used in the analysis is at least within 90-percent of the total mass of the structure. Modal analysis is usually performed using computer software capable of determining the periods of vibration and mode shapes for all contributing modes. Most structural analysis programs have this capability, and for many reasons this type of analysis is preferred over the ELF method of analysis which is limited to a single mode. The response-spectrum modal analysis procedure however has limitations and time history analysis is usually recommended for final design and evaluation in conformance with ER 1110-2-1806 when:

- The computed response-spectrum stresses or section forces exceed the allowable values, thus indicating nonlinear response might occur

- Soil-structure interaction, water-structure interaction, and reservoir bottom absorption effects are controlling response of the structure and could impact a new design or evaluation of an existing structure

- An estimate of the level of nonlinear behavior and thus damage is necessary to assess acceptability of the design or seismic safety of an existing structure (EM 1110-2-6051)

Detailed information on the response spectrum–modal analysis procedure can be found in EM 1110-2-6050 (1999). The response spectrum – modal analysis is part of the Linear Dynamic Procedure (LDP) described in Chapter 6.

d. Time history-modal analysis procedure. This procedure is similar to that described for the response spectrum – modal analysis procedure, except that earthquake demands are in the form of acceleration time histories, rather than response spectra and the results are in terms of displacement and stress (or force) histories. Peak values of various response quantities are extracted from the response histories. Time history-modal analysis provides valuable time-dependent information that is not available in the response spectrum–modal analysis procedure. Especially important is the number of excursions beyond displacement levels where the structure might experience strength degradation (strain softening). As with the response spectrum–modal analysis procedure, the time history-modal analysis is limited to a linear elastic response. The nonlinear response of a structure is computed by the time-history method using the direct integration procedure described in 4-2*e* below. Detailed information on the time history–modal analysis procedure can be found in EM 1110-2-6051 (2000). The time history–modal analysis is part of the Linear Dynamic Procedure (LDP) described in Chapter 6.

e. Nonlinear Time history – direct integration procedure. This type of time history analysis, described in Paragraph 6-6, involves the direct integration of the equations of motion, and therefore is the most powerful method available for evaluating the response of structures to earthquake ground motions. It is a step-by-step numerical integration procedure, which determines stresses (or forces) and displacements for a series of short time increments from the initiation of loading to any desired time. The time increments are generally taken of equal length for computational convenience. The condition of dynamic equilibrium is established at the beginning and end of each time increment. The motion of the system during each time

increment is evaluated on the basis of an assumed response mechanism. The advantage of this method is that it can be used for both linear and nonlinear analyses. In the case of nonlinear analyses, structure properties (including nonlinear behavior) can be modified during each time increment to capture response behavior appropriate to that deformed state. The application of nonlinear analysis to concrete hydraulic structures is limited to cases for which experimental or observational evidence of nonlinear behavior is available and that validity of the numerical models have been demonstrated. These include certain nonlinear behavior such as joint opening mechanisms in arch dams, tensile cracking of gravity dams, sliding and rotational stability of blocks isolated by opened joints and cracked sections, and yielding and cracking of free-standing intake towers.

4-3. Modeling of Structural Systems

a. Structural models. Structural models for dynamic analyses are developed much in the same manner as for static analyses. However, distribution of mass and stiffness and dynamic interaction between the structure and water and between the structure and foundation as well as with the backfill soil should be established accurately. The response of a structure under severe ground shaking may approach or exceed the yield/cracking state. This means that in a linear-elastic dynamic analysis the use of effective stiffness (Paragraph 4-4) is more appropriate than the initial elastic stiffness used in the static analysis, and that the damping should be selected consistent with the expected level of deformation and the extent of nonlinear behavior. Furthermore, concrete deterioration and cracking can reduce structural stiffness of an existing structure; thus these effects should be considered in estimation of a representative effective stiffness. The dynamic interaction with the foundation introduces flexibility at the base of the model and could provide additional damping mechanisms through material and radiation damping. Various foundation models suitable for concrete hydraulic structures are discussed in Paragraph *b* below. A hydraulic structure also interacts with the impounded, surrounding, or retained water through hydrodynamic pressures at the structure-water interface. This interaction is coupled in the sense that motions of the structure generate hydrodynamic pressures that affect deformations (or motions) of the structure, which in turn influence the hydrodynamic pressures. Various structure-water interaction models with varying degrees of sophistication are described in Chapter 2 of EM 1110-2-6051. They include models as simple as the added-mass concept to more vigorous finite-element formulation that accounts for water compressibility and boundary absorption effects. Often structure-foundation interaction and structure-water interaction effects can be accommodated in the special finite-element models developed for gravity and arch dam evaluation. Since foundation properties, structural properties, and boundary conditions can vary, it is advisable to systematically vary parameters that have a significant effect on structure response until the final results cover a reasonable range of possible responses the structure could experience during the design earthquake. Properties of concrete for use in seismic analysis are described in Chapter 5. Following is a brief description of structural idealization for seismic analysis of concrete hydraulic structures. For detailed discussions and more information refer to EM 1110-2-6050, EM 1110-2-6051, and respective manuals for a particular structure.

(1) A variety of models are used to represent different types of hydraulic structures or to capture certain modes of behavior. For example, the model may be as simple as a rigid block to perform sliding stability analysis of a dam section (Figure 4-1), a frame model to compute earthquake response of a freestanding intake tower, a 2D finite-element mesh for stress analysis a gravity dam, or a more elaborate 3D finite-element mesh with nonlinear joint elements to simulate contraction joints opening in an arch dam (see example in Appendix F).

(2) Frame type models. A frame type or stick model is composed of beam-column elements with nodal lumped masses for analyzing regular freestanding intake towers, or possibly U-frame or W-frame lock sections. Frame models are generally preferred for reinforced concrete where the earthquake demands are expressed in section moments, shears, and axial loads; the parameters needed to design and evaluate reinforced concrete members. The frame models could be developed in two or three dimensions. In 2D representation one horizontal component of the ground motion and sometimes also the vertical component will be used as the seismic input. Appendices D and E present two examples of frame models: a freestanding intake tower and a W-frame or dual-chamber navigation lock, respectively. One advantage of the frame models is that the beam-column elements include plastic hinge capability for modeling nonlinear behavior. In the examples cited here, this capability was used to conduct nonlinear static pushover analyses.

(3) 2D models. 2D finite-element idealization is used to model planar or very long structures such as gravity dams, lock structures, retaining walls, and outlet tunnels. These structures are usually built of independent segments separated by construction joints, and the loads perpendicular to the long axis are assumed not to change along each segment. In situations like this, the structure may be modeled as a 2D slice using either the plane stress or plane strain elements depending on whether the stress or strain can be ignored in the out-of-plane direction. In either case the foundation model is idealized using plane-strain elements. A 2D model is usually analyzed for two components of ground motion applied in the vertical and horizontal directions. Examples in Appendices G and H illustrate application of this type of modeling to a lock gravity wall with backfill soil and a non-overflow gravity dam section.

(4) 3D models. 3D finite-element idealization is used to analyze structures with complex or irregular geometry or nonuniform loading. Arch dams, inclined intake towers supported by the abutment foundations, irregular freestanding towers with significant torsional behavior, gravity dams built in narrow canyons, and certain lock monoliths with complicated components and loading conditions fall in this category. A 3D model is usually constructed using 3D solid elements, but shell elements may also be used for relatively thin sections of the structure. The seismic input for a 3D model includes three orthogonal components of ground motion, two horizontal and the vertical, applied along the principal axes of the structure. Appendix F provides an example of 3D modeling applied to linear and nonlinear earthquake analyses of an arch dam.

(5) Soil-structure-interaction (SSI) models. An SSI model refers to a case where interaction between the structure and its foundation requires special consideration in terms of the ground motion at the base of the structure and the flexible support provided by the soil foundation. At soil sites the bed rock motion is affected by the local soil conditions as it travels to the ground surface, and the presence of the structure produces a further change to this motion due to kinematic constraints. Furthermore, the foundation interacts with the structure by elongating periods of vibration and providing additional damping. An SSI condition requires a model which includes both the structure and foundation together (direct method) or separately (substructure method). These methods are briefly described in Paragraphs *c*(3) and *c*(4) below. Further discussions are provided in EM 1110-2-6050 and EM 1110-2-6051. An SSI analysis may be conducted using 2D or 3D models.

b. Foundation models. Foundation-structure interaction introduces flexibility at the base of the structure and provides additional damping mechanisms through material damping and radiation. The flexible foundation tends to lengthen the period of vibration and the material and radiation damping in the foundation region has the effect of reducing the structural response.

Such interaction effects generally introduce frequency-dependent interacting forces at the structure-foundation interface requiring more elaborate analysis. In practice however, simplified models that include only the flexibility of the foundation and not its inertia and damping are more common.

(1) Massless rock foundation model. Generally arch dams, gravity dams, and sometimes lock walls and intake towers are built on competent rock foundations. In these situations a massless finite-element model can adequately represent the effects of rock region supporting the structure. The size of foundation model need not be very large so long as it is comparable with dimensions of the structure. The earthquake input is applied directly at the fixed boundaries of the massless foundation model.

(2) Viscoelastic rock foundation model. The simplified massless foundation model discussed above accounts only for the flexibility of the foundation thus ignores its inertia and damping effects. This assumption may not be appropriate for rock sites whose elastic moduli are substantially lower than the massive concrete that they support. In such cases if similar rocks can be assumed to extend to large depths, the foundation may be idealized as a viscoelastic model. A viscoelastic model is represented by impedance functions whose terms are complex and frequency-dependent. The real component of the impedance function represents the stiffness and inertia of the foundation and the imaginary component characterizes its radiation and material damping. Two such viscoelastic models have been developed for the 2D analysis of gravity dams (Dasgupta and Chopra 1979) and 3D analysis of arch dams (Zhang and Chopra 1991).

(3) Finite-element soil-structure interaction (SSI) model. The interaction between the soil and structure can be fully accounted for by developing a direct SSI model, which includes both the structure and the supporting soil. The structure is modeled using frame and/or solid elements with linear material properties. The soil medium is represented by solid elements with strain-dependent soil properties. The two-dimensional direct method of SSI analysis can be carried out using the computer program FLUSH (Lysmer et al. 1975) or Q-FLUSH (Quest Structures 2001). These programs conduct SSI analyses in the frequency domain, where the nonlinear soil behavior is approximated by the equivalent linear method (Seed and Idriss 1969) and the response is evaluated by iteration. The iteration involves updating the stiffness and damping values in accordance with the prescribed strain-dependent material curves until the solution converges.

(4) Lumped-parameter soil foundation model. The soil-structure interaction effects can also be represented using a lumped-parameter model of the soil. A complete form of the lumped-parameter model consists of frequency-independent springs, dampers, and masses that closely reproduce the actual response of the soil. The simplest model that can be developed for each degree of freedom of a rigid basemat includes a spring and a damper connected to the basemat with a fictitious mass of the soil added to mass of the structure. The frequency-independent coefficients of this SDOF system are obtained by a curve-fitting procedure such that a good agreement between the dynamic stiffness of the SDOF model and that of the actual soil is achieved. Appendix B of EM 1110-2-6051 provides lumped-parameter models for a disk supported by a homogeneous half space, an embedded cylinder, an embedded prism, and a strip supported on the surface of a homogeneous half space. For application to finite-element analysis, distributed soil springs, dampers, and masses can be obtained by dividing the total soil parameters by the base area, and then assigning them to individual nodes according to the tributary area of each node.

c. Pile foundation models. Several analytical methods have been developed for the seismic-load analysis of soil-pile systems. The static-load "*p-y*" method of pile analysis, originated in the offshore industry, have been modified and extended to cyclic loading conditions, and is now routinely applied to dynamic or earthquake loading cases. At the same time, dynamic soil-pile analysis methods (elastic continuum solution) have been developed for single piles and pile groups embedded in homogenous and non-homogenous soil media. Such methods are more theoretically sound than the *p-y* method, and along with the finite-element method provide reasonable solutions for the soil-pile-structure interaction analysis. However these methods do not allow for the adequate characterization of the localized yielding at the soil-pile interface, and are generally suitable for relatively low levels of seismic loading. The results of dynamic pile analyses include seismic response as well as the dynamic stiffness of piles that can be used in the subsequent soil-pile-structure interaction analysis. In practice, four levels of soil-pile-structure-interaction (SPSI) analysis progressing from simple to complete interaction can be employed as follows:

(1) Single-pile kinematic seismic response analysis. This basic pseudo-static analysis incorporates nonlinear response and is performed as pile integrity evaluation. A pseudo-static method for pile integrity consists of transforming the horizontal profile of soil displacement (derived from a free-field site response analysis) to a curvature profile, and comparing peak values to allowable pile curvatures. This method assumes piles perfectly follow the soil, and that no inertial interaction takes place. Alternatively, a displacement time history may be applied to nodal points along the pile in a dynamic pile integrity analysis.

(2) Pile-head stiffness or impedance functions. In the second level of analysis, pile head stiffness or impedance functions may be obtained from linear or nonlinear soil-pile analyses and assembled into a pile-head stiffness matrix for use in a global response analysis (Figures 4-4 and 4-5). Secant stiffness values at design level deformations are normally prescribed from nonlinear soil-pile response analyses (Figure 4-6).
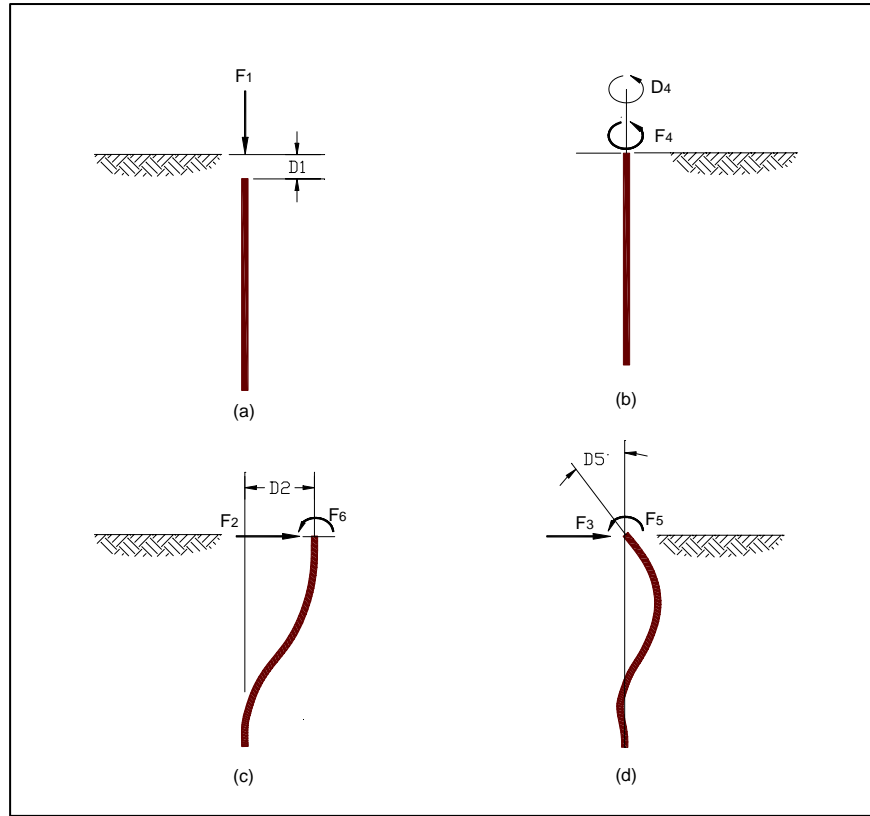
Figure 4-4. Pile Behaviors

$$\begin{bmatrix} K_{11} & 0 & 0 & 0 & 0 & 0 \\ 0 & K_{22} & 0 & 0 & 0 & K_{26} \\ 0 & 0 & K_{33} & 0 & K35 & 0 \\ 0 & 0 & 0 & K_{44} & 0 & 0 \\ 0 & 0 & K53 & 0 & K_{55} & 0 \\ 0 & K_{62} & 0 & 0 & 0 & K_{66} \end{bmatrix} \begin{Bmatrix} D_1 \\ D_2 \\ D_3 \\ D_4 \\ D_5 \\ D_6 \end{Bmatrix} = \begin{Bmatrix} F_1^1 \\ F_2^2 + F_6^2 \\ F_3^3 + F_5^3 \\ F_4^4 \\ F_5^5 + F_3^5 \\ F_6^2 + F_6^6 \end{Bmatrix} = \begin{Bmatrix} F_1 \\ F_2 \\ F_3 \\ F_4 \\ F_5 \\ F_6 \end{Bmatrix}$$

$$\underline{K} \quad \times \quad \underline{D} \quad = \quad \underline{F}_{dir} + \underline{F}_{coup.} = \underline{F}$$

where:

$\underline{K} = Stiffness$ $\qquad\qquad \underline{F}_{dir} = Direct\ Force$

$\underline{D} = Displacement$ $\qquad\qquad \underline{F}_{coup.} = Coupled\ Force$

$\qquad\qquad\qquad\qquad\qquad\qquad\quad \underline{F} = Total\ Force$

Figure 4-5. Flexible Pile Stiffness Matrix (after Kriger and Wright, 1980)
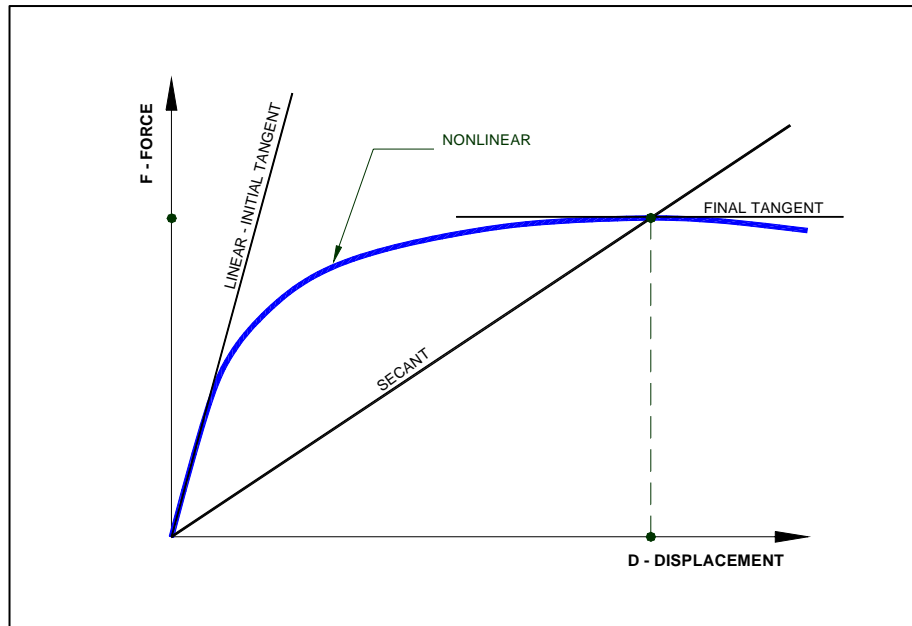
**Figure 4-6. Secant stiffness value selected at design level displacement from nonlinear
soil-pile force-displacement curve (after Kriger and Wright 1980)**

(3) Substructure method. Both inertia and kinematic interaction may be evaluated from a substructuring type analysis to determine pile head impedance and foundation level input motions (Figure 4-7). As described in EM1110-2-6050, the SPSI analysis may be performed in two steps consisting of the kinematic and inertia parts. The kinematic interaction is accomplished by setting mass of the superstructure to zero and obtaining the foundation level input motions (kinematic motions) for the subsequent inertia interaction analysis. The inertia interaction analysis is carried out in two steps. First pile-head impedance or dynamic stiffness is determined from a separate analysis of the soil-pile foundation system, and then used as spring supports in the inertia analysis of superstructure subjected to kinematic motions.
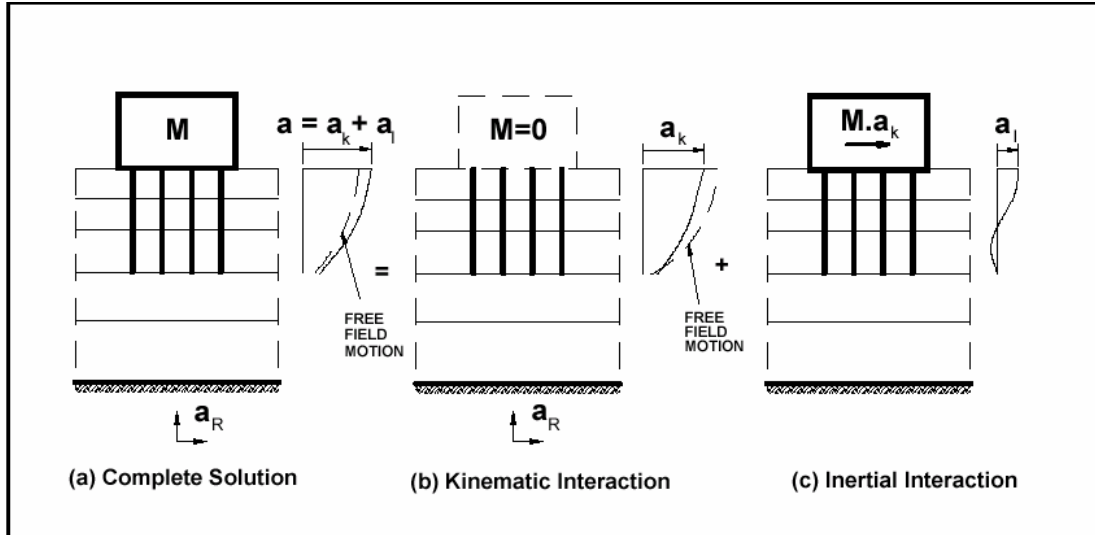
Figure 4-7. Substructuring concept: Decomposition of the problem into kinematic and inertia interaction problems.

(4) Complete or direct method of analysis. Finally a fully coupled SPSI analysis may be carried out to determine the complete system response. This can be accomplished by developing a complete finite-element model consisting of the structure and the soil-pile foundation and analyzing for a prescribed input motion. A 2D approximation of the soil-pile-structure system can be evaluated using the computer program FLUSH (Lysmer et al. 1975) or its enhanced web-based version Q-FLUSH at www.webdams.com (QUEST Structures 2001). Application of the SPSI analysis to lock structures is fully described in EM 1110-2-6051 and shown in Figure 4-8. An important aspect of the SPSI analysis is that large shear deformations that occur in soils during strong earthquake shaking introduce significant nonlinear behavior in the foundation region and must be considered in the analysis. In the FLUSH program the nonlinear response of the soil is approximated by the equivalent linear method (Seed and Idriss 1969). A similar 3D approximation of SPSI model can be evaluated using the computer program SASSI (Lysmer et al. 1981). However, the number of piles that can be included in 3D SASSI models is limited.

NOTES : 1. UNITS ASSUMED IN: METERS
2. NUMBER OF NODES   = 4716
3. NUMBER OF SOLID ELEMENTS = 3740
4. NUMBER OF BEAM ELEMENTS = 739
5. DIMENSION IN THE THIRD DIRECTION = 0.00
6. NODE 1 IS LOCATED AT TOP OF LEFT BOUNDARY

QUEST STRUCTURES

FLUSHQ Ver 1.01, Apr. 2000

GEOMETRY : LOCK SSI ANALYSIS EXAMPLE

FILE : lock01.def
DATE : 06/13/2000
TIME : 11:04:08

Figure 4-8. Q-FLUSH Two-dimensional Soil-Pile-Structure-Interaction Model of Olmsted Lock Chamber Monolith

d. Fluid-structure interaction. A hydraulic structure and water interact through hydrodynamic pressures at the structure-water interface. In the case of concrete dams, the hydrodynamic pressures are affected by the energy loss at the reservoir boundary. The complete formulation of the fluid-structure interaction produces frequency-dependent terms that can be interpreted as an added force, an added mass, and an added damping (Chopra 1987). The added hydrodynamic mass influences the structure response by lengthening the period of vibration, which in turn changes the response spectrum ordinate and thus the earthquake forces. The added hydrodynamic damping arises from the radiation of pressure waves and, for dams, also from the refraction or absorption of pressure waves at the reservoir bottom. The added damping reduces the amplitude of the struct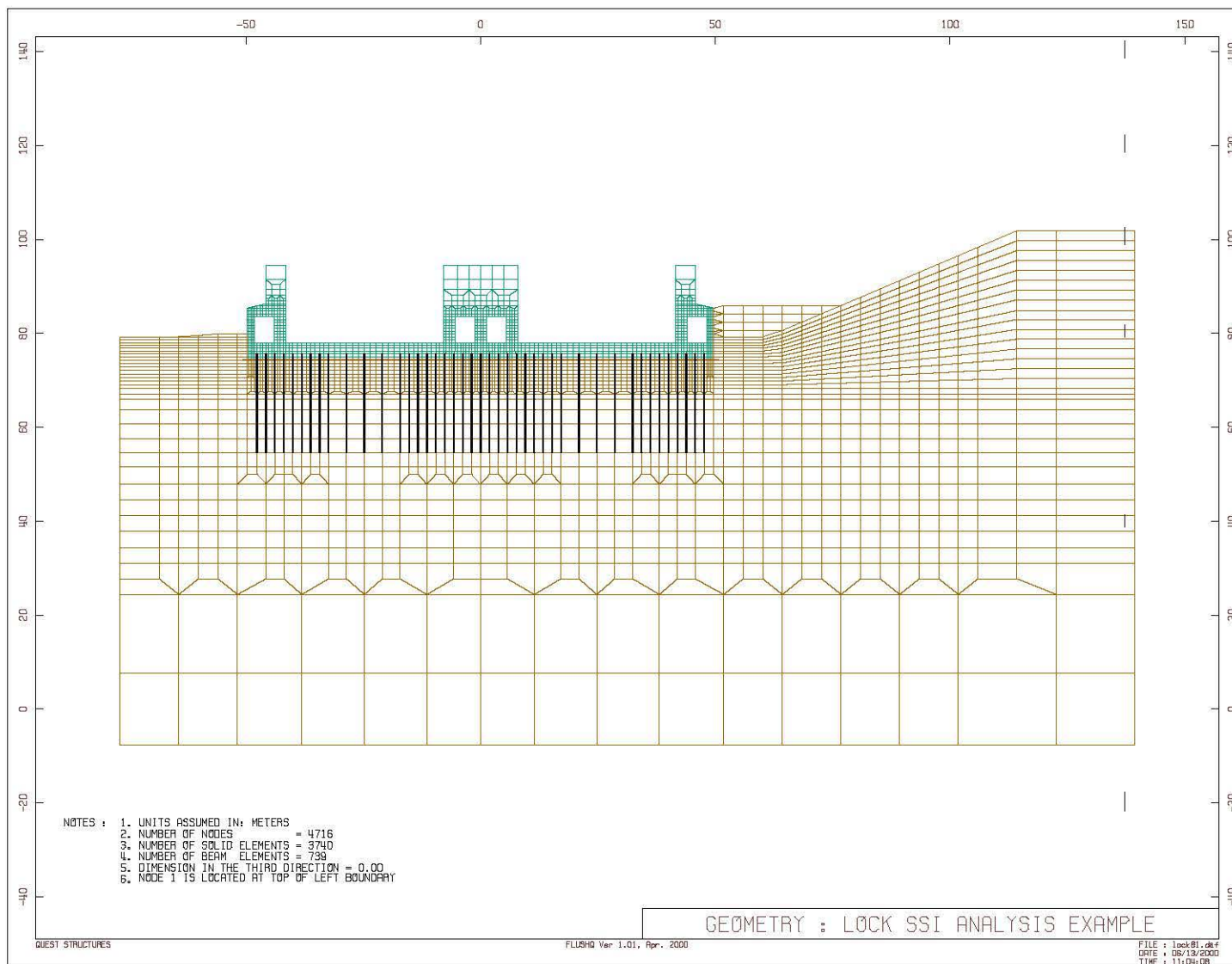ure response especially at the higher modes. Hydrodynamic effects for concrete hydraulic structures including dams, locks, and intake towers are fully described in EM 1110-2-6051. If the water is assumed incompressible, hydrodynamic effects are simply represented by added mass coefficients. Depending on the level of sophistication needed the added hydrodynamic mass may be computed using Westergaard, velocity potential, or finite-element procedures (EM 1110-2-6051). For high dams refined dam-water interaction analysis including water compressibility and reservoir-boundary absorption effects may be required (Hall and Chopra 1980; Fenves and Chopra 1984b; Fok and Chopra 1985.

e. Backfill-structure interaction effects. The interaction between the structure and backfill, and structure and surrounding water, as stated above, can be approximated using added mass concepts. It should be realized however, these interactions are complex and in some cases it may be necessary to use analytical methods, which deal with the interaction effects directly. Also important is the interaction between the structure and foundation. This interaction too is complex. In general, the effect of the foundation is to lengthen the fundamental period of the structure-foundation system, and to increase energy absorption due to energy radiation and material damping that occurs in the foundation material.

4-4. Effective Stiffness

When analyzing concrete hydraulic structures for static loads, it is generally acceptable to use stiffness values associated with the un-cracked section properties and to ignore the stiffening contribution of reinforcing steel. However, under seismic loads it is important that distribution of stresses and member forces be based on stiffness values that are representative of the near yield /cracking conditions. This is because the effective stiffness of CHS at near yield/cracking conditions can be significantly less than that represented by gross section properties. For reinforced concrete structures, the effective stiffness should be used in dynamic analyses to ensure that the hierarchy of member yielding conforms to assumed distributions, and that member plastic deformations are reasonably distributed through the structure. A reasonable estimate of the member stiffness is also required in computation of the structure period and hence seismic forces and displacements.

a. Plain concrete structures. Under severe earthquake ground shaking, it is probable that the elastic capacity of plain concrete structures such as gravity and arch dams would be exceeded, indicating some cracking with possible reduction in global stiffness of the structure. If cracking occurs near surfaces of these massive structures it will have minimal effects on the overall stiffness of the structure. Consequently in linear elastic analysis it is acceptable to use stiffness properties associated with the un-cracked sections. However, if cracking is pervasive and significant, its extent should be estimated and mapped so the stability of the cracked structure can be evaluated. Ideally, the evaluation should be conducted using nonlinear analyses if appropriate tools and procedures are available. Otherwise several approximate equivalent-linear analyses may be attempted, each with reduced stiffness and resistance

characteristics assigned to all finite-elements that have reached their tensile capacities. Such approximate analyses however are valid for static loading condition and not for the earthquake loading which is oscillatory. The stiffness modification and analysis of the modified structure are repeated until no further cracking would occur or the structure reaches a limit state indicating failure. Approximate equivalent-linear analyses must be carried out based on a rational interpretation of the results and sound engineering. The loss or reduction of stiffness should be applied in the direction perpendicular to the cracks. For each element the amount of stiffness reduction should be estimated approximately proportional to the area covered by cracks.

   b. Reinforced concrete structures. To obtain a best estimate of force and displacement demands the stiffness of cracked members (effective stiffness) should be used rather than the gross stiffness. The effective stiffness used is an average value for the entire member accounting for the distribution of cracking along the member length. The effective stiffness of reinforced concrete structures can be estimated based on the relationship between the cracking moment (i.e., the moment required to initiate cracking while ignoring the reinforcing steel) and the nominal moment capacity of the reinforced concrete section. The nominal moments and cracking moments are estimated at regions of the maximum positive or negative moments. Once the cracking moment (M_{CR}) and the nominal moment capacity (M_N) have been determined, the ratio of the effective stiffness (I_E) to the gross stiffness (I_G) can be estimated from:

$$\frac{I_E}{I_G} = 0.8 - 0.9\left[\frac{M_N}{M_{CR}} - 1\right] \tag{4-4}$$

The ratio of I_E / I_G should neither be greater than 0.8, nor less than 0.35 for walls reinforced with 40-grade steel, nor less than 0.25 for walls reinforced with 60-grade steel (EM 1110-2-2400). The nominal moment strength can be determined in accordance with standard ACI-318 procedures. The cracking moment (M_{CR}) can be determined from the following expression.

$$M_{CR} = \frac{I_G}{C}\left(\frac{P}{A_G} + f_r\right) \tag{4-5}$$

Where:

$\quad f_r$ = Modulus of Rupture $\quad = \quad 0.62\sqrt{f_c'} \quad\quad$ (MPa units)

$\quad\quad\quad\quad\quad\quad\quad\quad\quad\quad\quad = \left\{7.5\sqrt{f_c'}\right\} \quad\quad$ (psi units)

$\quad P$ = Axial Load

$\quad A_G$ = Gross Section Area

$\quad C$ = Distance from neutral axis to extreme fiber

4-5. Damping

   a. An effective damping of 5-percent of the critical provides a reasonable estimate of the dynamic response of concrete hydraulic structures at or near yield and cracking. However, damping could be as low as 2 to 3 percent for loads far below the yielding and cracking and higher than 5 percent if the structure is showing energy dissipation through joint opening, tension cracking, and yielding. In situations where such nonlinear responses could develop, a damping value as high as 10 percent can be justified in performing linear response analyses.

However, after increasing the damping to 10 percent, if the structure is still showing further nonlinear behavior, then a nonlinear response analysis should be performed.

b. Dynamic interaction between the structure and foundation could increase the effective damping if the subsurface condition suggests potential energy dissipation through radiation and the foundation deforms far enough to offer energy loss through hysteretic behavior. In addition dynamic interaction between the structure and impounded, surrounding, or retained water can also increase the effective damping due to energy radiation and absorption at fluid boundaries. Unless such interaction effects are significant, the damping value should be limited to 5-percent. Higher effective damping values between 5 to 10 percent could be justified if interaction effects of the foundation and impounded are significant but have not explicitly been included in the analysis.

4-6. Interaction with Backfill Soil

a. General. In addition to the foundation and water interaction effects discussed in Section 4.3*,* the soil behind the lock and retaining walls also affects earthquake response of the wall. During an earthquake, a lock wall is subjected to dynamic soil pressures caused by motions of the ground and the wall. Depending on the magnitude of wall movements the backfill soil is said to be in yielding, nonyielding, or intermediate state. Accordingly, the available methods of design and analysis of the backfill soil pressures also fall into similar categories.

b. Dynamic pressures of yielding backfill. Yielding backfill condition means wall movements due to earthquake ground motions are sufficient to fully mobilize shear resistance along the backfill wedge creating limit state conditions. The dynamic earth forces will then be proportional to the mass in the failure wedge times the ground accelerations. When designing retaining walls with yielding backfill conditions for earthquake ground motions, the Mononobe-Okabe (Mononobe and Matuo 1929; Okabe 1924) approach and its several variations are often used. Procedures for determining the failure wedge and dynamic soil pressure effects for active, at-rest and passive conditions are described in the US Army Technical Report No. ITL-92-11, "The Seismic Design of Waterfront Retaining Structures", (Ebeling and Morrison, 1992). The resulting dynamic pressures expressed in terms of equivalent added-mass coefficients are then added to the nodal masses of the wall in the dynamic analysis of the wall system as described in Section 4.3 above.

c. Dynamic pressures of non-yielding backfill. For massive structures with soil backfill, it is unlikely that movements sufficient to develop backfill yielding will occur during an earthquake. In this situation the backfill soil is said to be nonyielding and is treated as an elastic material. If idealized as a semi-infinite uniform soil layer, the dynamic soil pressures and associated forces for a nonyielding backfill can be estimated using a constant-parameter SDOF model (Veletsos and Younan 1994)) or a more elaborate MDOF system (Wolf 1995). The dynamic soil pressures for a more general nonyielding backfill soil can be determined by the finite-element procedure similar to that discussed in Paragraph 4-3*c*(4).

d. Intermediate case. The intermediate case in which the backfill soil undergoes nonlinear deformations can be represented by the finite element procedures using a soil-structure-interaction computer program such as QFLUSH. Figure 4-8 is an example of this approach where the lock structure, pile foundation, and the backfill soil are included in the model. The foundation and backfill soil are represented using plane-strain 2-D soil elements whose shear modulus and damping vary with level of shearing strains, and the nonlinear behavior is approximated by the equivalent linear method.

4-7. Permanent Sliding Displacement

a. Retaining walls and dams that are stable under static loading conditions may slide under severe earthquake ground motions, if the combined static plus seismic shear demands exceed sliding resistance along any potential sliding planes. The acceleration that generates sufficient force to initiate sliding is termed the critical acceleration (a_c). Every time the ground acceleration exceeds the critical acceleration the structure will slide. The ratio of the critical acceleration to the acceleration of gravity (a_c/g), is termed the yield coefficient (k_y). The ratio of the peak ground acceleration (a_m) to the acceleration of gravity (a_m/g), is termed the seismic coefficient (*A*). The expected permanent displacement of a retaining wall or dam treated as a rigid block can be estimated using the Newmark sliding block analogy (Newmark, 1965).

b. As shown in Figure 4-9, each time the ground acceleration exceeds the critical acceleration (a_c), some displacement at the structure-foundation interface will occur, and these will add up throughout the ground shaking and result in a final sliding permanent displacement. The total permanent sliding displacement will be a function of the earthquake characteristics such as duration and intensity, with the major factor being the number of times the critical acceleration is exceeded. As a part of extensive parametric studies, Richards and Elms have suggested the following equation for estimating permanent displacement, (Richards and Elms, 1977).

$$\Delta = 0.087 \frac{v_g^2}{Ag} \left[\frac{k_y}{A} \right]^{-4} \tag{4-8}$$

Where:
v_g = The peak ground velocity of the earthquake.

For preliminary design purposes the peak ground acceleration can be assumed equal to:

$v_g = 0.30A$ (distance in inches)

$v_g = 0.75\ A$ (distance in meters)

The relationship described above then can be simplified to:

$$\Delta = 0.2 \frac{A^5}{k_y^4} \quad \text{(inches)} \tag{4-9a}$$

$$\Delta = 5 \frac{A^5}{k_y^4} \quad \text{(mm)} \tag{4-9b}$$

A plot of the above relationship is shown in Figure 4-10. This plot can be used as a preliminary evaluation tool for estimating permanent displacement in retaining walls and dams. Additional information relative to the sliding displacement of dams can be found in Zhang and Chopra (1991).

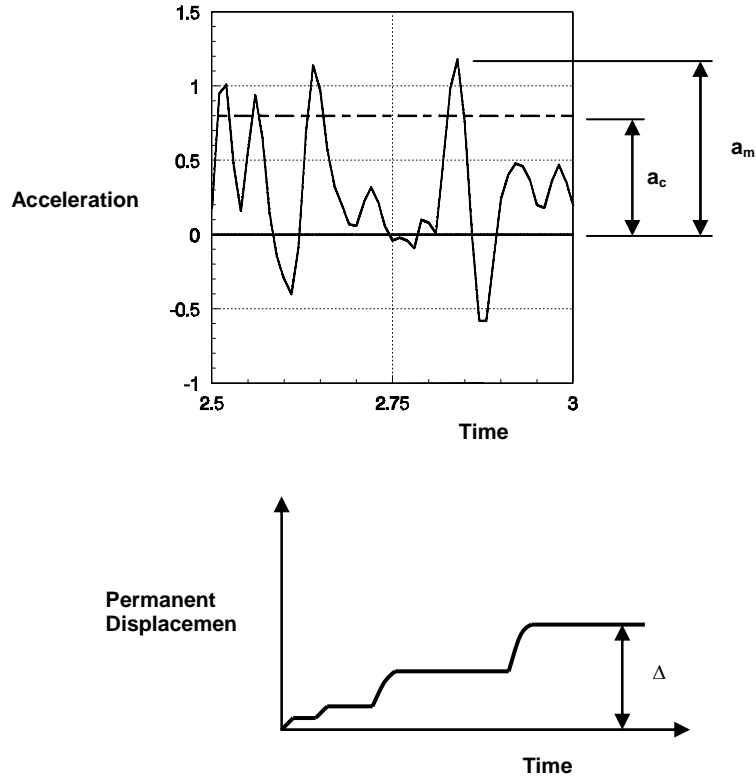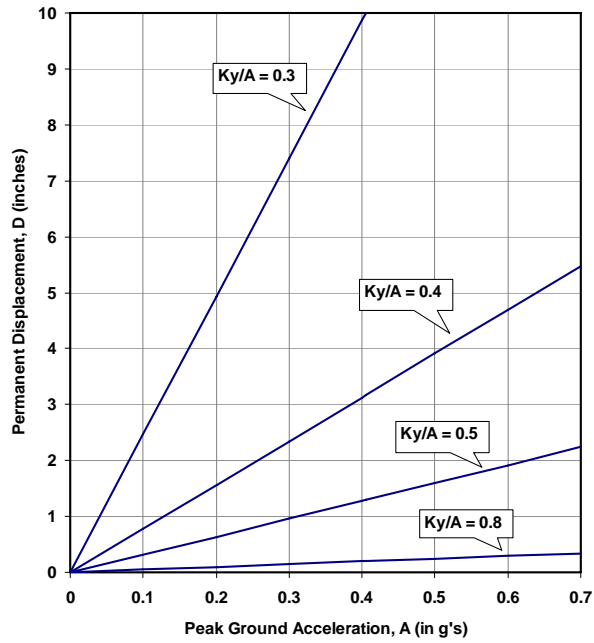**Figure 4-9. Permanent Sliding Displacement**

Figure 4-10. Permanent Displacement as a Function of k_y and A

4-8. Mandatory Requirements

Seismic evaluation of CHS should follow the progressive analysis methodology described in this chapter.

Chapter 5
Concrete Properties and Capacities

5-1. Plain Concrete Structures

a. General. The concrete properties important in the seismic design and evaluation of concrete dams are the unit weight, compressive, tensile, and shear strengths, modulus of elasticity, and Poisson's ratio. Properties of mass concrete at high rate of loading are higher than those under static loading conditions. Therefore, concrete properties used in the seismic analysis should reflect the effects of high deformation rates and cyclic loading response that the dam would experience under earthquake shaking. In general, the performance of a dam under earthquake loading is controlled by the tensile strength of the concrete, and by tensile crack propagation. However, the actual tensile strength used in performance evaluation of the dam should be determined by taking into account the effects of lift joints. The actual tensile strength across the poorly constructed lift joints of some older dams could be markedly lower than that for the homogeneous concrete. Thus it is important that such weaknesses in the mass concrete are accounted for in the seismic safety evaluation, and that the actual reduced strength at lift joints is determined by material testing. The properties of concrete for the final design and evaluation should also be determined by testing.

b. Testing. A comprehensive laboratory testing program is required to obtain the design mixture proportions for concrete strength and workability, to obtain the material properties important to structural analysis and thermal studies, and to validate in-place concrete strengths of both the parent concrete and lift joints. A measure of tensile strength of the concrete can be obtained from direct tension, modulus of rupture, or splitting tension tests. The direct tension tests of concrete are seldom carried out due to difficulties associated with the specimen holding devices. The modulus of rupture test is not favored for existing structures because of its beam specimen requirement. The most commonly used test for estimating the tensile strength of the concrete is the ASTM 496 splitting tension test, which uses a cylindrical specimen. Relationships between the tensile strength obtained from splitting tensile tests and direct tensile strength, for both conventional concrete and RCC, are given in EM 1110-2-2200.

c. Concrete Coring and Specimen Parameters. A concrete coring program to obtain test specimens should start with a random coring or non-destructive tests to establish the overall quality and uniformity of concrete, and to locate problem areas in existing structures. Once potential areas have been discovered, coring can concentrate in these areas to better define properties. While average values of strength and elastic modulus of the concrete are of some value for structural analysis, coring and testing should focus on "weak links" since these problem areas are more likely to govern performance of the structure, than the average properties. Another important factor in establishing the concrete properties is that sufficient number of specimens are taken and tested so that the uncertainty in the estimated parameter values are reduced to an acceptable level. The number of tests needed to establish the concrete properties depends on statistical considerations and cost. While for few tests (say less than 5), adding an additional test results in significant reduction in the uncertainty, for many tests, the reduction obtained by using an additional test is small. So the engineer must answer the question: "Is the additional precision obtained by using another test worth the additional expense?" As a general guideline the minimum number of tests for a specific parameter is about six, while more than nine tests would probably not be economical.

d. Dynamic Properties. Strength and elastic properties are strain rate sensitive. In the absence of test data, the following relationships between static and dynamic properties may be assumed (Bruhwiler, 1990):

(1) The dynamic modulus is equal to 1.15 times the static modulus.

(2) The dynamic Poisson's Ratio is equal to 0.70 times the static ratio.

(3) The dynamic compressive strength is equal to 1.15 times the static compressive strength.

(4) The dynamic tensile strength is equal to 1.50 times the static tensile strength.

(5) The dynamic shear strength is equal to 1.10 times the static shear strength.

e. Capacity (strength). The ultimate tensile strength of the parent concrete (concrete without joints) obtained from static load testing must be adjusted to account for lower strength at construction joints and strain rate effects. It is not reasonable to expect the bonding at construction joints to be equal to that of the parent concrete. The tensile strength of conventional mass concrete joints cleaned by high pressure water jet is approximately 70-percent of the tensile strength of the parent concrete (WES, 1973). This relationship is also applicable to roller compacted concrete (RCC) when lift joints are properly cleaned and covered with a mortar bedding (EP 1110-2-12). However, test results at some exiting dams show that tensile strengths of deteriorated or poorly construction joints could be more than 50% lower than that of the parent concrete. Raphael (Raphael, 1984) discusses the effects of dynamic loading (high strain rates) on the tensile strength of concrete, and the effect of nonlinear strain at failure on the results of linear elastic finite element analysis. According to Raphael, the static tensile strength of the concrete should be increased by a factor of 1.50 to obtain the dynamic tensile strength. As discussed in Chapter 6, a DCR allowable value equal to this ratio will be used for evaluation of the linear-elastic response-spectrum analysis. However, for the linear-elastic time-history analysis the ratio of the apparent dynamic tensile strength to the static tensile strength in conjunction with other parameters will be used for evaluation of the performance. Beyond yield levels apparent tensile stresses are higher than the actual tensile stresses. According to Raphael, the apparent dynamic tensile strength of the concrete is twice the static tensile strength.

5-2. Reinforced Concrete Structures

a. General. Earthquake related catastrophic failures have occurred in major civil works structures, reinforced concrete building and bridge structures. As a result structural codes have been revised dramatically in the past 20-years. Many of the earthquake related deficiencies in buildings and bridges designed by older codes also exist in most USACE structures. These deficiencies however should be examined with respect to the unique characteristics of major civil works structures. The major differences between major civil works structures and buildings / bridge type structures are that:

(1) Major civil works structures are lightly reinforced with reinforcement percentages generally less than 0.5-percent

(2) Major civil works structures have low axial load ratios

(3) Major civil works structures because of large cross-sectional dimensions have large shear capacities

(4) In major civil works structures the concrete protection (cover) and reinforcing bar spacing exceeds that found in bridge and building type structures

(5) Major civil works structures are generally of massive wall-slab construction rather than beam-column construction

b. Compressive strains in CHS. In most major civil works structures the compressive strains in the concrete are low and earthquake demands are usually not sufficient to cause a shear failure. Bond deterioration under cyclic loading only occurs if the maximum compressive strain at the location of reinforcing bar splices reaches levels where longitudinal micro-cracking develops. When compressive strains are below 0.2-percent (0.002) the chance for micro-cracking and bond deterioration that could lead to reinforcing steel splice failure is low. When compressive strains are below 0.4-percent the chance for concrete spalling is low. This means that in most civil works structures spalling would not occur, and that the disastrous consequences of spalling, such as the loss of concrete cover, the loss of confinement reinforcement, and the buckling of reinforcing steel would be unlikely.

c. Potential modes of failure. Performance requirements for reinforced concrete structures are met if all brittle modes of failure (all failure modes other than flexure) are suppressed. Brittle modes of failure include shear (diagonal tension), sliding shear (shear-friction) and fracture of flexural reinforcing steel. Inelastic flexural response will limit shear demands. Therefore, it is only necessary to provide shear strength equal to or greater than the shear demand associated with the maximum flexural strength. Fracturing of reinforcing steel is unique to lightly reinforced concrete members and will occur when strains in the reinforcing steel exceed 5-percent. This mode of failure can be prevented by limiting the displacement ductility capacity of members to that which will produce reinforcing steel strains less than 5-percent. Reinforcing steel used to resist flexural demands must also have splice and anchorage lengths sufficient to develop the maximum bar strength including strain hardening effects. The capacity of reinforced concrete members can be determined using the procedures described below. The capacity of members available to resist brittle modes of failure is discussed first. Brittle modes of failure are considered to be force-controlled actions (FEMA 273, 1997). For force-controlled actions, the capacity (nominal or ultimate strength) of the member at the deformation level associated with maximum flexural ductility demand must be greater than the force demands caused by earthquake, dead, and live loads (as represented by Equations 2-1 and 2-2). The flexural mode of failure is considered to be a displacement-controlled action. In a displacement-controlled action moment demands can exceed moment capacities, however, the displacement capacity of members must be greater than the inelastic displacement demands placed on the structure due to earthquake, dead, and live loads. The flexural displacement capacity will usually be limited either by the compressive strain in the concrete (a maximum of 0.02 % if bond deterioration is to be prevented), or by the tensile strain in the reinforcing steel (a maximum of 5% if fracture of the reinforcing steel is to be prevented). Another important potential mode of failure relates to piles supporting a navigation lock. As indicated in Example D2, performance of the lock structure is governed by yielding of the piles. In this particular example yielding should be limited to less than 10 percent of piles.

d. Shear (diagonal tension)

(1) General. Since shear failure is a brittle failure, it is necessary to inhibit shear failure by ensuring that shear strength exceeds the shear demand corresponding to that associated with

the maximum feasible flexural strength. Shear strength in plastic hinge regions is a function of the flexural displacement demand. As plastic-hinge rotations increase, shear cracks widen, and the capacity of the concrete to transfer shear by aggregate interlock decreases, as illustrated in Figure 5-2.

(2) Shear capacity. In order to meet damage control performance requirements for MDE loadings, the capacity of the reinforced concrete hydraulic structures in shear shall be equal to or greater than the lesser of:

- The full elastic demand placed on the member by the design earthquake, or

- The shear corresponding to 1.5 times the shear associated with the nominal flexural strength.

The capacity of the concrete in shear may be considered as the summation of shear due to aggregate interlock and the shear strength enhancement as the result of axial load (V_C), and to a lesser extent due to the shear resistance available from the transverse reinforcing (traditional truss mechanism), V_S. The total ultimate shear strength (V_U) can be expressed as:

$$V_U = \phi(V_C + V_S) = 0.85(V_C + V_S)$$
(5-1)

The concrete component of shear strength is given by:

$$V_C = 2\left[k + \frac{P}{2000A_g}\right]\sqrt{f_c'}(A_e)$$ (psi units)   (5-2)

$$V_C = 0.17\left[k + \frac{P}{2000A_g}\right]\sqrt{f_c'}(A_e)$$ (MPa units)

where,

$P =$ Axial load on section

$f_c' =$ Actual concrete compressive strength (The actual concrete compressive strength, which may be as high, or higher than 1.5 times the design compressive strength, should be used when calculating the shear capacity.)

$A_g =$ Gross concrete area

$A_e =$ 0.8(A_g)

In Equation 5-2, k = 1 for flexural displacement ductility demand μ = 1, and k = 0.5 for μ = 2.0, with linear interpolation between these values for μ greater than 1.0 but less than 2.0. The relationship between concrete shear strength and flexural displacement ductility is illustrated in Figure 5-1.

For rectangular sections the contribution of shear steel to the total shear capacity is:

$$V_S = \frac{A_h(f_y)(0.8d)}{s}$$
(5-3)

Where d is the section dimension in the direction of the seismic shear forces, f_y is yield strength of steel, s is spacing of reinforcement, A_h is the reinforcement cross section area, and V_S is the contribution from the shear reinforcement.

For circular sections the contribution of the shear reinforcement is given by:

$$V_S = \frac{\pi A_h (f_y)(0.8d)}{2s} \qquad (5\text{-}4)$$

$$2\left[1.0 + \frac{P}{2000 A_g}\right]\sqrt{f_c'}(A_e) \qquad \text{(psi units)}$$

$$0.17\left[1.0 + \frac{P}{2000 A_g}\right]\sqrt{f_c'}(A_e) \qquad \text{(Mpa units)}$$

$$2\left[0.5 + \frac{P}{2000 A_g}\right]\sqrt{f_c'}(A_e) \qquad \text{(psi units)}$$

$$0.17\left[0.5 + \frac{P}{2000 A_g}\right]\sqrt{f_c'}(A_e) \qquad \text{(MPa units)}$$

Concrete Shear Strength (V_c)

Flexural Displacement Ductility Demand (μ)
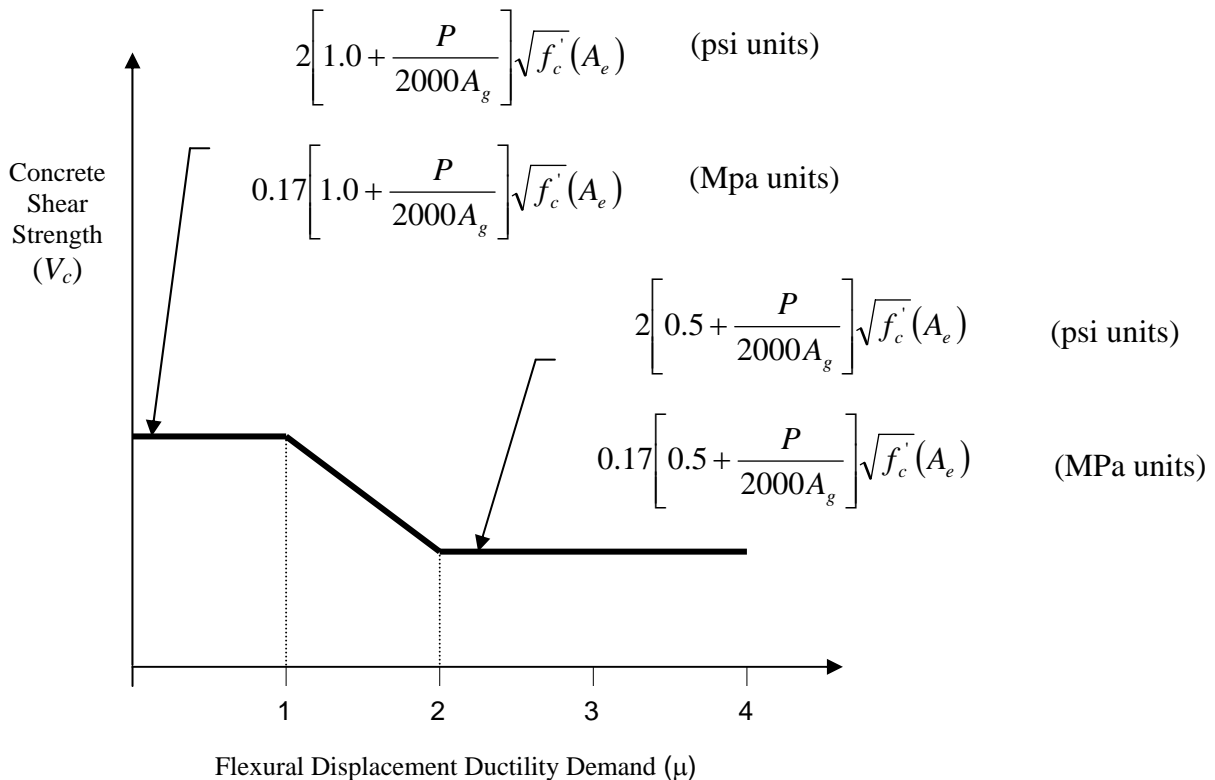
Figure 5-1. Concrete Shear Strength vs. Ductility

e. Sliding Shear. Sliding shear (shear friction) along the base of a structure or structural member should also be investigated. The shear friction shear capacity (V_{SF}) can be determined by the following expression:

$$V_{SF} = \mu_{SF} \ (P + 0.25 \ A_s \ f_y) \qquad (5\text{-}5)$$

Where:

μ_{SF} = sliding shear coefficient of friction, per ACI 318.

P = Axial load on section.

A_s = Area of the longitudinal reinforcing steel across the potential failure plane.

f_y = yield strength of the reinforcing steel.

f. Reinforcing Steel Anchorage. The flexural strength of a structure will deteriorate during a major earthquake if the vertical reinforcement provided for bending is not adequately anchored. For straight bars, the anchorage length provided (l_a) should be greater than:

$$l_a = \frac{f_y(d_b)}{13.8} \quad \text{mm} \qquad \text{(MPa units)} \qquad\qquad (5\text{-}6)$$

$$l_a = \frac{f_y(d_b)}{2000} \quad \text{inches} \qquad \text{(psi units)}$$

Where:

f_y = yield strength of reinforcing steel

d_b = diameter of reinforcing steel

g. Reinforcing Steel Splices.

(1) The lap splice length provided should not be less than:

$$l_s = \frac{A_b f_y}{0.94\sqrt{f'_{ca}}(c+d_b)} \qquad \text{mm} \quad \text{(Mpa units)} \qquad (5\text{-}7)$$

$$l_s = \frac{A_b f_y}{11.31\sqrt{f'_{ca}}(c+d_b)} \qquad \text{inches (psi units)}$$

Where:

f'_{ca} = Actual concrete compressive strength

c = the lesser of the clear cover over the reinforcing bars, or half the clear spacing between adjacent bars

A_b = Area of reinforcing bars

For existing structures, the actual compressive strength rather than the design compressive strength should be used when evaluating splice lengths and anchorages.

(2) Deterioration of bond and splice strengths of reinforcing bars is one of the major problems in the design of earthquake-resistant reinforced concrete structures. Transverse reinforcement provides the best protection against splice strength degradation. For new structures, adequate transverse reinforcing steel should be provided at all splice locations where concrete compressive strains are expected to exceed 0.002 in. /in. Perimeter transverse confinement reinforcement using smaller bars at close spacings is better than using larger bars

at wide spacings. However, close spacing of transverse reinforcement may not leave enough room for concrete placement. In situations like this, a design modification may be in order. Splice performance will be greatly improved if splices are located away from regions where yielding is expected to occur, and if lap splice locations are staggered (i.e., no more than half of the bars spliced at any horizontal plane). This is usually the case, but if yielding occurs near splicing, transverse reinforcement should be provided giving due consideration to concrete placement.

h. Fracture of reinforcing steel. Fracture of reinforcing steel can be prevented if enough flexural reinforcing steel is provided to produce a nominal moment strength equal to, or greater than, the 1.2 times the cracking moment capacity of the section. Existing massive concrete structures rarely meet this requirement. Even for new designs, the cost to provide this amount of flexural reinforcement may be prohibitive, but could be justified if seismic loading controls the design. Existing structures can be considered to meet MCE damage control performance requirements, if it can be demonstrated that brittle modes of failure will not occur. Alternatively, a displacement-based evaluation (Paragraph 5-3) can be performed to show that reinforcing steel strains are below 5-percent.

i. Flexure. The nominal moment strength of reinforced concrete members can be determined in accordance with EM 1110-2-2104 requirements. The nominal strength is the capacity to be used in determining demand to capacity ratios (DCR's) for the linear static and linear dynamic analysis methods described in Chapter 6. When DCR's exceed allowable values (see Chapter 6), a displacement-based evaluation can be performed to assess the inelastic flexural response of the structure (Paragraph 5-3).

5-3. Reinforced Concrete Displacement Capacities

When DCR values exceed allowable limits, the inelastic response of the structure is considered to be significant and should be assessed using a displacement-based analysis. The purpose of a displacement analysis is to ensure that flexural displacement capacities (elastic plus inelastic) are greater than flexural displacement demands of the earthquake ground shaking. Displacement-based analysis refers to either a nonlinear static pushover analysis described in Chapter 6, or an equivalent linear dynamic analysis procedure described in EM 1110-2-2400 for intake towers. In pushover analysis, a pushover or capacity curve is developed that shows structure displacement capacities at various stages of inelastic response. In the EM 1110-2-2400 displacement-based analysis, the earthquake displacement demands are computed by a response-spectrum analysis in which an effective stiffness is utilized for the plastic region at the base of the tower. The estimated displacement demand is then compared with the ultimate displacement capacity of the tower. The ultimate displacement capacity is related to the height, the length of plastic hinge, and the fracture strain of the reinforcement. The fracture or ultimate strain of the reinforcement is obtained over a standard 8-in gage length, and on the average can be taken as 18-percent.

5-4. Mandatory Requirements

a. Plain concrete structures.

(1) The tensile capacity of the concrete used in evaluation shall be representative of the concrete at construction joints.

(2) The tensile capacity values used in final design or evaluation shall be based on test results.

b. Reinforced concrete structures.

(1) Flexural capacity used in seismic design and evaluation shall be the nominal moment capacity determined in accordance with EM 1110-2-2104.

(2) Shear capacity shall be determined in accordance with Equation 5-1 with the shear contribution from the concrete (aggregate interlock) determined using Equation 5-2.

Chapter 6
Analysis Procedures and Evaluation of Results

6-1. Introduction

Four procedures are presented for the seismic evaluation of concrete hydraulic structures (CHS). They include: linear static, linear dynamic, nonlinear static, and nonlinear dynamic analyses. The linear static and linear dynamic analyses are commonly used in the design and evaluation of CHS. However, the use of nonlinear analysis in evaluation of existing structures under damaging earthquakes and in design of new structures with potential nonlinear response is gaining recognition. For existing structure, application of nonlinear analysis can eliminate unnecessary remediation and for new structures it can substantiate and verify the design. With respect to earthquake loadings, concrete hydraulic structures are designed and evaluated for both the Operational Basis Earthquake (OBE) and the Maximum Design Earthquake (MDE) earthquake loads in combination with the usual dead and live loads that occur during normal operating conditions. The seismic analysis may start with a seismic coefficient method or equivalent lateral force analysis (linear static procedures) and progress to a linear-elastic response-spectrum or linear-elastic time-history analysis (linear dynamic procedure). In some instances a nonlinear static or nonlinear dynamic analysis may be performed to assess the actual capacity or the level of damage that a structure may experience. The linear static and linear dynamic procedures are described in Paragraph 6-3, the nonlinear static procure in Section 6.5, and the nonlinear dynamic procedure in Paragraph 6-6.

6-2. Seismic Design and Evaluation Using DCR Approach

a. General. A demand to capacity comparison, utilizing a demand to capacity ratio (DCR) as a performance indicator, establishes the basis for performance evaluation of plain and reinforced concrete structures subjected to earthquake ground motions. For reinforced concrete structure, DCR is defined as the ratio of force or moment demand to force or moment capacity. For plain concrete structure, DCR is defined as the ratio of stress demands to static tensile strength of the concrete. Maximum permissible values of the DCR are established to assure serviceability and damage control performance objectives are met. The DCR approach is used in conjunction with linear analysis procedures to evaluate:

(1) Damage control performance for deformation-controlled actions (flexure) under Maximum Design Earthquake (MDE) loading conditions.

(2) Damage control performance for force-controlled actions (shear) under Maximum Design Earthquake (MDE) loading conditions.

(3) Serviceability performance for displacement-controlled actions (flexure) under Operational Basis Earthquake (OBE) loading conditions.

(4) Serviceability performance for force-controlled (shear) actions under Operational Basis Earthquake (OBE) loading conditions.

b. Flexural performance for MDE. In the linear procedures, a linear-elastic model of the structure is subjected to lateral forces of the design earthquake to determine displacements, stresses, and forces developed in the model. If the structure responds nonlinearly, as is often the case for MDE loading conditions, the lateral displacements and corresponding internal forces (or stresses) will exceed yield values. The degree to which the calculated internal forces

exceed flexural strength (or tensile stress capacity) is used as a measure of the extent of nonlinear deformations that develop in the member. The acceptance criteria for deformation-controlled actions, as expressed by Equation 6-1, are based on this concept. In Equation 6-1, the moment demands for damage control performance as represented by Equation 2-1 may exceed nominal moment capacity, i.e. the demand to capacity ratio (DCR) can be greater than one. For flexural demands associated with the MDE, the DCR allowable value in Equation 6-1 provides a measure of the displacement ductility capacity required of the member to meet damage control performance objectives. The DRC allowable values for damage control performance in flexure are listed in Table 6-1. These are based on the yield and performance characteristics of the concrete and reinforcing steel.

c. Shear performance for MDE. Shear failures are to be suppressed because they are brittle failures that involve rapid strength deterioration. Therefore under MDE loading conditions the shear demand should not exceed the shear capacity of the structure, or the shear DCR should be less than or equal to one. The allowable DCR values for damage control performance in shear are listed in Table 6-1.

d. Flexural performance for OBE. To keep yielding in flexure to levels that will not impair serviceability, the DCR should be equal to or less than one. The allowable DCR values for serviceability performance in flexure are set in Table 6-1.

e. Shear performance for OBE. The DCR for shear should be less than one to assure shear strength deterioration will not occur at levels of shear demand equal to, or slightly greater than, the OBE. The allowable DCR values for serviceability performance in shear are given in Table 6-1.

6-3. Linear Static and Linear Dynamic Procedures

a. General evaluation process. Concrete hydraulic structures must be designed and evaluated for unusual and extreme earthquake ground motion conditions represented by the OBE and MDE, respectively. It is not usually economical or practical to design new CHS to remain elastic during the MDE, nor can it be expected that existing CHS will respond elastically to an MDE event. In the linear static procedure, the inertia forces of the OBE and MDE are estimated by either the seismic-coefficient method or the equivalent lateral force (ELF) method. In the linear dynamic procedure, the seismic forces are determined by either a linear-elastic response-spectrum analysis or a linear-elastic time-history analysis. Information on the seismic coefficient method, the equivalent lateral force method, response-spectrum analysis, and time-history analysis can be found in Chapter 4.

b. Evaluation process for plain concrete structures. Plain concrete structures, such as dams, are usually evaluated for earthquakes using either a linear-elastic response-spectrum analysis, or a linear-elastic time-history analysis. A finite-element model (FEM) is used to represent the structure and its interaction with the foundation and water (Paragraph 4-3*a*(3) and (4)), and the results are output in the form of concrete stresses with tensile stresses as the primary quantity of interest. The peak tensile stresses obtained from the FEM analysis are those the structure would experience if it remained elastic. Evaluation is accomplished by comparison of elastic earthquake demands (tensile stress demands) to tensile capacity of the concrete. On the basis of linear-elastic analysis, performance is considered acceptable if the resulting demand to capacity ratios are less than the allowable values listed in Table 6-1 and that for the linear-elastic time-history analysis spatial extent and duration of high stresses also meet the

specific criteria set forth for each type of structure in Paragraphs 6-3*d*(2), 6.3*e*(2)*, and 6.3f*(2) below.

c. Evaluation process for reinforced concrete structures. Reinforced concrete structures, such as intake towers, navigation locks, and spillway piers, are commonly evaluated for earthquake ground motion effects using a linear-elastic response-spectrum analysis. Linear-elastic time-history modal analysis is also used to evaluate post-yield response with respect to cumulative duration of moment excursions exceeding the moment capacity as well as the spatial extent of yield region. Depending on the complexity of its geometry, an intake tower may be evaluated using an FEM model with frame or solid elements (Paragraph 4-3*a*(2) and (4)). A lock structure is usually evaluated by a 2D or 3D FEM using solid elements (Paragraph 4-3*a*(3), (4), and (5)) and by frame elements to perform pushover analysis (Paragraph 4-3*a*(2)). The results for FEM models with frame elements are output as forces (moments, shears, and axial load) rather than stresses. Force quantities facilitate the evaluation because they can be compared directly to capacity (nominal strength) of reinforced concrete members. Such comparison will show which part of the structure and to what extent, if any, will experience nonlinear behavior in the form of yielding of reinforcing steels and cracking of the concrete. For this purpose demand-capacity ratios for the bending moments, axial, and shear forces should be computed and compared with the allowable values in Table 6-1. The section force demands should also be compared with the axial force-bending moment interaction diagrams to account for the axial force-bending moment interaction effects. The results for FEM models using solid elements are output as element stresses, which must be converted into forces and moments at critical sections and then compared with section capacities. The evaluation should investigate all potential modes of failure (Paragraph 5-2*c*). Brittle failure mechanisms include shear failure, reinforcing steel anchorage failure, and reinforcing steel splice failure (Paragraphs 5-2*d* to *g*), for which the structure should respond elastically. Flexural failures (Paragraph 5-2*h*) are generally considered to be ductile failures. Performance is considered acceptable provided all brittle modes of failure are suppressed and demand to capacity ratios are less than the allowable values listed in Table 6-1.

d. Evaluation process for gravity dams. Gravity dams subjected to OBE ground motions should perform within the linear-elastic range to assure that very little or no tensile cracking will occur. Under MDE ground motion demands, gravity dams may respond in the inelastic range provided that the performance is within the strain hardening range (i.e. damage control range in Figure 2-5). Stresses in excess of the ultimate tensile stress capacity are assumed to initiate and propagate cracking. The results of the time-history analysis can be used to assess the damage potential of stress excursions that exceed the tensile capacity of the concrete and the effects that cracking might have on the performance of the dam.

(1) Response-Spectrum Analysis. A linear-elastic response-spectrum analysis is generally the first step in the evaluation process (Paragraph 4-2*c*). The earthquake demands in terms of stresses are computed and compared with the stress capacity of the concrete to assess whether the resulting DCR ratios are lower than allowable values listed in Table 6-1b. In cases where tensile stress demands exceed the allowable tensile capacity of the concrete (DCR's exceed acceptable limits), a linear-elastic time history analysis is generally performed.

(2) Linear Time-History Analysis. Linear time history analysis of gravity dams should be conducted and evaluated in accordance with procedures discussed in Paragraph 6-4*d*(1). A systematic interpretation and evaluation of the results of time-history analysis in terms of the demand-capacity ratios, cumulative inelastic duration, spatial extent of overstressed regions,

and consideration of possible modes of failure form the basis for estimation of probable level of damage or acceptable level of nonlinear response.

e. Evaluation process for arch dams. (From EM 1110-2-2201) The earthquake response analysis of arch dams is generally based on the linear-elastic dynamic analysis using finite-element procedures. It is assumed that the concrete dam and the interaction mechanisms with the foundation rock and impounded water exhibit linear-elastic behavior. Using this method, the arch dam and foundation rock are treated as 3-D systems. The analysis is performed using the response-spectrum modal superposition or time history method. The earthquake performance is evaluated using the numerical results obtained from such analyses. The results of linear analysis provide a satisfactory estimate of the dynamic response to low or moderate intensity OBE earthquake motions for which the deformations of the dam are within the linear-elastic range. In this case, the performance evaluation is based on DCR allowable values listed in Table 6-1b. Under MDE ground motions, it is possible that the calculated stresses would exceed the allowable values, and that some damage would occur. In such extreme cases, the dam may suffer significant damage but should retain the impounded water without rupture. Evaluation for the MDE should start with the DCR approach and progress to the linear time-history analysis and possibly to nonlinear time history analysis, as needed.

(1) Response-spectrum Analysis. The response-spectrum method of analysis (EM 1110-2-6050, EM110-2-2201) uses a response-spectrum representation of the seismic input motions to compute the maximum response of an arch dam to earthquake loads. Three orthogonal components of response spectra are used as the seismic input. This method provides an efficient procedure for the preliminary analyses of new and existing arch dams. It may also be used for the final analyses, if the calculated stress values meet the DCR allowable values listed in Table 6-1b. Otherwise, linear time-history analysis, and if needed, nonlinear time-history analysis should be considered. Using the response-spectrum procedure, the maximum response of the dam is obtained by combining the maximum responses for several modes of vibration computed separately.

(2) Linear Time-History Analysis. Linear time-history analysis of arch dams is conducted and evaluated in accordance with procedures and load combinations described in EM 1110-2-6051. It involves a systematic interpretation and evaluation of the results of time-history analysis in terms of the demand-capacity ratios, cumulative inelastic duration, and spatial extent of overstressed regions as described in Paragraph 6-4*d*(2).

f. Evaluation process for intake towers. Earthquake loadings generally govern the design of intake towers. Performance is considered acceptable if all brittle modes of failure are suppressed, and demand to capacity ratios are less than the allowable values listed in Table 6-1. The DCR requirements for flexure limit the ductility demand to levels acceptable for lightly reinforced structures. The DCR requirements for brittle modes of failure will suppress shear and sliding shear failures. Shear capacity for computation of DCR should be selected consistent with the level of displacement ductility demand associated with the peak flexural response (see Figure 5-3).

(1) Response-spectrum Analysis. The response-spectrum analysis of intake towers is carried out in accordance with EM 1110-2-2400 and EM 1110-2-6050. A model of the tower is developed as described in Paragraph 4-3 and is subjected to one horizontal and the vertical (2D model) or two horizontal and the vertical (3D model) components of response spectra. Section forces and moments are computed and combined in accordance with Paragraph 3-2, and compared with section capacities and axial force-bending moment diagram following the

procedure described in Paragraph 6-3*c*. In cases where force demand capacity ratios exceed the allowable values listed in Table 6-1a, a linear-elastic time history analysis may be performed to assess the level of damage.

(2) Linear Time-History Analysis. The damage for lightly reinforced freestanding intake towers is evaluated on the basis of demand-capacity ratios (DCR) and cumulative inelastic duration described in Paragraph 6-4*c*(2).

g. Evaluation process for navigation locks. The earthquake performance of reinforced concrete navigation locks is evaluated on the basis of demand-capacity ratios computed for the foundation piles when they are present) and the concrete sections in accordance with EM 1110-2-6051. The computation of earthquake demands starts with linear-elastic analysis using response-spectrum and/or time-history method.

(1) Response-spectrum analysis. Lock structures founded on rock with no backfill soil can adequately be analyzed using the response-spectrum modal superposition method, as described in EM 1110-2-6050. The performance is evaluated by computing and comparing force and moment DCRs with the allowable values listed in Table 6-1a. The total force and moment demands are obtained for the combined effects of static plus earthquake loads. The section shear capacity is determined according to Paragraph 5-2*d*(2). The section moment capacities are obtained from the axial force-bending moment interaction diagrams characterizing the strength of a reinforced concrete section.

(2) Time-history analysis. Locks founded on soil or pile foundation and with backfill soil may require SSI time-history analysis, as described in 4.3*c*. The earthquake performance of the lock is evaluated on the basis of demand-capacity ratios computed for the foundation piles and the concrete sections in accordance with EM 1110-2-6051. If all computed demand-capacity ratios are less than or equal to 1.0, then the lock structure and piles are expected to respond elastically with no damage. Otherwise demand-capacity ratios of greater than 1.0 show the structure will experience nonlinear behavior in the form of yielding of steel members and cracking or crushing of the concrete. The acceptability of the level of damage and nonlinear behavior will be determined on the basis of performance curves provided in EM 1110-2-6051. Performance of the pile-foundation under is evaluated using interaction factors or demand-capacity ratios computed in accordance with Equation 6-6. For the OBE excitation, the piles should respond within the linear elastic range of behavior. Under the MDE excitation, the piles interaction factor, I_p, should generally be less than or equal to 1. However, for severe and damaging earthquakes the pile interaction factor could approach 1.1 for less than 10 percent of the piles, provided that nonlinear pushover analysis is conducted to ensure that permanent later displacements of the pile foundation, if any, is small.

6-4. Acceptance Criteria for Linear Procedures

a. ELF and response-spectrum analysis. The earthquake load effects calculated in accordance with Chapter 4 combined with the effects of dead and live loads as specified in Equations 2-1 and 2-2 are used to calculate total demands on the structure. The expected capacity or strength of the structure is determined in accordance with Chapter 5, and demand to capacity ratios (DCRs) are calculated for each structural component of interest and for each potential failure mechanism (Flexure, shear, etc.). The seismic performance of the structure is considered acceptable if the DCR for each component and potential failure mechanism is less than or equal to the *allowable value* for that particular component and failure mechanism.

DCR ≤ *Allowable Value* (6-1)

The DCRs allowable values for concrete hydraulic structures are provided in Table 6-1. In some cases the forces obtained from the linear-elastic analysis are not sufficient to displace the structure to the maximum inelastic displacements expected in response to the design earthquake ground motions. This could occur in the case of an equal energy response (Paragraph 3-3*a*(2)). Therefore, for the flexural response when earthquake moment demands exceed nominal moment capacity, the moment demands from the ELF, or response spectrum analysis must be multiplied by a C_1 factor, where:

C_1 = Modification factor to relate expected maximum inelastic displacements to displacements obtained from the linear-elastic response

The C_1 factor is based on the FEMA 273 formulation for C_1, with the term SR in Equation 6-2 representing R in the FEMA formulation. Studies (Whittaker et al., 1998) suggest that for strength ratios (nominal flexural strength to moment demand) of 0.5 the use of the FEMA C_1 factor will produce inelastic displacements that are representative of mean elastic displacements obtained from linear elastic analyses. This however is not true for strength ratios lower than 0.5 where the inelastic displacements can substantially exceed the C_1 adjusted mean elastic displacements. The strength ratios for hydraulic structures are generally in the 0.5 range, and therefore the FEMA 273 formulation for C_1 is considered to be appropriate.

For an equal displacement response (or for $T \geq T_0$), $C_1 = 1.0$.

For an equal energy response (or for $T \leq T_0$):

$$C_1 = \left[1.0 + (SR-1)\frac{T_0}{T}\right]\left(\frac{1}{SR}\right) \leq 1.5 \qquad (6\text{-}2)$$

Where:

$$SR = \frac{M_D}{M_N} \qquad (6\text{-}3)$$

M_D = Elastic moment demand from linear analysis

M_N = Nominal moment capacity

Table 6-1a
DCR *Allowable Values* for Reinforced Concrete Hydraulic Structures

Action	Performance Objectives	
In terms of forces	Damage Control (MDE)	Serviceability (OBE)
Flexure	2.0	1.0
Shear	1.0	0.8
Sliding Shear	1.0	0.8

Table 6-1b
DCR Allowable Values for Response-Spectrum Analysis of Plain Concrete Hydraulic Structures

Action	Performance Objectives	
In terms of stresses	Damage Control (MDE)	Serviceability (OBE)
Tension due to flexure	1.5	1.0
Diagonal tension due to shear	0.9	0.8
Shear due to sliding	1.0	0.8

Table 6-1a is based on the assumptions that:

1. Concrete hydraulic structures are lightly reinforced

2. Beams, slabs, walls and other load carrying members are controlled by flexure

3. The members are non-conforming meaning they do not meet confinement steel and other seismic detailing requirements of ACI 318

4. Wall and other vertical load carrying members have axial load ratios $\dfrac{P}{A_g f_c'}$ less than 0.1

5. DCR *allowable values* for conditions other than those described above can be selected from Tables 6-10 and 6-11 of FEMA 273

   (1) Illustrating the use of Table 6-1a for flexure. For damage control requirements, DCR allowable values for the flexural response in a reinforced concrete structure must be less or equal to 2. This means that the ratio of the elastic moment demand (modified by C_1) to the nominal moment capacity, must be less than or equal to 2:

$$\frac{M_{DC}(C_1)}{M_N} \le 2.0 \qquad (6\text{-}4)$$

Where:

M_{DC} = Total moment demand (See Equation 2-1) obtained from a linear-elastic response spectrum or time history analysis.

C_1 = Modification factor to relate maximum inelastic displacements to displacements obtained from linear elastic response (see EQ 6-2)

M_N = Nominal moment capacity.

(2) Illustrating the use of Table 6-1b for flexure. For damage control requirements, DCR allowable values for the flexural response in a plain concrete structure must be less than 1.5. This means that the ratio of the flexural tensile stress demand from the linear-elastic response-spectrum analysis to the splitting static tensile stress capacity, must be equal to, or less than 1.5, or:

$$\frac{\sigma_{ta(DC)}}{f_t^s} \leq 1.5 \qquad\qquad (6\text{-}5)$$

Where:

$\sigma_{ta(DC)}$ = Total tensile stress demand (See Equation 2-1) obtained from a linear-elastic response- spectrum analysis for MDE ground motions

f_t^s = Static tensile strength (see Chapter 5)

In other words, Equation 6-5 is the same as requiring the tensile stress demand obtained from a linear elastic FEM analysis to be equal to or less than the dynamic tensile strength.

b. Pile interaction factors (demand-capacity ratios). Performance of the pile-foundation under the MDE loading combination is evaluated using interaction factors or demand-capacity ratios computed in accordance with Equation 4-1.

$$I_p = \left(\frac{f_a}{F_a} + \frac{m_x}{M_x} + \frac{m_y}{My}\right)_{static} + \left(\frac{f_a}{F_a} + \frac{m_x}{M_x} + \frac{m_y}{M_y}\right)_{dynamic} \qquad (6\text{-}6)$$

Where:

I_p = pile interaction factor
f_a, m_x, m_y = the axial force and bending moments (force and moment demands) computed either from the static or dynamic analysis
F_a = allowable axial force (force capacity) for combining with allowable moment (moment capacity)
M_x, M_y = allowable moments (moment capacities), respectively, about the strong and weak axes of the pile

c. Time history analyses – reinforced concrete structures

(1) FEMA 273 approach. In Table 6-1a, the DCR allowable values for flexure are based on the assumption that the structure has the capacity to resist three fully reversed deformation cycles at the deformation levels represented by the allowable values, in addition to similar cycles at lesser deformation levels. When time history analyses are used to verify performance acceptability, the evaluations shall be relative to acceptable moment demand levels represented by the DCR allowable values. The acceptable moment demand level is equal to (*DCR Allowable Value/ C₁*) times M_N, which is illustrated as being 850 ft-kips in Figure 6-1. The moment

demand response as represented by Figure 6-1 suggests that there are five cycles above the acceptable moment demand level (850 ft-kips), indicating the structure may not perform to expectations. With a longer duration earthquake of similar magnitude the performance would surely be unacceptable. Short period structures subjected to long duration earthquakes are particularly vulnerable to numerous cycles at the deformation levels represented by the DCR allowable values. In some cases, the energy contained in each cycle may not be sufficient to impair strength. In other cases, the increased number of cycles can lead to reductions in force and deformation capacity. The effects on strength and deformation capacity of more numerous cycles beyond what is considered the ductility capacity of the structure should be considered. In those cases where the number of cycles, beyond what is considered to be acceptable moment demand levels exceed three, the cumulative duration approach as described in EM 1110-2-6051 should be used.
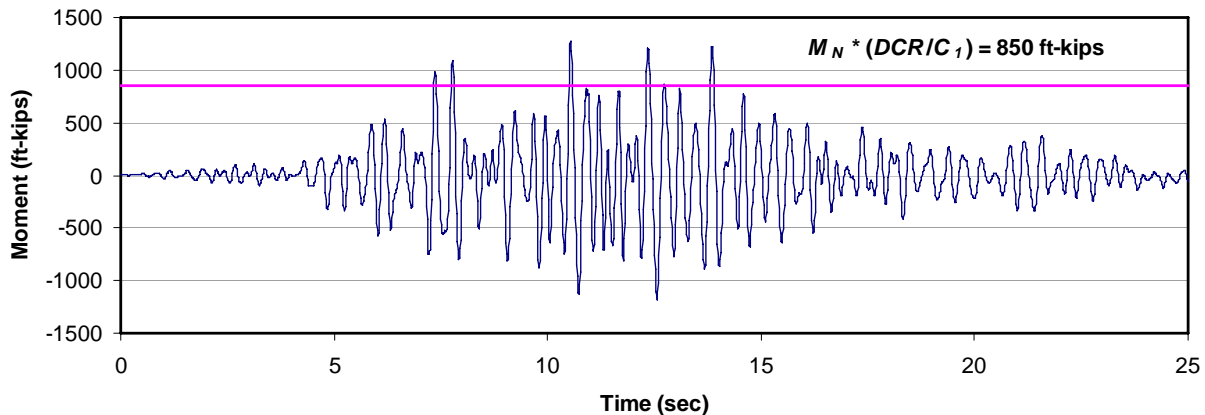
Figure 6-1. Moment Time History Evaluation

(2) EM 1110-2-6051 cumulative duration approach. The acceptance criteria for linear-elastic time-history evaluation of lightly reinforced freestanding intake towers is assessed on the basis of demand-capacity ratios (DCR) and cumulative duration, as described in EM 1110-2-6051. The basic procedure is to perform linear time-history analysis with appropriate amount of damping to obtain bending moment DCR ratios for all finite elements. Initially a damping ratio of 5 percent is used and then increased to 7 percent if DCR ratios are approaching 2 and to 10 percent if they exceed 2. After adjustment for the damping, the damage is considered moderate and acceptable if the following conditions are met:

- Bending moment DCR ratios computed on the basis of linear time-history analysis remain less than 2

- Cumulative duration of bending-moment excursions above DCR ratios of 1 to 2 fall below the acceptance curve given in Figure 6-2

- The extent of yielding along the height of tower (i.e., plastic hinge length for DCR ratios of 1 to 2) is limited and falls below the acceptance curve.

If DCR ratios exceed 2.0 or the cumulative duration and the yield lengths rise above the acceptance curves, the damage is considered to be severe and should be assessed using nonlinear analysis procedures. The term cumulative inelastic duration is defined as the total time of bending-moment excursions above a particular capacity corresponding to DCR ratios of

1 to 2. The yield height ratio refers to the yielded length of tower normalized with respect to the tower height. To keep the damage to a moderate level, the yield length should be less than one-third of the tower height, as shown in Figure 6-2.
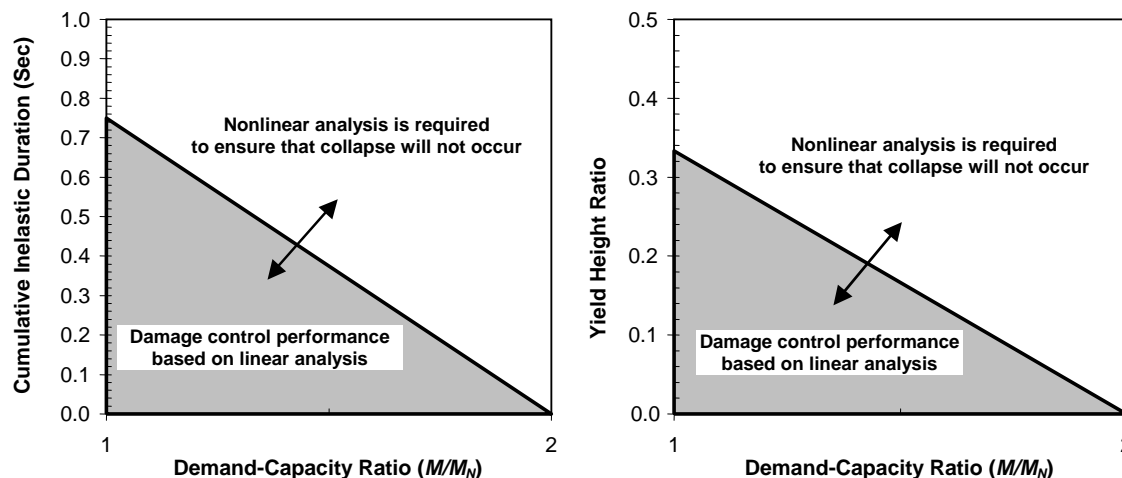

Figure 6-2. Acceptance Criteria for Freestanding Intake Towers

d. Time history analyses – plain concrete structures

(1) Concrete gravity dams. The acceptance criteria for linear-elastic time-history analysis of gravity dams is based on DCRs and cumulative inelastic duration described in EM 1110-2-6051. DCR for plain concrete structures are computed as the ratio of stress demands to static tensile strength of the concrete. A systematic interpretation and evaluation of the results of time history analysis in terms of the demand-capacity ratios, cumulative inelastic duration, spatial extent of overstressed regions, and consideration of possible modes of failure form the basis for estimation of probable level of damage or acceptable level of nonlinear response. The dam response to the MDE is considered to be within the linear-elastic range of behavior with little or no possibility of damage if the computed stress demand-capacity ratios are less than or equal to 1.0. The dam would exhibit nonlinear response in the form of cracking of the concrete and/or opening of construction joints if the estimated stress demand-capacity ratios exceed 1.0. The level of nonlinear response or cracking is considered acceptable if demand-capacity ratios are less than 2.0 and limited to 15 percent of the dam cross-sectional surface area, and the cumulative duration of stress excursions beyond the tensile strength of the concrete falls below the performance curve given in Figure 6-3. Consideration should also be given to relation between the fundamental period of the dam and peak of the earthquake response spectra. If lengthening of the periods of vibration due to nonlinear response behavior causes the periods to move away from the peak of the spectra, then the nonlinear response would reduce seismic loads and improve the situation by reducing stresses below the values obtained from the linear time-history analysis. When these performance conditions are not met, or met only marginally with the nonlinear response increasing the seismic demand, then a nonlinear time-history analysis might be required to estimate the damage more accurately.
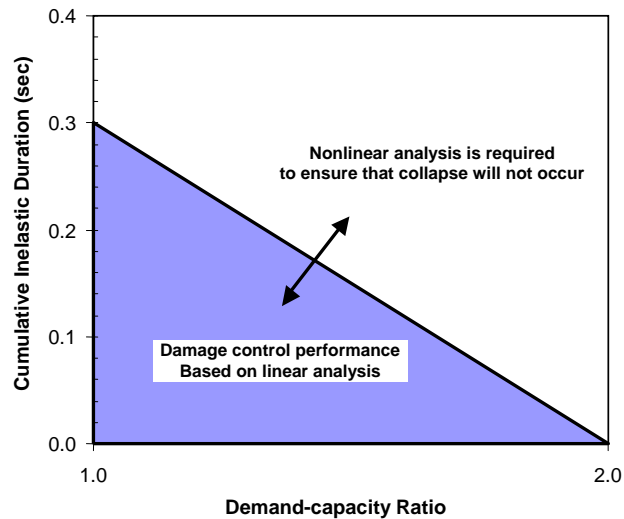
The chart shows Cumulative Inelastic Duration (sec) on the vertical axis ranging from 0.0 to 0.4, and Demand-capacity Ratio on the horizontal axis ranging from 1.0 to 2.0. A line descends from (1.0, 0.3) to (2.0, 0.0). The shaded region below is labeled "Damage control performance Based on linear analysis" and the region above is labeled "Nonlinear analysis is required to ensure that collapse will not occur".

Figure 6-3. Performance Curve for Concrete Gravity Dams

(2) Concrete arch dams. The acceptance criteria for the linear-elastic time-history analysis of arch dams are based on procedures and load combination cases described in EM 1110-2-6051. It involves a systematic interpretation and evaluation of the results of time history analysis in terms of the demand-capacity ratios, cumulative inelastic duration, spatial extent of overstressed regions, and consideration of possible modes of failure that form the basis for estimation of probable level of damage or acceptable level of nonlinear response. The dam response to the MDE is considered to be within the linear elastic range of behavior with little or no possibility of damage if computed demand-capacity ratios are less than or equal to 1.0. Considering that the ability of contraction joints to resist tension is limited, the joints may still open even if demand-capacity ratios are less than or equal to 1.0. The amount of contraction joint opening at a DCR ≤ 1, however, is expected to be small with negligible or no effects on the overall stiffness of the dam. The dam is considered to exhibit nonlinear response in the form of opening and closing of contraction joints and cracking of the horizontal joints (lift lines) if the estimated demand-capacity ratios exceed 1.0. The level of nonlinear response or opening and cracking of joints is considered acceptable if DCR < 2, overstressed region is limited to 20 percent of the dam surface area, and the cumulative inelastic duration falls below the performance curve given in Figure 6-4. The relation between the fundamental period of the dam and peak of the response spectra should also be considered to determine whether the nonlinear response behavior would increase or decrease the seismic demand. If these performance criteria are not met, or met marginally with increasing demand due to nonlinear behavior, then a nonlinear analysis would be required for more accurate estimate of the damage.
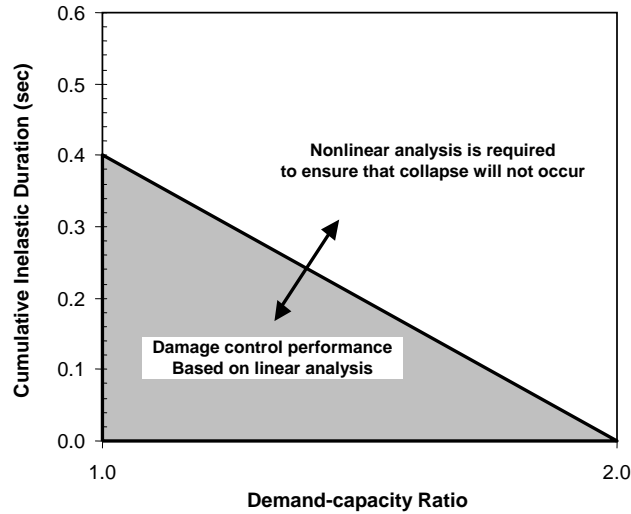
Figure 6-4. Performance Curve for Concrete Arch Dams

6-5. Nonlinear Static Procedures

Two different nonlinear static procedures are available for the evaluation of reinforced concrete structures. They are the displacement ductility evaluation and the pushover analysis. The displacement ductility approach at this time is limited to cantilever type structures as described in Chapter 5. The pushover method is applicable to all types of structures, as long as structural members of the reinforced concrete structure can be represented by frame elements for which nonlinear response behavior has been established.

   a. Displacement ductility evaluation. In displacement ductility evaluation the displacement ductility capacity of the structure is determined as described in Chapter 5. Displacement ductility demands are estimated based on a linear elastic response-spectrum analysis. Since all inelastic action will be due to the flexural response, the elastic moment demand (M_D) and the nominal moment capacity of the section (M_N) are used to determine the displacement ductility demand (μ_D) on the structure. The ductility demand will depend on whether the structure exhibits an equal energy response or an equal displacement response (see Chapter 3). A formulation for displacement ductility demand can be developed using Formula 6-2 based on the following:

   (1) The displacement ductility demand (μ_D) is equal to the displacement demand (δ_D) divided by the displacement at yield (δ_y), or

$$\mu_D = \frac{\delta_D}{\delta_y} \qquad (6\text{-}6)$$

   (2) Since in linear analysis displacements are proportional to forces, Equation (6-6) can be expressed:

$$\mu_D = \frac{M_D(C_1)}{M_N} \qquad (6\text{-}7)$$

(3) Recalling that SR = M_D / M_N (see Equation 6-3), the displacement ductility demand can be calculated using the following equation:

$$\mu_D = \left[\frac{M_D}{M_N} - 1 \right] \frac{T_0}{T} + 1 \qquad (6\text{-}8)$$

This should neither be less than M_D/M_N for equal displacement response, nor greater than 1.5 M_D/M_N for equal energy response. The above formulation provides a smooth transition between the equal energy and equal displacement regions of the response spectrum. The structure is considered to perform acceptably if all modes of brittle failure are suppressed and the displacement ductility capacity exceeds the displacement ductility demand. Shear should be reexamined to make sure the shear capacity has not been reduced to unacceptable levels due to high flexural ductility demand. A pushover analysis is required when it becomes necessary to evaluate collapse prevention performance. Collapse prevention performance could be the performance objective for critical structures where the MDE is equal to the Maximum Credible Earthquake (MCE).

b. Pushover method. For complex structures where plastic hinges can form in several locations, a pushover type analysis (collapse mechanism analysis) should be used to assess the actual performance of the structure. Pushover analysis is a nonlinear static procedure in which the magnitude of loading is increased incrementally according to a predefined pattern. The analysis with increasing loads continues until the structure is displaced to a large enough displacement (target displacement) capable of mobilizing principal nonlinear modes of behavior up to collapse of the structure. The computer model of the structure incorporates inelastic material response, thus allowing for redistribution of forces and deformations as structural members undergo nonlinear response in the form of yielding of reinforcing steel and cracking of the concrete. The pushover analysis is conducted using a load controlled or displacement controlled procedure. Load-controlled procedure involves incremental application of a monotonic load to the structure until the maximum load is reached or the structure collapses, whichever occurs first. Force control should be used when the magnitude of load is known (such as gravity), and the structure is expected to support the load. Displacement-controlled procedure involves incremental application of a monotonic load until the control displacement is reached a pre-specified value or the structure collapses, whichever occurs first. Displacement control is used when the value of applied load is not known in advance, or when the structure is expected to lose strength. Since the final value of earthquake load can not be determined precisely in advance, the displacement-controlled method is usually employed. In addition to the load and displacement-controlled procedures, the capacity spectrum method is also available for seismic evaluation of structures with multiple plastic hinge regions. The capacity spectrum is an approximate nonlinear static procedure that predicts the inelastic displacement demand of the structure by combining structural capacity obtained from a pushover analysis with seismic demand represented by response spectra (ATC-40 and example in Appendix D).

(1) The displacement-controlled approach, also known as the target displacement approach, is the pushover analysis procedure selected in FEMA 356 (2000) for seismic assessment of building structures. The same approach is also applicable to hydraulic structures, as demonstrated in examples in Appendices D and E. In pushover procedure, a series of nonlinear static analyses carried out to develop a capacity or pushover curve for the structure. With increasing the magnitude of loading during the pushover analysis, the structural members undergo nonlinear response, and thus weak links and failure modes of the structure are found. The yield regions are monitored as lateral loads representing inertial forces in an earthquake

are increased until the ultimate rotational capacity is reached, or the structure fails due to instability. The displacement capacity, as represented by rotational failure or by structure instability, is then compared with the earthquake displacement demand to determine if the displacement capacity of the structure is sufficient to prevent failure. The pushover method, using the target displacement approach of FEMA 356, is illustrated by Figure 6-5 and 6-6. Figure 6-5 represents a center wall section of a navigation lock. The structural idealization is shown along with potential yield regions (plastic hinge zones). The pushover loads are distributed as shown, and are proportioned in accordance with the first mode shape. The structure is displaced by increasing the lateral load (keeping the same distribution) until the force demand equals the capacity of the most critical member. Assuming shear modes of failure are suppressed, the most critical member is the one where the nominal moment capacity is reached first. The displacement at the top of the structure is plotted vs. the total lateral load. A plastic hinge element is then inserted in the model. The stiffness of the plastic hinge element is based on its load-rotation characteristics. Generally stiffness equal to 5-percent of the effective section stiffness is used. The new model (model with the plastic hinge) is pushed in a similar manner until the next critical element or elements are located. The load and displacement increment associated with the formation of the new hinge is plotted and the process continues until the rotation of one of the plastic hinges reaches its ultimate rotational capacity, or until instability occurs. The displacement capacity as determined from the capacity curve is compared to the displacement demand (δ_D) to see if performance is satisfactory.

Center Wall Section   Structure Idealization
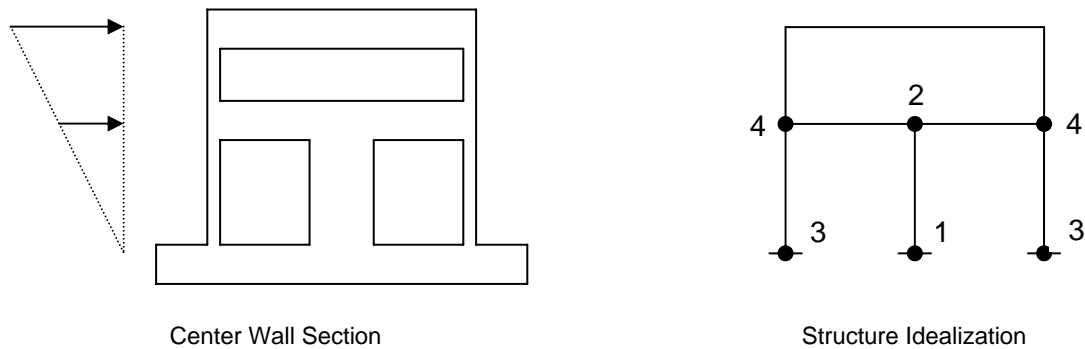
Figure 6-5. Pushover Model for Navigation Lock Center Wall
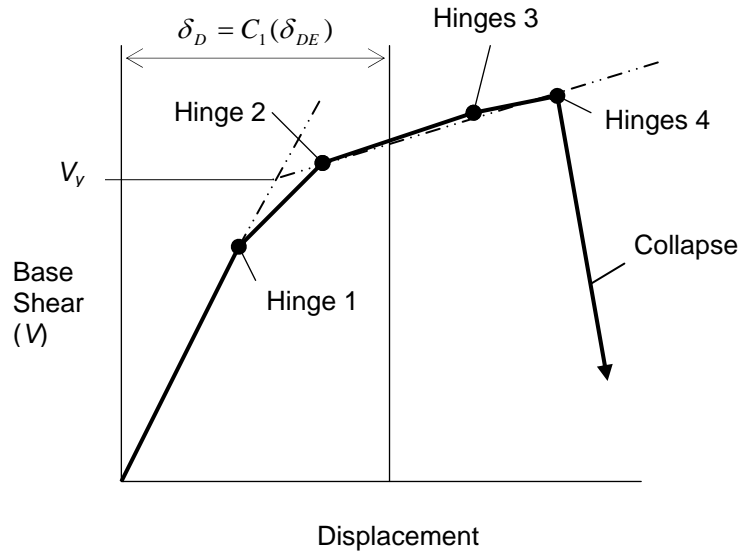
Figure 6-6. Force – Displacement from Pushover Analysis

The displacement demand is determined using the following equation:

$$\delta_D = C_1(\delta_{D1})$$
(6-9)

Where:

δ_{D1} = The first mode displacement demand of the structure. Obtained from linear elastic response-spectrum analysis, or by the following equation:

$$\delta_{D1} = C_0(S_a)\frac{T^2}{4\pi^2}$$
(6-10)

Where:

S_a = Response spectrum acceleration for the first mode of vibration.

T = First mode period of vibration

C_0 = Modification factor to relate spectral displacement to top of structure displacement. Use first mode participation factor, or assume C_0 = 1.5.

C_1 is the modification factor to relate expected maximum inelastic displacements to displacements obtained from the linear elastic response. For an equal displacement response (or for $T \geq T_0$), C_1 = 1.0. For $T \leq T_0$:

$$C_1 = \left[1.0 + (SR-1)\frac{T_0}{T}\right]\left(\frac{1}{SR}\right) \leq 1.5$$
(Repeat of Equation 6-2)

Where:

$$SR = \text{Strength ratio} = C_0 \frac{S_a(m_T)}{V_y} \qquad (6\text{-}11)$$

And where:

$m_T =$ Total Mass (structure mass + added water mass + added soil mass)

$V_y =$ Structure yield strength calculated from the pushover analysis assuming an idealized bilinear load-displacement relationship (see Figure 6-6).

The term $S_a(m_T)$ represents the total shear demand on a single degree of freedom system with a period (T), spectral acceleration (S_a), and mass (m_T). Performance is acceptable if the relationship between the displacement demand and the displacement capacity meets project performance objectives, and provided all brittle modes of failure are suppressed.

6-6. Nonlinear Dynamic Procedure

  a. General. Under nonlinear dynamic analysis procedure, the induced displacements, stresses, and section forces (seismic demands) are obtained from the step-by-step solution of the equations of motion including nonlinear force-displacement relationship. Seismic demands in the form of response histories are computed using ground motion acceleration time histories as the seismic input, and then compared with the structure capacity to determine if the desired performance has been achieved. The nonlinear dynamic analysis for plain concrete structures is carried out using a nonlinear finite-element representation of the structure. Performance is evaluated by investigating the formation and propagation of tensile cracking to determine whether or not the cracking would lead to failure of the structure. The failure mechanisms may involve sliding along the joints and cracked sections, rotational instability, or both. Prediction of crack patterns in mass concrete can be accomplished using fracture mechanics techniques. For crack analysis of 3D structures both linear elastic fracture mechanics (LEFM) and nonlinear fracture mechanics (NLFM) may be considered. These methods are based on various material models that depend on critical values of parameters characterizing the crack-tip stress and strain fields. The application of these methods to concrete structures has somewhat been limited to static loading conditions. Conducting a meaningful non-linear fracture mechanics analysis of a concrete gravity dam is extremely difficult and should be undertaken only under the supervision of experts in the field of fracture mechanics, and with approval by and in consultation with CECW-CE. In the case of concrete hydraulic structures such as dams, the nonlinear behavior mostly involves opening and closing of the vertical joints and tensile cracking along the horizontal lift lines and the dam-foundation interface. These conditions can be identified using the linear-elastic dynamic analysis described earlier and then analyzed for structural stability using nonlinear dynamic procedures described in the following paragraphs. The performance of dams for the MDE is considered satisfactory if the cracks that develop during intense ground shaking have not opened to the extent that significant leakage through the dam can occur, or to the extent that significant permanent irrecoverable displacements within the dam or foundation occur.

b. Gravity dams

(1) While it is possible to model material and other sources of nonlinearity in analysis of gravity dams, the required parameters are either not known or well defined. For this reason the nonlinear dynamic analysis of a gravity dam should focus on capturing the potential failure modes that would have the most impact on the stability of the dam. A typical gravity dam is built as individual monoliths separated by vertical joints, and construction of each monolith involves placement of concrete in lifts that produces horizontal joints whose tensile strength could be less than that of the parent concrete. Consequently, in a major earthquake it is likely that the vertical joints would open and close repeatedly and tensile cracking would occur along the lift lines, at the dam-foundation interface, and at the change of slope in upper part of the dam where stress concentration occurs. The nonlinear performance evaluation of gravity dams therefore starts with a linear-elastic time-history analysis to identify overstressed regions that would experience cracking, followed by nonlinear dynamic analyses incorporating slippage and rotation with respect to opened joints and cracked sections, as well as post-earthquake analyses for static loads and after-shock excitations.

(2) The results of nonlinear analysis will include sliding displacement and rotation demands that must be sufficiently small not to jeopardize safety of the dam during the main event as well as during the after shocks. This means that after the level of damage has been established for the main event, the damaged structure should be tested against the probable aftershock that could be one to two magnitudes smaller than the main shock. In addition, post-earthquake static stability analyses should be carried out so that the ability of the damaged structure to resist the operating loads can be demonstrated.

(3) For example, a linear-elastic dynamic analysis may indicate that the gravity dam shown in Figure 6-7 will experience high tensile stresses at the dam-foundation interface and that the dam does not pass the acceptance criteria set forth in Paragraph 6-4c(2). In subsequent nonlinear dynamic analyses gap-friction elements are introduced at the high tensile-stress region of the base to allow formation and propagation of cracks, which are found to extend through the entire base of the dam. The results may indicate that the dam fully cracked at the base will undergo sliding and rocking leading to a permanent displacement (offset) at the end of the shaking. The magnitude of the permanent sliding displacement is estimated and compared with operational and safety requirements. The performance of dams for the MDE is considered satisfactory if the cracks that develop during intense ground shaking have not opened to the extent that significant leakage through the dam can occur, or to the extent that significant permanent irrecoverable displacements within the dam or foundation occur. Appendix H provides an example of nonlinear time-history analysis and performance evaluation of a non-overflow gravity dam section.
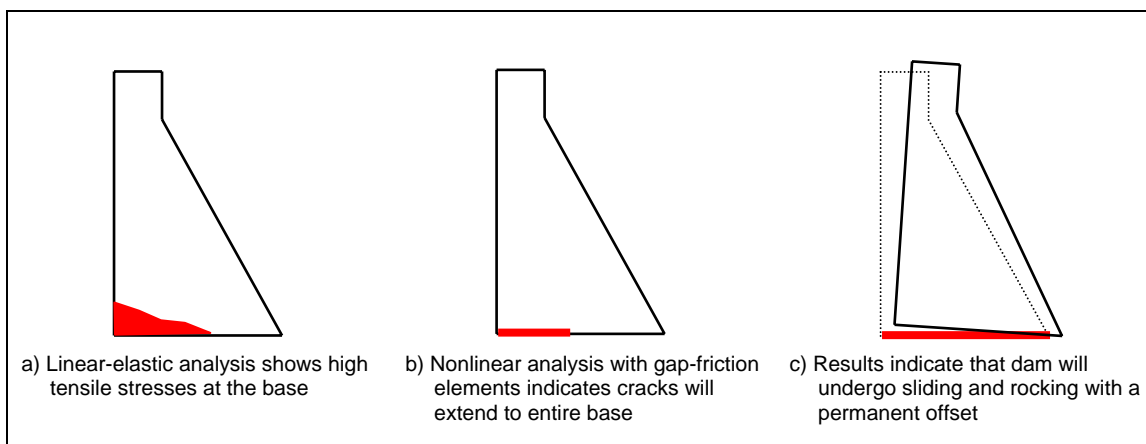
Figure 6-7. Example of sliding and rocking of a typical gravity dam

a) Linear-elastic analysis shows high tensile stresses at the base

b) Nonlinear analysis with gap-friction elements indicates cracks will extend to entire base

c) Results indicate that dam will undergo sliding and rocking with a permanent offset

c. Arch Dams

(1) Arch dams are generally built as independent cantilever monoliths separated by vertical contraction joints. Since contraction joints cannot transfer substantial tensile stresses in the arch direction, the joints can be expected to open and close repeatedly as the dam vibrates in response to severe earthquake ground motions. Construction of arch dams also involves horizontal construction joints known as lifts that may exhibit lower tensile strength than the mass concrete. Consequently opening of contraction joints and cracking of lift joints are the most likely nonlinear mechanisms that could occur in arch dams. Such conditions can be modeled and analyzed using QDAP (Quest Structures, 2001) or other finite-element programs with nonlinear joint capabilities. As in the case of linear analysis the concrete arch and the foundation rock are discretized using standard 3D solid elements, but joints and fractures in the dam, at the dam-foundation interface, or within the foundation are represented by nonlinear 3D joint elements. Therefore the only nonlinear effects considered for the response of the dam are those associated with the opening, closing, and sliding of the along the joints and cracked sections. Since opening of the contraction joint and cracking of the lift joints relieve high tensile stresses, the traditional stress-based criteria will not be applicable to the QDAP results. Instead, under nonlinear dynamic analysis, the magnitude of compressive stresses, the extent of joint opening or cracking, and the amplitude of non-recoverable movements of concrete blocks bounded by failed joints that control the overall stability of the dam should be assessed, as opposed to the magnitude of calculated tensile stresses. Appendix F provides an example of nonlinear time-history analyses conducted to assess the earthquake performance of an arch dam.

(2) The nonlinear dynamic analysis of arch dams should also assess stability of potentially moveable blocks in the abutments if there are adversely jointed rock blocks directly beneath the dam. This problem is best handled as a coupled dynamic problem in which the moveable blocks are modeled as part of the dam finite-element model to allow joint slippage in the abutments and the effects it might have on the stability of the dam. The block joints can be modeled using 3D joint elements discussed above which resist bearing and shear but not tension. The sensitivity of the results to shear strength of the joints and strength degradation with movement and uplift pressures should be investigated.

d. Reinforce Concrete Hydraulic Structures. Similar to static nonlinear analysis, reinforced concrete hydraulic structures such as intake towers and lock structures can be evaluated using nonlinear dynamic analysis. Nonlinear evaluation of reinforced concrete hydraulic structures involves step-by-step solution of equations of motion with nonlinear force-displacement relationship for members exhibiting nonlinear behavior. A nonlinear dynamic analysis of reinforced hydraulic structures may be carried out when the contribution of higher modes are significant. In situation like this, the pushover analysis, which simulates only the effects of the fundamental mode, is not appropriate. The nonlinear dynamic analysis of reinforced concrete hydraulic structures should be attempted when the structure can be idealized by frame elements for which nonlinear behavior is well defined. The structural models for the nonlinear dynamic analysis will be similar to those considered for the pushover analysis (see Examples D1 and D2), except that the seismic input will consist of two or three-component acceleration time histories. Accordingly the results will include displacement, stress, and force demand histories.

6-7. Design vs. Evaluation

Most existing hydraulic structures have been designed for load combinations that considered very little or no provisions for the effects of earthquake ground motions. For these structures, earthquake ground motion effects are often part of an evaluation process rather than the original design process. However, for design of new structures in highly active seismic regions earthquake loads could control the design. In situations like this, the structure must be designed for the effects of seismic loads and performance levels prescribed in Chapter 2. To accomplish this, the structural configurations and dimensions should be adjusted until the desired performance is achieved. In addition to such adjustments the design of reinforced concrete hydraulic structures should also involve practices that ensure ductile behavior while suppressing brittle failure modes. Every attempt should be made to:

    (1) Meet minimum reinforcing steel requirements

    (2) Provide adequate confinement at splice locations

    (3) Provide adequate splice and anchor lengths

    (4) Avoid locating splices in inelastic regions

    (5) Provide direct and continuous load paths

6-8. Minimum Steel Design Requirements for New Reinforced Concrete Hydraulic Structures

For economy reason, structures located in high seismic regions should be designed to perform inelastically for the MDE ground motions. To ensure ductile performance, the flexural steel provided should as a minimum result in nominal moment strength equal to 1.2 times the cracking moment (i.e. $M_N/M_{cr} \geq 1.2$). This will provide displacement ductility greater than that exhibited by existing structures whose nominal moment capacities are less than cracking moment capacities. Structures detailed in accordance with modern seismic detailing practices and designed to have $M_N/M_{cr} \geq 1.2$ will have flexural displacement ductilities greater than those indicated by the DCR allowable values in Table 6-1a. The selection and use of higher DCR allowable values for such structures should be in consultation with CECW-ET. For concrete elements with deep cross-section dimensions, i.e. spillway piers for instance, the amount of reinforcing steel needed to satisfy minimum steel requirements may be excessive. When it is impractical to design for $M_N/M_{cr} \geq 1.2$, sufficient quantities of reinforcing steel should still be provided to ensure nearly elastic performance under the MDE. Meeting minimum reinforcing

requirements ensures that plastic hinge cracking is not limited to a discrete location; rather it is spread out to improve plastic hinge rotational capability and displacement ductility.

6-9. Mandatory Requirements

a. Linear static and linear dynamic evaluations. Tables 6-1a and 6-1b establish maximum permissible demand to capacity ratios (DCR's) for the linear static and linear dynamic evaluations. The use of higher DCR allowable values must be justified on a project by project basis in consultation with CECW-ET.

b. Nonlinear static and nonlinear dynamic evaluations. Nonlinear static and nonlinear dynamic evaluations shall be performed when performance can not be assured by the linear static and linear dynamic evaluations (when DCR's exceed the allowable values). Nonlinear static and nonlinear dynamic evaluations shall also be performed when it becomes necessary to evaluate collapse performance for critical structures where the MDE demands are those of the Maximum Credible Earthquake (MCE).

c. Minimum reinforcing steel requirements. New reinforced concrete structures where the design is controlled by earthquake loadings shall be reinforced as required by Paragraph 6-7.

Chapter 7
Methods to Evaluate the Seismic Stability of Structures

7-1. Introduction

Structures must be evaluated with respect to sliding and rotation to ensure that they remain stable during an earthquake. Sliding stability of CHS under earthquake loading is evaluated using the limit equilibrium method (seismic coefficient) and permanent sliding displacement approaches (EM 1110-2-6050). Rotational stability of CHS under earthquake loading is evaluated using the energy-based formulation and the limit equilibrium method (EM 1110-2-6050). In addition to these methods, a new method based on rocking spectrum is introduced for assessment of rotational stability after a tipping of the structure has been indicated. All of these stability methods assume rigid structural behavior. This assumption is reasonable for most massive hydraulic structures, because the period of a sliding or rocking structure is much longer than the vibration period of the flexural response of the structure. However, the effects of structure flexibility on sliding and rotation could be important for more flexible and less massive structures and should be investigated. The structure flexibility can significantly affect the earthquake demands, which are used to determine whether or not sliding or rotation would take place. Sliding or rocking of a structure during an earthquake may not lead to failure of the structure. For a sliding failure to occur, the sliding displacement of the structure must be of sufficient magnitude to impair lateral load carrying capacity or life safety protection (for example, uncontrolled release of water from a reservoir). For a rotational stability failure to occur, the ground motion energy imparted to the structure after tipping occurs must be sufficient to cause rotational instability, or otherwise impair lateral load carrying capacity and life safety protection. Since bearing pressures can increase significantly as the resultant moves towards the edge of the base during a rotational response to earthquake ground motions, the load carrying capacity of the structure can be impaired due to a foundation bearing failure.

7-2. Rigid Structure vs. Flexible Structure Behavior

While a rigid structure will be subjected to a maximum acceleration equal to the peak ground acceleration (PGA) during earthquake ground shaking, a flexible structure will experience an average acceleration that depends on vibration period of the structure and on characteristics of the earthquake ground motion. This is illustrated by the acceleration response spectrum in Figure 7-1. The figure represents the typical acceleration responses of single-degree-of-freedom (SDOF) systems on a rock or firm soil site. Although most structures are not SDOF, a similar relationship can be assumed for the first-mode acceleration response of multi-degree of vibration systems. From Figure 7-1 it can be seen that only very rigid structures, with vibration period close to zero seconds, can be expected to experience peak accelerations equal to the PGA. For structures with periods between 0.02 seconds and 1 second (the typical range for most concrete hydraulic structures)
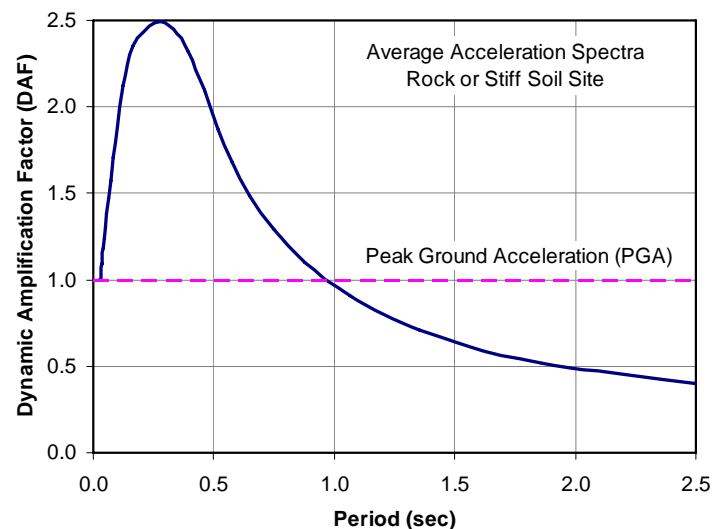
Figure 7-1. Dynamic Amplification Effects

the average structure acceleration will be greater than the PGA, with Dynamic Amplification Factors (DAF) as high as two to three.

7-3. Sliding Stability

a. Seismic coefficient method. In the limit equilibrium or seismic coefficient method, the sliding stability is expressed in terms of a prescribed factor of safety. A seismic coefficient, equal to 2/3 the peak ground acceleration divided by the acceleration of gravity (g), is used by the Corps to evaluate the potential for sliding. This coefficient when multiplied by the effective weight (structure weight + hydrodynamic added weight) provides the total lateral inertial force on the structure due to earthquake ground motions. The total lateral inertial force when added to static lateral forces, if any, provides the total driving force for the sliding stability analysis. The Maximum Design Earthquake (MDE) is considered an extreme load condition requiring a safety factor of 1.1 against sliding failure (Refer to EM 1110-2-2100 for stability requirements). A permanent sliding displacement analysis is required for structures that do not meet the required sliding factor of safety determined by the seismic coefficient method.

b. Permanent sliding displacement approach

(1) Upper bound estimate - rigid behavior. Sliding of a structure on its base will not occur until the total driving force exceeds the resisting force, or in other words when the sliding factor of safety is less than one. The total driving force can be due to static earth pressures, hydrostatic pressures, earthquake inertia forces, and earthquake induced hydrodynamic forces. Hydrodynamic forces are commonly determined by the Westergaard's added hydrodynamic mass (EM 1110-2-6051). The total mass of the system is therefore represented by the sum of the structure mass plus the hydrodynamic added mass. The static component of the driving force can easily be determined. The maximum inertia force for a rigid structure is a product of the total mass times the peak ground acceleration. The peak ground acceleration that will initiate sliding (i.e. when the driving force equals the resisting force) is defined as the critical acceleration. If the critical acceleration is greater than the peak ground acceleration of the design earthquake then the structure will not slide. Conversely, if the critical acceleration is less than the peak ground acceleration the structure will slide. An upper bound estimate of the permanent sliding displacement can be made using Newmark's rigid block analysis procedures (Newmark, 1965) or by methods developed by Richards and Elms (Richards and Elms, 1977). The Newmark procedure has been incorporated into the Corps program CSLIP. Newmark developed rigid block analysis procedures for rigid structures that slide in one direction only (dams, retaining walls, etc.) and for structure, which have the potential to slide equally in both directions (intake towers, lock monoliths, etc.). Newmark's sliding block analysis is demonstrated for a concrete gravity dam in Chopra and Zhang (1991), and the results from the Newmark analysis are compared to those obtained from a response history analysis. The potential for sliding, and the upper bound estimate of permanent sliding displacements can be reasonably determined using a Newmark-type sliding block analysis provided that the foundation sliding resistance is based on a best estimate (mean value) of the foundation shear strength, and that foundation shear strength parameters are adjusted for dynamic loading effects. Although the permanent sliding displacement is to be based on a mean shear strength value, permanent-sliding displacements should also be calculated using upper and lower bound estimates of foundation shear strength parameters.

(2) Upper bound estimate - flexible behavior. An approximate method based on rigid block analysis procedures (Chopra and Zhang, 1991) has been developed to estimate upper bound permanent displacements for flexible behavior. The analysis is similar to that used in the rigid

block analysis except that the sliding potential and estimate of upper bound displacements are based on the average peak structure acceleration rather than the peak ground acceleration. The average peak structure acceleration will generally be larger than the peak ground acceleration (see Figure 7-1) and therefore the upper bound permanent sliding displacement will be larger for a flexible structure than it is for a rigid structure. The average peak acceleration of the structure can be estimated by dividing the total first mode inertial force (base shear) obtained from a linear elastic response spectrum analysis by the total mass. Procedures for estimating average peak structure accelerations for flexible structures are provided in Chopra and Zhang, 1991.

c. Response history analysis procedures

(1) Linear time-history analysis – instantaneous factor of safety. The results of linear-elastic time-history analysis can be used to compute time-history or instantaneous sliding factor of safety along any desired sliding plane(s). The instantaneous factor of safety for the earthquake loading condition is obtained by combining the interface (i.e. sliding plane) force histories due to the earthquake loading with the interface forces due to the static usual loads plus the uplift. At each time step, the static and dynamic nodal forces are combined and then resolved into a resultant force having components normal and tangential to the sliding plane. The resisting forces are obtained from the normal component of the resultant force using the Mohr-Coulomb law, and the driving force is computed from vector summation of tangential components of the resultant force. The time-history of factor of safety is then obtained from the ratio of the resisting to driving forces at each time step. Figure 7-2 is an example of instantaneous factors of safety. The time-history starts at value equal to static factor of safety and then oscillates as the structure responds to the earthquake ground shaking. Under earthquake excitation, the stability is maintained and sliding does not occur if the factor of safety is greater than 1. However, a factor of safety of less than one indicates a transient sliding, which if repeated numerous times, could lead to excessive permanent displacement that could undermine safety of the structure. For example, Figure 7-1 shows that the factor of safety repeatedly falls below one, an indication that sliding of the structure could be expected. The magnitude of sliding displacement and its impact on the stability of the structure need to be evaluated by performing a nonlinear sliding displacement analysis discussed next.
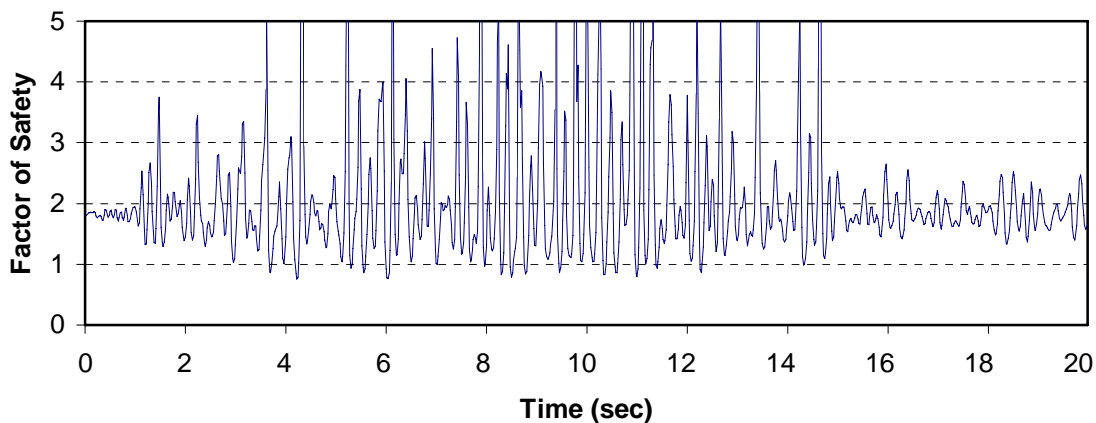
Figure 7-2. Time-history or instantaneous factors of safety

(2) Nonlinear time history analysis -- permanent sliding displacement. In nonlinear time-history analysis, governing equations of motion for the sliding structure are derived with respect to time and solved using step-by-step procedures (Chopra and Zhang 1991, Chavez and Fenves, 1993). A sliding structure is subjected to the ground acceleration plus the acceleration associated with the sliding displacement. If the sliding structure is assumed to be rigid, the governing equations involve dynamic equilibrium of inertia and static forces in the direction of sliding. Sliding is initiated when the acceleration reaches a critical or yield acceleration, i.e. a value at which the driving and resisting forces are equal; and the sliding ends when the sliding velocity becomes zero and the ground acceleration falls below the critical acceleration. If the sliding structure is flexible, two sets of governing equations will represent the sliding phase: 1) equations representing equilibrium of forces for the portion of the structure above the sliding plane, and 2) equations representing equilibrium for the entire sliding structure including all forces acting on the sliding plane. The structure's total permanent sliding displacement is then obtained by step-by-step solution of these coupled sets of equations. Alternatively, the nonlinear sliding behavior can be estimated using gap-friction elements along the sliding plane followed by a direct step-by-step integration of the equations of motion to obtain the total permanent sliding displacement.

7-4. Rotational Stability

a. General. A structure will tip about one edge of its base when earthquake plus static overturning moment (M_o) exceed the structure restoring moment capacity (M_r), or when the resultant of all forces falls outside the base. Depending on the magnitude of the peak ground acceleration, duration of main pulses, and slenderness of the structure, different rotational or rocking responses can be expected. As with sliding stability the inertia forces are likely to be larger for flexible structures than they are for rigid structures. Rotational or rocking responses to ground motions may include:

(1) No tipping because $M_o < M_r$

(2) Tipping or uplift because $M_o > M_r$, but no rocking due to insufficient ground motion energy

(3) Rocking response ($M_o > M_r$) that will eventually stop due to the energy loss during impact

(4) Rocking response that leads to rotational instability (extremely unlikely).

The likelihood of tipping can be determined by the following simple tipping potential evaluation. Even if tipping occurs, it is unlikely that it would result in rotational instability for the massive concrete hydraulic structures (Paragraph 7-4*d*). However, high bearing pressures can develop during tipping and rocking responses. A bearing failure evaluation is required to determine whether bearing pressures associated with the tipping and rocking responses could lead to foundation failure. Rocking spectrum and nonlinear time-history procedures are available to evaluate the potential for rotational instability (Paragraph 7-4d).

b. Tipping Potential Evaluation. Hydraulic structures subjected to large lateral forces produced by earthquakes may tip and start rocking when the resulting overturning moment becomes so large that the structure breaks contact with the ground. For a nearly rigid structure as shown in Figure 7-3, or for a flexible structure idealized as an equivalent single degree of freedom system, the tipping occurs when the overturning moment exceeds the resisting moment due to the weight of the structure. Note that in both cases it is assumed that the

structure is not bonded to the ground, but it may be keyed into the soil with no pulling resistance. This condition is expressed by:

$M_o > Mr$

$m\,S_a\,h > m\,g\,b$ or, $S_a > g\,(b/h)$ (7-1)

where:

M_o = overturning moment

M_r = resisting moment

S_a = spectral acceleration

g = gravitational acceleration

b = one-half width of the structure

h = distance from the base to the center of gravity

m = mass of the structure

This expression can also be used for hydraulic structures, except that the moments due to hydrostatic and hydrodynamic forces should be included and that the added hydrodynamic mass of water be also considered in determination of the structure's center of mass.
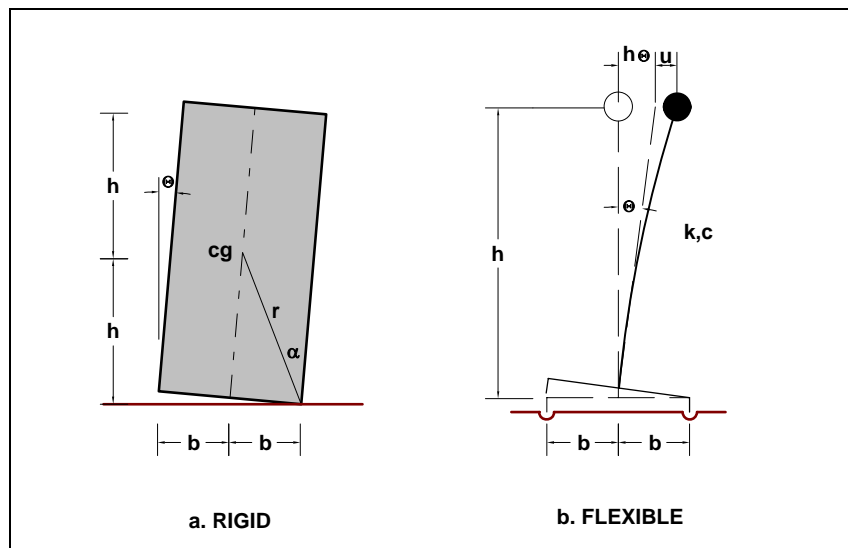
Figure 7-3. Rigid block and SDOF models for rigid and flexible structures

c. Energy Based-Rotational Stability Analysis. The structure will eventually overturn if the moment $M_o>M_r$ is applied and sustained. However, under earthquake excitation large overturning moments occur for only a fraction of second in each cycle, with intermediate opportunities to unload. Although rocking occurs, the structure may not become unstable rotationally if the energy loss during impact results in reduction of the angular velocity when the rotation reverses. By comparing the earthquake average energy input with the required average energy for overturning the structure, Housner provided the following approximate relationship as a criterion for the overturning stability of a rocking structure (Housner 1963):

$$\alpha = S_v \sqrt{\frac{mr}{gI_o}} \qquad (7\text{-}2)$$

where:

α = angle between the vertical and the line segment R as illustrated in Figure 7-2.

r = distance from the center of gravity to the corner about which rotation occurs.

I_o = mass moment of inertia about that corner.

S_v = spectral velocity of the earthquake ground motion.

Based on the average energy formulation used, this equation is interpreted as stating that for a given spectral velocity S_v, a block having an angle α given by Equation 7-2 will have approximately a 50 percent probability of being overturned (Housner 1963). For slender structures such as intake towers Equation 7-1 can be approximated by:

$$\alpha = \frac{S_V}{\sqrt{gr}} \qquad (7\text{-}3)$$

By combining Equations 7-1 and 7-3 and using the relationships among the spectral acceleration, velocity, and displacement, R. E. Scholl (ATC-10-01, 1984) found that consideration of one spectral parameter alone as the earthquake demand is not sufficient for evaluating overturning and suggested the following relationships:

$$S_d = b \quad \text{when} \quad S_d = g\frac{b}{h} \qquad (7\text{-}4)$$

These equations show that when S_a is just sufficient to cause tipping, the structure will start rocking, but its displacement approximated by spectral displacement S_d must reach the value b before it can overturn. These equations also demonstrate why larger structures such as buildings do not overturn during earthquakes, whereas smaller rigid blocks having the same aspect ratio are expected to overturn. This is because, in general, S_d is never large enough to tip over a building, but it can approach one-half the base width (i.e. b) of smaller rigid blocks such as tombstones. A better and more accurate procedure for evaluation of rocking response is the use of rocking spectra and nonlinear time-history method described next.

d. Time-history and rocking spectrum procedures

(1) Time history and rocking spectra can be used to estimate the uplift or overturning of hydraulic structures that tend to undergo rocking motion (Makris and Konstantinidis, 2001). There are distinct differences between a SDOF oscillator and the rocking motion of a rigid block, as shown in Figure 7-4. As such, an equivalent SDOF oscillator and standard displacement and acceleration response spectra should not be used to estimate rocking motion of structures. For example, the restoring mechanism of the SDOF oscillator originates from the elasticity of the structure, while the restoring mechanism of the rocking block from gravity. The SDOF oscillator

has a positive and finite stiffness, k, and energy is dissipated as the force-displacement curve forms closed loops. The rocking block, on the other hand, has infinite stiffness until the magnitude of the applied moment reaches the restoring moment, and once the block is rocking, its stiffness decreases and reaches zero when the of rotation of the block becomes equal to α (the block slenderness). The vibration frequency of a rigid block is not constant because it depends on the vibration amplitude (Housner 1963). The vibration frequency $p = (3g/4R)^{1/2}$ is a measure of the dynamic characteristic of the block. It depends on the size of the block, R, and the gravitational acceleration, g. This indicates that rocking response cycles of larger block is longer than the corresponding rocking response-cycles of the smaller block.

(2) Governing equations. The governing equations of rocking motion under horizontal ground acceleration are given by Yim et al. 1980, Makris and Roussos 2000, among others):

$$I_o \ddot{\theta}(t) + m\,g\,R\,sin(-\alpha - \theta) = -m\ddot{u}_g(t)R\,cos(-\alpha - \theta), \qquad for \quad \theta < 0 \qquad (7\text{-}5)$$

$$I_o \ddot{\theta}(t) + m\,g\,R\,sin(\alpha - \theta) = -m\ddot{u}_g(t)R\,cos(\alpha - \theta), \qquad for \quad \theta > 0 \qquad (7\text{-}6)$$

which in its compact form can be expressed as:

$$\ddot{\theta}(t) = -p^2\left\{sin[\alpha\,sgn[\theta(t)] - \theta(t)] + \frac{\ddot{u}_g}{g}cos[\alpha\,sgn[\theta(t)] - \theta(t)]\right\} \qquad (7\text{-}7)$$

where for rectangular blocks;

$\alpha \quad = tan^{-1}(b/h)$

$I_o \quad = (4/3)\,m\,R^2$

$P \quad = (3g/4R)^{1/2}$
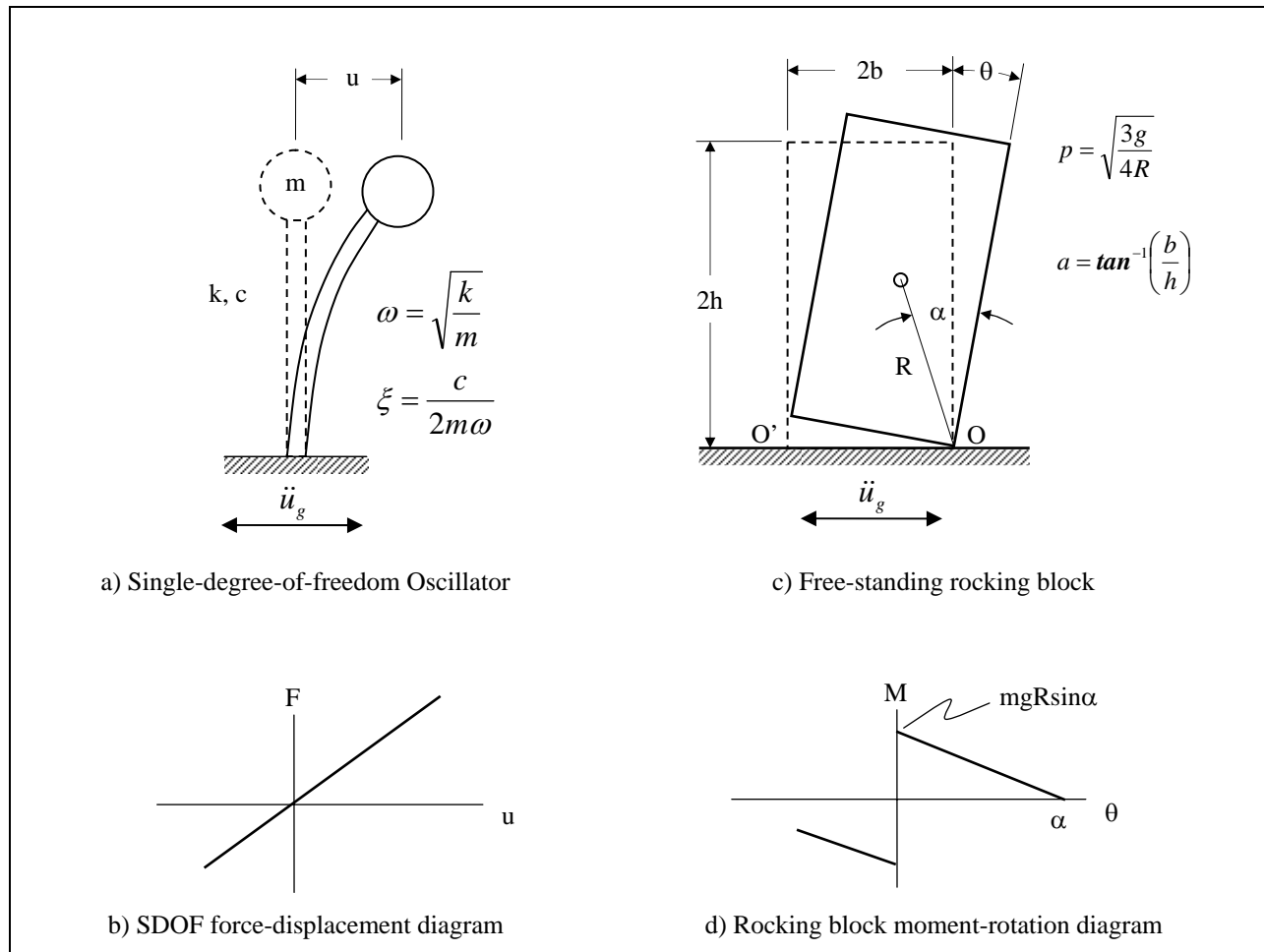
Figure 7-4. Comparison of a single-degree-of-freedom oscillator with a freestanding block in rocking motion (adopted from Makris and Konstantinidis, 2001)

(3) Time-history solution. The solution of Equation 7-7 is obtained by step-by-step numerical procedures. The rocking response quantity of interest include the block rotation, θ, and its angular velocity, $\dot{\theta}$. The resulting time-histories of θ and $\dot{\theta}$ will indicate how many impacts the block will experience and whether or not it will overturn (i.e. θ becomes greater than α).

(4) Rocking spectra. Same as the standard response spectra, one can generate rotational and angular velocity spectra (rocking spectra) as a function of the "period" $T=2\pi/p$ for different values of slenderness (damping), $\alpha = \tan^{-1}$ (b/h). This can be accomplished by solving Equation 7-7 for the maximum rotation of similar blocks of different sizes subjected to a given earthquake acceleration time history. This was done for similar blocks with $\alpha = 15°$ subjected to Pacoima Dam motion recorded during the 1971 San Fernando earthquake. The resulting rocking spectrum and the input acceleration record are shown in Figure 7-5. In the rocking spectrum, as $2\pi/p$ increases, the size of the block becomes larger. Larger values of the slenderness α correspond to larger amount of energy lost during impact. Figure 7-4 indicates that any block with slenderness α =15° that is small enough so that $2\pi/p<3.3$ sec (*or R<6.7* ft) will overturn when subjected to the Pacoima Dam record. Larger blocks with $2\pi/p>3.3$ sec *(or R>6.7* ft), will

uplift, but the maximum rotation is only a fraction of their slenderness. From this example, it should be obvious that rocking spectra provides a powerful and accurate tool for assessment of overturning potential of hydraulic structures. New research and development in this area are necessary to develop computation tools needed to make such assessments.
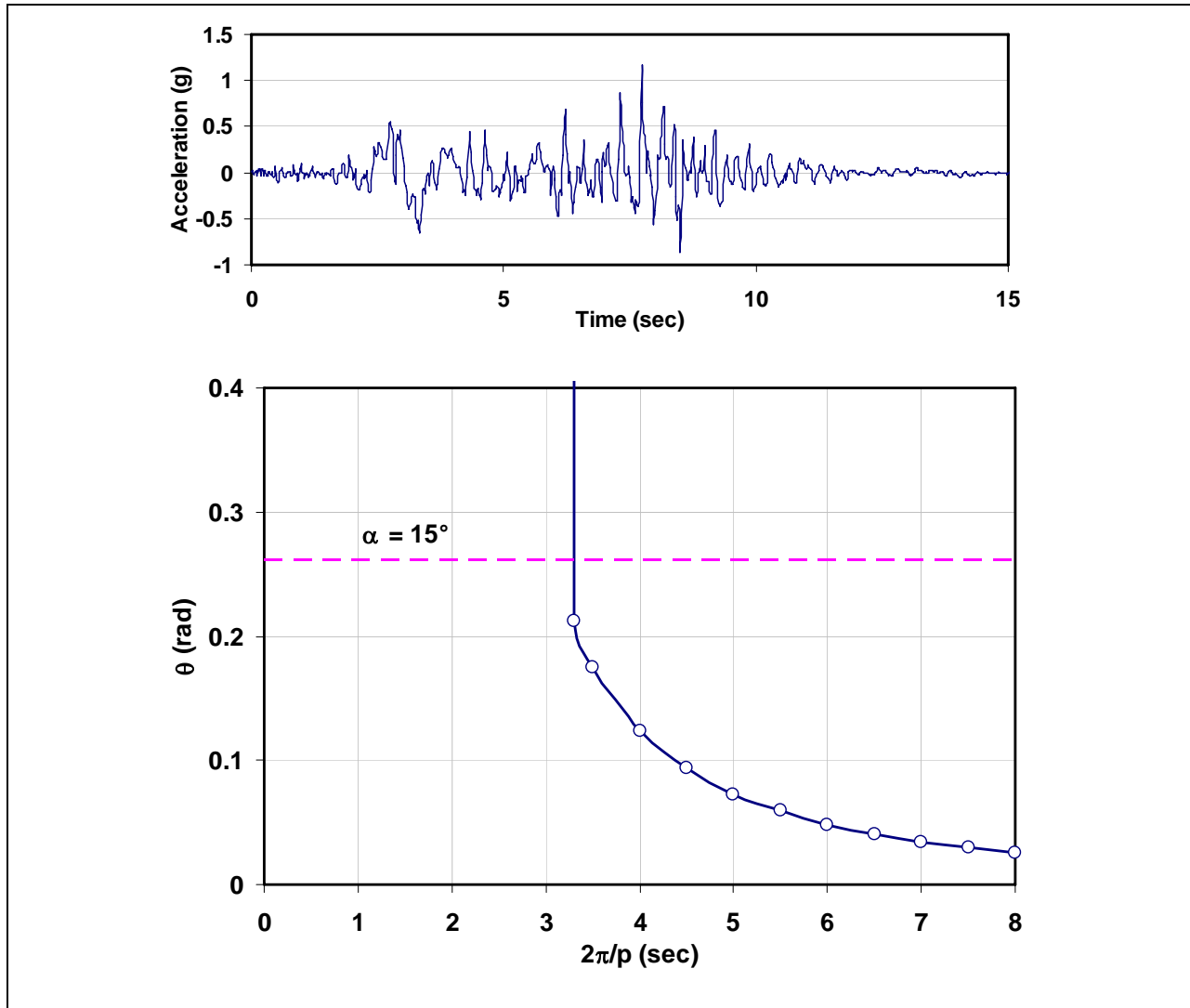
Figure 7-5. Pacoima Dam motion recorded during the 1971 San Fernando earthquake (top) and rocking spectrum of similar blocks with $\alpha = 15°$ (bottom).

7-5. Mandatory Requirements

 a. Performance requirements for stability shall be in accordance with EM 1110-2-2100, Stability Analysis of Concrete Structures.

 b. Seismic stability evaluation other than seismic coefficient method shall be in accordance with procedures discussed in this chapter.

APPENDIX A
REFERENCES

A-1. Required Publications

DEQAS
Ground Motion Analysis System, Engineer Research and Development Center

EM 1110-2-2100
Stability Analysis of Concrete Structures

EM 1110-2-2104
Strength Design for Reinforced-Concrete Hydraulic Structures

EM 1110-2-2200
Structural Design and Analysis of Gravity Dams and Spillways

EM 1110-2-2201
Arch Dam Design

EM 1110-2-2400
Structural Design and Evaluation of Outlet Works

EM 1110-2-6050
Response Spectra and Seismic Analysis for Concrete Hydraulic Structures

EM 1110-2-6051
Time History and Seismic Analysis for Concrete Hydraulic Structures

EP 1110-2-12
Seismic Design Provisions for Roller Compacted Concrete Dams, Appendix E, Tensile Strength
of Roller Compacted Concrete by Robert W. Cannon ,30 September 1995

ER 1110-2-1806
Earthquake Design and Evaluation for Civil Works Projects

A-2. Related Publications

ACI 318-95
ACI Manual of Concrete Practice (1998), Part 3. Building Code Requirements for Structural
Concrete (ACI 318-95) and Commentary (ACI 318R-95). ACI International.

ATC-3 1978
Applied Technology Council, 1978. Tentative provisions for the development of seismic
regulations for buildings, ATC-3-06 (NBS SP-510), U.S Government Printing Office,
Washington, DC.

ATC-40 (1996)
 "Seismic evaluation and Retrofit of Concrete Buildings," Applied Technology Council,
November 1996.

COE 2001

Seismic Evaluation Procedures for Existing Civil Works Powerhouse, draft report June 2001.

FEMA 273 and 274 (1997)

NEHRP Guidelines for the Seismic Rehabilitation of Buildings, 1997 Edition and Commentary.

FEMA 302 and 303 (1998)

NEHRP Recommended Provisions for the Development of Seismic Regulations for New Buildings, 1998 Edition and Commentary.

FEMA 356 (2000)

"Pre-standard and Commentary for the Seismic Rehabilitation of Buildings," Federal Emergency Management Agency, November 2000.

FEMA 368 (2000)

NEHRP Recommended Provisions for New Buildings and Other Structures, 2000 Edition.

NEHRP 1997

NEHRP Recommended Provisions for Seismic Regulations for New Buildings and Other Structures, 1997 Edition.

NEHRP 2003

2003 Hazards Reduction Program (NEHRP) Recommended Provisions for New Buildings and Other Structures (FEMA 450).

Bruhwieler 1990

Bruhwiler, E., Fracture of Mass Concrete under Simulated Seismic Action, Dam Engineering, Vol. 1, Issue 3, 1990.

Campbell 1994

Campbell, S. D. (1994), "Nonlinear Elements for Three Dimensional Frame Analysis". Ph.D. thesis, UC Berkeley.

Cannon 1995

EP 110-2-12, Seismic Provisions for Roller Compacted Concrete Dams, Appendix E, Tensile Strength of Roller Compacted Concrete by Robert W. Cannon, 30 September 1995.

Chakrabarti and Chopra 1972

Chakrabarti, P., and Chopra, A. K., 1972. Hydrodynamic Pressures and Response of Gravity Dams to Vertical Earthquake Component, *Journal of the International Association for Earthquake Engineering*, 1:325-335.

Chakrabarti and Chopra 1973

Chakrabarti, P., and Chopra, A. K., 1973. *A Computer Program for Earthquake Analysis of Gravity Dams Including Reservoir Interaction*, EERC 73-7, Earthquake Engineering Research Center, University of California, Berkeley AD 766 271 A04.

Chakrabarti and Chopra 1973
Chakrabarti, P., and Chopra, A. K., 1973. Earthquake Analysis of Gravity Dams Including Hydrodynamic Interaction EADHI, *Earthquake Engineering and Structural Dynamics*, 2:143-160.

Chakrabarti and Chopra 1974
Chakrabarti, P., and Chopra, A. K., 1974. Hydrodynamic Effects in Earthquake Response of Gravity Dams,@ *ASCE Journal of the Structural Division*, 106ST6:1211-1225.

Chang and Chen 1982
Chang, M. F., and Chen, W. F., 1982. *Lateral Earth Pressures on Rigid Retaining Walls Subjected to Earthquake Forces*, SM Archives 7, pp 315-362.

Chavez and Fenves 1993
Chavez, J.W. and Fenves, G.L., "Earthquake Analysis and Response of Concrete Gravity Dams Including Base Sliding," Report No. UCB/EERC-93/07, Earthquake Engineering Research Center, University of California, Berkeley, December 1993.

Chopra 1970
Chopra, A. K., 1970. Earthquake Response of Concrete Gravity Dams, *Journal of the Engineering Mechanics Division*, American Society of Civil Engineers, pp: 443-454.

Chopra 1980
Chopra, A. K., 1980. *Dynamics of Structures, A Primer*, Earthquake Engineering Research Institute, Berkeley, CA.

Chopra 1987
Chopra, A. K., 1987. Simplified Earthquake of Concrete Gravity Dam, *ASCE Journal of the Structural Division*, 113ST8: pp1688-1708.

Chopra and Chakrabarti 1972
Chopra, A. K., and Chakrabarti, P., 1972 Oct-Dec. The Earthquake Experience at Koyna Dam and Stresses in Concrete Gravity Dams, *Journal of the International Association for Earthquake Engineering*, 12.

Chopra and Chakrabarti 1981
Chopra, A. K., and Chakrabarti, P., 1981. Earthquake Analysis of Concrete Gravity Dams Including Dam-Water-Foundation Rock Interaction, *Earthquake Engineering and Structural Dynamics*, pp. 262-383.

Chopra, Chakrabarti, and Gupta 1980
Chopra, A. K., Chakrabarti, P., and Gupta, S., 1980. *Earthquake Response of Concrete Gravity Dams Including Hydrodynamic and Foundation Interaction Effects*, EERC 80-01, Earthquake Engineering Research Center, University of California, Berkeley ADA 087297.

Chopra and Gupta 1982
Chopra, A. K., and Gupta, S., 1982. Hydrodynamic and Foundation Interaction Effects in Frequency Response Functions for Concrete Gravity Dams, *Earthquake Engineering and Structural Dynamics*, 10:89-106.

Chopra and Tan 1989
Chopra, A. K., and Tan, H., 1989, Simplified Earthquake Analysis of Gated Spillway Monoliths of Concrete Gravity Dams,@ Technical Report SL-89-4, U.S. Army Engineer Waterways Experiment Station, Vicksburg, MS.

Chopra and Zhang 1991
Chopra, A.K., and Zhang L. (1991). "Base Sliding Response of Concrete Gravity Dams to Earthquakes," Report No. UCB/EERC-91/05, University of California, Berkeley, May 1991.

Clough and Penzien 1993
Clough, R. W., and Penzien, J., 1993. Dynamics of Structures, McGraw-Hill, New York.

Clough and Zienkiewicz 1982
Clough, R. W., and Zienkiewicz, O. C., 1982. *Finite Element Methods in Analysis and Design of Dams*, Committee on Analysis and Design of Dams.

Clough and Niwa 1980,
Earthquake Simulator Research on Arch Dam Models, ACI Special Publication SP 73-5.

Cole and Cheek 1986
Cole, R. A., and Cheek, J. B., 1986. Seismic Analysis of Gravity Dams, Technical Report SL-86-44, U.S. Army Engineer Waterways Experiment Station, Vicksburg, MS.

Dasgupta and Chopra 1979
G. Dasgupta and A. K. Chopra, "Dynamic Stiffness Matrices for Homogenous Viscoelastic Half Plane," Journal of the Engineering Mechanics Division, ASCE, Vol. 105, No. EM5, October 1979.

Dove 1998
Dove, R. C., "Performance of Lightly Reinforced Concrete Intake Towers under Selected Loadings". Technical Report SL-98-1, US Army Corps of Engineers, Waterways Experiment Station, March 1998.

DRAIN-2DX 1994
DRAIN-2DX User Guide (1994), Department of Civil Engineering, University of California, Berkeley, California.

Ebeling 1992
Ebeling, R. M., 1992. Introduction to the Computation of Response Spectrum for Earthquake Loading, Technical Report ITL-92-4, USACEWES.

Ebeling and Morrison 1992
Ebeling, R. M. and Morrison, E. E., The Seismic Design of Waterfront Structures, Report ITL-92-11, Department of the Army, Army Corps of Engineers, Waterways Experiment Station, November 1992.

Ebeling et al. 1992
Ebeling, R. M., Clough, G. W., Duncan, J. M., Brandon, T. M., 1992 Technical Report REMR-CS-29, Methods of Evaluating the Stability and Safety of Earth Retaining Structures Founded on Rock, U.S. Army Engineer Waterways Experiment Station, Vicksburg, MS.

Ehsani and Marine 1994
Ehsani M.R., Marine M.E. (1994), "User's Guide for Concrete Moment-Curvature Relationship (M-Phi)". MRE and Associates, Contract Report SL-94-.

EPRI 1992
Uplift pressures, Shear Strengths, and Tensile Strengths for the Stability Analysis of Concrete Gravity Dams, Vol. 1, Electric Power Research Institute, August 1992.

Fenves and Chopra 1986
Fenves, G., and Chopra, A. K., UCB/EERC-85-10, Simplified Analysis for Earthquake Resistant Design of Concrete Gravity Dams, June 1985.

Fenves and Chopra 1983
Fenves, G., and Chopra, A. K., 1983. Effects of Reservoir Bottom Absorption on Earthquake Response of Concrete Gravity Dams, *Earthquake Engineering and Structural Dynamics*, 11.

Fenves and Chopra 1984
Fenves, G., and Chopra, A. K., 1984. Earthquake Analysis of Concrete Gravity Dams Including Reservoir Bottom Absorption and Dam-Water-Foundation Rock Interaction, *Earthquake Engineering and Structural Dynamics*, 12:663-680.

Fenves and Chopra 1985
Fenves, G., and Chopra, A. K., 1985. Effects of Reservoir Bottom Absorption and Dam-Water-Foundation Rock Interaction on Frequency Response Functions for Concrete Gravity Dams, *Earthquake Engineering and Structural Dynamics*, 13:13-31.

Fenves and Chopra 1985
Fenves, G., and Chopra, A. K., 1985. Reservoir Bottom Absorption Effects in Earthquake Response of Concrete Gravity Dams, *ASCE Journal of Structural Engineering*, American Society of Civil Engineers, pp.545-562.

Fenves et al. 1989
Fenves, G.L., Mojtahedi, S. and Reimer, R.B.,"ADAP-88: A   Computer Program for Nonlinear Earthquake Analysis of Concrete Arch Dams," Report No. UCB/EERC-89/12, Earthquake Engineering Research Center, University of California at Berkeley, CA, 1989.

French et al. 1994
French, S. E., Ebeling, R. M., and Strom, R., Dynamics of Intake Towers and Other MDOF Structures Under Earthquake Loads, Report ITL-94-4, September, 1994.

Fronteddu, Leger, and Tinawi 1998
Fronteddu, L., Leger, P., and Tinawi, R., Static and Dynamic Behavior of Concrete Lift Joint Surfaces, ASCE Journal of Structural Engineering, Vol. 124, No. 12, Dec. 1998.

Ghanaat 1993
Ghanaat, Y., 1993. "GDAP: Graphics-Based Dam Analysis Program, User's Manual", U.S. Army Corps of Engineers, Waterways Experiment Station, Vicksburg, MS.

Ghanaat 1993
Ghanaat, Y., 1993. "Theoretical manual for Analysis of Arch Dams," Instruction Report ITL-93-1, U.S. Army Corps of Engineers, Waterways Experiment Station, Vicksburg, MS.

Goyal and Chopra 1989
Goyal, A., and Chopra, A. K., 1989. Earthquake Analysis and Response of Intake-Outlet Towers, Report No. UCB/EERC-89-04, Earthquake Engineering Research Center, University of California, Berkeley, CA.

Hall and Chopra 1982
Hall, J. F., and Chopra, A. K., 1982. *Hydrodynamic Effects in the Dynamic Response of Concrete Gravity Dams*, Earthquake Engineering and Structural Dynamics, pp. 333-345.

Housner 1963
Housner , G.W. (1963). "The Behavior of Inverted Pendulum Structures During Earthquakes," *Bulletin of the Seismological Society of America,* Vol. 53, No. 2, pp. 403-417.

Houghton 1976
Houghton, D. L., 1976, Determining Tensile Strain Capacity of Mass Concrete, *ACI Journal*, pp. 691-700.

Jansen 1988
Jansen, R. B., 1988. *Advanced Dam Engineering for Design, Construction, and Rehabilitation*, Van Nostrand Reinhold, New York.

Kriger and Wright 1980

Liaw and Chopra 1973
Liaw, C. Y., and Chopra, A. K., 1973. Earthquake Response of Axisymmetric Tower Structures Surrounded by Water, Report No. 73-25, Earthquake Engineering Research Center, University of California, Berkeley, CA.

Liu and McDonald 1978
Liu, T. C., and McDonald, J. E., 1978, Prediction of Tensile Strain Capacity of Mass Concrete, *ACI Journal*, pp. 192-197.

Lopez and Torres 1997
Lopez, O.A. and Torres R., "The critical angle of seismic incidence and the maximum structural response," J. of Earthquake Engineering and Structural Dynamics, Volume 26, 881-894 (1997).

Lopez, Copra and Hernandez 2000
Lopez, O.A., Copra, A.K., and Hernandez, J.J., "Critical response of structures to multi-component earthquake excitation," J. of Earthquake Engineering and Structural Dynamics, Volume 29, 1759-1778 (2000).

Lukose, Gergely, and White 1982
Lukose, K., Gergely, P., and White, R. N., 1982 (Sept-Oct), Behavior of Reinforced Concrete Lapped Splices for Inelastic Cyclic Loading, *ACI Structural Journal* pp. 355-365.

Lysmer et al. 1975
Lysmer, J., Udaka, T., Tsai, C.-F., and Seed, H.B., 1975, "FLUSH - a program for approximate 3-D analysis of soil-structure interaction problems," Report No. EERC 75-30, Earthquake Engineering Research Center, University of California, Berkeley.

Lysmer et al. 1981
Lysmer, J., Tabatabaie-Raissi, M., Tajirian, F., and Vahdani, S. (1981), "A System for Analysis of Soil-Structure Interaction," University of California, Berkeley.

Makris and Konstantinidis 2001
Makris, N. and Konstantinidis, D., "The Rocking Spectrum and the Shortcomings of Design Guidelines," PEER Report 2001/07, Pacific Earthquake Engineering Research Center, University of California, Berekeley, August 2001.

Makris and Roussos 2000
Makris, N., and Roussos, Y. (2000). "Rocking Response of Rigid Blocks under Near-Source Ground Motions," Geotechnique 50(3): 24362.

Mlakar and Jones 1982
Mlakar, P. F., and Jones, P. S., 1982. Seismic Analysis of Intake Towers, Technical Report SL-82-8, U.S. Army Engineer Waterways Experiment Station, Vicksburg, MS.

Mlakar, Vitaya-Udom, and Cole 1985
Mlakar, P. F., Vitaya-Udom, K. P., and Cole, R. A., 1985. Dynamic Tensile-Compressive Behavior of Concrete, *ACI Journal*, pp. 484-491.

Moehle 1992
Moehle, J. P., 1992, Displacement-Based Design of RC Structures Subjected to Earthquakes, *Earthquake Spectra, Vol. 8, No. 3,* pp. 403-428.

Mononobe and Matsou 1929
Mononobe, N., and Matsuo, H. 1929, On the Determination of Earth Pressures During Earthquakes, Proceedings, World Engineering Congress, 9.

Newmark 1965
Newmark, N. M., Effects of Earthquakes on Dams and Embankments, Geotehnique, Vol. 15, No. 2., 1965, pp139-160.

Newmark and Hall 1982
Newmark, N. M., and Hall, W. J. 1982. "Earthquake Spectra and Design," Engineering Monographs on Earthquake Criteria, Structural Design, and Strong Motion Records, Earthquake Engineering Research Institute, University of California, Berkeley, CA.

Newmark 1965
Newmark, N. M., "Effects of Earthquakes on Dams and Embankments", Geotechnique, Vol. 15, No. 2., 1965, pp139-160.

Okabe 1924

Orangun, Jirsa and Breen 1977
Orangun, C. O., Jirsa, J. O., Breen, J. E., 1977 (March), A Reevaluation of Test Data on Development Length and Splices, *ACI Journal* pp. 114-122.

Pauley 1980
Pauley, T., 1980 (May-Jun), Earthquake-Resisting Shearwalls--New Zealand Design Trends, *ACI Structural Journal.*

Priestley and Benzoni 1996
Priestley, M. J. N., and Benzoni, G. Seismic Performance of Concrete Circular Columns with Low Longitudinal Reinforcement Ratios, ACI Structural Journal, July-August, 1996.

Paulay and Priestley 1992
Paulay, T., and Priestley, M.J.N., Seismic Design of Reinforced Concrete and Masonry Buildings, John Wiley and Sons, Inc., 1992.

Priestley and Park 1987
Priestley, M.J.N. and Park, R., Strength and Ductility of Concrete Bridge Columns under Seismic Loading, ACI Structural Journal, January-February 1987.

Priestley, Seibel and Calvi 1996
Priestley, M. J. N., Seible, F., and Calvi, G. M., Seismic Design and Retrofit of Bridges, John Wiley & Sons, Inc., 1996.

Priestley, Verma, and Xaio 1994
Priestley, M.J.N., Verma, R., and Xaio, Y., Seismic Shear Strength of Reinforced Concrete Columns, ASCE Journal of Structural Engineering, Vol. 120, No. 8, August 1994.

QDAP
QDAP, a Web-based nonlinear dam analysis program developed by QUEST Structures, available at www.WebDams.com. QDAP is an enhanced version of the previous ADAP-88 program developed at University of California at Berkeley.

QUEST Structures 2001
WebDams (www.WebDams.com) - a web-based program for earthquake analysis of concrete arch dams, user's manual, QUEST Structures, 2001.

QUEST Structures 2001
QUEST Structures, 2001, an enhanced version of FLUSH with pre- and post-processing capabilities (www.WebDams.com).

Raphael 1984
Raphael, J. M., Tensile Strength of Concrete, ACI Journal, March-April 1984, pp. 158-165.

Rea, Liaw and Chopra 1975
Rea, D., Liaw, C. Y., and Chopra, A. K., 1975, Dynamic Properties of San Bernardino Intake Tower.

Richards and Elms 1977
Richards, R., and Elms, D. G., Seismic Behaviour of Retaining Walls and Bridge Abutments, Report 77-10, Department of Civil Engineering, University of Canterbury, Christchurch, New Zealand, 1977.

Rosenbloeth, and Contreas 1977
Rosenbloeth, E., and Contreas, H., 1977 (Oct), Approximate Design for Multicomponent Earthquakes, *ASCE Journal of the Engineering Mechanics Division.*

Saouma, Bruhwiler and Boggs 1990
Saouma, V.E., Bruhwiler, E., and Boggs, H.L., 1990, A Review of Fracture Mechanics Applied to Concrete Dams, *Dam Engineering* 1(1).

SAP2000 1997
SAP2000 Analysis Reference and User Guide (1997), Computers and Structures, Inc.

Seed, Ugas, and Lysmer 1976
Seed, H. B., Ugas, C., and Lysmer, J., 1976, *Site-Dependent Spectra for Earthquake-Resistant Design*, Bulletin of the Seismological Society of America, pp:221-243.

Seed and Whitman 1970
Seed, H. B., and Whitman, R. V., 1970, Design of earth retaining structures for dynamic loads, *ASCE Specialty Conference, Lateral Stresses in the Ground and Design of Earth Retaining Structures*, 103-147.

Scholl 1984
Scholl, R., 1984. "Overturning of Rigid Bodies during Earthquakes," Applied Technology Council Publication ATC 10-01, Redwood City, CA, pp 105-111.

Seed and Idriss 1969
Seed, H. B. and Idriss, I. M., 1969, "Influence of Soil Conditions on Ground Motions During Earthquakes," Journal of the Soil Mechanics and Foundation Division, ASCE, Vol. 94, No. SM1, January 1969.

Smedy and Der Kiureghian 1985
Smedy, W. and Der Kiureghian A., "Modal combination rules for multi-component earthquake excitation," Earthquake Engineering and Structural Dynamics, Volume 13, 1-12 (1985).

Veletsos and Younan 1994 (pp:4-15)
Veletsos, A.S., and Younan, A.H., 1994. "Dynamic Soil Pressures on Rigid Vertical Walls," *Earthquake Engineering and Structural Dynamics*, Vol. 23, pp 275-301.

WES 1973
U. S. Army Engineer Waterways Experiment Station, Investigation of Methods of Preparing Horizontal Construction Joints in Concrete, Technical Report No. 6-518, July 1959, Testing of Joints in Large Blocks, Report No. 2, July 1963, and Evaluation of High-Pressure Water Jet and Joint Preparation Procedures, Report No. 4, August 1973.

Westergaard 1933
Westergaard, H. M. 1933, Water Pressures on Dams during Earthquakes, *Transaction, American Society of Civil Engineers*, 98:418-433.

Whitman and Liao 1985
Whitman, R. V., and Liao, S., 1985, Seismic Design of Gravity Retaining Walls, Miscellaneous Paper GL-85-1, U. S. Army Engineer Waterways Experiment Station, Vicksburg, MS.

Whitman 1990
Whitman, R. V., Seismic Design and Behavior of Gravity Retaining Walls, 1990 ASCE Soil Mechanics Specialty Conference, Geotechnical Special Publication No. 25, entitled: Design and Performance of Earth Retaining Structures.

Whittaker, Constantinou and Tsopelas 1998
Whittaker, A., Constantinou, M. and Tsopelas, P., Displacement Estimates for Performance-Based Seismic Design, Journal of Structural Engineering, ASCE, August 1998.

Wilson and Button 1982
Wilson, E.L. and Button, M., "Three-dimensional dynamic analysis for multi-component earthquake spectra," Earthquake Engineering and Structural Dynamics, Volume 10, 471-476 (1982).

Wilson et al. 1995
Wilson, Edward L., Suharwardy, Iqbal, and Habibullah, Ashraf, Earthquake Spectral, Volume 11, No.4, November 1995, A Clarification of the Orthogonal Effects in a Three-Dimensional Seismic Analysis.

Winter and Nilson 1973
Winter G., Nilson A. H., (1973). "Design of Concrete Structures. 8th ed." McGraw-Hill Book Company, New York.

Wolf 1995 (pp:4-15)
Wolf, J.P., 1995. "Discussion on a paper by A.S. Veletsos and A.H. Younan," *Earthquake Engineering and Structural Dynamics,* Vol. 24, pp 1287-1291.

Yim et al. 1980
Yim, S.C., Chopra, A.K., and Penzien, J. (1980). "Rocking Response of Rigid Blocks to Earthquakes," Earthquake Engineering and Structural Dynamics 8(6):56587.

Zhang and Chopra 1991a
Zhang, L., and Chopra, A. K., 1991, "Base Sliding Response of Concrete Dams to Earthquakes", Report No. UCB/EERC-91/04, University of California at Berkley, May 1991.

Zhang and Chopra 1991b
Zhang, L. and Chopra, A. K., "Computation of Spatially Varying Ground Motion and Foundation-Rock Impedance Matrices for Seismic Analysis of Arch Dams," Report NO. UCB/EERC-91/06, Earthquake Engineering Research Center, University of California, Berkeley, May 1991.

U.S. Army Corps of Engineers 1983
U.S. Army Corps of Engineers, 1983. A Three-Dimensional Stability Analysis/Design Program 3DSAD; Report 4, Special Purpose Modules for Dams CDAMS, Instruction Report K-80-4, Office, Chief of Engineers, Washington, DC.

USBR 1976
USBR, 1976, U.S. Bureau of Reclamation, Design of Gravity Dams.

FHWA-RD-94-052 (1995)
U.S. Department of Transportation, Federal Highway Administration
Seismic Retrofitting Manual for Highway Bridges.

TM 5-809-10-1 (1986)
Seismic Design Guidelines for Essential Buildings, 27 February 1986.

Bazant, 1990
Bazant, Z.P., 1990.   A critical appraisal of no-tension dam design: a fracture mechanics view point, *Dam Engineering*, 1(4).

Wood 1973
Wood, J., 1973, Earthquake-Induced Soil Pressures on Structures, Report No. EERL 73-05, California Institute of Technology, Pasadena, CA, pp.311.

Wood 1989
Wood, Sharon L., 1989 (Sept-Oct), Minimum Tensile Reinforcement Requirements in Walls, *ACE Structural Journal,* pp. 582-591.

Wood 1990
Wood, Sharon L., 1990, (Jan-Feb), Shear Strength of Low-Rise Reinforced Concrete Walls, *ACE Structural Journal,* and pp. 99-107.

**Appendix B
Developing Standard Response Spectra and Effective Peak Ground
Accelerations for Use in the Design and Evaluation of Civil Works Projects**

B-1. Introduction

a. Purpose. The purpose of this appendix is to provide a procedure for developing standard acceleration response spectra and effective peak ground accelerations for use in the seismic design and evaluation of structural features of USACE projects as required by ER 1110-2-1806. The standard response spectra can be used as a starting point for performing seismic designs and evaluations, and, if needed, for determining dynamic analysis requirements for more refined analysis. A specific goal of this appendix is to update previous guidance documents to include the information available in the 2000 National Earthquake Hazards Reduction Program (NEHRP) Recommended Provisions for New Buildings and Other Structures (FEMA 368), which are based on the most recent representation of the national ground shaking hazard.

b. Scope. Guidance is provided for using the most recent national seismic hazard data for determining both horizontal and vertical acceleration response spectra. Guidance is also provided for determining effective peak ground accelerations and seismic coefficients for use in seismic stability analyses.

c. Background. Previous guidance memoranda were prepared before the 2000 NEHRP Recommended Provisions were published. The recommended procedures in those documents were initially based on the spectral maps contained in the 1991 NEHRP provisions, and later on the maps contained in the 1994 NEHRP provisions. Over the years, there have been significant changes in the seismic hazards maps and their application to estimate ground shaking hazard levels. The 1997 NEHRP provisions introduced a more detailed procedure for estimating site specific design response spectra. The procedure in the current provisions is based on probabilistic estimates associated with a 2% probability of occurrence in 50 years bounded in some areas by deterministic thresholds, provide spectral ordinates at periods of 0.2 and 1.0 seconds. In addition, probabilistic seismic hazard information is currently available in the form of maps for peak ground acceleration and spectral ordinates at periods of 0.2 and 1.0 seconds which are available for probabilities of exceedance of 10% in 50 years and 2% in 50 years. Note that only the USGS probabilistic seismic hazard maps may be used in seismic design and evaluation of hydraulic structures, and not the MCDE maps. The MCDE maps are used in seismic design and evaluation of building structures and are mentioned here to provide background on NEHRP provisions.

d. Definitions

(1) Peak ground acceleration. The peak ground acceleration (PGA) is the maximum amplitude of the ground acceleration time history. In terms of structural response, it represents the peak value of the absolute acceleration of a single degree of freedom (SDOF) system with infinite stiffness, that is, with a natural period of vibration equal to zero.

(2) Effective peak ground acceleration and effective peak ground velocity.

(a) Several definitions and different physical interpretations have been proposed for this parameter with the purpose of quantifying the severity of design ground shaking. The concepts of effective peak acceleration (EPGA) and effective peak velocity (EPGV) have been employed to define design ground motions for use in model building codes. They were introduced in the Applied Technology Council (ATC-3 1978) seismic provisions as convenient normalizing factors for construction of design response spectra for ground motions of normal duration. The EPGA is proportional to spectral ordinates for periods in the range of 0.1 to 0.5 seconds, while the EPGV is proportional to spectral ordinates at a period of about 1 second. The constant of proportionality (for a 5 percent damping spectrum) was set at a standard value of 2.5 in both cases. The EPGA and EPGV are related to peak ground acceleration and peak ground velocity but are not necessarily the same as or directly proportional to peak acceleration and velocity. When very high frequencies are present in the ground motion, the EPGA may be significantly less than the peak ground acceleration. In general, if one examines the ratio between the spectral ordinate at period 0.2 seconds and the corresponding PGA value at individual locations in the national probabilistic hazard maps, the value of the ratio is variable and generally less than 2.5.

(b) Newmark and Hall (1982) characterized the effective peak acceleration as the acceleration value that is most closely related to structural response and to damage potential of an earthquake. That is, this concept of effective peak acceleration is intended to reflect the actual damage potential of the seismic excitation, which cannot be completely described only by the peak value of the ground acceleration. The definition of the effective peak acceleration therefore must take into account not only the amplitude of the excitation, but also of its frequency content and the type and characteristics of the general structural system under consideration.

(3) Response spectra.

(a) A response spectrum is a plot of the peak values of the response (displacement, velocity, or acceleration) of a number of SDOF systems with different natural vibration periods subjected to the same seismic input. Therefore, an acceleration response spectrum represents the peak accelerations that a suite of SDOF systems with a range of natural periods may exhibit for a given component of ground motion.

(b) In general, the acceleration response spectrum associated with a specific time history recorded at a given location has a jagged shape with significant peaks and valleys. The response spectrum for another ground motion recorded at the same site during a different earthquake will exhibit also an irregular shape, but the peaks and valleys will not necessarily coincide with those in the previous one.

(c) Therefore, appropriately smoothed spectra are usually defined for design and evaluation purposes. These spectra are termed design response spectra. They do not represent the acceleration response from a single ground motion time history, but rather they are intended to be representative of all the ground motions that can be expected at a given site. There are two basic approaches for the development of design response spectra: site-specific procedure or standard procedure.

(d) Site-specific response spectra. Site-specific response spectra are developed using source to site distances, appropriate attenuation relationships, expected magnitudes and actual local site conditions. Therefore, it is typically assumed that site

specific studies will provide more accurate acceleration spectra than using the codified standard acceleration spectra. EM 1110-2-6050 describes the conditions requiring a site specific ground motion study. Site-specific response spectra can be generated by means of a deterministic seismic hazard analysis (DSHA) or a probabilistic seismic hazard analysis (PSHA). In the DSHA, the site ground motions are estimated for a specific earthquake, defined as a seismic event of a certain magnitude for a particular seismic source occurring at a certain distance from the site. The representation of the ground motions in terms of the corresponding site-specific response spectra is achieved by using appropriate attenuation relationships. Information on this approach can be found in EM 1110-2-6050. The PSHA is an approach that uses the likelihood (probability) that a given level of ground motion will occur during a specific exposure period. In the PSHA, the site ground motions are defined for selected values of the probability of exceedance in a given time exposure period, or for selected values of annual frequency or return period for ground motion exceedance. This approach incorporates the frequency of occurrence of earthquakes of different magnitudes on the seismic sources, the uncertainty of the earthquake locations on the sources, and the ground motion attenuation including its uncertainty. The response spectra developed by a PSHA represent equal or uniform hazard spectra, in which each spectral ordinate has an equal probability of exceedance. EM 1110-2-6050 describes the procedures for probabilistically estimating earthquake ground motions.

(e) Standard response spectra. Standard response spectra are based on a general characteristic shape that is defined in terms of estimates of selected ground motion parameters, which can be effective peak ground accelerations or spectral accelerations. EM 1110-2-6050 describes the approach proposed by Newmark and Hall (1982) to develop design response spectra using peak ground motion parameters (peak ground acceleration, velocity and displacement), multiplied by a series of appropriate spectral amplification factors that depend on the damping level.

(4) Probability of exceedance. The probability of exceedance represents the chance, expressed as a percentage (%), that a more severe ground motion will occur within a specified exposure time expressed in number of years. Assuming that the temporal occurrence of the earthquake follows a Poisson process, the probability of exceedance (P_e) in a given exposure time (T_e) is related to the annual probability of exceedance (λ_m) as follows:

$$P_e = 1 - e^{-\lambda_m T_e} \tag{1}$$

The reciprocal of the annual probability of exceedance is the return period ($T_R = 1/\lambda_m$), which represents the average number of years between exceedances. For a given (P_e, T_e) pair, the corresponding return period can be obtained as follows:

$$T_R = -\frac{T_e}{\ln(1 - P_e)} \tag{2}$$

As an example, an earthquake having a probability of exceedance of 2% in 50 years would have a mean return period of 2,475 years, whereas an earthquake having a probability of exceedance of 10% in 50 years would have a mean return period of 475

years. The following table summarizes the return periods for some of the most common combinations of probabilities of exceedance and exposure time:

Table B-1. Approximate return periods for different probabilities of exceedance and exposure times

Prob. of Exceedance	Exposure Time [years]	Return Period [years]
50%	100	144
10%	50	475
10%	100	950
5%	100	1,950
2%	50	2,475
1%	100	9,950

(5) Operating basis earthquake (OBE). The OBE is an earthquake that can reasonably be expected to occur within the service life of the project, that is, with a 50 percent probability of exceedance during the service life. (This corresponds to a return period of 144 years for a project with a service life of 100 years.) The associated performance requirement is that the project will show little or no damage without interruption of function. The purpose of the OBE is to protect against economic losses from damage or loss of service. Therefore alternative choices of return period for the OBE may be based on economic considerations. In a site-specific study the OBE is determined by a PSHA (ER 1110-2-1806).

(6) Maximum design earthquake (MDE). The MDE is the maximum level of ground motion for which a structure is designed or evaluated. The associated performance requirement is that the project performs without catastrophic failure, such as uncontrolled release of a reservoir, although severe damage or economic loss may be tolerated. The MDE can be characterized as a deterministic or probabilistic event (ER 1110-2-1806).

(7) Maximum credible earthquake (MCE). The maximum <u>credible</u> earthquake represents the earthquake hazard level used for design and evaluation of critical features of high hazard projects as defined by ER 1110-2-1806. The Maximum Credible Earthquake is defined as the greatest earthquake that can reasonably be expected to be generated by a specific source on the basis of the available seismological and geological evidence. The Maximum Credible Earthquake is determined by a deterministic seismic hazard analysis. Since buildings are not classified as critical facilities, the use of a Maximum Credible Earthquake as defined in ER 1110-2-1806 is not required for the building structures.

(8) Seismic coefficient method. In the seismic coefficient method, the inertial force is assumed to act in a horizontal direction at the center of mass of the structure, based on the assumption that the structure is a rigid body. However, the use of the rigid body concept often underestimates the magnitude of the actual inertial actions because of the amplification effects associated with the flexibility of the structure.

(9) Dynamic analysis procedures. Linear dynamic analysis procedures are presently used for earthquake-resistant design and safety evaluation of hydraulic structures. Linear dynamic analysis is typically based on modal decomposition techniques, in which the total response of a structure is obtained by combining the response of its individual modes of vibration, calculated separately. Linear dynamic analysis is adequate for structures whose seismic response stays within the linear elastic range and it can be performed using response spectrum analysis or time-history analysis.

(a) Response spectrum analysis. In the response spectrum analysis, the peak response of the structure is evaluated by combining estimates of the maximum responses from individual modes and multicomponent input. The seismic input is defined in terms of ground response spectra.

(b) Time history analysis. This type of analysis involves the computation of the complete response history of the structure to the earthquake, and not just the peak values. The seismic input is given by actual or simulated acceleration time histories.

B-2. Seismic hazard and design maps

a. USGS probabilistic maps. The U.S. Geological Survey (USGS) National Hazard Mapping Project supported by NEHRP provides the latest peer reviewed and published seismic hazard data for the US. This data is provided in probabilistic hazard maps and interactive web based query for certain ground motion parameters. The current link to this project site is located at the following address: http://eqhazmaps.usgs.gov/. However, this could change and it may be necessary to search for the most current web link. The available probabilistic maps for downloading or viewing correspond to PGA values and 0.2 sec and 1.0 sec spectral acceleration values for probabilities of exceedance of 10% in 50 years (return period of 475 years) and 2% in 50 years (return period of 2,475 years). The site also provides an interactive menu where the user can obtain the above mapped values for a given location specified by latitude / longitude. Ground motion values for the 48 states have been calculated for a grid spacing of 0.05 degrees. Interpolated values are typically calculated using the four surrounding corner points. For guidance, 0.1 degree latitude is about 6.8 miles, and 0.1 degree longitude varies but for the 48 states is on the order of 5.6 miles. Figures B-1 and B-2 show the probabilistic maps for the 0.2 and 1-second spectral acceleration values corresponding to a probability of exceedance of 2% in 50 years.
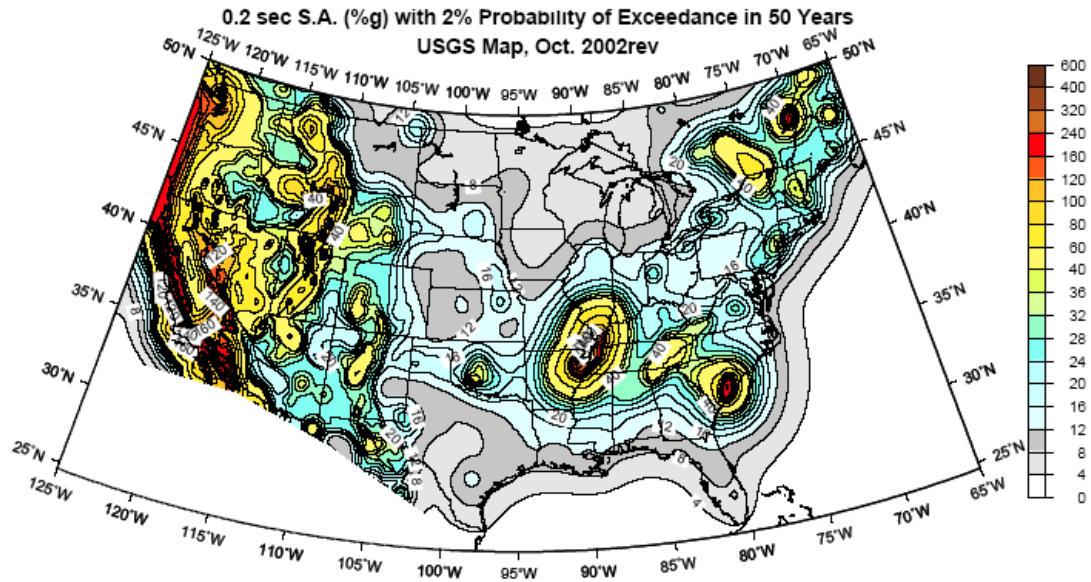
Figure B-1. 0.2-second spectral acceleration with 2% probability of exceedance in 50 years
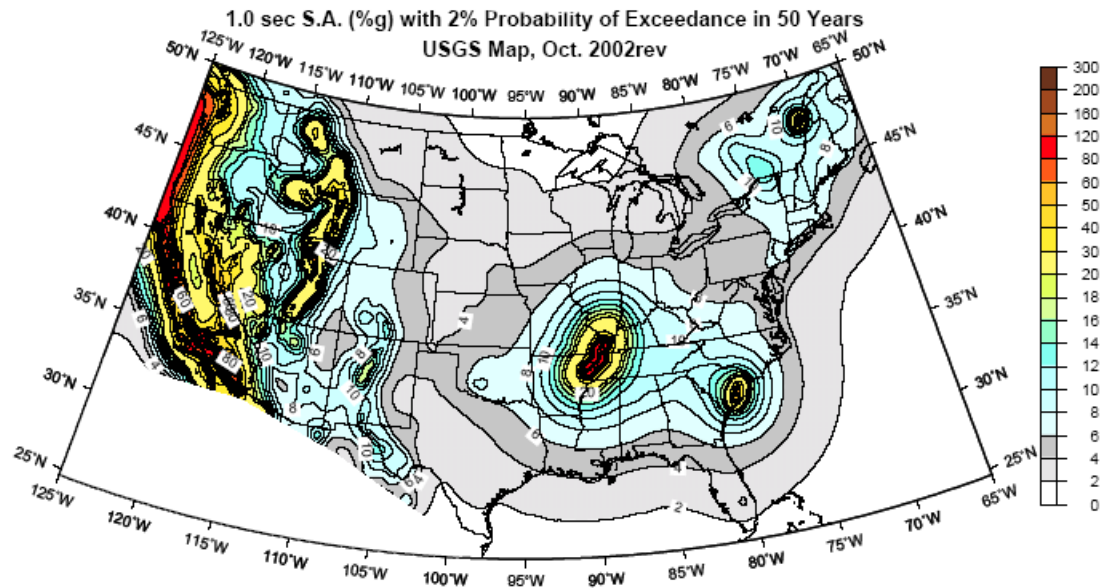
Figure B-2. 1-second spectral acceleration with 2% probability of exceedance in 50 years

b. MCE design maps. Most recent NEHRP provisions define seismic hazards in terms of "Maximum Considered Earthquake" ground motions, which are based on a set of rules that depend on the seismicity of a region. The design ground shaking level for new building structures is defined as 1/1.5 = 2/3 of the maximum considered earthquake ground motion. For most regions of the nation, the maximum considered earthquake ground motion is defined with a uniform probability of exceedance of 2% in 50 years (return period of about 2,500 years). For regions of high seismicity (such as coastal California) the seismic hazard is typically controlled by large-magnitude events occurring on a limited number of well-defined fault systems. The ground shaking calculated at a

2% PE / 50 years would be much larger than that which would be expected based on the characteristic magnitudes of earthquakes on these known active faults. For regions of high seismicity, it is more appropriate to directly determine the maximum considered earthquake motions based on the actual characteristics of these faults. The ground shaking in these cases is defined based on the median estimate of the ground motion resulting when the characteristic earthquake is multiplied by 1.5 to achieve the appropriate level of conservatism.

B-3. Development of standard horizontal response spectrum

a. Seismic hazard data. The following recommended procedure for developing standard spectra for use in the preliminary design and analysis of USACE civil works structures is based on the current probabilistic seismic hazard data. For a given site location, the spectral ordinates at periods of 0.2 and 1.0 seconds are available for probabilities of exceedance of 10% in 50 years and 2% in 50 years. These ground motion values are calculated for firm rock sites. The spectral ordinate at periods 0.2 and 1 seconds are denoted as S_S and S_1.

b. Site effects.

(1) The shape of the standard response spectra can be modified to reflect site characteristics. The effects of the soil and foundation conditions can greatly affect the structural response. These site effects are accounted for in the development of the standard response spectra by the use of site coefficients that scale the spectral ordinates to the appropriate values for other local conditions such as those defined in Table B-2.

(2) Site class F is omitted from the table because this site classification requires site-specific investigations and a standard response spectrum should not be employed for this case. The site coefficients F_a and F_v are given in Tables B-3 and B-4. These two coefficients F_a and F_v scale the values of S_S and S_1, respectively, which were determined for firm rock conditions (characterized by a shear-wave velocity of about 2,500 ft/sec in the top 100 ft).

(3) The independent scaling of the spectral parameters using these factors modifies not only the spectral amplitudes but also the shape of the spectrum by changing the maximum amplification plateau. The scaled maximum considered earthquake spectral values are designated as $\overline{S}_S$ and $\overline{S}_1$, for short and 1-second period responses. They are given by the following expressions:

$$\overline{S}_S = F_a S_a$$
$$\overline{S}_1 = F_v S_1$$

(3)

Table B-2. Site classification

Site Class	Description
A	Hard rock with $\bar{v}_s > 5,000\,\text{ft/sec}$
B	Rock with $2,500\,\text{ft/sec} < \bar{v}_s \leq 5,000\,\text{ft/sec}$
C	Very dense soil and soft rock with $1,200\,\text{ft/sec} < \bar{v}_s \leq 2,500\,\text{ft/sec}$ or with either $\bar{N} > 50$ or $\bar{s}_u > 2,000\,\text{psf}$
D	Stiff soil with $600\,\text{ft/sec} \leq \bar{v}_s \leq 1,200\,\text{ft/sec}$ or with either $15 \leq \bar{N} \leq 50$ or $1,000\,\text{psf} \leq \bar{s}_u \leq 2,000\,\text{psf}$
E	A soil profile with $\bar{v}_s < 600\,\text{ft/sec}$ or with either $\bar{N} < 15$ or $\bar{s}_u < 1,000\,\text{psf}$, or any profile with more than 10 ft of soft clay

Table B-3. Site correction coefficient F_a

Site Class	Coefficient F_a				
	$S_S \leq 0.25$	$S_S = 0.50$	$S_S = 0.75$	$S_S = 1.00$	$S_S \geq 1.25$
A	0.8	0.8	0.8	0.8	0.8
B	1.0	1.0	1.0	1.0	1.0
C	1.2	1.2	1.1	1.0	1.0
D	1.6	1.4	1.2	1.1	1.0
E	2.5	1.7	1.2	0.9	0.9

Table B-4. Site correction coefficient F_v

Site Class	Coefficient F_v				
	$S_1 \leq 0.10$	$S_1 = 0.20$	$S_1 = 0.30$	$S_1 = 0.40$	$S_1 \geq 0.50$
A	0.8	0.8	0.8	0.8	0.8
B	1.0	1.0	1.0	1.0	1.0
C	1.7	1.6	1.5	1.4	1.3
D	2.4	2.0	1.8	1.6	1.5
E	3.5	3.2	2.8	2.4	2.4

   c. Damping. The seismic hazard information is based on an inherent structural damping of 5%. If spectral values for other damping ratios are required, then the standard spectral accelerations have to be adjusted using the correction coefficients B_S and B_1 provided in Table B-5.

   d. Construction of standard horizontal spectrum.

(1) To determine the standard horizontal response spectrum it is necessary to compute first the values of the two periods defining the interval of maximum spectral amplification. They are denoted as T_0 (start of maximum amplification plateau) and T_S (end of maximum amplification plateau), and they are defined as follows:

$$T_S = \frac{B_S \overline{S}_1}{B_1 \overline{S}_S}$$

$$T_0 = \frac{1}{5} T_S$$

(4)

(2) The standard horizontal spectrum is then defined as follows:

$$S_A(T) = \begin{cases} \overline{S}_S \left(\left(\frac{5}{B_S} - 2 \right) \frac{T}{T_S} + 0.4 \right) & \text{for } 0 \leq T < T_0 \\ \dfrac{\overline{S}_S}{B_S} & \text{for } T_0 \leq T < T_S \\ \dfrac{\overline{S}_1}{B_1 T} & \text{for } T_S \leq T \end{cases}$$

(5)

Table B-5. Damping correction coefficients B_S and B_1

Damping [%]	Coefficient B_S	Coefficient B_1
≤ 2	0.80	0.80
3	0.87	0.87
4	0.93	0.93
5	1.00	1.00
6	1.06	1.04
7	1.12	1.08
8	1.18	1.12
9	1.24	1.16
10	1.30	1.20
20	1.80	1.50

e. Spectrum construction for different probability levels

(1) The two values of spectral ordinates at periods of 0.2 and 1.0 seconds (S_S and S_1) are available for probabilities of exceedance of 10% in 50 years and 2% in 50 years, which correspond to average return periods of 475 and 2,475 years, respectively. If a standard spectrum associated with a different probability of exceedance or return period is required, then it is necessary to appropriately modify those values.

(2) It is assumed that the hazard curves relating the spectral acceleration (S_A) with the return period (T_R) can be approximated by power curve functions of the following form:

$$S_A = b(T_R)^m \tag{6}$$

This assumption implies that spectral values and return periods are linearly related in a log-log representation, that is:

$$\log(S_A) = \log(b) + m\log(T_R) \tag{7}$$

The coefficient m represents the slope of the straight line and $\log(b)$ is the intercept on the ordinate axis.

(3) Considering the available data points, which are represented by ($S_A^{T_R=475}$) and ($S_A^{T_R=2475}$), then it is possible to obtain spectral accelerations at different return periods by linear log-log interpolation. The curve coefficients are given by

$$m = \frac{\log(S_A^{T_R=2475}) - \log(S_A^{T_R=475})}{0.7169}$$

$$\log(b) = 4.7338\log(S_A^{T_R=475}) - 3.7338\log(S_A^{T_R=2475}) \tag{8}$$

Using this approach, two approximated hazard curves can be defined for the spectral accelerations at periods of 0.2 and 1.0 seconds (S_S and S_1), which can be then used to determine the corresponding spectral values for other return periods different from 475 and 2,475 years.

B-4. Development of standard vertical response spectrum

a. Vertical-to-horizontal response spectral ratio. Vertical response spectra may be necessary for design and analysis of certain structures. The commonly adopted vertical-to-horizontal response spectral ratio of 2/3 (Newmark and Hall 1978) may be significantly exceeded at short periods for near-source distance conditions. Therefore, the vertical standard response spectrum should be obtained considering the source to site distance (R) by means of the factors given in Table B-6. These factors were based on the information provided in EM 1110-2-6050. In most cases of preliminary design the source-to-site distance will be unknown, and for those cases $R = 25\,\text{km}\,(15\,\text{miles})$ may be assumed. This general procedure can be applied to both standard and site-specific spectra, although in this last case vertical response spectra can also be derived directly by some attenuation relationships.

Table B-6. Conversion factor F_V for vertical response spectrum

Source to Site Distance (R)	Conversion Factor
≤ 10 km	1.00
25 km	0.84
≥ 40 km	0.67

b. Construction of standard vertical spectrum.

(1) To determine the standard spectrum it is necessary to compute first the period defining the upper limit of the maximum vertical amplification plateau, given by

$$T_{SV} = \frac{0.67}{F_V} T_S \tag{9}$$

(2) The standard vertical spectrum is then defined as follows:

$$S_{AV}(T) = \begin{cases} F_V S_A(T) & \text{for } T < T_{SV} \\ \\ 0.67 \dfrac{\overline{S}_1}{B_1 T} & \text{for } T_{SV} \leq T \end{cases} \tag{10}$$

B-5. Multi-component earthquake input

a. Second orthogonal component of horizontal ground motion. The NEHRP hazard maps are based on attenuation relationships for the random horizontal component of the ground motion, not the stronger component. If a second orthogonal component of horizontal motion is required for preliminary seismic analysis, then it should be set equal to the first orthogonal component determined as indicated in the previous section.

b. Combining multi-component earthquake input. For most structures, preliminary seismic analysis can be conducted considering a single horizontal component of earthquake ground motion. However, for those cases where the effects due to two or three components of ground motion must be taken into account, the maximum structural responses should be obtained by combining the effects of the components in accordance with the procedures described in EM 1110-2-6050.

B-6. Seismic stability analysis

a. Determination of effective peak ground acceleration (EPGA). For a given return period, the effective peak ground acceleration (EPGA) is determined by dividing by 2.5 the corresponding 5%-damping short period spectral acceleration value as follows:

$$EPGA(T_R) = \frac{\overline{S}_S^{T_R}}{2.5} \tag{12}$$

b. Seismic coefficient. The seismic coefficient used for the preliminary seismic stability evaluation of concrete hydraulic structures should be equal to 2/3 of the EPGA value corresponding to the OBE or the MDE, expressed as a decimal fraction of the acceleration of gravity.

B-7. DEQAS-R computer program

a. Description. Due to the availability of the national probabilistic seismic hazard data, it is now possible to provide tools to assist in developing design spectra without the need to manually extract data from maps or to explicitly query the USGS web site. A set of integrated software tools has been developed to provide the needed seismic hazard data based on the most recent national probabilistic seismic hazard information. For user-specified location and return period, the current version of this program can calculate and display the horizontal and vertical standard spectra based on the procedure provided in this document. In addition, the program can generate the equal hazard spectrum for the location and return period indicated as well as the corresponding seismic hazard curves for periods of 0.2 and 1.0 seconds. The program also includes additional options to display different maps containing the most recent seismic hazard data and it provides access to relevant USACE reference documents.

b. Availability. The program DEQAS-R can be downloaded from the following website: http://chl.erdc.usace.army.mil/.

B-8. Examples

Typical example problems illustrating step-by-step implementation of the procedures in this guidance document are provided in Appendix C. The first example describes the development of a 5%-damping horizontal standard spectrum for an OBE. The second example describes the development of both horizontal and vertical standard spectra for an MDE and for a 6% damping level. The last example describes the determination of EPGA values for a specified set of return periods. The solution of each one of these examples using the computer program DEQAS-R is illustrated in Section II of Appendix C.

Appendix C
Ground Motion Example Problems

Section I: Manual Calculations

C-1. Example problem 1

This problem will demonstrate the development of a 5% damping horizontal standard response spectrum for an Operational Basis Earthquake (OBE).

a. Project data

Name: Mud Mountain Dam
Location: King County, WA
Latitude: 47.1 deg
Longitude: -121.9 deg
Site Conditions: Soft rock foundation (site class C)

b. Mapped spectral values.

Accessing the USGS web site with the appropriate site location information, we obtain the corresponding PGA and spectral acceleration values corresponding to 0.2 seconds and 1 second:

	10% PE in 50 years	**2% PE in 50 years**
PGA [g]	0.2666	0.4858
S_S [g]	0.5951	1.1005
S_1 [g]	0.1918	0.3601

c. Return period for design earthquake

If the OBE is defined as an event with 50% chance of exceedance in 100 years, then the corresponding return period is given by

$$T_R = -\frac{100\,\text{years}}{\ln(1-0.50)} = 144\,\text{years}$$

d. Adjust spectral values to specified return period

For the spectral acceleration at 0.2 seconds:

$$m_S = \frac{\log(S_S^{T_R=2475}) - \log(S_S^{T_R=475})}{0.7169}$$

$$m_S = \frac{\log(1.1005) - \log(0.5951)}{0.7169} = 0.3724$$

$$\log(b_S) = 4.7338 \log(S_S^{T_R=475}) - 3.7338 \log(S_S^{T_R=2475})$$
$$\log(b_S) = 4.7338 \log(0.5951) - 3.7338 \log(1.1005)$$
$$\log(b_S) = -1.2223$$
$$b_S = 10^{\log(b_S)} = 0.0599$$

Therefore

$$S_S^{T_R=144} = 0.0599(144)^{0.3724}$$
$$S_S^{T_R=144} = 0.3815$$

For the spectral acceleration at 1 second:

$$m_1 = \frac{\log(S_1^{T_R=2475}) - \log(S_1^{T_R=475})}{0.7169}$$
$$m_1 = \frac{\log(0.3601) - \log(0.1918)}{0.7169} = 0.3816$$

$$\log(b_1) = 4.7338 \log(S_1^{T_R=475}) - 3.7338 \log(S_1^{T_R=2475})$$
$$\log(b_1) = 4.7338 \log(0.1918) - 3.7338 \log(0.3601)$$
$$\log(b_1) = -1.7386$$
$$b_1 = 10^{\log(b_1)} = 0.0183$$

Therefore

$$S_1^{T_R=144} = 0.0183(144)^{0.3816}$$
$$S_1^{T_R=144} = 0.1216$$

e. Construct standard spectrum

Adjust for site conditions

$$\overline{S}_S = F_a S_S^{T_R=144} = (1.20)0.3815$$
$$\overline{S}_S = 0.4578$$
$$\overline{S}_1 = F_v S_1^{T_R=144} = (1.69)0.1216$$
$$\overline{S}_1 = 0.2041$$

Compute periods defining the amplification plateau

$$T_S = \frac{B_S \overline{S}_1}{B_1 \overline{S}_S} = \frac{(1.00)0.2041}{(1.00)0.4578} = 0.45\,\text{sec}$$

$$T_0 = \frac{1}{5}T_S = \frac{0.45}{5} = 0.09\,\text{sec}$$

Define the horizontal standard spectrum

$$S_A[g] = \begin{cases} 3.0806\,T + 0.1831 & \text{for } 0 \le T < 0.09\,\text{sec} \\ 0.4578 & \text{for } 0.09\,\text{sec} \le T < 0.45\,\text{sec} \\ 0.2041/T & \text{for } 0.45\,\text{sec} \le T \end{cases}$$

Therefore the spectrum exhibits a maximum value of 0.4578 g between the periods of 0.09 and 0.45 seconds. The following figure shows the resulting horizontal standard spectrum:
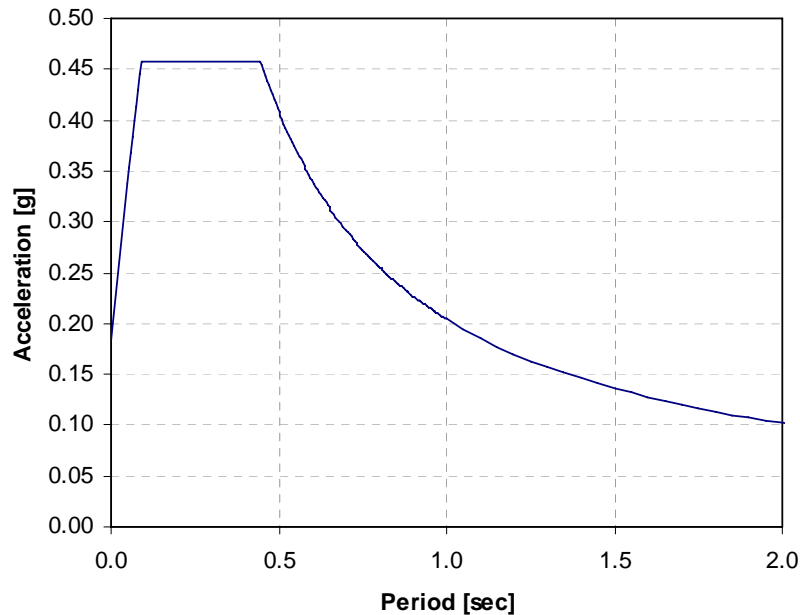
Figure C-1. Standard horizontal acceleration response spectrum for example C-1

C-2. Example problem 2

This problem will demonstrate the development of 6% damping horizontal and vertical standard response spectra for a Maximum Design Earthquake (MDE) characterized by a return period of 1,000 years.

a. Project data

Name: Blue River Dam
Location: Lane County, OR
Latitude: 44.2 deg
Longitude: -122.3 deg
Site Conditions: Rock foundation (site class B)

b. Mapped spectral values

Accessing the USGS web site with the appropriate site location information, we obtain the corresponding PGA and spectral acceleration values corresponding to 0.2 seconds and 1 second:

	10% PE in 50 years	**2% PE in 50 years**
PGA [g]	0.1020	0.2216
S_S [g]	0.2371	0.5262
S_1 [g]	0.0987	0.2231

c. Return period for design earthquake

For this case the specified MDE is characterized by a return period of 1,000 years.

d. Adjust spectral values to specified return period

For the spectral acceleration at 0.2 seconds:

$$m_S = \frac{\log(S_S^{T_R=2475}) - \log(S_S^{T_R=475})}{0.7169}$$

$$m_S = \frac{\log(0.5262) - \log(0.2371)}{0.7169} = 0.4830$$

$$\log(b_S) = 4.7338 \log(S_S^{T_R=475}) - 3.7338 \log(S_S^{T_R=2475})$$

$$\log(b_S) = 4.7338 \log(0.2371) - 3.7338 \log(0.5262)$$

$$\log(b_S) = -1.9178$$

$$b_S = 10^{\log(b_S)} = 0.0121$$

Therefore

$$S_S^{T_R=1000} = 0.0121(1000)^{0.4830}$$
$$S_S^{T_R=1000} = 0.3397$$

For the spectral acceleration at 1 second:

$$m_1 = \frac{\log(S_1^{T_R=2475}) - \log(S_1^{T_R=475})}{0.7169}$$
$$m_1 = \frac{\log(0.2231) - \log(0.0987)}{0.7169} = 0.4941$$

$$\log(b_1) = 4.7338\log(S_1^{T_R=475}) - 3.7338\log(S_1^{T_R=2475})$$
$$\log(b_1) = 4.7338\log(0.0987) - 3.7338\log(0.2231)$$
$$\log(b_1) = -2.3281$$
$$b_1 = 10^{\log(b_1)} = 0.0047$$

Therefore

$$S_1^{T_R=1000} = 0.0047(1000)^{0.4941}$$
$$S_1^{T_R=1000} = 0.1426$$

e. Construct standard spectra

Adjust for site conditions

$$\overline{S}_S = F_a S_S^{T_R=1000} = (1.00)0.3397$$
$$\overline{S}_S = 0.3397$$
$$\overline{S}_1 = F_v S_1^{T_R=1000} = (1.00)0.1426$$
$$\overline{S}_1 = 0.1426$$

Compute periods defining the amplification plateau

$$T_S = \frac{B_S \overline{S}_1}{B_1 \overline{S}_S} = \frac{(1.06)0.1426}{(1.04)0.3397} = 0.43\,\text{sec}$$
$$T_0 = \frac{1}{5}T_S = \frac{0.43}{5} = 0.086\,\text{sec}$$

Define the horizontal standard spectrum

$$
S_A[g] = \begin{cases} 2.1573\,T + 0.1359 & \text{for } 0 \le T < 0.086\,\text{sec} \\ 0.3205 & \text{for } 0.086\,\text{sec} \le T < 0.43\,\text{sec} \\ 0.1371/T & \text{for } 0.43\,\text{sec} \le T \end{cases}
$$

Therefore, the horizontal response spectrum exhibits a maximum value of 0.3205 g between the periods of 0.086 and 0.43 seconds. A source-to-site distance of 25 km is assumed to define the vertical standard spectrum. Considering the corresponding conversion factor $F_V = 0.84$, the periods defining the vertical amplification plateau are given by

$$
T_{SV} = \frac{0.67}{F_V} T_S = \frac{0.67}{0.84} 0.43 = 0.34\,\text{sec}
$$

Define the vertical standard spectrum

$$
S_{AV}[g] = \begin{cases} 0.84\,S_A & \text{for } 0 \le T < 0.34\,\text{sec} \\ 0.0919/T & \text{for } 0.34\,\text{sec} \le T \end{cases}
$$

The vertical response spectrum shows a maximum value of 0.2692 g between the periods of 0.086 and 0.34 seconds. The following figure displays both horizontal and vertical standard response spectra:
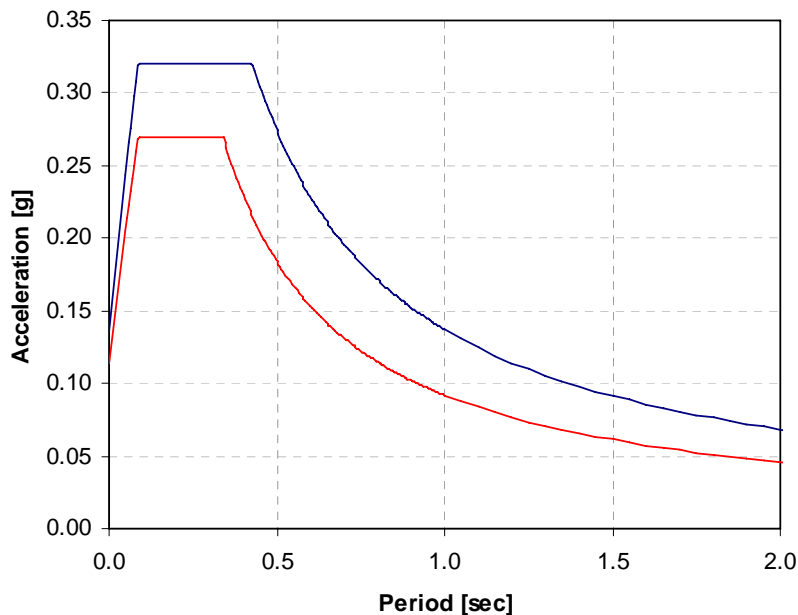
Figure C-2. Standard horizontal (blue) and vertical (red) acceleration response spectra for example C-2

C-3. Example problem 3

This problem will demonstrate the determination of Effective Peak Ground Acceleration (EPGA) values for different return periods (100, 500, 1000, 2000, 5000, and 10000 years).

a. Project data

Name: Montgomery Point Lock and Dam
Location: AR
Latitude: 33.9 deg
Longitude: -91.1 deg
Site Conditions: Stiff soil (site class D)

b. Mapped spectral values

Accessing the USGS web site with the appropriate site location information, we obtain the corresponding PGA and spectral acceleration values corresponding to 0.2 seconds and 1 second:

	10% PE in 50 years	**2% PE in 50 years**
PGA [g]	0.0612	0.2008
S_S [g]	0.1417	0.4562
S_1 [g]	0.0452	0.1553

c. Compute short-period spectral values for specified return periods

For the spectral acceleration at 0.2 seconds:

$$m_S = \frac{\log(S_S^{T_R=2475}) - \log(S_S^{T_R=475})}{0.7169}$$

$$m_S = \frac{\log(0.4562) - \log(0.1417)}{0.7169} = 0.7083$$

$$\log(b_S) = 4.7338\log(S_S^{T_R=475}) - 3.7338\log(S_S^{T_R=2475})$$

$$\log(b_S) = 4.7338\log(0.1417) - 3.7338\log(0.4562)$$

$$\log(b_S) = -2.7446$$

$$b_S = 10^{\log(b_S)} = 0.0018$$

Therefore, the spectral acceleration values can be approximated as follows:

$$S_S^{T_R} = 0.0018(T_R)^{0.7083}$$

d. Determine effective peak ground acceleration values

To adjust for site conditions, we determine the site coefficients based on the short-period spectral accelerations corresponding to the different return periods:

Return Period [years]	S_s [g]	F_a	$\overline{S}_s$ [g]
100	0.0470	1.60	0.0752
500	0.1469	1.60	0.2351
1000	0.2401	1.60	0.3841
2000	0.3923	1.49	0.5830
5000	0.7507	1.20	0.9006
10000	1.2266	1.01	1.2381

Finally, the EPGA values for the required return periods can be tabulated as follows:

Return Period [years]	EPGA [g]	Site Specific PGA [g]
100	0.0301	0.0180
500	0.0940	0.0390
1000	0.1537	0.0520
2000	0.2332	0.0700
5000	0.3603	0.1100
10000	0.4952	---

For the same return periods, the table also shows the associated PGA values obtained by a site-specific probabilistic seismic hazard study as described in EM 1110-2-6050 (Appendix G, Example 3). The results show that the computed EPGA values are much larger than the site-specific PGA values. The local site condition (deep soil site) was included in the site-specific study by employing special ground motion attenuation relationships for deep-soil-site motions. This site condition was consistently taken into account in the determination of the EPGA values by using the corresponding site coefficient F_a .

SECTION II: Use of Computer Program DEQAS-R

C-4. Solution of example problem C-1 using the program DEQAS-R

a. Start the program
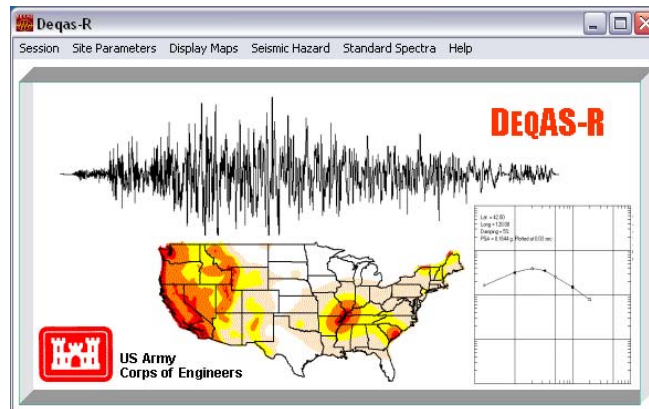
b. Enter site location and site class
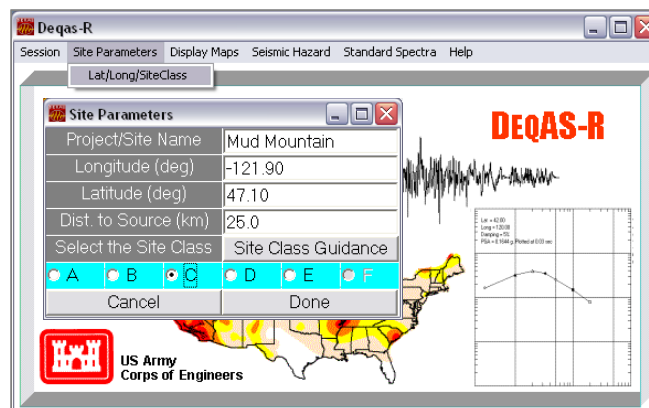
c. Define return period
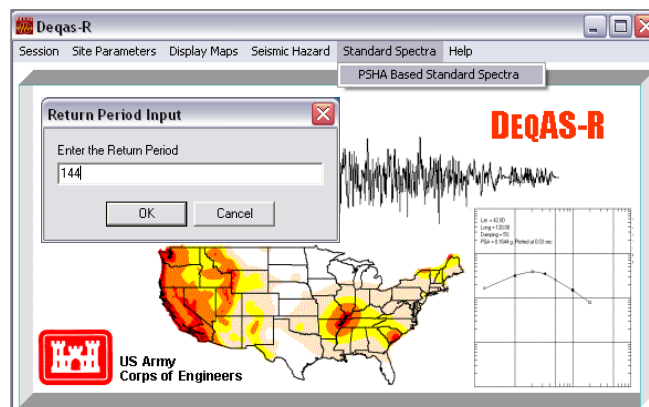
d. Plot horizontal standard spectrum
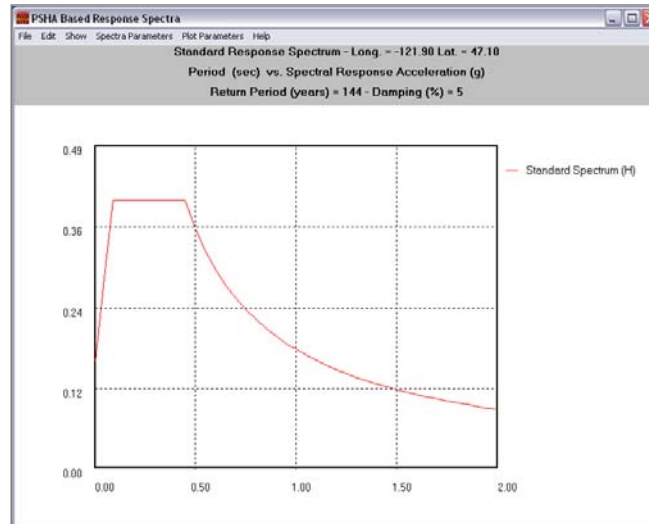
Figure C-3. Standard horizontal acceleration response spectrum for example C-1 obtained using the program DEQAS-R

e. Discussion

(1) As shown in Figure C-3, the program plots the horizontal standard spectrum for the required location, site class and return period. If required, the spectral data can be saved in a text file for future use. The spectrum shows an amplification plateau that extends between the periods of 0.09 and 0.44 seconds, with a maximum spectral value of 0.4043 g. This value is about 88% of the maximum spectral acceleration obtained with the previous procedure (0.4578 g).

(2) By taking advantage of the fact that the program can also display the 0.2- and 1.0-second period seismic hazard curves for the specified location, an explanation for the difference in the spectral results can be found by examining these curves. These hazard curves are shown in Figure B-2. These two curves represent the actual seismic hazard data used by the program to compute the spectral values S_S and S_1 that are used in the construction of the standard response spectrum. To obtain the values corresponding to the specified return period (e.g., $S_S^{T_R=144}$ and $S_1^{T_R=144}$), the program performs a linear log-log interpolation using the two closest available values. This is a "local" interpolation scheme which is adopted to represent a return period interval in the vicinity of the available data points. The resulting values may be different from those obtained based on direct interpolation of the data available from the USGS website, which offers only two spectral acceleration values (for return periods of 475 and 2,475 years). The values in this case are then based on a "global" 2-point interpolation that is used to represent the entire return period range.
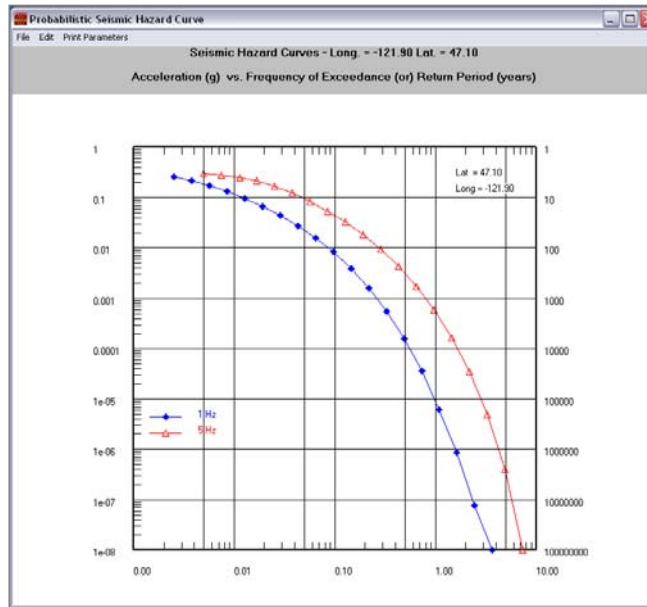
**Figure C-4. Seismic hazard curves for example C-1 obtained
using the program DEQAS-R**

(3) Figure C-5 depicts this situation for the case of the S_S spectral acceleration. The figure shows that the 144-year value (0.3815 g) computed based on the values for return periods of 475 and 2475 years is different from the 144-year value (0.3369 g) determined by the **DEQAS-R** program by interpolating the two closest data points in the database (which for this case correspond to approximate return periods of 107 and 232 years).
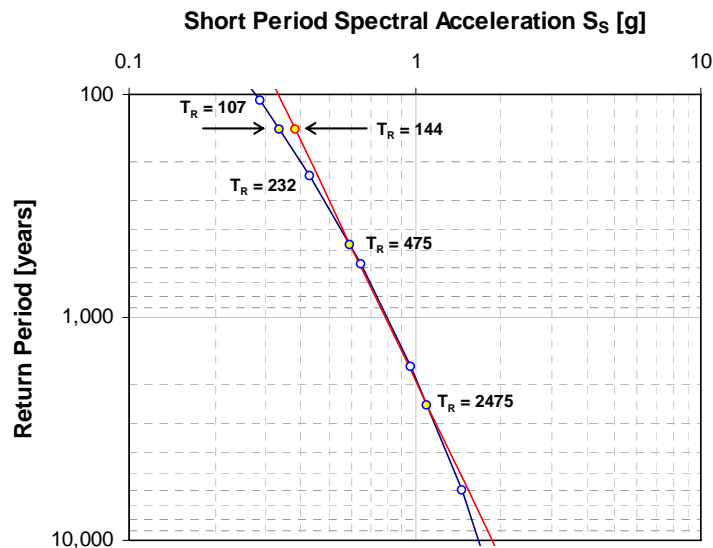
**Figure C-5. Comparison of 0.2-second seismic hazard curves for example C-1
obtained by local (red) and global (blue) log-log interpolation**

(4) Figure C-6 shows the same situation for the S_1 spectral acceleration. The 144-year value (0.1216 g) computed based on the values for return periods of 475 and 2475 years is different from the 144-year value (0.1060 g) determined by the **DEQAS-R** program by interpolating the two closest data points available in the database (which for this case correspond to approximate return periods of 120 and 253 years).

1-Second Spectral Acceleration S$_1$ [g]
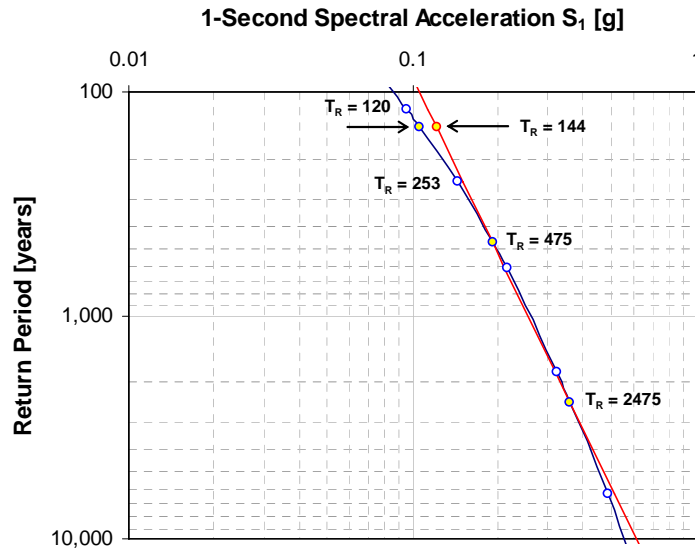
Figure C-6. Comparison of 1-second seismic hazard curves for example C-1 obtained by local (red) and global (blue) log-log interpolation

C-5. Solution of example problem C-2 using the program DEQAS-R

a. Start the program
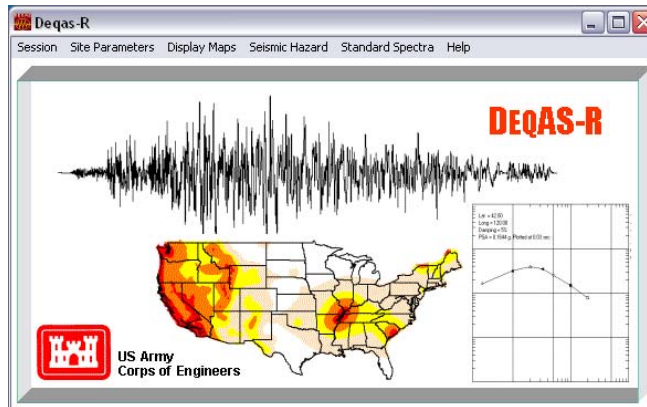
b. Enter site location and site class
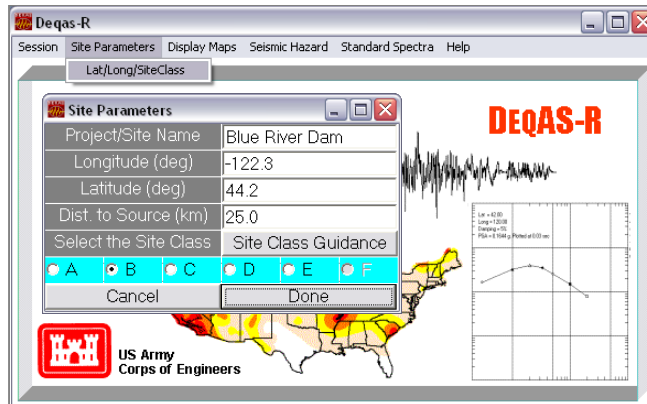
c. Define return period
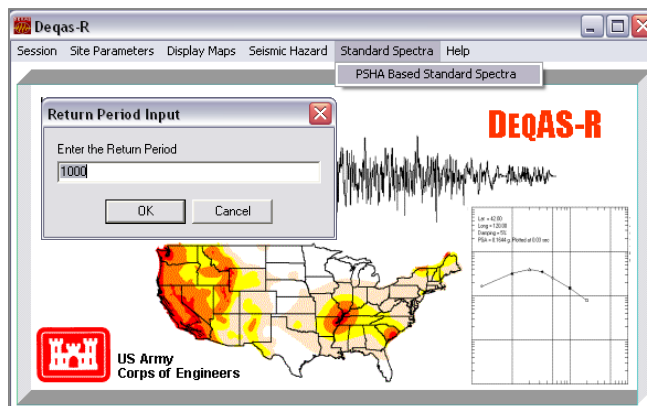
d. Adjust damping level
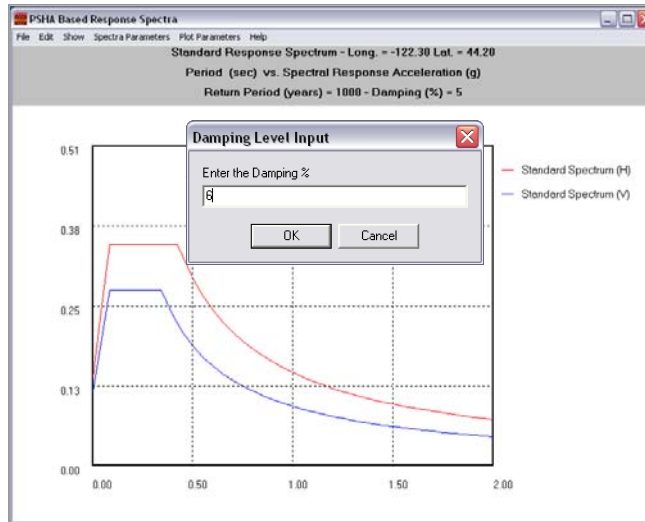
e. Plot horizontal and vertical response spectra
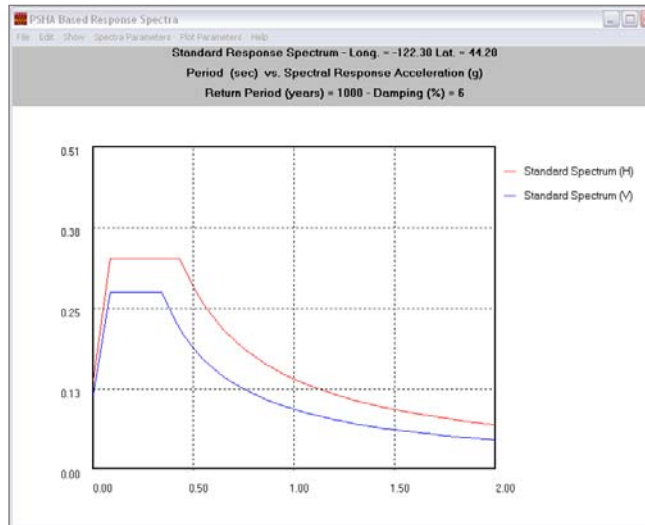
**Figure C-7. Standard horizontal and vertical response spectra for example C-2
obtained using the program DEQAS-R**

f. Discussion

As shown in Figure C-7, the horizontal response spectrum computed by the program exhibits a maximum value of 0.3313 g between the periods of 0.086 and 0.43 seconds. The vertical response spectrum shows a maximum spectral value of 0.2783 g between the periods of 0.086 and 0.34 seconds. Therefore, these maximum horizontal and vertical spectral values represent an increase of about 3% with respect to those values previously computed manually in Section I.

C-6. Solution of example problem C-3 using the program DEQAS-R

a. Start the program
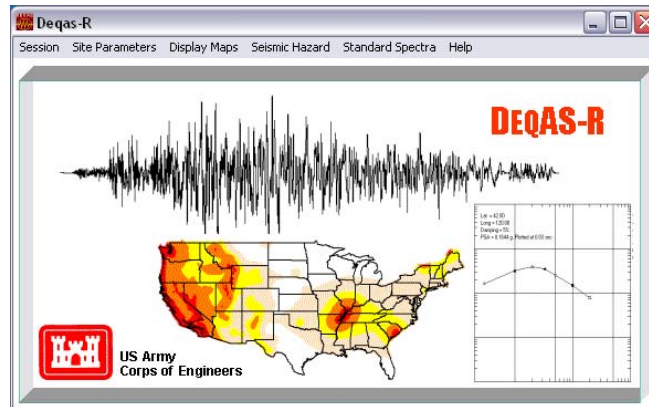
b. Enter site location and site class
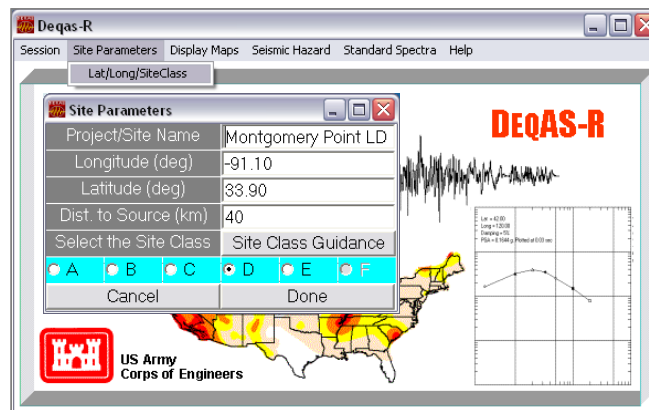
c. Enter required return periods
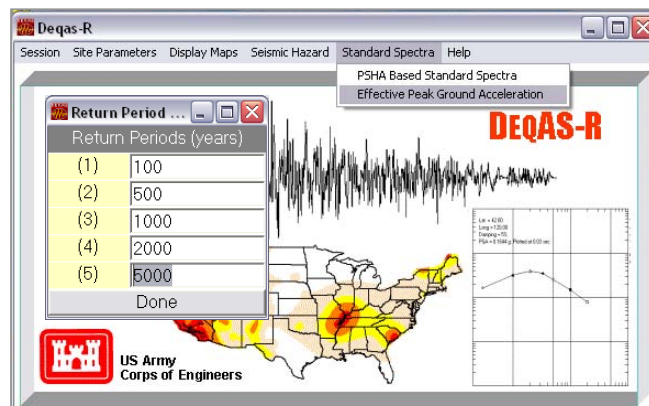
d.   Obtain EPGA values
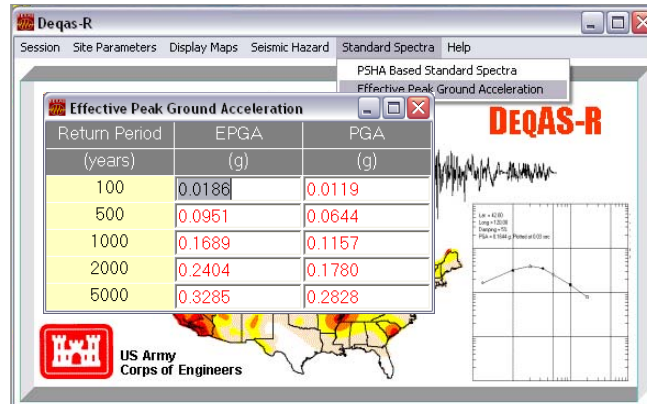
e.   Discussion

(1) The EPGA values computed by the program DEQAS-R are based on a more accurate interpolation of the data in the database, and this explains the differences between these results and those previously obtained in Section I.

(2) For reference purposes, the program also outputs the PGA values corresponding to the required return periods. However, it must be considered that these PGA values are only available for the default site class (firm rock). On the other hand, the EPGA values are calculated as a function of the short-period spectral value modified by site conditions.

Appendix D
Pushover Analysis of Intake Towers

D-1. Introduction

a. This appendix provides an example pushover analysis for a free-standing intake tower that has been analyzed previously to illustrate seismic design procedures in EM 1110-2-2400, response-spectrum mode superposition method in EM 1110-2-6050, and the linear time-history dynamic analysis methodology in EM 1110-2-6051. In this appendix the same free-standing intake tower is used to illustrate the nonlinear static pushover analysis procedures.

b. The nonlinear static pushover analysis or simply pushover analysis is carried out to assess damage vulnerability of structures. A pushover procedure is a series of nonlinear static analyses carried out to develop a capacity curve for the structure. With increasing the magnitude of loading during the pushover analysis, the structural members undergo nonlinear response, and thus weak links and failure modes of the structure are found. The lateral loads representing inertia forces in an earthquake are increased until a target displacement is exceeded or the structure collapses. The target displacement represents the maximum displacement that the structure would likely experience during the design earthquake. The results of pushover analysis are summarized as a plot of lateral load vs. displacement, from which the actual load capacity and ultimate displacement of the structure can be determined.

D-2. Purpose and Objectives

The purpose of this example is to illustrate application of the nonlinear static procedures to pushover analysis of free-standing intake towers. The objectives of the example are:

 a. To compute section capacities of the tower using various procedures.

 b. To obtain pushover curve showing yielding, cracking, and ultimate displacement of the intake tower.

 c. To identify the sequence of plastic hinging and potential failure modes.

D-3. Scope

The scope of this example includes the following:

 a. Idealization of the intake tower using various frame elements that account for effects of material inelastic response.

 b. Examination of various modeling techniques to identify their strengths and shortcomings.

 c. Conducting pushover analyses to obtain capacity curves for various models.

 d. Evaluation of results to assess inelastic response behavior and ultimate displacement capacity of the tower.

D-4. Assumptions

The following simplifying assumptions were made to reduce the calculation efforts and to focus on more important aspects of the analysis procedure:

   a. Effects of axial load is not considered.

   b. Axial force-bending moment (i.e. P-M_x-M_y) interaction is not considered.

   c. P-Δ effect is not considered.

   d. Shear failure is not considered and tower is therefore assumed to fail in flexure.

D-5. Description of Tower

   a. Tower Geometry. The intake tower used in this example is described in EM 1110-2-2400. It is a freestanding tower with a height of 60.96 m (200 ft). The tower cross sections vary from 14.63 m %11.28 m (48 ft % 37ft) at the base to 13.41 m % 8.84 m (44 ft % 29 ft) at the top in five steps. The section thicknesses vary from 1.83 m (6 ft) at the base to 0.61 m (2 ft) at the top of the tower. Figure D-1 shows upstream and side elevation views of such a tower. The tower has a 0.61-m- (2.0-ft-) thick concrete slab at the top and a heavy 1.83-m- (6.0-ft-) thick slab at its base. The unit weight of the concrete (γ_{conc}) is 2,403 kg/m^3 (150 lb/ft^3).
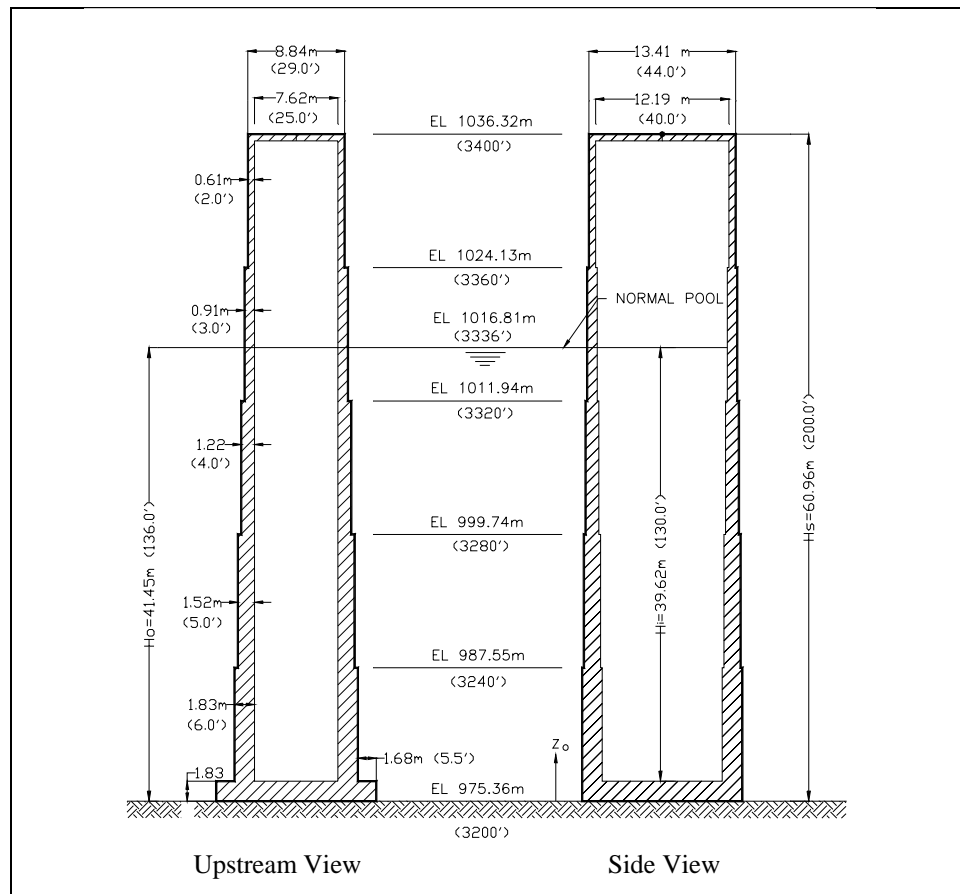
Figure D-1. Example Intake Tower

b. Material and section properties. Table D-1 below summarizes the material properties used for the concrete and reinforcing steel. The concrete is assumed to have a compressive strength of 20.7 MPa (3,000 psi) with an ultimate strain of 0.3 percent. The assumed yield strength and ultimate strain for the reinforcing steel are 413.69 MPa (60 ksi) and 5%, respectively. The stress-strain relationship for the concrete and reinforcing steel are discussed later as part of the reinforced concrete fiber element in Paragraph D-8*d*(4). Figure D-2 shows the geometry and reinforcement arrangement at the bottom section of the tower. There is one layer of #11 vertical bars at 30.48-cm (12-inch) spacing along the faces of each wall. Each reinforcement layer is made of 36 bars along the short axis and 47 bars along the long axis of the tower. The section properties including cross-section area, moment of inertia, nominal moment, and cracking moment for pushing along the longitudinal (x) and transverse (y) directions are listed in Table D-2.

Table D-1. Assumed material properties

Parameter		Value	
		Metric Units	English Units
Re-bar Material Properties			
Modulus of Elasisity	(E_s)	199,947.95 MPa	29,000.00 ksi
Specified Yield Strength	(f_y)	413.69 MPa	60.00 ksi
Strain Hardening			0.80 %
Steel Ultimate Stress		517.11	75.00 ksi
Ultimate Strain Hardening			5.00 %
Concrete Matrial Properties			
Modulus of Elasisity	(E_c)	21,525.43 MPa	3,122.00 ksi
Concrete Compressive Strength	(f'_c)	20.68 MPa	3.00 ksi
Modulus of Rupture	(f_r)	2.83 MPa	0.41 ksi
Concrete Ultimate Strain	(ε_c)		0.30 %
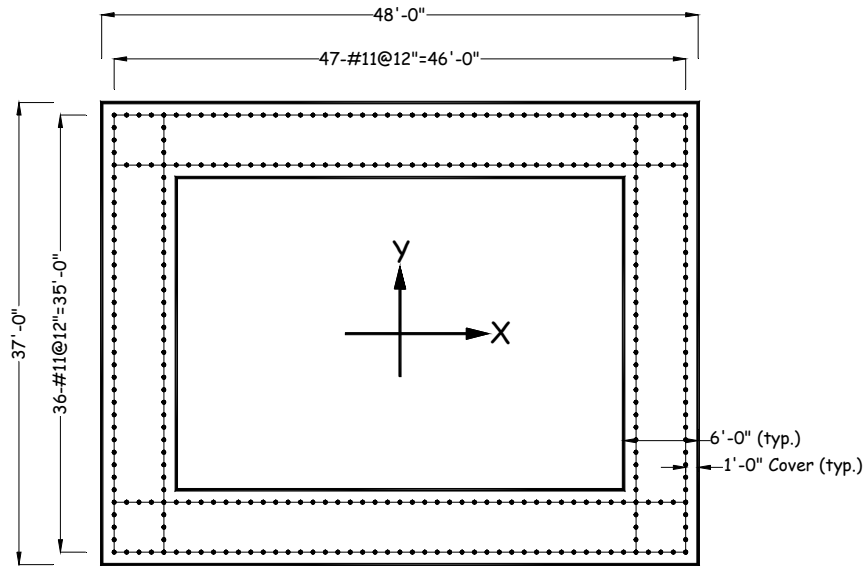
Figure D-2. Geometry and re-bar arrangement at base section of tower

Table D-2. Calculated section properties of the base section shown on Figure 1

For Pushing in X-X direction			
Parameter		Value	
		English Units	Metric Units
Width	(b)	37.00 ft	11.28 m
Depth	(h)	48.00 ft	14.63 m
Cross Section Area	(A)	876.00 ft^2	81.38 m^2
Moment of Inertia	(I_{yy})	243,792 ft^4	2,104.16 m^4
Nominal Moment	(M_{ny})	718,814 k-ft	974.58 N-m
Cracking Moment	(M_{cr})	620,900 k-ft	841.83 N-m
For Pushing in Y-Y direction			
Parameter		Value	
		English Units	Metric Units
Width	(b)	48.00 ft	14.63 m
Depth	(h)	37.00 ft	11.28 m
Cross Section Area	(A)	876.00 ft^2	81.38 m^2
Moment of Inertia	(I_{xx})	155,737 ft^4	1344.16 m^4
Nominal Moment	(M_{nx})	518,879 k-ft	703.51 N-m
Cracking Moment	(M_{cr})	507,900 k-ft	688.62 N-m

D-6. Selection of Analysis Procedures

The following procedures were considered for nonlinear static analysis:

a. Simplified displacement-based analysis. This method involves hand calculations that can be effectively used for the analysis of relatively simple structures such as freestanding towers and bridge piers.

b. Pushover analysis. The pushover analysis is conducted using a load controlled or displacement controlled procedure. Both procedures involve intense calculations requiring the use of computer programs with nonlinear analysis capabilities.

(1) Load-controlled procedure involves incremental application of a monotonic load to the structure until the maximum load is reached or the structure collapses, whichever occurs first. Force control should be used when the magnitude of load is known (such as gravity load), and the structure is expected to support the load.

(2) Displacement-controlled procedure involves incremental application of a monotonic load until the control displacement is reached a pre-specified value or the structure collapses, whichever comes first. Displacement control is used when the value of the applied load is not known in advance, or when the structure is expected to lose strength. Since the final value of earthquake load can not be determined precisely in advance, the displacement-controlled method is employed in this example.

D-7. Simplified displacement-based analysis

Simplified displacement-based analysis for reinforced concrete structures is described in the reference (COE 2001).

When the nominal moment capacity (M_N) is less than 1.2 times the cracking moment (M_{cr}), the plastic hinge length needed for estimation of rotational capacity can be obtained from:

$$l_p = 0.30 f_y (d_b)$$ (ksi units)

where f_y is yield strength of the reinforcing steel in ksi and d_b is diameter of the reinforcing steel in inches. For the example tower the ratio of nominal moment to cracking moment for both the x and y directions are less than 1.2:

$$\frac{M_{Ny}}{M_{cry}} = \frac{718,814}{620,900} = 1.16 < 1.20$$

and

$$\frac{M_{Nx}}{M_{crx}} = \frac{518,737}{507,900} = 1.02 < 1.20$$

Thus the plastic hinge length can be obtained as follows:

$$l_p = 0.30 f_y(d_b) = 0.30(60.0)(1.56) = 28.08 \; in = 2.34 \; ft$$

The ultimate rotational capacity is estimated from:

$$\theta_u = \phi_u(l_p) = 0.0003125 \cdot (2.34) = 0.000731(rad) = 0.042(\deg)$$

The ultimate displacement capacity in the strong axis direction x-x is estimated using:

$$\delta_u = \frac{11}{40}\phi_y l^2 + (\phi_u - \phi_y)l_p\left(l - \frac{l_p}{l}\right) = \frac{11}{40}(0.0000539)(200)^2 +$$

$$(0.001302 - 0.0000539)(2.34)\left(200 - \frac{2.34}{200}\right)$$

$$\delta_u = 1.18 \; ft = 14.16 \; in$$

Where:

$$\phi_y = \frac{\varepsilon_y}{0.8\,h} = \frac{0.00207}{0.8(48)} = 0.0000539$$

and

$$\phi_u = \frac{\varepsilon_u}{0.8\,h} = \frac{0.05}{0.8(48)} = 0.001302$$

The ultimate displacement ductility is given by:

$$\mu = 1 + 3.64\left(\frac{\phi_u}{\phi_y} - 1\right)\frac{l_p}{l}\left(1 - 0.5\frac{l_p}{l}\right) = 1 + 3.64 \cdot (24.15 - 1) \cdot \left(\frac{2.34}{200}\right) \cdot \left(1 - 0.5 \cdot \frac{2.34}{200}\right) = 1.98 \approx 2$$

Where:

$$\frac{\phi_u}{\phi_y} = \frac{0.05}{0.00207} = 24.15$$

D-8. Nonlinear Static Procedures Using Computer Program (Pushover)

a. Various computer programs with nonlinear analysis capabilities can be used to perform a pushover analysis. In this example, SAP2000 (1997) and DRAIN-2DX (1994) programs are used to illustrate the displacement-controlled pushover analysis. In each case, a computer model of the tower is developed and subjected to appropriate lateral loads that are increased incrementally until a target displacement is reached or the tower collapses. The lateral load patterns and target displacements are described below.

b. Controlling Node, Lateral Load pattern and Target Displacement

(1) *Controlling node* is a node at which the displacement is computed and monitored. In this example Node 13 at the top of the tower is selected for this purpose (Figure D-3).

(2) *Lateral load pattern* should closely resemble the probable distribution of the earthquake loads. In this example, a load pattern proportional to the fundamental mode shape of the tower is selected. The lateral loads representing the seismic inertia forces are then obtained from production of the fundamental mode shape and the associated mass tributary.

(3) *Target displacement* of the controlling node shall be at least three times of the yield displacement. The yield displacement is the displacement associated with the first yielding of the reinforcing steel.

c. Pushover Analysis using SAP2000

(1) *Structural model.* The basic geometry and section properties defined in Paragraph D-5 are used to develop a SAP2000 model for the pushover analysis. The model is created like any other analysis, except that frame hinges are introduced to model nonlinear response. Plastic hinges are restricted to frame elements only, even though other types of elements can be present in the model. As shown in Figure D-3, the model consists of 13 nodal points and 12 frame elements. The model is fixed at the base nodal point, while other nodes are free with respect to translation and rotation. SAP2000 can handle for both the material nonlinearity and the geometric nonlinearity. As mentioned earlier only the material nonlinearity is considered in this example for simplicity reason and also because axial loads for intake towers are relatively small. The material nonlinearity is specified at discrete, user-defined hinges along the length of frame elements. Since concrete cracking and steel yielding tend to concentrate at the base of the tower, only a single hinge immediately above the bottom slab was included in the model. Figure D-3 provides two views of the model, an extruded view showing 3D geometry of the tower, and a frame view depicting the nodal points and frame elements.

(2) *Moment-rotation relationship.* For pushover analysis, moment-rotation relationship for plastic hinges should be defined. The default moment-rotation relationships available in SAP2000 have been developed for building structural members. They are generally not appropriate for the lightly reinforced hydraulic structures such as the example tower. For this reason the computer program "*M-Phi*" (Ehsani and Marine 1994) is used to develop a moment-curvature for the bottom section of the tower where the plastic hinges will occur (Figure D-2). Then the moment-rotation for the section is obtained by multiplying the curvature by a plastic hinge length. The plastic hinge length is assumed to be 2.34ft, the same as that estimated in the simplified displacement-based analysis in Section D-7. The estimated moment-rotation diagrams for the bottom section with respect to longitudinal (x) and transverse (y) axes of the

tower are shown in Figure D-4. Also shown on this figure are the nominal moments for comparison.
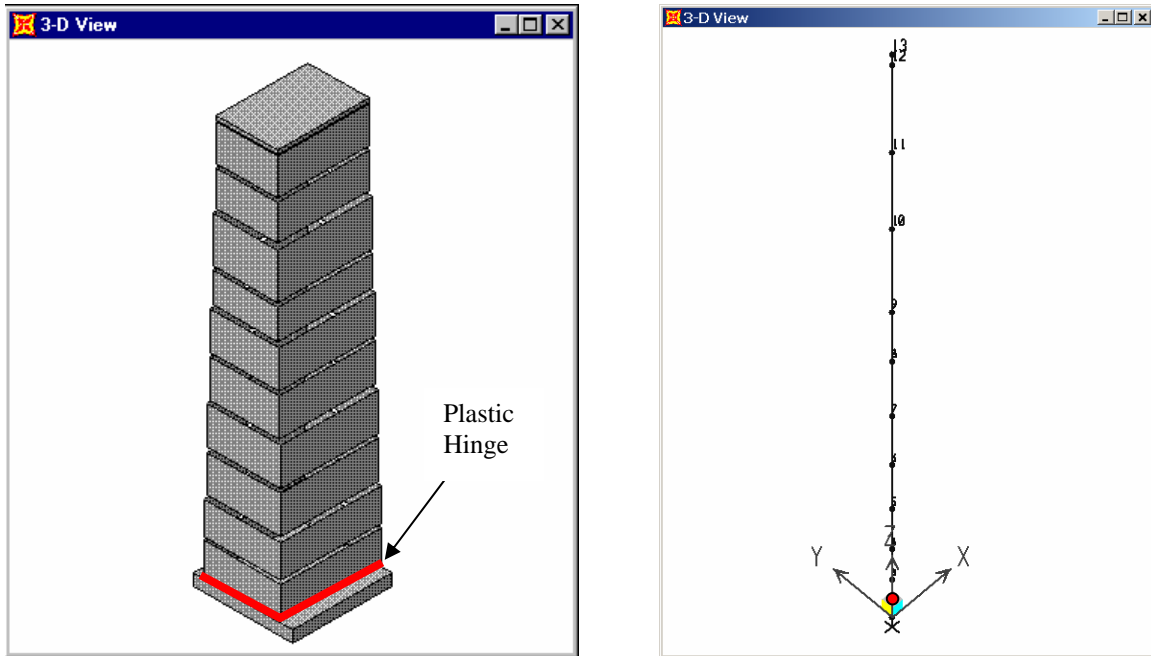
Figure D-3. 3-D view of the sample tower in SAP2000
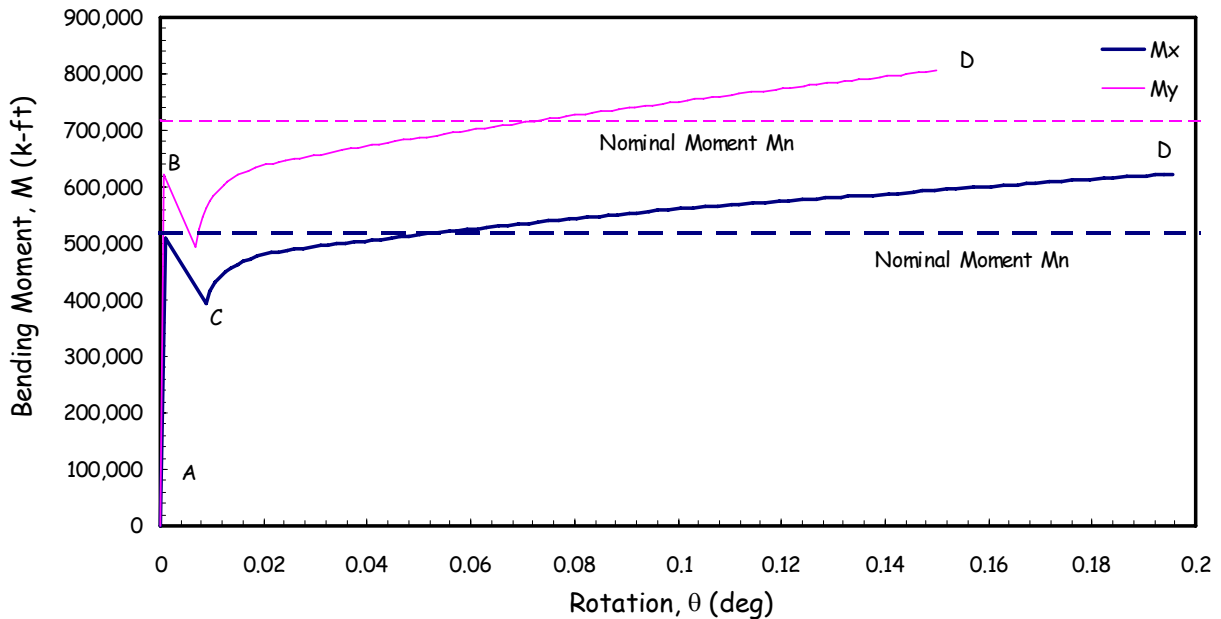
Figure D-4. Moment-rotation relationship for bottom section with l_p= 2.34ft

(3) *Plastic Hinge Properties*. The moment-rotation in Figure D-4 is idealized to define hinge properties for SAP2000 pushover analysis. SAP2000 allows only 4 points to define the hinge properties in accordance with NEHERP (1997). As such the estimated moment-rotation should be idealized according to this restriction. Figure D-5 is a normalized moment-rotation diagram

showing how the four basic points are picked to prepare input for SAP2000. For the lightly-reinforced example tower the ratio of nominal moment to cracking moment is close to one. The yielding moment in SAP2000 is therefore taken equal to the cracking moment obtained from the *M-Phi* analysis. This approach facilitates the identification of most critical steps in the plastic hinge development. However, for pre-existing cracks where the concrete has no initial tensile strength, points B and C in Figure D-5 could be lumped into one point corresponding to the yield point of re-bars. The selected Points A to E in Figure D-5 correspond to similar points in SAP2000 used to define the hinge properties, as shown in Figure D-6.
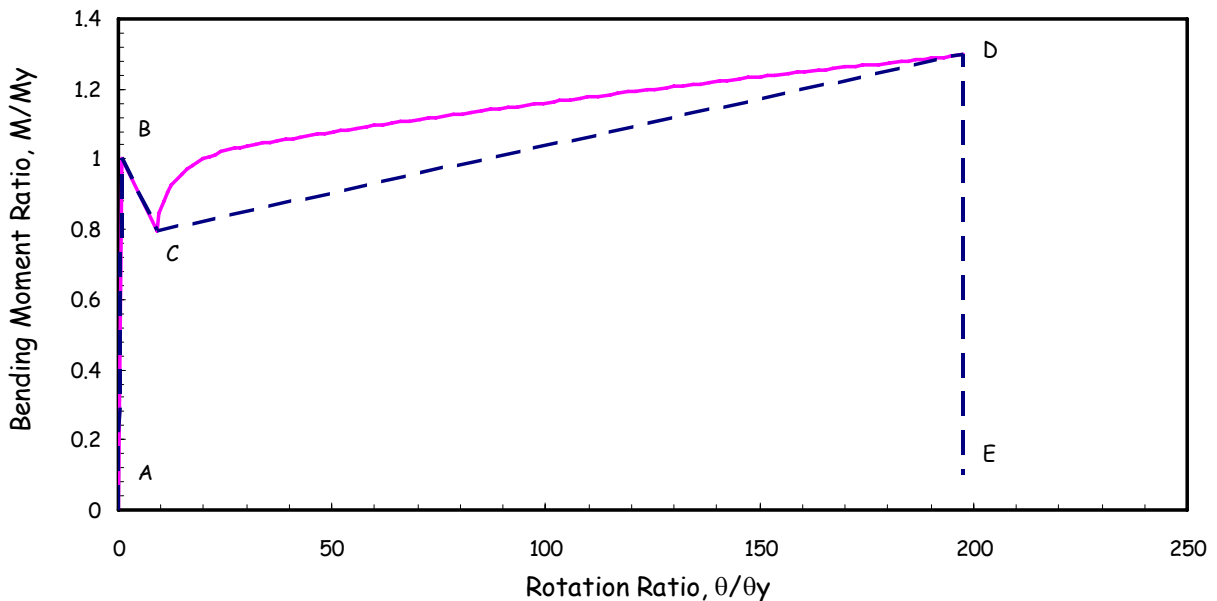
Figure D-5. Idealized moment-rotation diagram for SAP2000 input $(M_y\text{-}\theta_y)$

Point	Moment/Yield	Rotation/Yield
E-	-0.1	-200.7263
D-	-1.2272	-200.7263
C-	-0.7755	-9.0409
B-	-1	-1
A	0	0
B	1.	1.
C	0.7755	9.0409
D	1.2272	200.7263
E	0.1	200.7263

M_x vs. θ_x

Point	Moment/Yield	Rotation/Yield
E-	-0.1	-197.4979
D-	-1.2975	-197.4979
C-	-0.7977	-8.8868
B-	-1	-1
A	0	0
B	1.	1.
C	0.7977	8.8868
D	1.2975	197.4979
E	0.1	197.4979

M_y vs. θ_y
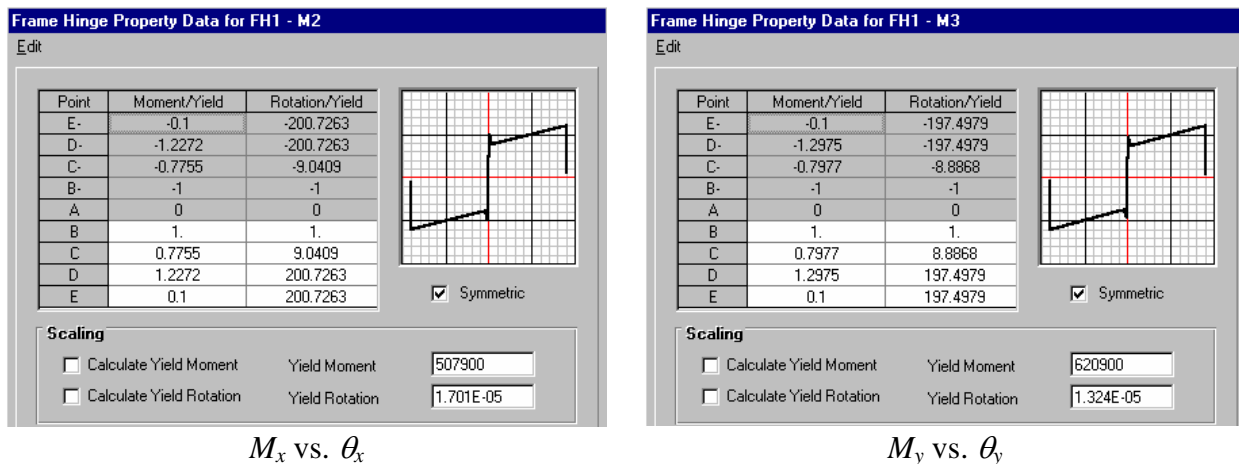
Figure D-6. Frame hinge property setup in SAP2000

(4) *Summary of SAP2000 pushover analysis.* In summary the following steps are required to perform static pushover analysis using SAP2000 program:

(a) Develop a structural model as you would do for any other analysis using frame and other types of elements. Assign material and section properties as needed.

(b) Perform the basic static analysis and, if desired, a linear-elastic analysis to check the model and compute mode shapes that may be used in defining pushover load patterns.

(c) Define hinge properties for frame elements corresponding to appropriate moment-rotation and force-displacement diagrams. Assign hinges at frame element ends or at any location along the element length, as appropriate.

(d) Define static pushover load cases (load pattern) that best describe the seismic inertia forces affecting the structure. For example, these may be taken proportional to the fundamental mode shape.

(e) Perform static pushover analysis.

(5) *Results of pushover analysis.* The results generated by SAP2000 include both pushover curves and capacity spectrum graphical representation. The pushover curves for the example tower are shown in upper graphs of Figure D-7 for loading along the longitudinal (x) and transverse (y) axes. The results for the capacity spectrum method for loading in the x and y directions are presented in the lower graphs of Figure D-7. The capacity spectrum method is an approximate nonlinear static procedure that predicts the inelastic displacement demand of the structure by combining structural capacity obtained from a pushover analysis with seismic demand represented by response spectra (ATC-40). In capacity spectrum method the demand response spectra and pushover curve are displayed in terms of spectral acceleration vs. spectral displacement. The resulting diagram shows a family of demand response spectra (shown as red) at various level of damping, a capacity spectrum (shown as black), and a family of straight lines representing constant periods (shown as green). The graph also includes a single demand spectrum with variable damping (shown as blue) whose intersection with the capacity spectrum gives the Performance Point, a point corresponding to the expected inelastic displacement demand of the structure. It is interesting to note that for this example the ratio of the inelastic displacement to the yield displacement is about 2, an indication that the performance of the tower beyond the performance point will be marginal because ductility ratio for the lightly reinforced example tower is expected not to exceed two.

(6) *Advantages of SAP2000 pushover analysis*

(a) Excellent pre-processing capabilities

(b) Built-in default plastic hinge properties for building structure based on FEMA-273 recommendations. However, user should define plastic hinge properties for lightly reinforced concrete structures

(c) Load patterns are easy to create

(d) Axial and shear failures along with bending failures can be considered, if desired

(e) Plastic hinges can be located at any point along the length of a frame element

(f) Rupture of the re-bar or the breakage of the connection is determined

(7) *Disadvantages of SAP2000 pushover analysis*

(a) Plastic hinges are available for beam elements only

(b) The approximate location of plastic hinges should be known prior to the analysis

(c) Nonlinear link elements behave linearly during the pushover analysis.
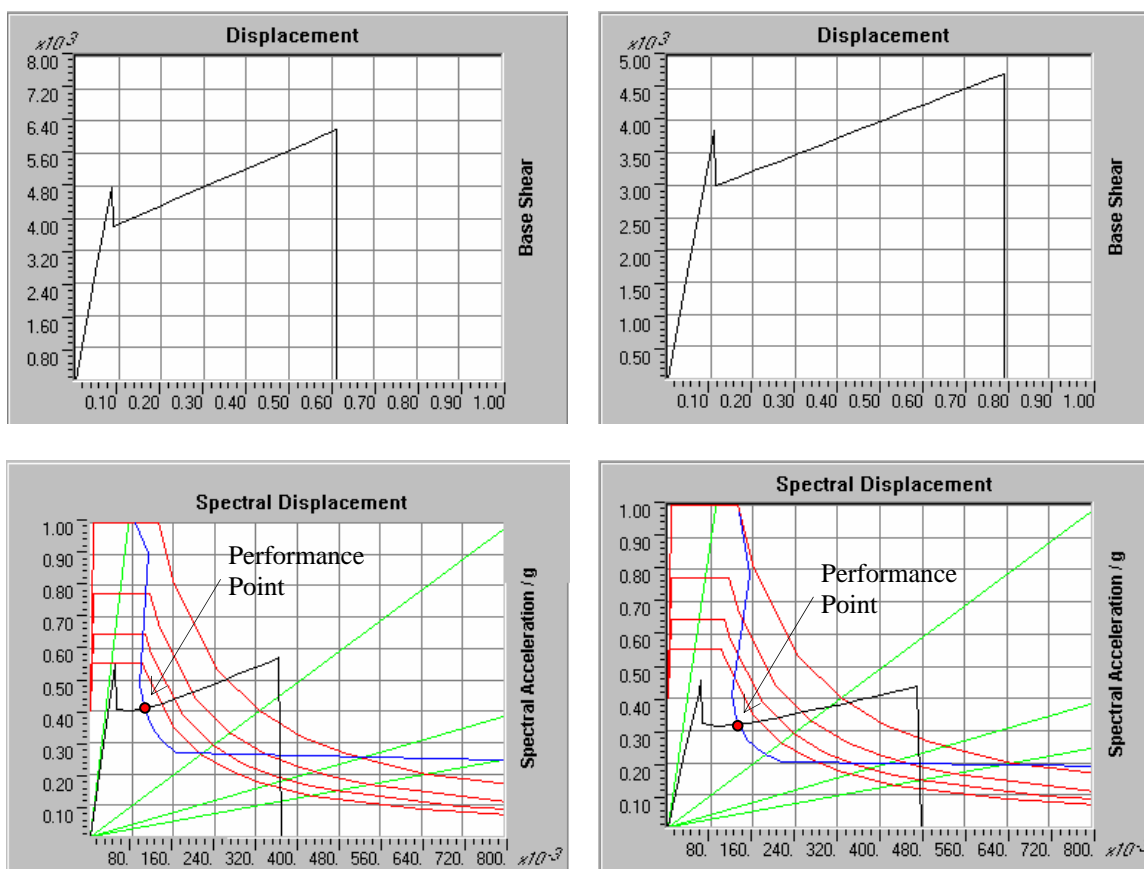
Pushing in X-X direction   Pushing in Y-Y direction

Figure D-7. Base shear vs. top displacement (above) and demand-capacity spectra (below)

d. Pushover Analysis using DRAIN-2DX program

(1) DRAIN-2DX is used to illustrate the application of a general nonlinear structural analysis program to push-over analysis. Three different element types are used for comparison purposes to show their strengths and shortcomings. These include: plastic hinge beam-column element (type 02), simple connection element (type 04), and fiber beam-column element (type 15). Each of these is briefly described below.

(2) *Plastic hinge beam-column element (type 02).* This element uses plastic hinge formation in bending to represent the nonlinear behavior. The plastic hinges are lumped at the element ends. The input for the plastic hinges includes an idealized bilinear moment-rotation relationship, which is defined by an initial stiffness, yield strength, and the post-yield strain hardening ratio. The idealized bilinear relationship may be obtained from approximation of an actual moment-rotation curve estimated using "*M-Phi*" program. Figure D-8 shows a possible approximation of the *M-Phi* moment-rotation curve, in which the yield strength B is obtained as an average of B and C and strain-hardening portion by connecting B to D. Also shown on this figure is the idealized moment-rotation relationship for SAP2000 program (i.e. ABCDE). The main advantage of the element is its ease of use, and disadvantages include:

(a) Element remains linear in axial and shear

(b) Plastic hinges form only at the element ends and have no length

(c) Since strain hardening is modeled by placing an additional parallel element, the stiffness of the parallel element should be estimated carefully so that it results in a correct strain-hardening ratio

(d) Requires moment-rotation relationship to be known prior to the analysis. In this example, it was obtained from "M-Phi" analysis.
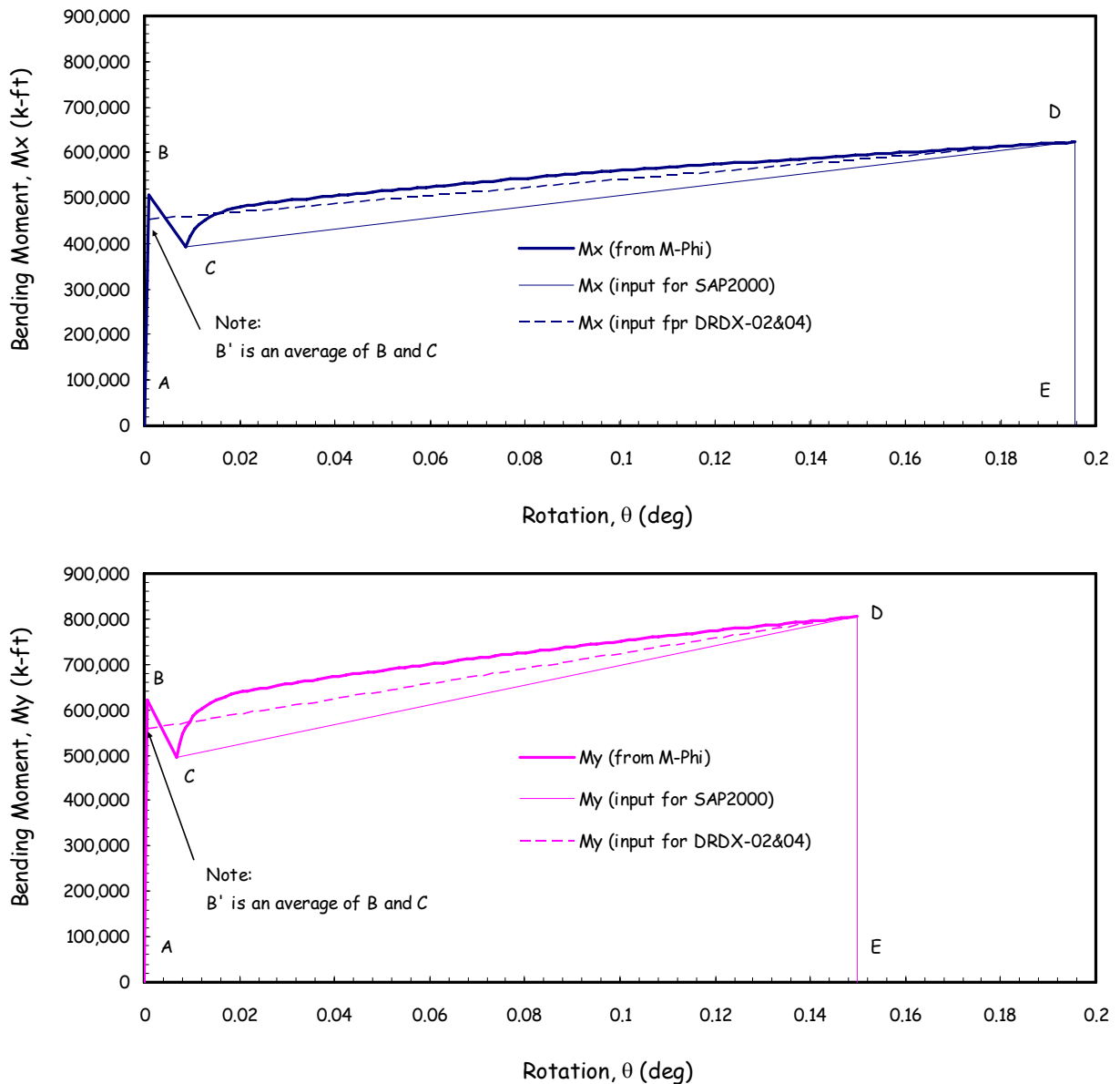
Figure D-8. Idealization and comparison of moment-rotation for SAP2000 and Drain-2D

(3) *Simple connection element (type 04).* Simple connection element allows the user to insert a nonlinear hinge and gap type connection at any location in the structure. The hinges can behave in tension, compression, bending, or shear deformation. One connection element for each type of deformation is permitted. The connection element is idealized by a bilinear relationship defined by an initial stiffness, yield force or moment, and the post yield stiffness ratio. The idealized bilinear moment-rotation for the connection element is obtained similar to that described for the Element Type 02 and shown in Figure D-8. The connection element has advantages of the ease of use and the ability to model axial and shear failure modes in addition to the bending. However, the use of additional elements with additional nodal points, prior knowledge about the possible locations and types of plastic hinges needed, as well as prior knowledge of the moment-rotation or force-displacement relationships are some of the drawbacks.

(4) *Fiber beam-column element (type 15).* Fiber beam-column element is more comprehensive than the Type-02 and Type-04 elements. The numerical models of the tower are developed by dividing the tower into a number of fiber elements. Each fiber element, in turn, is divided into several segments. The fiber element section consists of numerous fibers, each with its own material properties. In this example, the fiber element at the bottom of the tower where nonlinear behavior is expected is divided into a total of 95 fibers, 48 concrete fibers, and 47 steel fibers, as shown in Figure D-9. Note that for pushing in the y-direction fiber elements are developed parallel to the x-axis. Generally, more fibers increase the accuracy of the analysis; however the time of the computation also increases. Each fiber element is identified by its distance from the neutral axis and its section area. For example in Figure D-9 the hatched concrete fiber is located 6.55m (21'-6") from the y-axis and has a section area of 4.46 m^2 (48 ft^2). Similarly, the farthest steel fiber along the positive x-axis is located 7 m (23 ft) from the y-axis with a section area of 0.036 m^2 (0.39 ft^2) for the 36 #11 bars located at this distance. The basic fiber element used in this example assumes full bond between the concrete and the reinforcing steel. The material model for the fiber element consists of the uni-axial stress-strain relationship for the concrete and steel fibers. No force-displacement or moment-rotation relationship is needed. The assumed material properties for the concrete and steel are given in Table D-1 and the corresponding stress-strain curves are shown in Figure D-10. The pushover analysis proceeded with the displacement control and the tower model was subjected to increasing lateral load until a lateral displacement of 30.48 cm (1 foot) was achieved.
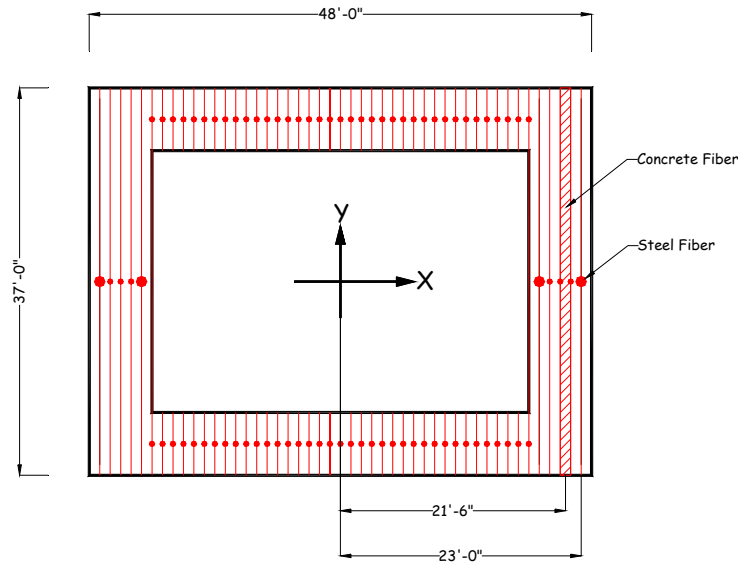
Figure D-9. Fiber element idealization of tower section for pushing in x direction
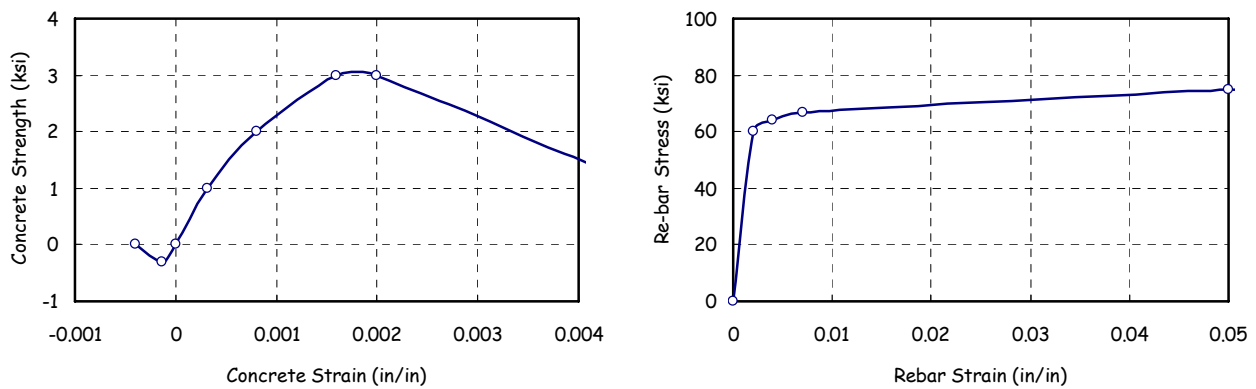
Figure D-10. Assumed stress-strain curves for concrete and reinforcing bar

(5) *Advantages of DRAIN-2DX fiber element (type 15)*

(a) Plastic hinges can be developed at any location in the element and plastic deformations are distributed along the element length and through the element cross-section.

(b) Plastic hinges have a final length.

(c) Re-bar bond-slippage and concrete crack opening and closing can be considered.

(d) Concrete strength degradation is considered.

(e) Reinforcing bar strength degradation can be considered.

(f) Concrete cracking, concrete crushing and re-bar yielding are identified in the output.

(g) No moment-rotation or force-displacement relationship is required.

(h) Developed strains and curvatures of the plastic hinge are directly output and can be plotted and evaluated.

(6) *Shortcomings of DRAIN-2DX fiber element*

(a) Relatively complicated to use.

(b) Very sensitive to material and section properties.

(c) Element remains linear in shear.

D-9. Evaluation and comparison of results

a. The results indicate that the inelastic response primarily occurs at the base of the tower. At this location the inelastic response starts with concrete tensile cracking followed by concrete crushing in compression prior to complete cracking of the section and yielding of steel reinforcements.

b. Moment Curvature. Figure D-11 shows moment-curvature relationships for bottom section of the tower computed for bending with respect to x and y axes. The figure compares moment-curvature relationships obtained from the *M-phi* and DRAIN-2D fiber element analyses. The figure also includes the idealized bending moment-curvature used in the DRAIN-2D analysis utilizing the connection element Type 04. The results for bending along x-axis (top graph of Figure D-11) indicate a cracking moment of about 687,400 kN-m (507,000 k-ft) for *M-Phi* and 650,793 kN-m (480,000 k-ft) for the fiber element. The concrete cracking is followed by a sudden drop in moment, but it is picked up as the load is fully transferred to the reinforcing bars. The moment drop caused by concrete cracking is more abrupt for the fiber element than it is for the *M-phi* analysis. Similarly, for bending with respect to y-axis, a cracking moment of about 840,608 kN-m (620,000 k-ft) was obtained from M-phi and slightly higher than 786,375 kN-m (580,000 k-ft) for the fiber element analysis (lower graph of Figure D-11). Again the moment drop due to concrete cracking is more abrupt for the fiber element than it is for the *M-phi* analysis. Overall there is a good agreement between the fiber element and *M-phi* moment-curvature analysis. The slight difference between the two models is due to the effects of shear and axial force inherent in the fiber model but not included in the *M-phi* calculation. The moment-curvature relationship in Figure D-11 is a measure of the local damage. The acceptance of local damage can be determined by comparing the induced inelastic curvature (or rotation) with the ultimate curvature capacity of the section. The ultimate curvature or rotation capacity of a section is computed according to the procedure outlined in Section D-7. Note that the moment-curvature in Figure D-11 was developed assuming that bond between the concrete and reinforcing steel will not fail and that post-elastic deformation of the steel can develop fully. If this bond is not strong and the bond slippage can occur, then the tower will fail prematurely before inelastic deformation of the reinforcing steel is fully realized. Bond slippage can be modeled to account for this failure mode but requires a special modeling technique which is beyond the scope of this example.

c. Pushover Curve. The global response of the tower as a plot of the base shear versus the lateral top displacement of the tower is shown in Figure D-12. In this figure the top graph is for loading along the strong x-axis and the lower graph for loading along the weak y-axis. These graphs summarize pushover curves for one SAP 2000 analysis and three DRAIN-2D analyses with three different types of elements. Generally, the results for all models are in good agreement up to completion of the concrete cracking and differ beyond this point where the

inelastic deformation and yielding of reinforcing steel begin. In general the fiber element is better suited for capturing the inelastic response behavior and provides a more accurate pushover curve than the other models. At about 25 mm (1 inch) of lateral displacement along the x-axis (top graph of Figure D-12), the tower fully cracks at the bottom on the tension side, followed by transfer of tensile forces from the cracked concrete to reinforcing bars and crushing of the concrete on the compression side. The concrete crushing and load transformation occur at a slightly lower strength and continue without resistance for a lateral displacement of about 15 mm (0.6 inches), at which point the strength increases as the reinforcing bars are fully engaged in carrying the load (plateau portion of the DRDX-15 curve in upper graph of Figure D-12). Note that the basic fiber element used in this example assumes full bond between the concrete and reinforcing bars, thus the pullout or bond slip observed in the laboratory tests (Dove, 1998) were not included in this example. If the bond slip had been considered. the resulting pushover curve would have shown strength deterioration rather than strength gain. The pushover curve for loading in the weak direction shows similar behavior, except that force demands are lower and displacements are higher. For this example, the performance of the tower is considered acceptable if displacement ductility is limited to 2.5, which translates into a global displacement of about 70 mm (2.75 inches) in the strong direction and 89 mm (3.5 inches) in the weak direction. Note that these ultimate displacements are much smaller than the 360 mm (14.16 in.) predicted by the simplified displacement method.
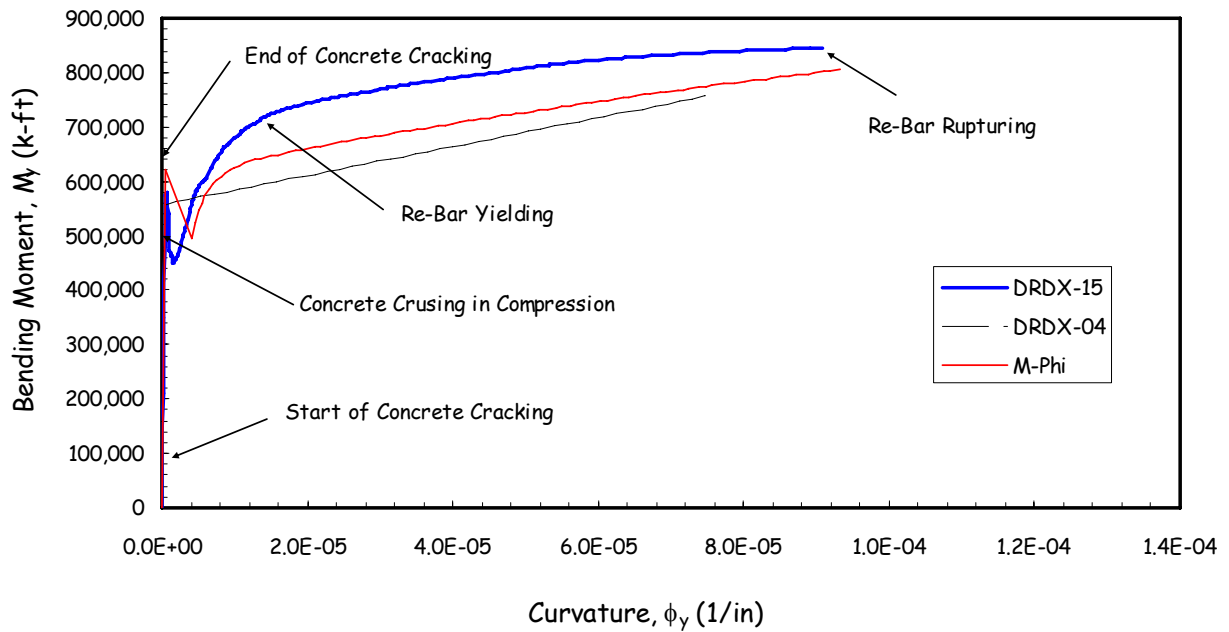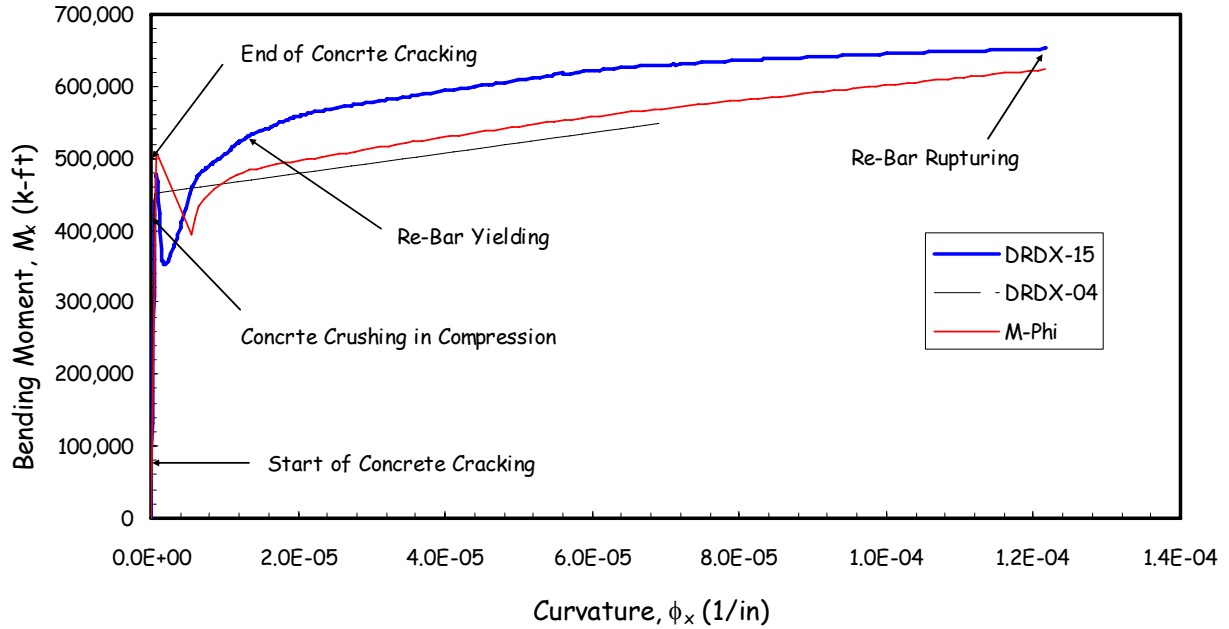
Figure D-11. Comparison of moment-curvature relationships obtained through different procedures
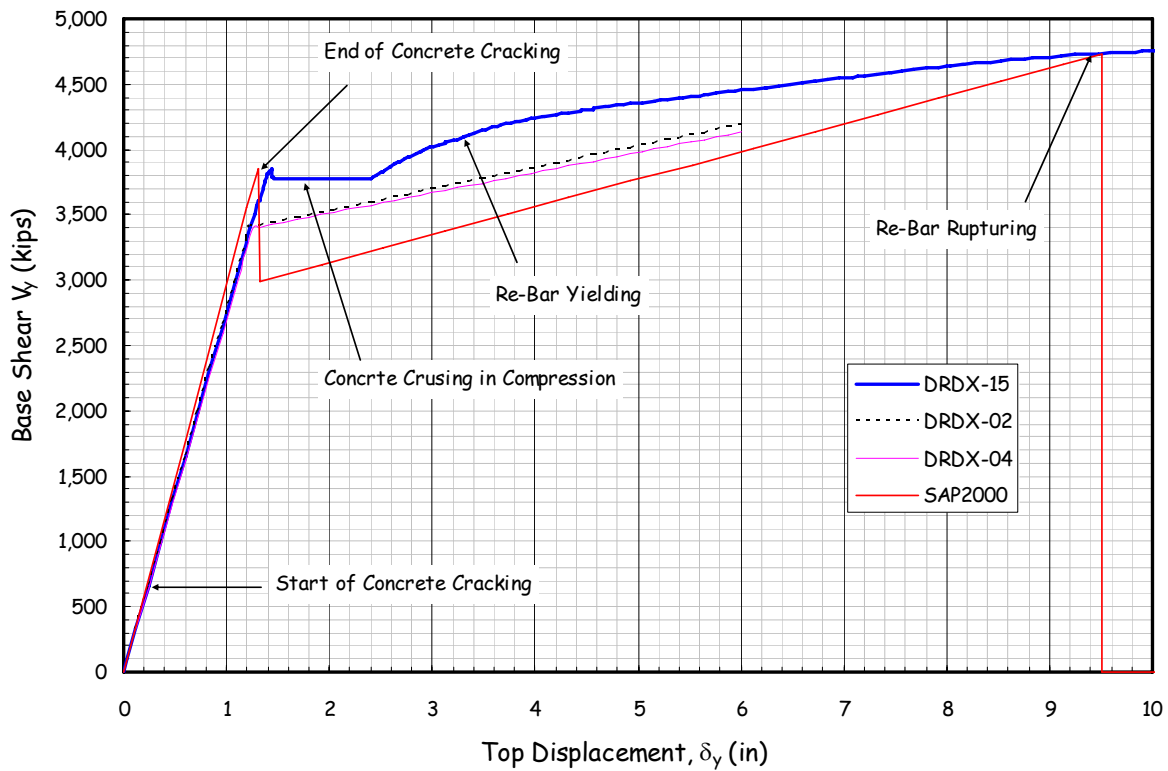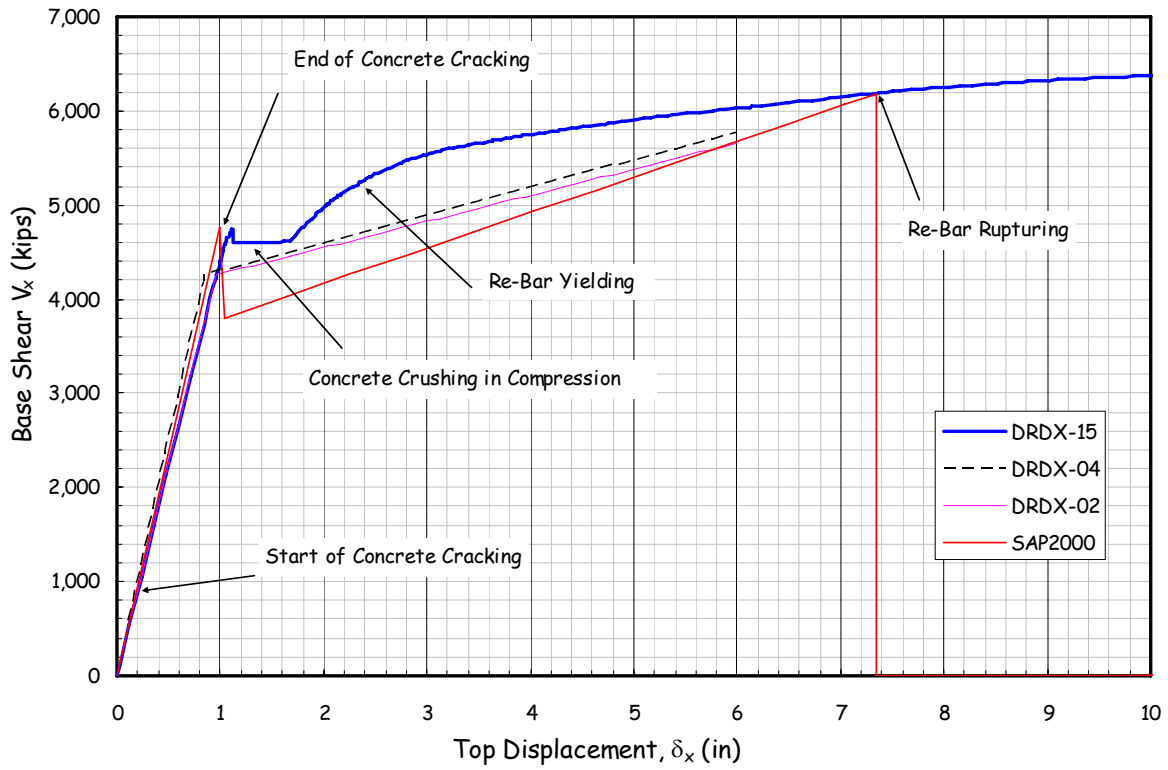
Figure D-12. Comparison of pushover curves from different procedures

D-10. Summary and Conclusions

Four different nonlinear models were used to illustrate nonlinear pushover analysis procedures for the example intake tower. They included a SAP2000 model with plastic-hinge frame element and three DRAIN-2DX models with lumped-plastic hinge (Type 02), connection hinge (Type 04), and fiber (Type 15) elements. The effectiveness and shortcomings of each model were briefly discussed. SAP2000 has excellent graphics capabilities and also provides spectrum capacity analysis. However, plastic hinges can be used only with frame elements and gap elements cannot be used in static analysis to model crack opening and separation. DRAIN-2DX element Type 02 permits plastic hinges to form at the end of beam-column elements only. The element's behavior is linear with respect to axial load and shear and nonlinear with respect to bending. The nonlinear behavior is represented by an idealized bilinear moment-rotation relationship, which is defined and input by the user. DRAIN-2DX element Type-04 allows the user to insert a nonlinear hinge and gap type connection at any location in the structure; the nonlinear hinges can model axial, bending, or shear deformation. Finally, DRAIN-2DX fiber element can be used that allows distributed plastic hinge formation at any location in the element. No moment-rotation or force-displacement relationship is required. Only uni-axial stress-strain curves for various materials are needed as the input. Overall, the fiber element provided more accurate results, except that strength degradation due to bond slip needs to be also modeled. The results showed that at a lateral displacement of about 25 to 35 mm (1 to 1.4 inches), the tower first fully cracks at the bottom on the tension side, followed by transfer of tensile forces from the cracked concrete to reinforcing bars and crushing of the concrete on the compression side. The concrete crushing and load transformation occur at a slightly lower strength and continue without resistance for a lateral displacement of about 15 to 25 mm (0.6 to 1 inch), at which point the strength increases if the concrete and reinforcing steel are fully bonded, otherwise strength degradation will occur due to bond slippage. Based on the results of this example, it appears that a displacement ductility of 2.5 is appropriate for lightly reinforced towers but should not be exceeded.

Appendix E
Pushover Analysis of Pile-Founded Navigation Locks

E-1. Introduction

a. This appendix provides an example pushover analysis for a pile-founded navigation lock. The example lock is Olmsted Locks and Dam located on the Ohio River near town of Olmsted, Illinois. The lock structure consists of two 33.5-m by 365.8-m (110-ft by 1200-ft) locks supported by more than 11,700 H-piles (HP 14x117). The H-piles are 12.2 to 13.7 m (40 to 50 ft) long and are spaced 1.5 to 2.1 m (5 to 7 ft) in the upstream-downstream direction and 1.8 to 3.8 m (6 to 12.5 ft) in the cross-stream direction. The Olmsted Locks were designed for the MDE ground motion with a return period of 1,000 years. The design calculations consisted of the seismic coefficient method as well as the dynamic soil-pile-structure-interaction (SPSI) procedure. In the SPSI analysis, the nonlinear soil behavior was approximated by the equivalent linear techniques described in EM 1110-2-6051, but the H piles and reinforced concrete were assumed to behave linearly.

b. In this example, the mathematical model of the lock incorporates inelastic material response, thus allowing for redistribution of forces and deformations as structural members undergo nonlinear response in the form of yielding and cracking. With increasing the magnitude of loading during the pushover analysis, weak links and failure modes of the lock structure are found. The results of static pushover analysis are summarized as a plot of lateral load vs. displacement (pushover or capacity curve), from which the actual load capacity and ultimate displacement of the structure can be determined.

E-2. Purpose and Objectives

The purpose of this example is to illustrate application of nonlinear static pushover analysis described in Paragraph 6.5b to performance evaluation of navigation locks founded on piles. The objectives of the pushover analysis are:

a. To compute concrete section and pile capacities

b. To obtain pushover curve showing yielding, cracking, and ultimate displacement of the lock

c. To identify the sequence of plastic hinging and potential failure modes

E-3. Scope

The scope of this example includes pushover analyses for two structural idealizations and involves the following:

a. Idealization of lock monoliths using frame elements

b. Idealization of soil-pile-foundation using lumped nonlinear springs (Lumped Model)

c. Idealization of soil-pile-foundation using nonlinear frame elements to represent the piles and nonlinear springs to model the soil (Full Model)

    d. Conducting pushover analyses to obtain performance curves for the lumped and full models

    e. Evaluation of results to assess inelastic response behavior and ultimate displacement capacities of the lock

E-4. Assumptions

The following assumptions were made to reduce the amount of calculations and better demonstrate the effects of most important parameters on the inelastic response.

    a. Piles were modeled using lumped plasticity, where plastic hinges are assumed to form at the two ends of the element.

    b. The effect of axial load on bending moment was ignored in developing section moment-curvature relationships for the piles.

    c. Reinforced concrete members were modeled using fiber elements with distributed plasticity. The fiber elements are characterized by the constitutive models of the concrete and reinforcing steel.

    d. In 3D structures, the axial load interacts with both the in-plane and out-of-plane bending moments (i.e. $P\text{-}M_x\text{-}M_y$). In 2D-pushover analysis, the structure is restricted to in-plane bending, and thus only axial load interaction with the in-plane bending moment was accounted for.

    e. The P-δ effect is not considered.

    f. The structure is assumed not to fail in shear.

E-5. Finite Element Models

    a. The example lock is a typical chamber monolith section of the Olmsted Locks and Dam. It consists of lightly reinforced concrete slab floor and walls founded on steel piles producing two chambers, each 110 ft and 1 in. wide. The upper graph in Figure E-1 shows the basic geometry and dimensions of the chamber monolith.

    b. For reasons of simplicity and available analytical capabilities, the nonlinear static pushover analysis is carried out using beam-column (frame model) idealization of the lock structure. To insure accuracy of this approach, the frame model was calibrated against a 2D finite-element (solid elements) representation of the lock. Two computer models, one based on 2D solid elements (Figure E-1, upper graph) and another using equivalent 2D beam-column elements (Figure E-1, lower graph) were developed and analyzed. The rigid panel zones in the frame model were adjusted to obtain the same or nearly the same deformations, vibration frequencies, and mode shapes for the two models. The lengths of rigid zones were selected based on the geometry, but their rigidity was determined by trial and error.

    c. The final calibrated frame model is shown in Figure E-1 (lower graph). In this figure thick lines show the assumed rigid zones and fine lines represent the flexible beam-column elements. A rigidity factor of 1.0 was obtained from the equivalence analysis. Tables E-1 and E-2 show material properties and reinforcements for various lock sections, respectively.

d. The pushover analysis of the example soil-pile-lock system was performed using a two-dimensional slice. The depth or thickness of the slice was chosen such that the relative rigidities of the soil-pile-lock system are preserved. The pile spacing along the length of the lock is 2.13 m (7 ft). The thickness of the slice is chosen equal to the pile spacing so that pile forces and moments are obtained directly without scaling.

E-6. Section Strength Capacities and Moment-Curvature Relationship

Using the material properties listed in Table E-1, reinforcing steel listed in Table E-2, and dimensions indicated in Figure E-1, the lock section capacities were calculated. The results are presented in Table E-3 and Figure E-2. Based on geometry and amount of reinforcements, lock sections are grouped into six sections designated as Base-1, Base-2, Beam-2, Col-1, Col-2, and Col-3, as shown in Figure E-1. The reinforcing steel ratios for these sections vary from the lowest 0.3 percent for Col-3 to the highest 0.8 percent for Col-1. Computer program "*M-phi*" (Ehsani and Marine 1994) was used to estimate strength capacities and moment-curvature relationship for each of the sections. The *M-phi* moment-curvature relationships were estimated for verification of the same obtained by fiber elements, as discussed later in Paragraph E-10b. The results show that the cracking moments for all concrete sections are 2 to 3 times smaller than the nominal moments, except for Col-3 section whose cracking moment is only slightly lower than the corresponding nominal moment. Figure E-2 shows moment-curvature relationships computed for various lock sections. This provides information necessary for evaluation of the inelastic response of the lock when the lumped plasticity model is used. The concrete cracking and steel yielding for each section can easily be identified on this figure.

Table E-1. Assumed material properties

Parameter		Value	
Re-bar Material Properties			
Modulus of Elasticity	(E_s)	199,958.46 MPa	29,000.00 ksi
Specified Yield Strength	(f_y)	413.71 MPa	60.00 ksi
Strain Hardening			0.80 %
Steel Ultimate Stress		517.13 MPa	75.00 ksi
Steel Ultimate Strain			5.00 %
Concrete Material Properties			
Modulus of Elasticity	(E_c)	23,457.77 MPa	3,402.08 ksi
Shear Modulus	(G)	9,774.07 MPa	1,417.53 ksi
Poisson's Ratio	(ν)		0.20
Concrete Compressive Strength	(f'_c)	20.69 MPa	3.00 ksi
Modulus of Rupture (per ACI)	(f_r)	2.83 MPa	0.41 ksi
Concrete Ultimate Strain	(ε_c)		0.30 %

Table E-2. Reinforcing steel properties

Section ID	Reinforcing Bar (per foot of depth)					
	Upper			Lower		
Base-1	1- #18	2.58 mm^2	4.00 in^2	1- #18	2.58 mm^2	4.00 in^2
Base-2	1- #18 & 1- #14	4.03 mm^2	6.25 in^2	1- #18 & 1- #14	4.03 mm^2	6.25 in^2
Beam-2	2- #11	1.82 mm^2	2.82 in^2	2- #11	1.82 mm^2	2.82 in^2
Col-1	2- #11	1.82 mm^2	2.82 in^2	2- #11	1.82 mm^2	2.82 in^2
Col-2	2- #11	1.82 mm^2	2.82 in^2	2- #11	1.82 mm^2	2.82 in^2
Col-3	2- #11	1.82 mm^2	2.82 in^2	2- #11	1.82 mm^2	2.82 in^2

Table E-3a. Calculated section capacities (English units)

Parameter		Base-1	Base-2	Beam-2	Col-1	Col-2	Col-3
Depth	b (ft)	7.00	7.00	7.00	7.00	7.00	7.00
Width	h (ft)	12.00	12.00	6.00	5.00	8.00	14.00
Section Area	A (ft^2)	84	84	42	35	56	98
Moment of Inertia	I_{yy} (ft^4)	1,008	1,008	126	73	299	1,601
Nominal Moment	M_n (k-ft)	18,771	28,847	6,241	5,057	8,610	15,717
Cracking Moment	M_{cr} (k-ft)	9,938	9,938	2,484	1,725	4,417	13,527
Shear Capacity	V_x (kips)	530,020	530,020	265,010	220,842	353,347	618,357
Tension Capacity	P_t (kips)	3,360	5,250	2,369	2,369	2,369	2,369
Compression Capacity	P_c (kips)	36,288	36,288	18,144	15,120	24,192	42,336

Table E-3b. Calculated section capacities (metric units)

Parameter		Base-1	Base-2	Beam-2	Col-1	Col-2	Col-3
Depth	b (m)	2.13	2.13	2.13	2.13	2.13	2.13
Width	h (m)	3.66	3.66	1.83	1.52	2.44	4.27
Section Area	A (m^2)	7.80	7.80	3.90	3.25	5.20	9.10
Moment of Inertia	I_{yy} (m^4)	8.70	8.70	1.09	0.63	2.58	13.82
Nominal Moment	M_n (kN-m)	25,451	39,113	8,463	6,857	11,674	21,310
Cracking Moment	M_{cr} (kN-m)	13,475	13,475	3,369	2,339	5,989	18,341
Shear Capacity	V_x (kN)	2,357,771	2,357,771	1,178,885	982,405	1,571,847	2,750,733
Tension Capacity	P_t (kN)	14,947	23,354	10,538	10,538	10,538	10,538
Compression Capacity	P_c (kN)	161,426	161,426	80,713	67,261	107,617	188,330
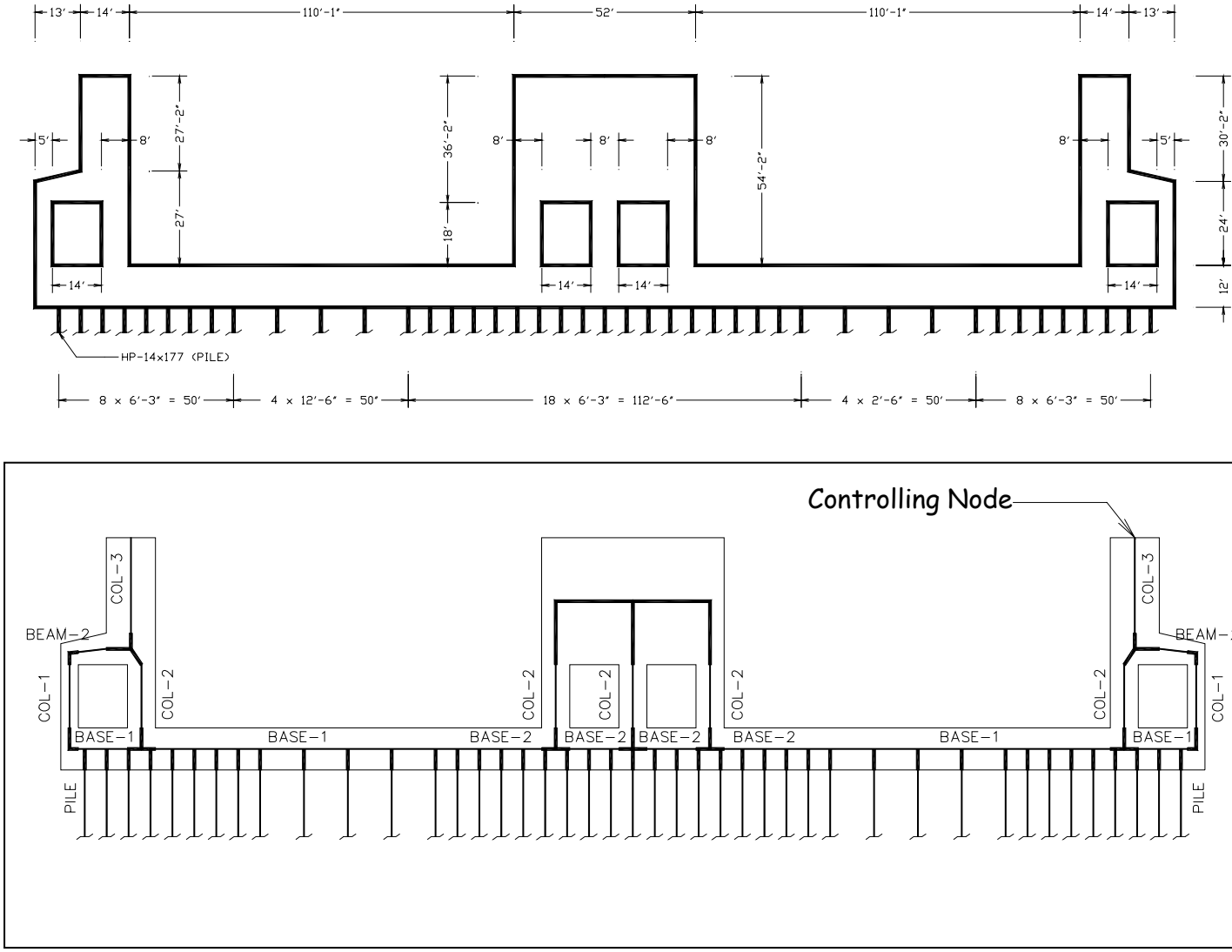
Figure E-1. Basic geometry and frame model of reinforced concrete lock
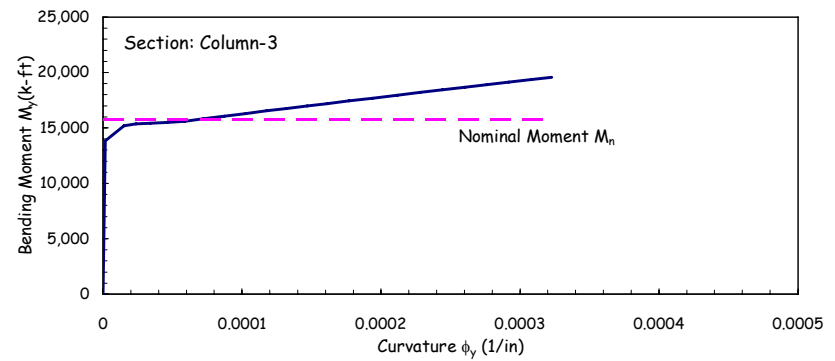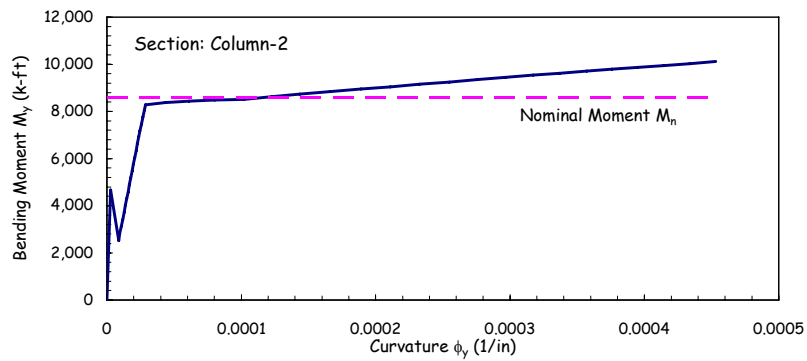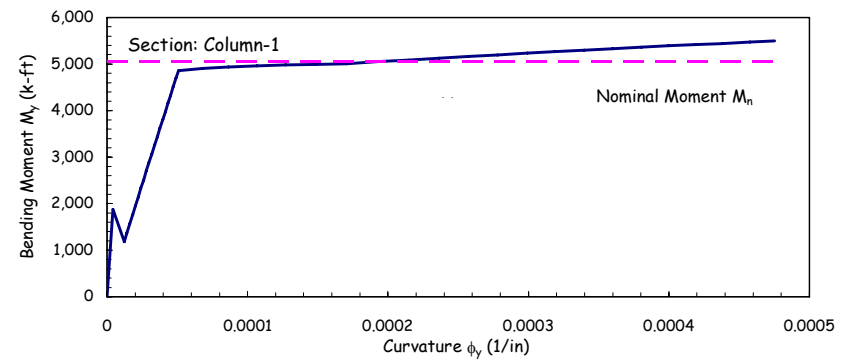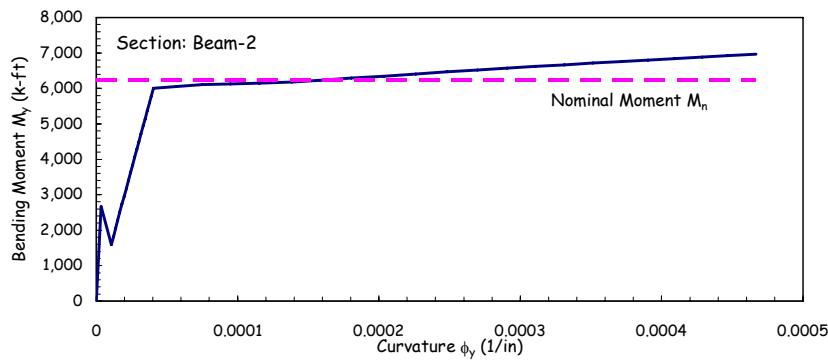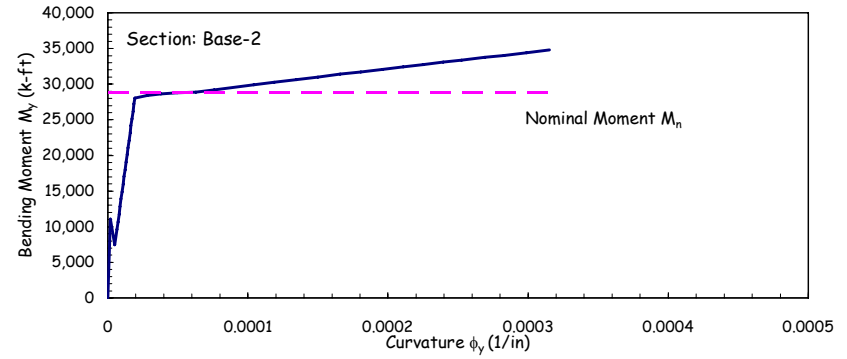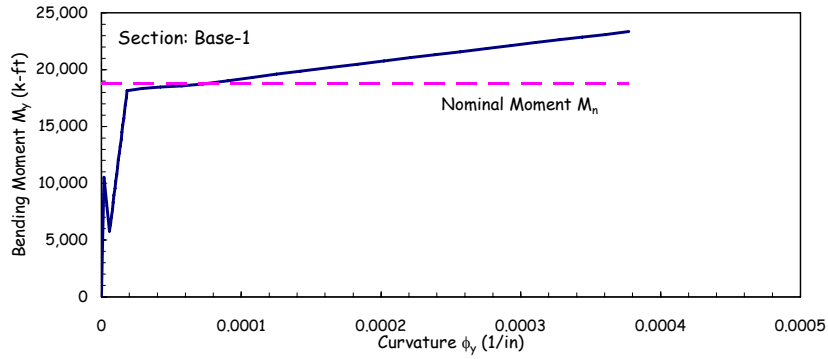
Figure E-2. Calculated moment capacities of various lock sections (shown in Figure E-1)

E-7. Analysis Procedures

a. Non-linear static pushover analysis implies monotonic application of static load to mathematical model of the structure. The load is applied in increments until the maximum load (load controlled) or a target displacement is reached (displacement controlled). This procedure requires considerably more analysis effort than does the linear static procedure. It is therefore conducted using a computer program having nonlinear analysis capabilities.

b. The maximum seismic load demands in the load-controlled pushover analysis cannot easily be determined. Consequently, the displacement-controlled method of analysis is commonly used to conduct pushover analysis. Accordingly, static lateral loads are applied incrementally to a mathematical model of the structure until a target displacement is exceeded. The target displacement represents the maximum displacement that the structure is likely to experience when subjected to the design earthquake. An estimate of target displacement for building structures is given by FEMA-356 (2000). The target displacement for lock structures has not been developed. Consequently, the step-by-step nonlinear pushover analysis for lock structures should continue until the resulting displacement is large enough to mobilize principal nonlinear mechanisms or the structure collapses.

c. The main objective of pushover analysis is to obtain a pushover or capacity curve by which performance of the structure can be assessed. The performance is considered satisfactory if permissible deformation and strength demands for a prescribed performance level are met. For deformation-controlled actions (such as flexural moment) deformation demands are compared with the maximum permissible values for the component. While for force-controlled actions (such as shear forces in beams) the force demands are compared with the strength capacity. If either the force demand in force-controlled elements or deformation demand in deformation-controlled members exceeds permissible values, then the element is deemed to violate the performance criteria. The applied load pattern should closely resemble the probable earthquake load pattern. As an example for structures whose response is governed by the fundamental mode of vibration, the lateral load pattern may be selected proportional to the fundamental mode shape of the structure. Since dynamic response of the example lock structure is dominated by the fundamental mode, it seems reasonable to assume a load pattern (i.e. lateral inertia forces) proportional to the product of fundamental mode shape and nodal masses. In other cases, a dominant load pattern may not exist. In those situations, two or more load patterns should be considered. It is also a good idea to normalize the load pattern such that the sum of all horizontal components is equal to unity. The benefit of such normalization is that the load scale factor, computed by some programs such as DRAIN-2DX (1994), directly gives the base shear.

d. To speed up the computations the size of computer model is reduced by replacing the pile-soil-foundation system with equivalent lumped pile-head stiffness. The pile-head stiffness is represented by sets of non-linear springs arranged at appropriate locations. This model referred to as the "Lumped Model" is discussed in Paragraph E-7*e*. The computation of pile-head stiffness coefficients is described in Section E-8. Alternatively, one may develop a complete pile-soil-foundation model using nonlinear frame elements to represent the piles and nonlinear springs to idealize the pile-soil foundation. This model referred to as the "Full Model" is discussed in Paragraph E-7*f*. Obviously, the Full Model requires significantly more computational efforts than does the Lumped Model, thus limiting the engineer's ability to perform parameter sensitivity study. The need for the parameter sensitivity study could frequently arise from the poor or lack of convergence of numerical algorithms. In this example, the Lumped Model was first used to perform initial analyses and to make any necessary

adjustments to the model before a Full Model could be developed and analyzed. In Paragraph E-10, the results from the Lumped and Full Models are discussed and compared to validate the assumptions regarding the Lumped Model.

e. Lumped Model. Figure E-3 shows a plot of lock model with the lumped pile-head system. *Load pattern* for this model is chosen as a product of the first mode shape and the corresponding nodal masses. The lateral loads that would have been acting along the length of piles are lumped at the location of each pile-head spring. The lateral load is applied to "push" the lock model to the left. The *controlling node*, at which the lateral displacement is monitored, is taken at the top of the right wall. A *target displacement* of 1.0 ft is selected.
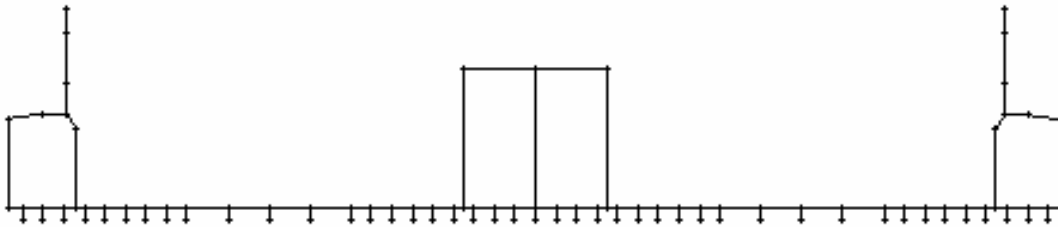
Figure E-3. Lumped pile-head model of reinforced concrete lock

f. Full Model. Figure E-4 shows a plot of lock model with the full pile-soil-foundation system. Each pile is represented by 11 nonlinear beam-column or frame elements supported by 11 lateral nonlinear soil springs. The nonlinear force-displacement relationship for soil springs are represented by *p-y* curves estimated for each soil layer. *Load pattern* for this model is also chosen as the product of the first mode shape and the corresponding nodal masses. The load pattern is applied to push the lock to the left. The *controlling node* is selected at the top of the right wall. A *target displacement* of 1.0 ft is selected.
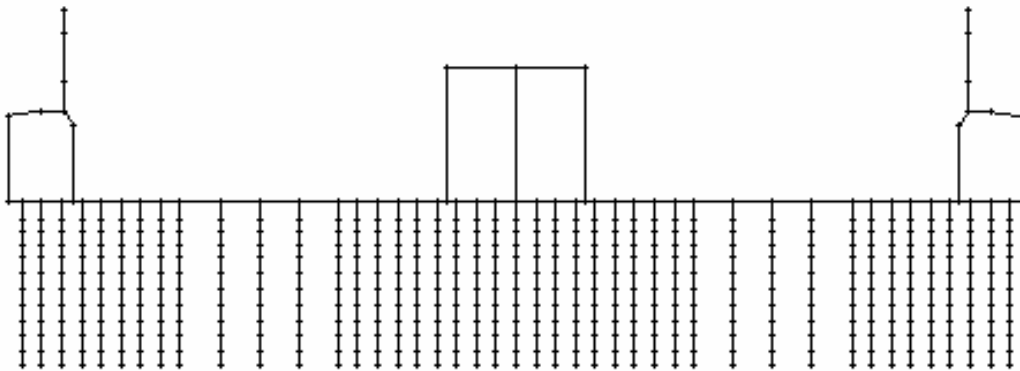
Figure E-4. Full model of reinforced concrete lock

E-8. Single Pile Analysis

 a. This section describes computation of the equivalent pile-head stiffness used in the Lumped Model. The effects of pile-soil-foundation system can be approximated by sets of equivalent nonlinear springs attached to the base of the lock model. The stiffness of these springs is calculated by conducting a nonlinear static analysis of a single pile-soil model subjected to either a lateral load or moment. The pile is modeled with nonlinear beam-column elements and the soil is represented by nonlinear *p-y* curves. In the first analysis the pile head is constrained against the rotation and subjected to an incrementally increasing lateral load. A plot of lateral load versus lateral displacement produces the lateral stiffness K_{xx} shown in the upper left graph of Figure E-5. Whereas a plot of the induced pile-head moment as a function of the lateral displacement gives the coupling stiffness, $K_{\theta x}$ shown in the lower left graph of Figure E-5. In the second analysis the pile head is constrained against lateral displacement and subjected to incrementally increasing moment. A plot of the applied moment versus the rotation produces the nonlinear rotation stiffness, $K_{\theta\theta}$, shown in the lower right graph of Figure E-5. The applied moment generates a lateral reaction at the fixed pile head, which if plotted against rotation produces the coupling stiffness $K_{x\theta}$, as shown in the upper right graph of Figure E-5.

 b. The presence of large off-diagonal terms in Figure E-5 suggests a strong coupling between the rotation and lateral stiffness. The incorporation of coupling stiffness terms in the analysis is not straightforward if the computer program lacks such capabilities. However, the coupling terms can be accounted for indirectly if the springs are placed at an offset equal to the ratio of $K_{\theta x}/K_{xx}$, as illustrated in Figure E-6. This ratio or offset remains constant within the linear-elastic range of behavior, but varies significantly in the inelastic deformation range.

 c. Figure E-7 displays variation of offset *h* with respect to load steps. Since the location of springs (i.e. value of *h*) cannot be changed within a single computer run, some average value of *h* should be assumed. Separate analyses could also be run using either the maximum or the minimum *h* to envelop the results. Other approaches are to select *h* based on the expected deformations, or run several analyses with different possible values of *h*. All of these approaches, however, require several computer runs.

 d. In this example, a single value of $h = 3.5$ was selected to avoid numerous computer runs, with the understanding that these results will later be compared with the Full Model for further validation.
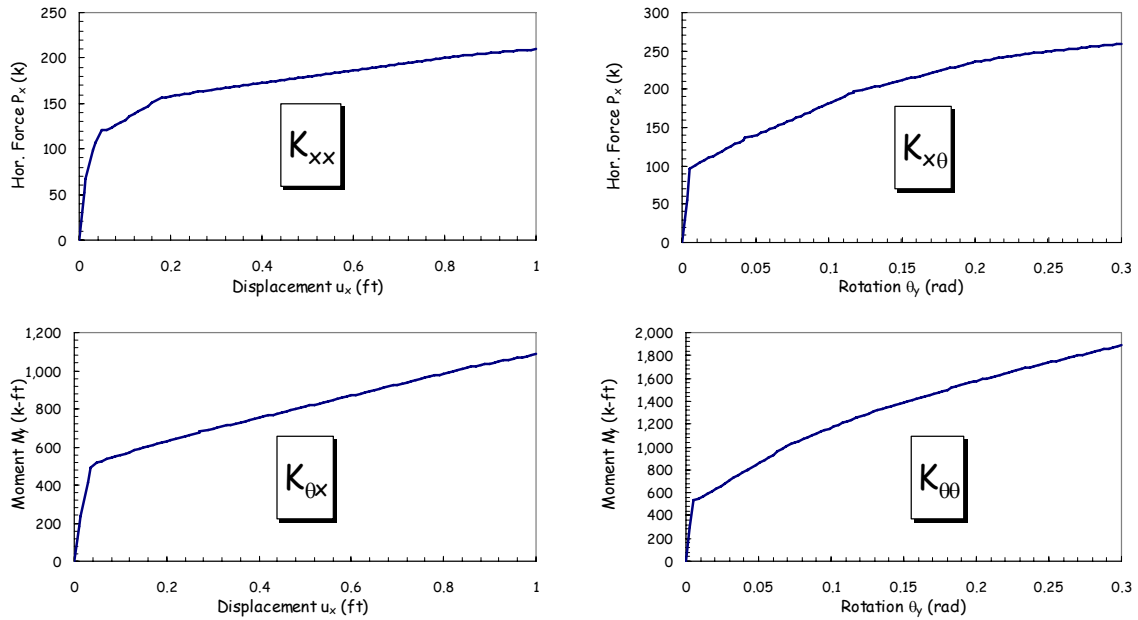
Figure E-5. Nonlinear pile-head stiffness matrix

$$\begin{Bmatrix} V_x \\ M_y \end{Bmatrix} = \begin{bmatrix} K_{xx} & K_{x\theta} \\ K_{\theta x} & K_{\theta\theta} \end{bmatrix} \times \begin{Bmatrix} u_x \\ \theta_y \end{Bmatrix}$$
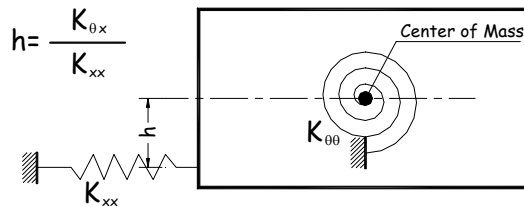
Figure E-6. Pile-head springs
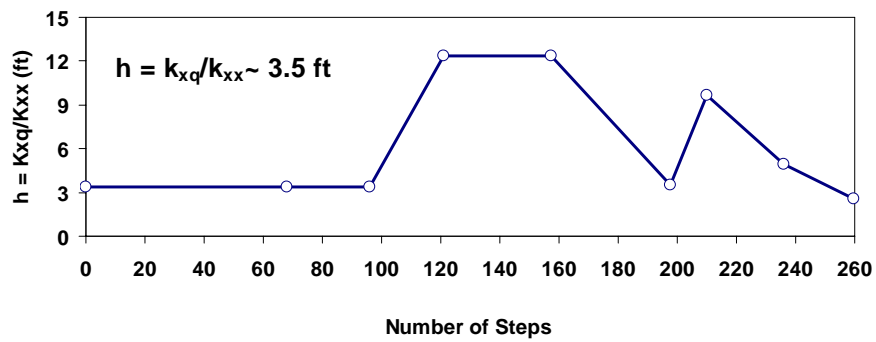
Figure E-7. Variation of offset *h* as a function of load step

E-9. Pushover analysis using computer program DRAIN-2DX

a. An enhanced version of the computer program DRAIN-2DX is used to illustrate the application of nonlinear static procedures to pushover analysis of navigation locks. Three types of elements are used to model the lock-pile-foundation system: 1) a distributed plasticity fiber beam-column element (Type 15), 2) a lumped plastic-hinge beam-column element (Type 02), and 3) a simple connection or spring element (Type 04). Fiber beam-column elements are used to model the reinforced concrete lock, as shown in Figures E-1, E-3, and E-4. Plastic-hinge beam-column elements are used to model steel piles. While simple connections or spring elements are used to represent the nonlinear soil.

b. Fiber Model. The reinforced concrete lock is represented using fiber beam-column elements available in DRAIN-2DX. Each lock section is divided into 18 concrete and 2 steel fibers, as shown in Figure E-8. This "distributed plasticity" modeling permits for the spread of inelastic behavior both over the cross section and along the member length (Campbell 1994). The fiber modeling is in contrast to a conventional "lumped plasticity" model, where the inelastic behavior is concentrated in zero length plastic "hinges." The use of fibers to model cross sections accounts rationally for axial force-moment interaction, while no yield surface or plastic flow rule needs to be defined explicitly. The concrete and reinforcing bars are represented by separate fibers, each with its own material properties, as shown in Figure E-9. Such model can account for yielding of steel including strain hardening, cracking and crushing of concrete including post-crushing strength loss, crack opening, and reinforcing bar pullout if desired. The same fiber model of the lock was used for the Lumped and Full Models of the pile-soil-foundation system.
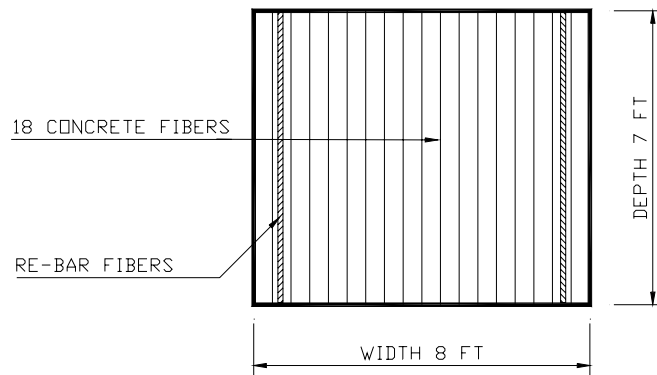
Figure E-8. Fiber element cross-section for Col-3
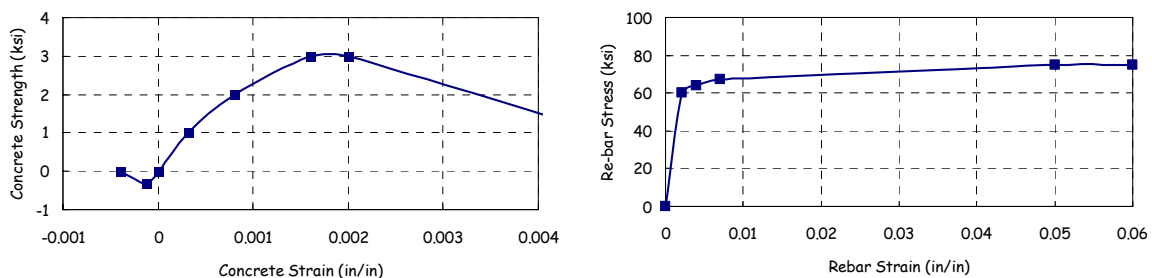
Figure E-9. Assumed stress-strain relationship for concrete and reinforcing bar

E-11

c. Lumped Plastic-Hinge Model. The conventional lumped plastic-hinge beam-column elements (Type 02 in DRAIN-2DX) were used to model steel piles in the Full Model representation of the pile-soil-foundation system. In the Full Model, the same nonlinear spring elements (Type 04 in DRAIN-2DX) discussed next were used to model the nonlinear soil along the length of piles. Except that the stiffness of the soil springs was based on the *p-y* curves.

d. Nonlinear Springs. The pile-soil-foundation system in the Lumped Model was modeled using nonlinear spring elements (Type 04 in DRAIN-2DX). The effects of each pile and the surrounding soil were represented by three sets of nonlinear springs estimated according to the procedure discussed in Section E-8. Each set of springs included a vertical, horizontal, and rotational springs. The horizontal and rotational springs were positioned with an offset according to Figure E-4 to produce coupling stiffness terms between lateral and rotational degrees of freedom.

E-10. Evaluation of Results

a. Deflected Shapes. Figures E-10 and E-11 show deflected shapes of the Lumped and Full Models respectively after being pushed to a target displacement of about 1 foot. Red symbols indicate the locations where nonlinear deformation takes place. Nonlinear behavior includes cracking and crushing of the concrete, yielding of the reinforcing steel, and yielding of the pile-soil foundation. A quick examination of Figure E-10 shows that all pile-head springs in the Lumped Model have yielded and that reinforced concrete sections have experienced cracking and yielding at the base slab and at the top of the lock walls. A yielding of the pile-head springs indicates a yielding of the steel piles, or soil, or both. Similarly the Full Model also indicates yielding of the piles with some cracking and yielding of the base slab but no cracking of the lock walls.
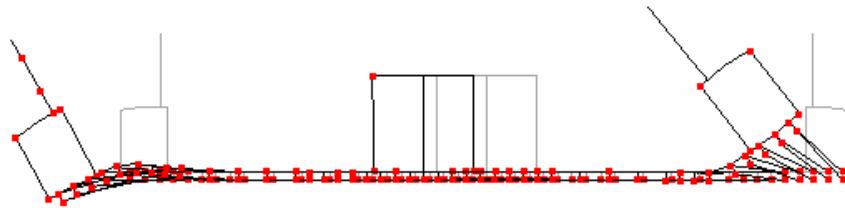
Figure E-10. Lumped model deflected shape
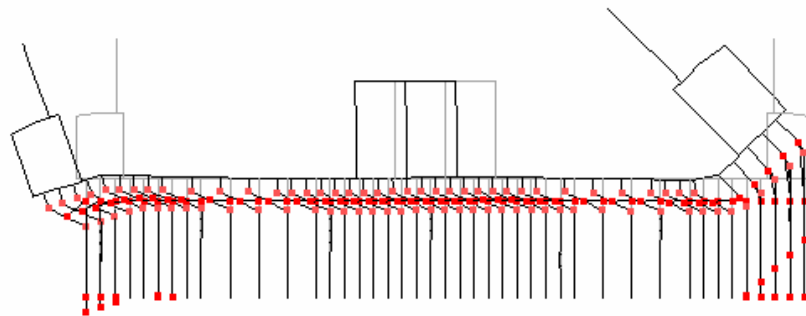
Figure E-11. Full model deflected shape

b. Moment-Curvature. A more detailed evaluation of the structural performance is carried out by a careful examination of the location, extent, and sequence of inelastic deformations. All sections and members exhibiting inelastic response are identified and their moment-curvature or force-displacement relationships are plotted and evaluated to assess the damage. The level of damage is then compared against the acceptance criteria. Figure E-12 is one such moment-curvature relationship for the base slab section of the lock. The figure compares moment-curvature relationships obtained from the Full Model, Lumped Model, and the *M-phi* program. The figure also includes the nominal bending moment as a reference. The results indicate that the concrete cracking starts at a bending moment of about 1,3558 kN-m (10,000 k-ft), followed by a stiffness reduction of the lock section due to cracking and yielding of reinforcing steel at about 27,116 kN-m (20,000 k-ft). The agreement among different models is quite reasonable. The difference between the *M-phi* and DRAIN-2DX fiber model is due to effects of shear and axial force inherent in the fiber model but not accounted for in the *M-phi* calculation of the section moment-curvature. The moment-curvature relationship in Figure E-12 is a measure of the local damage. The acceptance of local damage can be determined by comparing the induced inelastic curvature (or rotation) with the ultimate curvature or rotation capacity of the section.
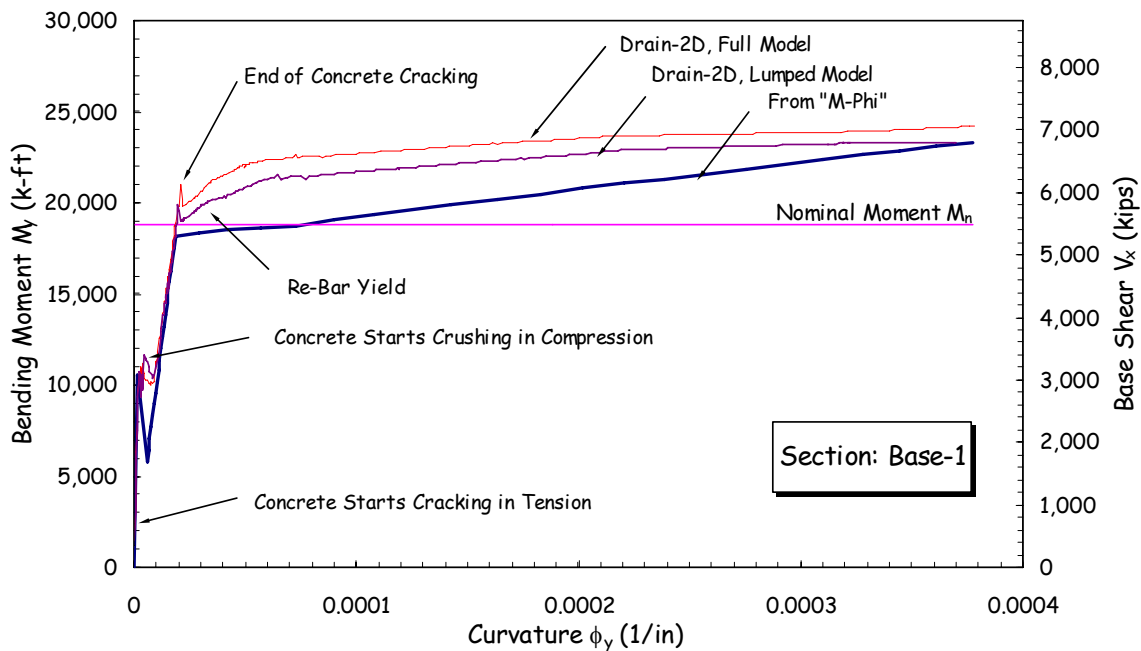
Figure E-12. Moment capacities and moment-curvature relationship of base slab from various procedures

c. Pushover Curve. In pushover analysis, the global response of the structure is commonly represented by a plot of the base shear versus lateral displacement. For the example lock, the plot of base shear versus a control node at the top of the lock wall is shown in Figure E-13 for both the Full and Lumped Models. Also shown in this figure and listed in Table E-4 are the base shear levels at which the soil begins yielding and 10%, 50%, 80%, or 100% of the piles experience yielding. Generally, the results of the Lumped and Full Models are in good agreement, except that the Lumped Model appears slightly stiffer than the Full Model (FigureE-13). This is probably due to bilinear approximation of the pile-head stiffness in the Lumped Model, which causes instant yielding as opposed to a gradual yielding with softening effect in the Full Model. The pile yielding for the Lumped Model is more sudden due to lumping nature of the pile-head stiffness. The first yielding in pile springs occurs at a lateral displacement of 3.5 cm (1.2 in.) and spreads to all pile springs at a lateral displacement of 5.31 cm (2.09 in.). While, in the case of Full Model, the first pile yielding starts at a lateral displacement of 5.34 cm (2.10 in.) and spreads to all piles at a much higher displacement of 15.81 cm (6.22 in.).

d. Percentage of Pile Yielding. Another interesting result is a graph of the base shear against the percentage of yielded piles, as shown in Figure E-14. This graph reveals that as soon as a few pile-head springs yield in the Lumped Model, the yielding spreads almost instantly to all other pile-head springs with no increase in the base shear. In the case of Full Model the pile yielding quickly spreads from a few percent to 75 percent of piles with very little increase in the base shear. However, the spread of yielding from 75 percent to 100 percent of the piles requires a significant additional base shear. For this example the pile-founded lock is considered safe and the level of damage acceptable if:

(1) The global displacement is not more than twice the first pile-yielding displacement

(2) The element or section curvature is not more than twice the section yield curvature
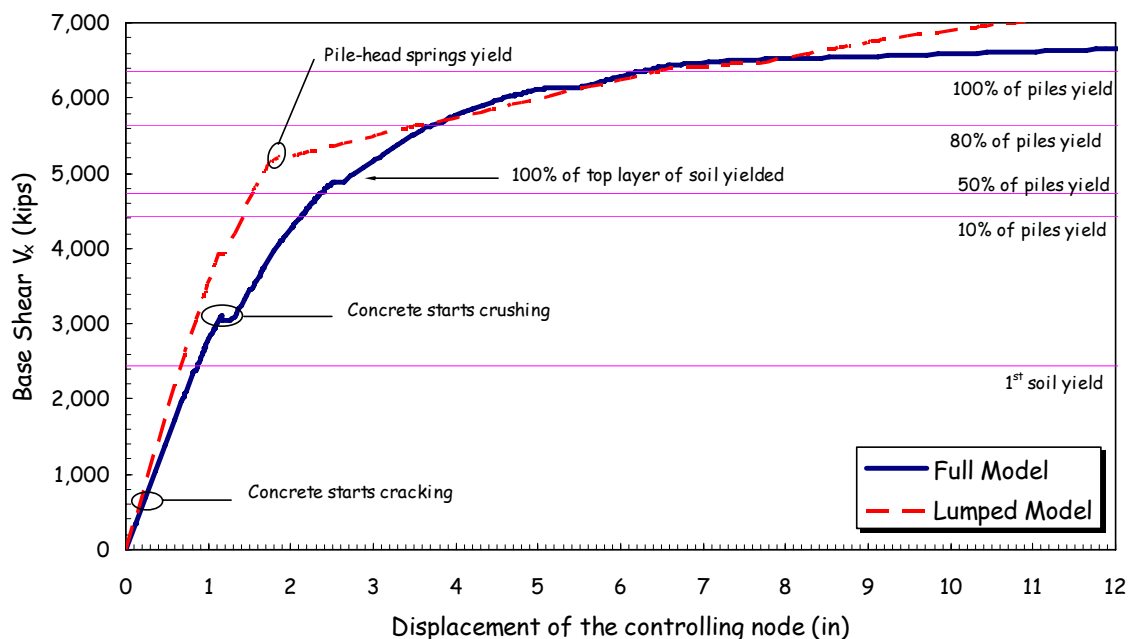
Figure E-13. Pushover curve indicating inelastic response (or level of damage) for Full and Lumped Models of example lock-pile system

Table E-4. Identification and estimate of damage for Full- and Lumped-Model representation of example lock-pile system

DAMAGE DESCRIPTION	FULL MODEL		LUMPED MODEL	
	Base Shear kN (kips)	Controlling Node Displacement cm (in)	Base Shear kN (kips)	Controlling Node Displacement cm (in)
1st Soil Yield	10,885 (2,447)	2.21 (0.87)		
1st Pile-Head Spring Yield			17,525 (3,940)	3.05 (1.20)
1st HP Pile Yield	19,564 (4,398)	5.34 (2.10)		
10% of Piles Yield	19,724 (4,434)	5.41 (2.13)		
30% of Piles Yield	20,349 (4,574)	5.67 (2.23)		
50% of Piles Yield	21,021 (4,725)	5.98 (2.36)		
100% of top soil layer yield	21,718 (4,882)	6.67 (2.63)		
10% of Pile-Head Springs Yield			22,438 (5,044)	4.29 (1.69)
65% of Pile-Head Springs Yield			22,817 (5,129)	4.40 (1.73)
100% of Pile-Head Springs Yield			23,346 (5,248)	5.31 (2.09)
80% of Piles Yield	25,054 (5,632)	9.45 (3.72)		
100% of Piles Yield	28,254 (6,351)	15.81 (6.22)		
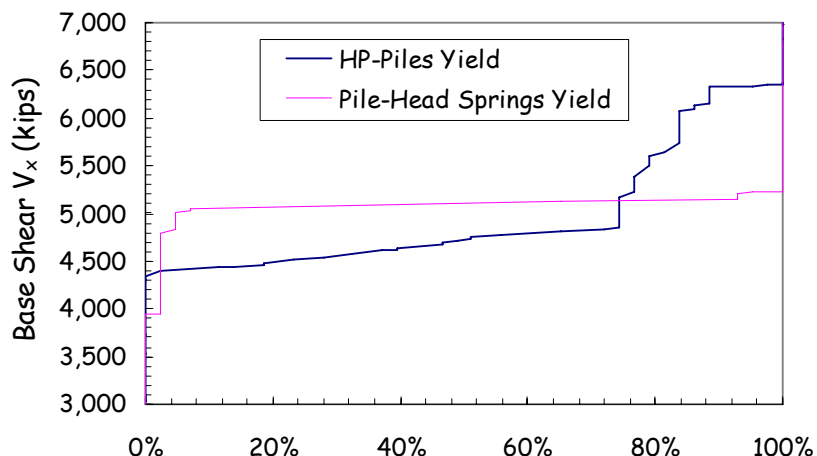
Figure E-14. Percent of Full Model piles and Lumped Model pile-head springs yielded vs. base shear

E-11. Conclusions and Recommendations

In general, lumped model representation of the pile foundation provides reasonable results, if pile-head stiffness properties are estimated accurately based on the single pile analysis discussed in this example and the coupling stiffness terms are considered in the analysis. If computation time is of no concern, the full model may be used for more accuracy. The full model also provides section forces and moments along the entire length of the piles, from which locations of maximum pile forces can be determined. The results show that the yielding spreads instantly from a few piles to more than 75 percent of the piles. Consequently, a sound acceptance criterion is to limit yielding to less than 10 percent of the piles.

Appendix F
NONLINEAR ANALYSIS OF ARCH DAMS

F-1. Introduction

The example dam is a double-curvature thin arch structure 142.65 m (468 ft) high and 220.68 m (724 ft) long along the crest. The dam is 3.66 m (12 ft) thick at the crest and 15.85 m (52 ft) thick at the base. In this example, the dam is first evaluated using the linear time history analysis for comparison with the damage criteria discussed in Paragraph 6.4*d*(2). Nonlinear time-history analyses are then performed to obtain quantitative estimates of probable damage in the form of joint opening and lift line cracking for several postulated MCE ground motions.

F-2. Purpose and Objectives

The purpose of this example is to illustrate the application of nonlinear time-history method to earthquake response analysis of arch dams. The objectives of this nonlinear time-history analysis are: 1) to model and estimate the amount of contraction joint opening and lift line cracking, 2) to compute displacement and stress response histories of the dam due to six sets of three-component acceleration time histories, and 3) to provide stress contours, stress time histories, and joint displacement time histories for assessing the earthquake performance of the dam.

F-3. Scope

The scope of this example includes the following:

   a. Establishment of design earthquake and earthquake ground motions including acceleration time-histories.

   b. Computation of linear earthquake response of the dam-water-foundation system.

   c. Development of nonlinear model with contraction joint opening and lift line cracking.

   d. Computation of earthquake responses of the nonlinear dam model for four sets of acceleration time-histories with various contraction joints and lift lines configurations.

   e. Evaluation of sensitivity of dam response to numbers of contraction joints and lift line joints.

   f. Evaluation of sensitivity of dam response to characteristics of acceleration time histories.

F-4. Earthquake Ground Motions

For evaluation of the earthquake damage using linear and nonlinear time-history analyses, the example arch dam was assumed to be located in the near field of a maximum earthquake event having a moment magnitude M_w of about 6-1/2. A total of six sets of records were selected for the analysis, five of which included natural acceleration time-histories from four recent earthquakes, and the sixth consisted of a spectrum-matched time-history derived using the 1971 Pacoima Dam record. The smooth response spectra for the horizontal and vertical components of ground motion were constructed to be representative of median ground motions for an M_w 6-1/2 earthquake occurring at a distance of $R \approx 5$ km (3.1 miles). The records

considered are listed in Table F-1 and the smooth response spectra are shown in Figure F-1. The ground motions were scaled such that the sum of ordinates for the response spectra of each natural record would match the sum for the smooth response spectra in the period range of 0.1 to 0.5 sec. This period range was selected to contain the most significant modes of vibration for the example dam (i.e., all periods longer than 0.1 sec). The resulting scale factor for each record is listed in Table F-1, and the response spectra for all records in the period range of 0.1 to 0.5 sec are compared in Figure F-2. Time-histories of the larger horizontal component of the records are plotted in Figure F-4. This figure clearly demonstrates the pulsive ("fling") type motions contained in the Pacoima Dam and Morgan Hill records.

Table F-1. Near-Source Earthquake Records		
Earthquake Record	**Designated Name**	**Scale**
Coyote Lake Dam 1984 Morgan Hill earthquake, M_w 6.2, R = 0.1 km	CLD	0.64
Gilroy Array No. 1 1989 Loma Prieta earthquake, M_w 6.9, R = 11 km	GLY	0.81
Spectrum-matched 1971 Pacoima Dam record	PACB	1.00
Pacoima Dam, downstream record 1994 Northridge earthquake, M_w 6.7, R = 8 km	PACN	1.13
Pacoima Dam, downstream record 1971 San Fernando earthquake, M_w 6.6, R = 2.8 km	PACX	0.52
Newhall, West Pico Canyon Boulevard 1994 Northridge earthquake, M_w 6.7, R = 7.1 km	U56	1.80
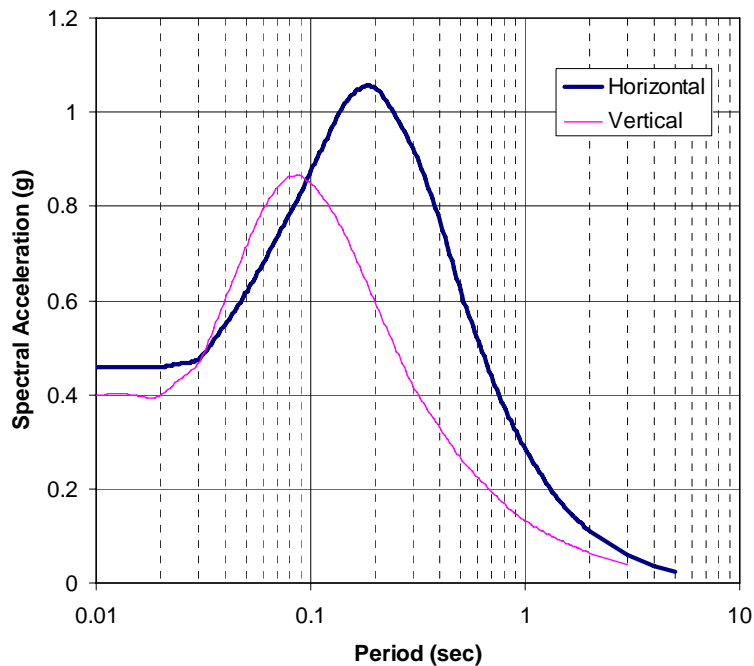
Figure F-1. Horizontal and vertical smooth response spectra
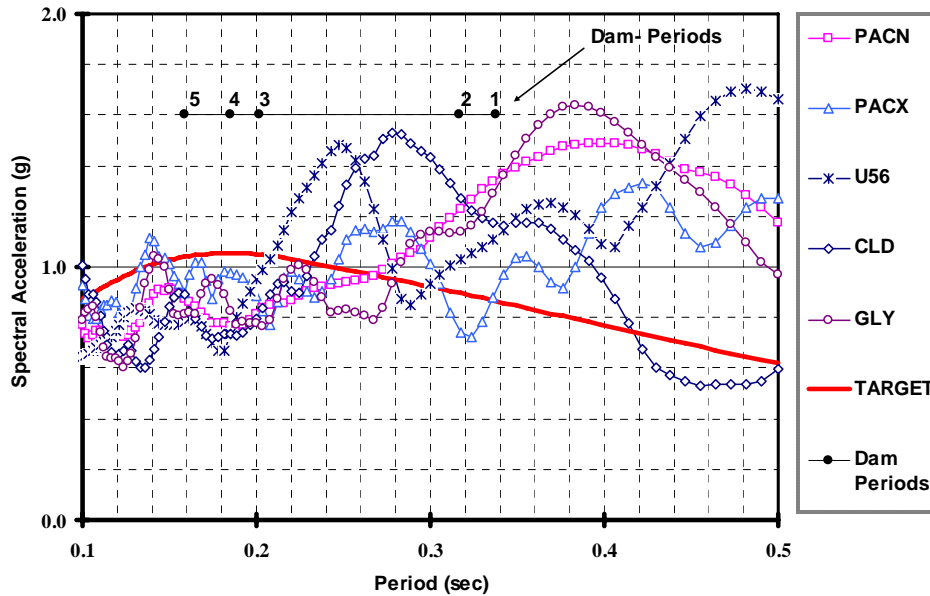
Figure F-2. Response spectra of scaled records

F-5. Computation of Linear-elastic Response

The linear-elastic time-history analysis of the example dam is based on the 3-D finite-element procedures discussed in Chapter 2 of EM 1110-2-6051. Finite-element models for the concrete arch, foundation rock, and the impounded water were developed using the GDAP program and loading combinations were established in accordance with EM 1110-2-2201. Material properties were selected from the available data. The ground motion acceleration time history inputs for the dynamic analysis were selected based on the procedures discussed in Chapter 5 of EC 1110-2-6051. Interaction effects of the impounded water and foundation rock with the dam were included in the finite-element stress analyses by modeling a sufficiently large portion of the foundation rock and the impounded water. A 5% structural damping ratio was assumed in the analyses.
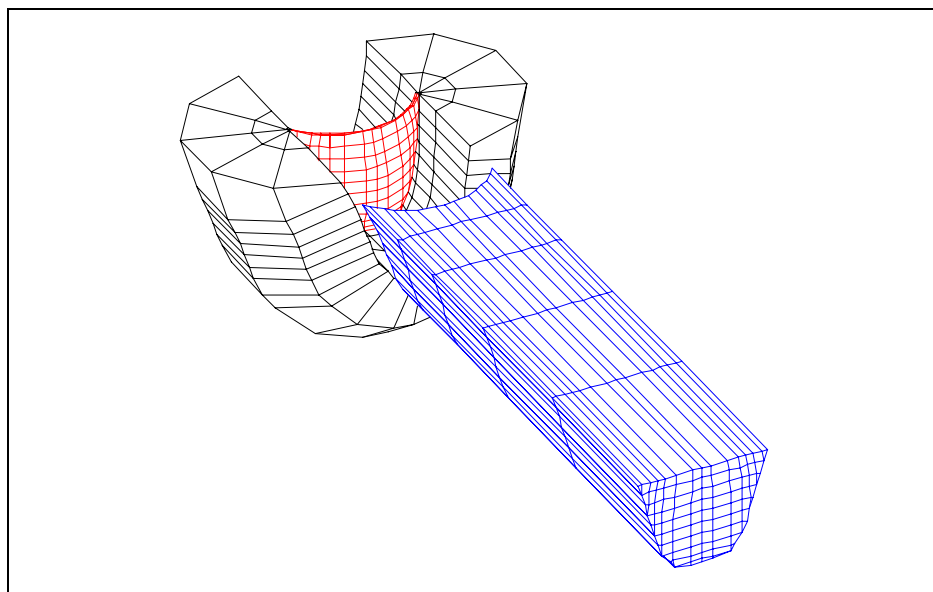
Figure F-3. Three-dimensional view of dam-rock-reservoir system
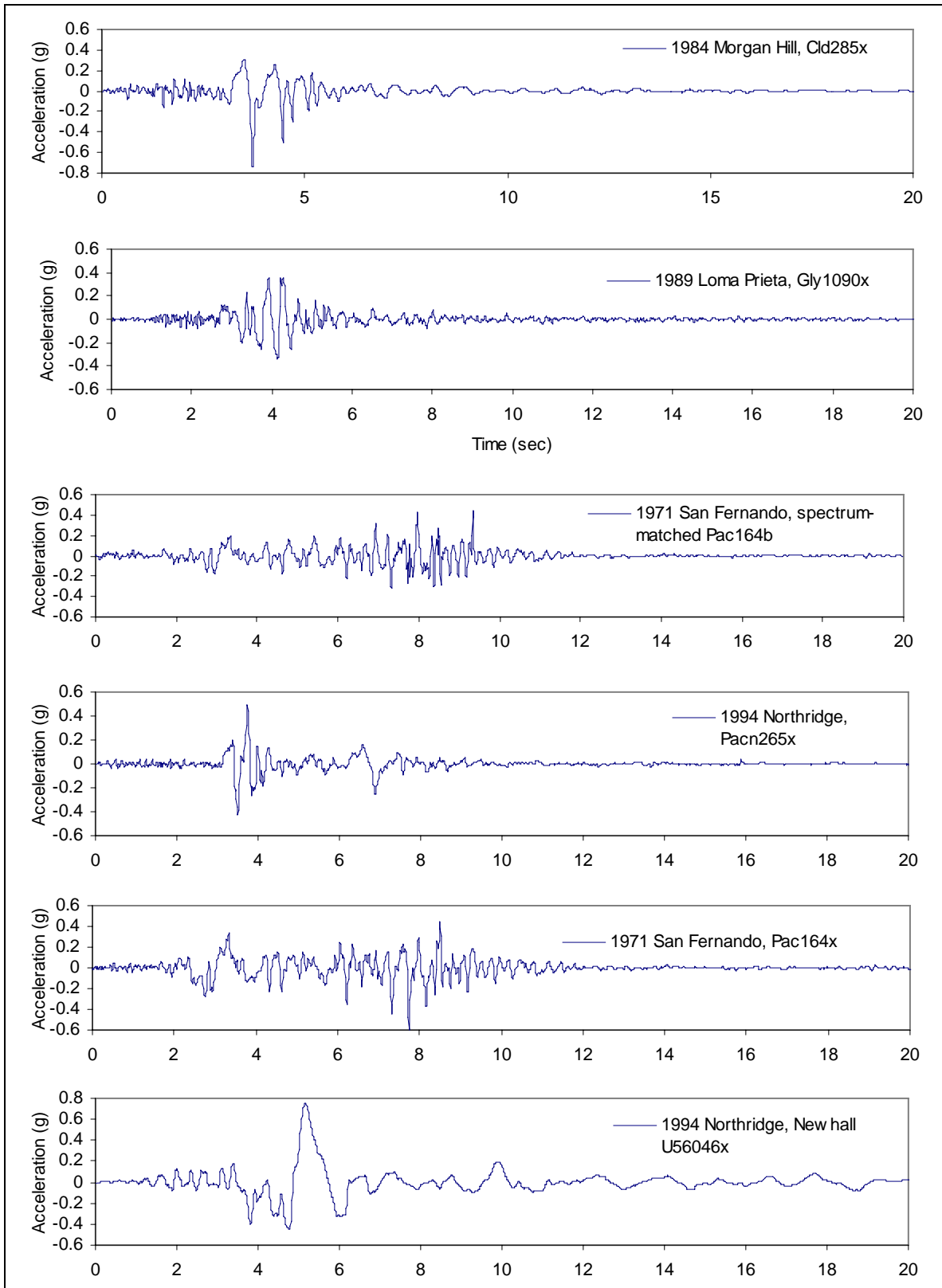
Figure F-4. Scaled acceleration time-histories for near-source, *M_w*~6-1/2 earthquake

F-6. Evaluation of Linear-elastic Analyses Results

The dam-water-foundation model in Figure F-3 was analyzed for six sets of three-component acceleration time histories discussed above in Section F-4. The Web-based GDAP program (Quest Structures 2001), a three-dimensional finite-element program for linear-elastic analysis of concrete dams was used. The results are presented and evaluated with the damage criteria in Paragraph 6.4*d*(2). Figure F-5 compares the magnitude and extent of high arch and high cantilever tensile stresses with the performance curves established for arch dams (see Chapter 4 of EM 1110-2-6051). The upper graphs show that the surface areas and cumulative inelastic duration of arch tensile stresses exceed the permissible values set for the linear-elastic analysis. The lower graphs show that the surface areas of cantilever tensile stresses are below the permissible values but their cumulative inelastic duration exceeds the permissible values. The results suggest that the nonlinear response of the dam in the form of contraction joint opening and lift line cracking is significant and well above the established threshold. Therefore, the evaluation of dam safety should proceed with nonlinear analysis including contraction joint opening and lift line cracking.
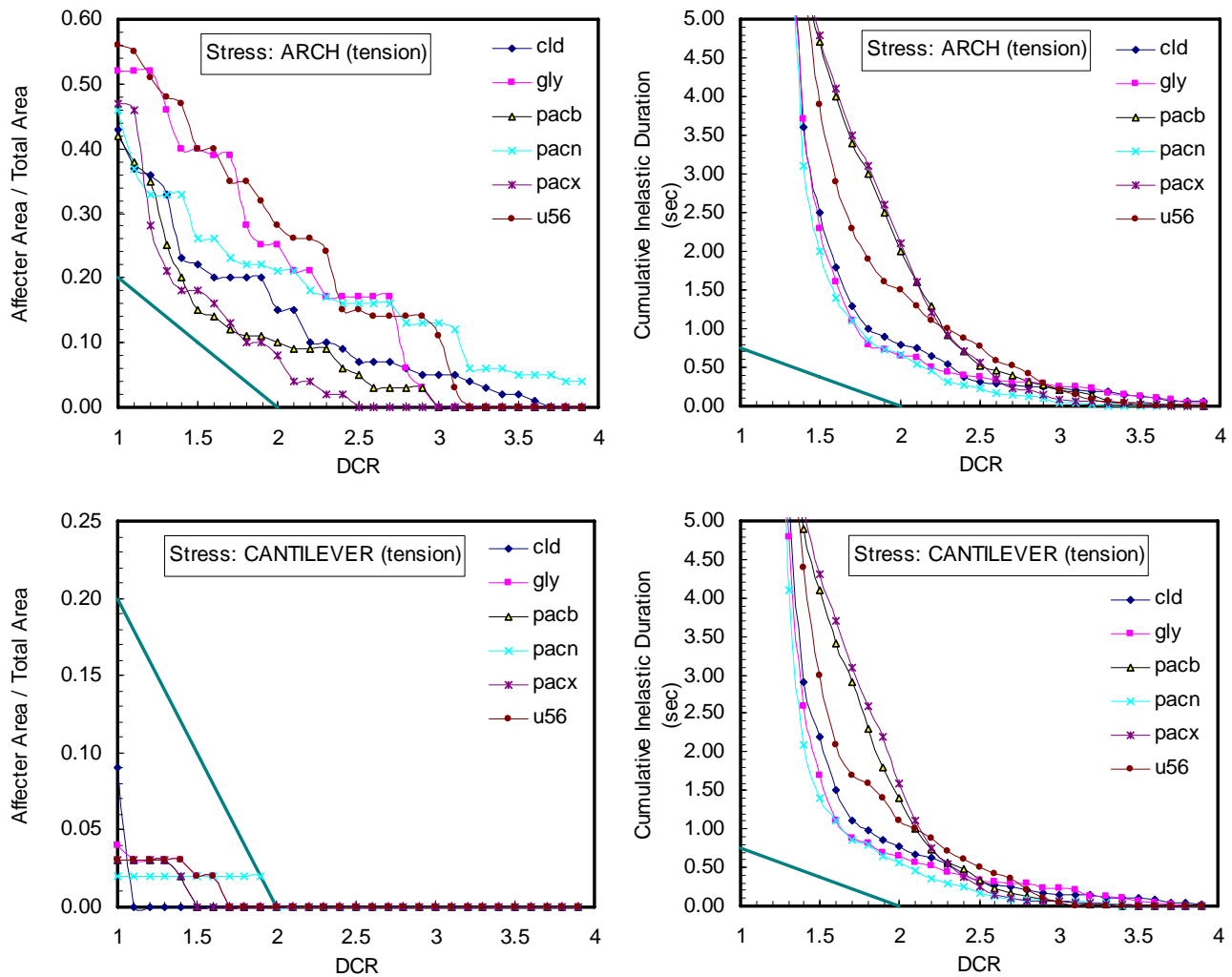
Figure F-5. Performance evaluation curves for Morrow Point Dam

F-7. Selection of Nonlinear Analysis Procedures

The results of linear analyses indicated that the high tensile arch stresses are well above the tensile strength of contraction joints and would lead to significant joint opening requiring nonlinear analysis. The Web-based dam analysis program QDAP was used to perform earthquake nonlinear analyses for the example arch dam (www.WebDams.com). QDAP is a 3D finite-element nonlinear analysis program with capabilities to account for nonlinear effects due to opening and closing of contraction joints and cracking/opening of lift lines during the earthquake ground shaking. The program uses a substructure technique to reduce the amount of computational effort. In substructure technique nonlinear equations of motion are formed only for the degrees of freedom at the contraction joints, or at the dam-foundation interface. Each cantilever bounded by the contraction joints and dam-rock abutment is considered as a substructure behaving in a linear manner under static and dynamic loads. The foundation rock is also a linear substructure in the entire system. The hydrodynamic loads are represented by the added mass terms. Any opening of the joints under hydrostatic and temperature loads are also considered in the analysis. QDAP is an enhanced version of the ADAP-88 program developed at UC Berkeley (Fenves et. al, 1989).

F-8. Nonlinear Finite-element Model

   a. Nonlinear earthquake response of an arch dam is sensitive to the modeling assumptions and characteristics of the earthquake ground motion. In this example several analyses are conducted to examine the effects that numbers and configuration of joints and characteristics of earthquake acceleration time histories might have on response of the dam. The finite-element model of the dam system will include the body of the dam, several contraction joints and lift lines represented by nonlinear joint elements, a portion of the foundation rock, and inertia effects of the impounded water represented by added mass terms. The analysis will start with three vertical contraction joints and proceed with more contraction joints and lift lines, as appropriate.

   b. Dam Model. The dam model is developed using mesh generation capability of the GDAP program. The body of the dam is modeled similar to that used in the linear-elastic analysis. It includes three layers of 8-node solid elements through the dam thickness. The 8-node solid elements are three-dimensional isoparametric elements with linear geometry and displacement interpolation in three directions. The finite-element mesh of the dam is arranged along horizontal and vertical planes to facilitate modeling of the joints. The vertical planes are oriented in the radial direction same as the contraction joints. This way, when needed, nonlinear joint elements can easily be inserted along the horizontal lift lines and the vertical contraction joints. A total of 270 8-node solid elements, 90 elements in each of the three layers were used to model the body of the dam, as shown in Figure F-6.
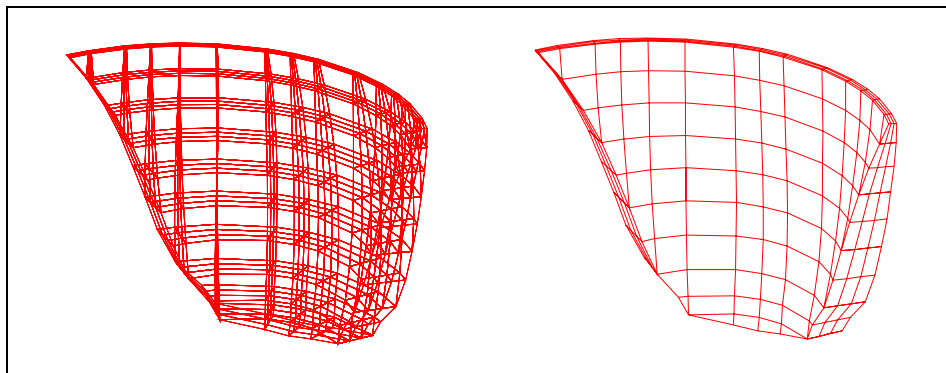
Figure F-6. Finite-element mesh of dam body

c. Nonlinear Joint Model. Concrete arch dams are constructed as individual cantilever blocks separated by vertical contraction joints. The contraction joints usually are grouted at the completion of the dam or in stages and may also include shear keys for additional resistance. However, contraction joints have limited tensile resistance and can open and close repeatedly during the earthquake ground shaking that produces net tensile forces across the joints. Such opening and closing of the joints is transient in nature, but if severe, can lead to unstable cantilever blocks and concrete crushing due to impact. The joint opening relieves tensile stresses across the joint but compressive stresses are increased due to the impact and reduced contact surfaces. This nonlinear behavior therefore needs to be investigated to ensure that the amount of joint opening and compressive stresses are not excessive. The contraction joint opening is modeled using a nonlinear joint element shown in Figure F-7 (Fenves et al., 1989). The nonlinear joint element consists of two coincident surfaces, each defined by four nodes that may lie on a plane (Figure F-7a). The element stiffness properties, displacements, and stresses are computed at four Gauss integration points shown in Figure F-7b. The relative displacements between the two element surfaces, v, produce stresses, q, according to the nonlinear relationship described in Figure F-7c. As shown in this figure, the element is characterized by the tensile strength, q_0, and the stiffness, k. The tensile strength q_0 can be selected to represent different joint types. For example, $q_0 = 0$ represents an ungrouted joint or a grouted joint with zero tensile strength. Whereas a nonzero q_0 represents a grouted joint for which some tensile strength can be assumed. Finally, a large value of q_0 may be used to simulate a linear analysis for which the joints are not permitted to open. The nonlinear joint elements are placed between cantilever blocks to model opening and closing of contraction joints, between lift lines to model cracking and opening and closing of the lift lines, and at the dam-foundation contact to model cracking and separation of the dam from the foundation.

(a) Local and global coordinate systems

(b) Integration points

(c) Stress-relative displacement relationship
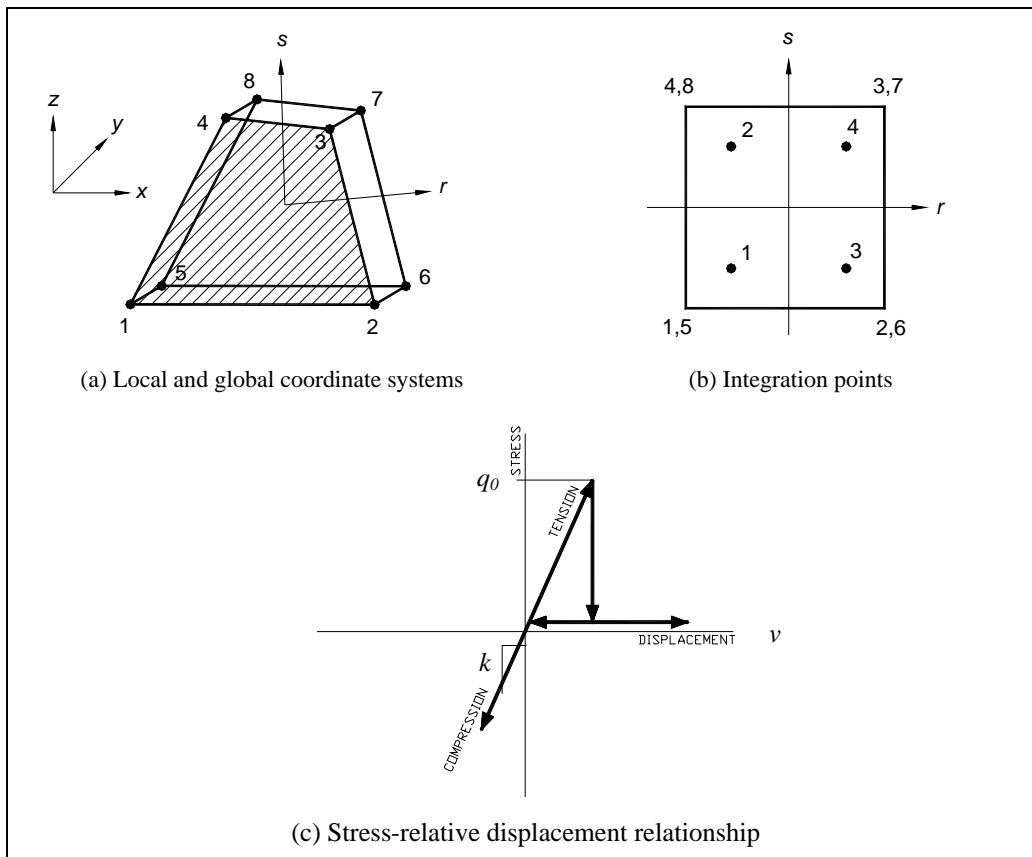
Figure F-7. Nonlinear Joint Element

d. Foundation Model. The finite-element model of the foundation rock is similar to that used in the linear analysis and shown in Figure F-3. The finite-element mesh for the foundation was constructed on the semi circular planes cut into the canyon wall perpendicular to the dam-foundation interface. The radius of the semi-circle was selected twice the dam height. A total of 396 8-node solid elements were used. The foundation model was assumed to be massless, an assumption that is commonly used in practice to eliminate reflection of seismic waves at the fixed boundaries of the foundation model and to apply the earthquake records measured at the ground surface directly at the base of the foundation model.

e. Incompressible Water Model. The inertia forces of the impounded water due to earthquake shaking were represented by the equivalent added mass terms applied to the upstream nodes of the dam. The added-mass of water was computed using a finite-element mesh of incompressible water, as shown in Figure F-3. The fluid mesh, which was developed in the linear analysis, included five element layers and was constructed by projecting the upstream nodes of the dam about five times the water depth in the upstream direction. This prismatic fluid mesh included a total of 450 3D fluid elements to represent the body of the water and 90 2D fluid elements to establish the dam-water interface. The water level was assumed at the crest elevation. The computer program QRES (www.WebDams.com) was used for solution of the incompressible added mass. The resulting added-mass is a full matrix that couples all degrees-of-freedom at the upstream face of the dam. If left this way, this matrix couples all substructures together, thus negating the major advantage of the substructure solution for the joint opening mechanism. For this reason, the added-mass matrix is diagonalized in the nonlinear analysis using QDAP.

F-9. Selection of Nonlinear Analysis Parameters

a. As mentioned earlier, the nonlinear earthquake response of arch dams is sensitive to the numbers and configuration of the joints as well as on characteristics of the earthquake ground motion. In this example both of these issues are examined. With respect to joint opening three models are considered: 1) a model with three vertical contraction joints, 2) a model with five vertical contraction joints, and 3) a model with five vertical contraction joints, two lift-line joints, and a peripheral joint at the dam-foundation contact. The sensitivity to ground motion is addressed by using six sets of three-component acceleration time histories with a wide range of ground motion characteristics including the near field effects. Other analysis parameters such as the concrete and foundation rock material properties, joint properties, and damping are kept the same for all eighteen analyses.

b. Material Properties. Material properties for the concrete and foundation rock are listed in Table F-2 below. Whenever applicable they are given for both the static and dynamic loading to account for the effects of rate of loading on modulus values and material strengths. A nominal compressive strength of 3,000 psi was assumed for the concrete. Note that the foundation rock is assumed not to be affected by thermal loading; thus a coefficient of thermal expansion of zero is assigned to the rock. Furthermore, the unit weight of the rock is set to zero to satisfy the assumption of massless foundation discussed earlier.

Table F-2. Assumed material properties

Concrete Material Properties					
Static Compressive Strength	$(f_c')_{st}$	4,000.00	psi	27.50	MPa
Dynamic Compressive Strength	$(f_c')_d$	5,000.00	psi	34.50	MPa
Static Tensile Strength	$(f_t)_{st}$	450.00	psi	3.10	MPa
Apparent Dynamic Tensile Strength	$(f_t)_{ad}$	900.00	psi	6.2	MPa
Modulus of Elasticity (static)	E_{st}	454,700.00	ksf	21,771.00	MPa
Modulus od Elasticity (Dynamic)	E_d	604,800.00	ksf	28,958.00	MPa
Coefficient of Thermal Expansion	α	5.00E-06		5.00E-06	
Unit Weight	γ	0.15	kcf	2402.77	Kg/m^3
Poisson's Ratio	ν	0.20		0.20	
Rock Material Properties					
Modulus of Elasticity	E	460,800.00	ksf	22,063.00	MPa
Coefficient of Thermal Expansion	α	0.00		0.00	
Unit Weight	γ	0.00	kcf	0.00	kcf
Poisson's Ratio	ν	0.20		0.20	

c. Joint Properties. The joint properties needed for the analysis are the normal stiffness and tangential stiffness with the corresponding joint strengths. The normal and tangential stiffness for the joint element are assigned large values to enforce displacement continuity at the contraction joints. However, these values should not be too large to cause numerical problems. Appropriate stiffness values for the joint may be selected equal to (n.E/L) where E is the modulus of elasticity of the concrete and L is the length of the adjacent 3D solid element in the direction normal to the joint. Depending on the floating point precision, n may range from 10 to 100 with larger values for higher precision floating point representation. In this example a stiffness value of 157x109 N/m3 (1x109 lb/ft3) was assumed in the normal and tangential directions. The joint strength (q0) was set to zero assuming that the joint cannot resist any tension.

d. Damping. QDAP requires that proportional Rayleigh damping be used. Ten modes of vibration were used to approximate 5% critical damping for the concrete dam. The periods of vibration needed for this purpose were computed using the GDAP program.

e. Number and Configuration of Joints. Three joint configurations were analyzed. Initially three vertical contraction joints were modeled at the location of maximum tensile arch stresses from the linear analysis. These locations were at the quarter span points and at the crown section of the dam. Each of these contraction joints was modeled by many nonlinear joint elements that covered the entire length of the joint from the top to bottom and through the thickness of the dam. Based on the results of this initial model, a second configuration with five contraction joints was analyzed. The locations of these joints were also selected on the basis of tensile arch stresses. A third and final configuration included three types of joints: five vertical, two horizontal, and one peripheral joint at the dam-foundation interface. The purpose of the vertical joints was to relieve high tensile arch stresses. The horizontal joints were to permit cracking and opening of the lift lines experiencing excessive tensile cantilever stresses; while the peripheral joint was intended to relieve tensile stresses at the dam-foundation contact caused by the assumption of linear-elastic behavior. Additional joints may be used to redistribute the joint openings. However, too many joints can significantly affect the computation time.

F-10. Computation of Nonlinear Earthquake Response

a. Analysis with Three Contraction Joints (Model 1)

(1) *Description of Model*. The nonlinear analysis for joint opening should start with a minimum number of contraction joints at the locations of maximum tensile arch stresses. The stress results from the linear-elastic analysis show that high tensile arch stresses develop on the upstream face at the crown section and on the downstream face near the quarter span points (see Figure 4-18 in EM 1110-2-6051). Thus the obvious choice is to start with three vertical contraction joints, one at the crown section and one each at the ¼ span points, as shown in the upstream view of the dam in Figure F-8 below. In this figure the thick lines indicate the locations where the nonlinear joint elements will be inserted. The addition of contraction joints increases number of nodal points, but the number of three-dimensional solid elements remains the same. A total of 72 contraction joint elements were used in this model.

(2) *Results*. The analysis began with the application of gravity, hydrostatic, and temperature loads as the initial conditions, followed by the step-by-step nonlinear time-history dynamic analysis for the seismic loads. Results are summarized in Table F-3 and in Figures F-9 to F-14 for the six input acceleration time history records. The table shows the maximum amount of joint opening with the peak tensile and peak compressive stresses. The figures display deflected shapes at the time of maximum joint opening, time-history of the maximum joint opening, envelopes of maximum arch and cantilever stresses, and vector plots of maximum principal stresses for the upstream and downstream faces of the dam. As expected, the maximum joint opening occurs at the crown section. Table F-3 indicates that the maximum joint opening varies from 1.2 inches for the spectrum-matched 1971 Pacoima Dam record (PACB) to 3.36 inches for the Gilroy record of 1989 Loma Prieta earthquake (GLY). The contraction joint at the crown-section opens 8 to 20 times during the ground shaking provided by six different acceleration time-history records. The 20 openings occur during the application of the spectrum-matched 1971 Pacoima Dam record (PACB). This confirms that the spectrum-matched records tend to increase the number of strong motion cycles. Each joint opening cycle lasts between 0.1 to 0.2 seconds, except for the Newhall record of 1994 Northridge earthquake (U56) during which the joint stays open about 0.5 second (Figure F-14). The reason for this long-duration opening is the presence of the long-period acceleration pulse in the Newhall record (Figure F-4). The results also show that tensile arch stresses have significantly reduced but not vanished. Therefore, it appears more contraction joints could be beneficial. In the next analysis, the number of contraction joints were increased to five, as discussed in Paragraph F-10b.

Table F-3. Summary of maximum joint opening and stresses for case with three contraction joints
(1 MPa = 145 psi)

Ground Motion Record	Max. Displ (in)	Max. Joint Opening (in)	Peak Tensile stresses (psi)			Peak Compressive Stresses (psi)		
			Arch	Cantilever	Principal	Arch	Cantilever	Principal
CLD	5.31	1.56	910	976	1,752	-3,451	-3,359	-3,932
GLY	9.67	3.36	1,193	1,008	1,679	-3,394	-2,395	-3,574
PACB	4.62	1.20	799	792	1,265	-2,509	-2,139	-3,349
PACN	5.83	1.38	907	881	1,537	-3,119	-2,290	-3,703
PACX	8.07	2.40	1,204	899	1,743	-3,490	-2,584	-4,014
U56	8.95	2.88	680	979	1,169	-2,648	-3,294	-3,404

Table F-4. Summary of maximum joint opening and stresses for case with five contraction joints
(1 MPa = 145 psi)

Ground Motion Record	Max. Displ (in)	Joint Opening (in.)	Peak Tensile stresses (psi)			Peak Compressive Stresses (psi)		
			Arch	Cantilever	Principal	Arch	Cantilever	Stress
CLD	5.63	1.56	1,028	1,315	1,441	-2,536.	-1,964	-3,478
GLY	10.02	2.58	897	1,193	1,852	-3,526	-2,439	-3,584
PACB	4.60	1.08	1,331	756	1,338	-2,715	-2,027	-3,311
PACN	5.80	1.44	1,017	1,046	1,430	-3,225	-2,510	-3,754
PACX	8.23	2.16	1,162	936	1,641	-3,385	-2,667	-4,051
U56	8.61	2.15	869	990	1,140	-2,711	-3,295	-3,598

Table F-5. Summary of maximum joint opening and stresses for case with vertical, horizontal, and peripheral joints (1 MPa = 145 psi)

Ground Motion Record	Max. Displ. (in)	Joint Opening (in.)	Peak Tensile stresses (psi)			Peak Compressive Stresses (psi)		
			Arch	Cantilever	Principal	Arch	Cantilever	Principal
CLD	5.99	1.80	846	994	1,208	-2,576	-1,890	-2,638
GLY	10.59	4.32	1,308	1,365	2,113	-3,094	-2,089	-3,355
PACB	5.43	1.98	823	786	1,355	-2,038	-1,719	-2,202
PACN	6.26	2.40	1,223	1,186	1,822	-3,352	-1,944	-3,629
PACX	9.75	3.72	1,187	1,408	2,023	-3,198	-1,922	-3,256
U56	15.35	9.50	1,117	1,438	2,300	-3,758	-1,994	-3,759
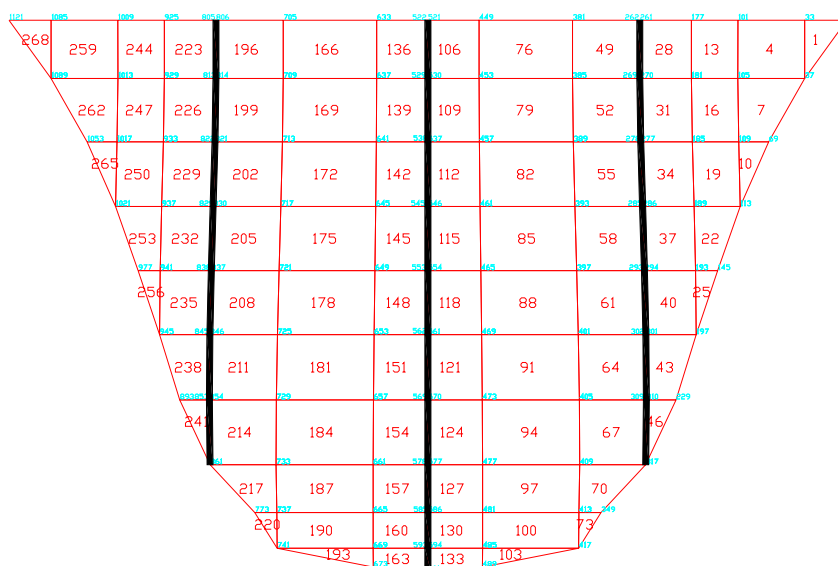
Figure F-8. Finite-element mesh with three contraction joints (Model 1)
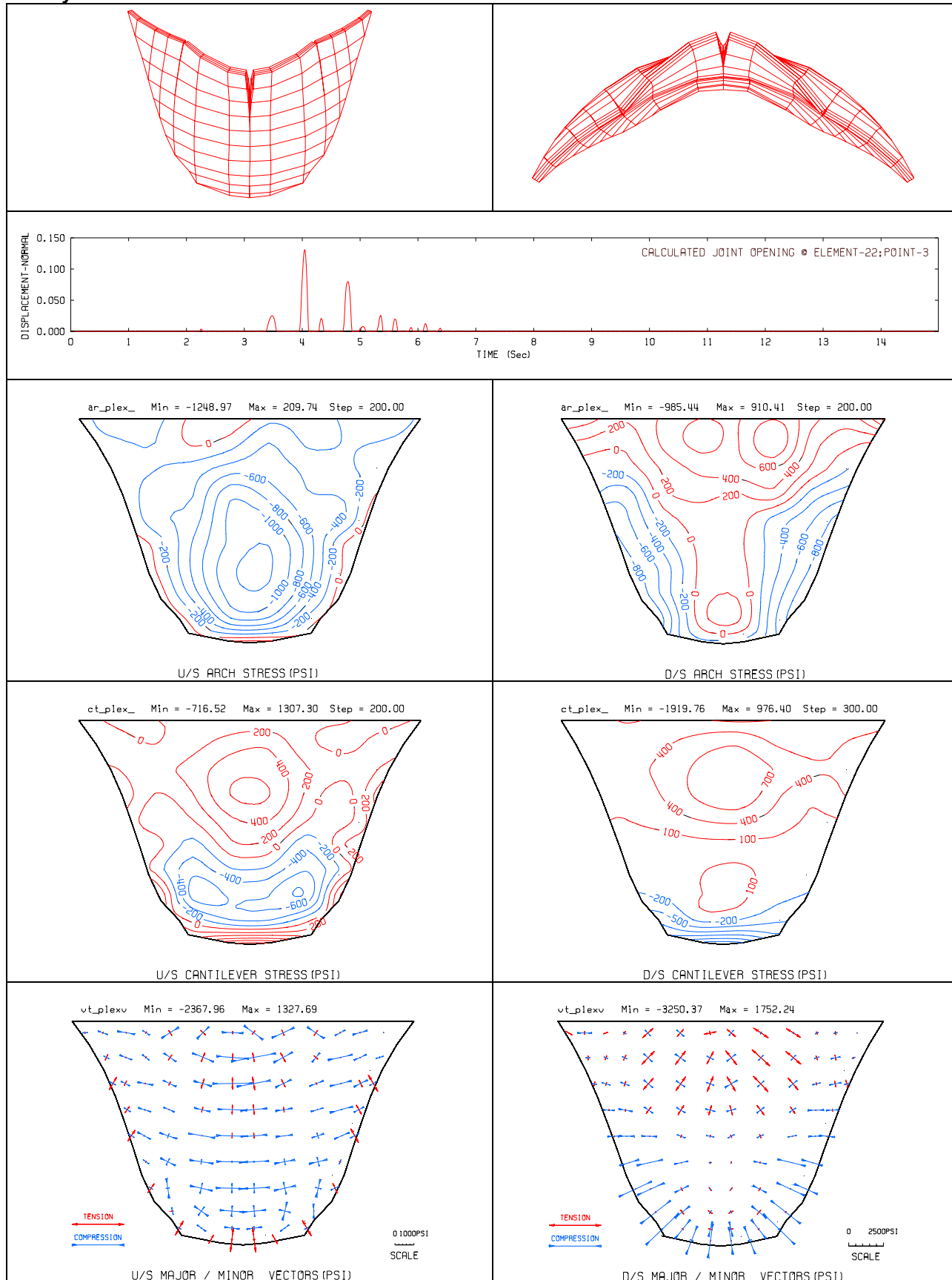
Figure F-9. Deflected shapes, maximum joint opening time history (in units of ft), envelopes of maximum arch and cantilever stresses, & envelopes of principal stress vectors due to CLD record
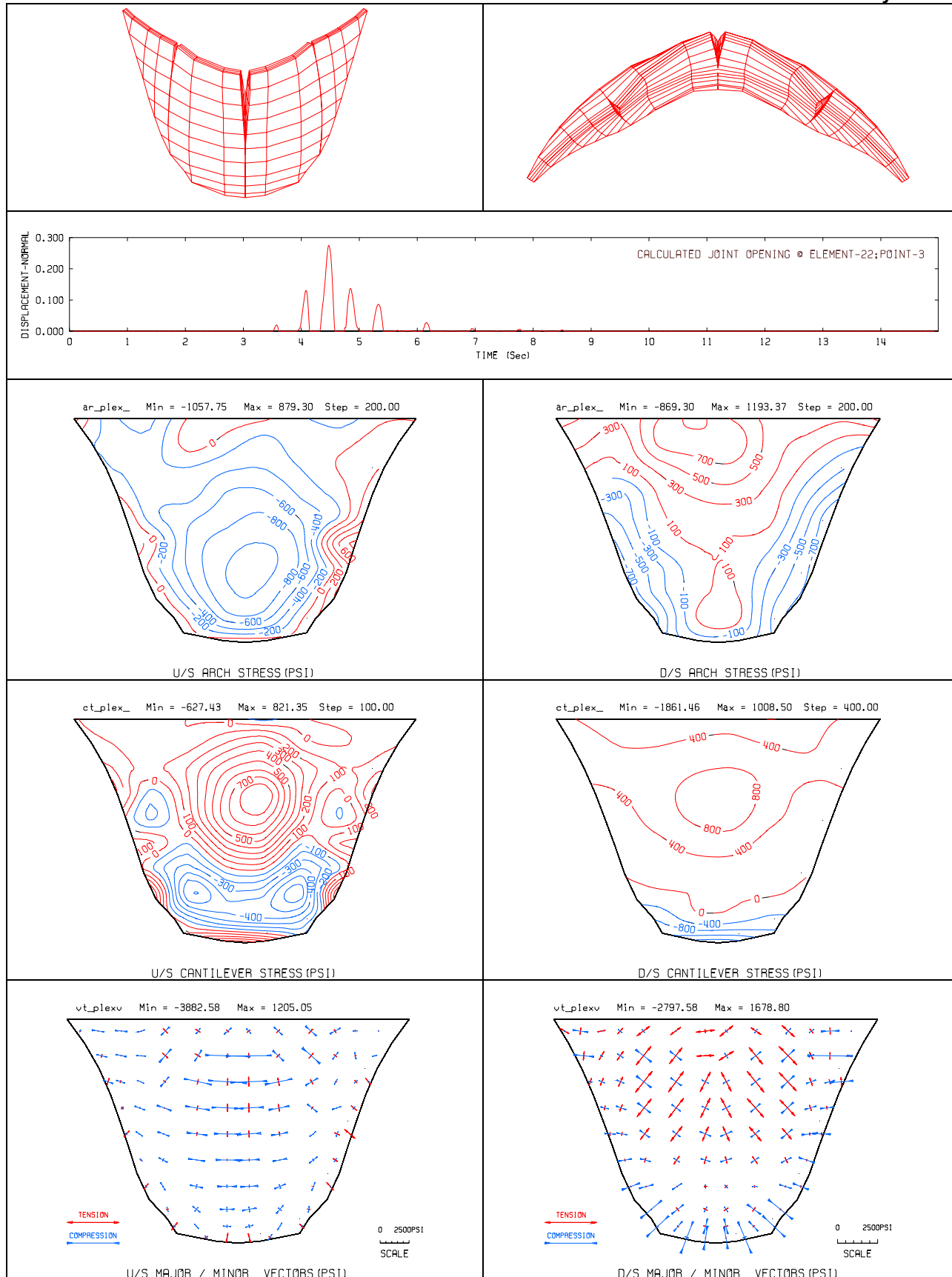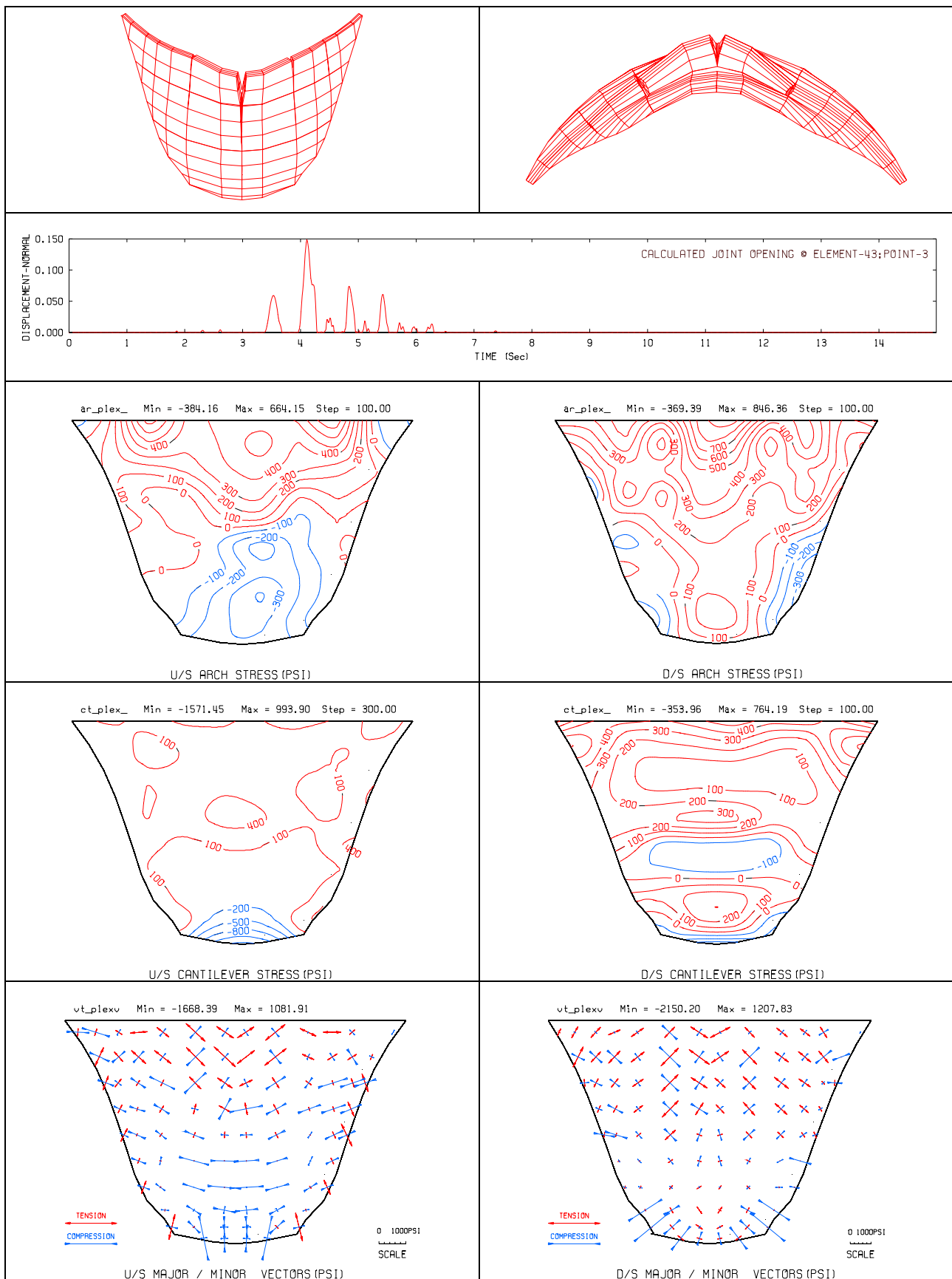
Figure F-10. Deflected shapes, maximum joint opening time history (in units of ft), envelopes of maximum arch and cantilever stresses, & envelopes of principal stress vectors due to GLY record
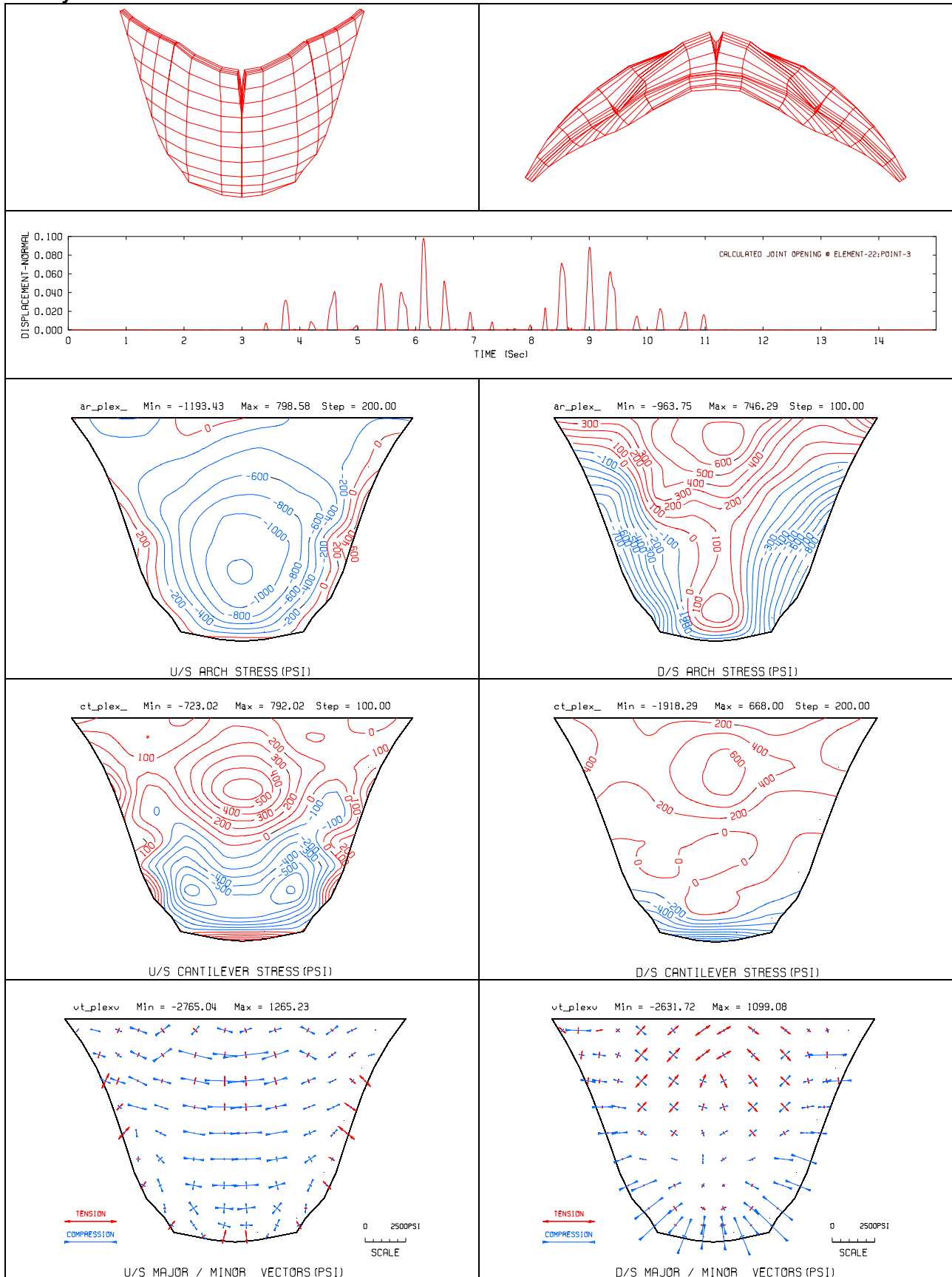
Figure F-11. Deflected shapes, maximum joint opening time history (in units of ft), envelopes of maximum arch & cantilever stresses, & envelopes of principal stress vectors due to PACB record
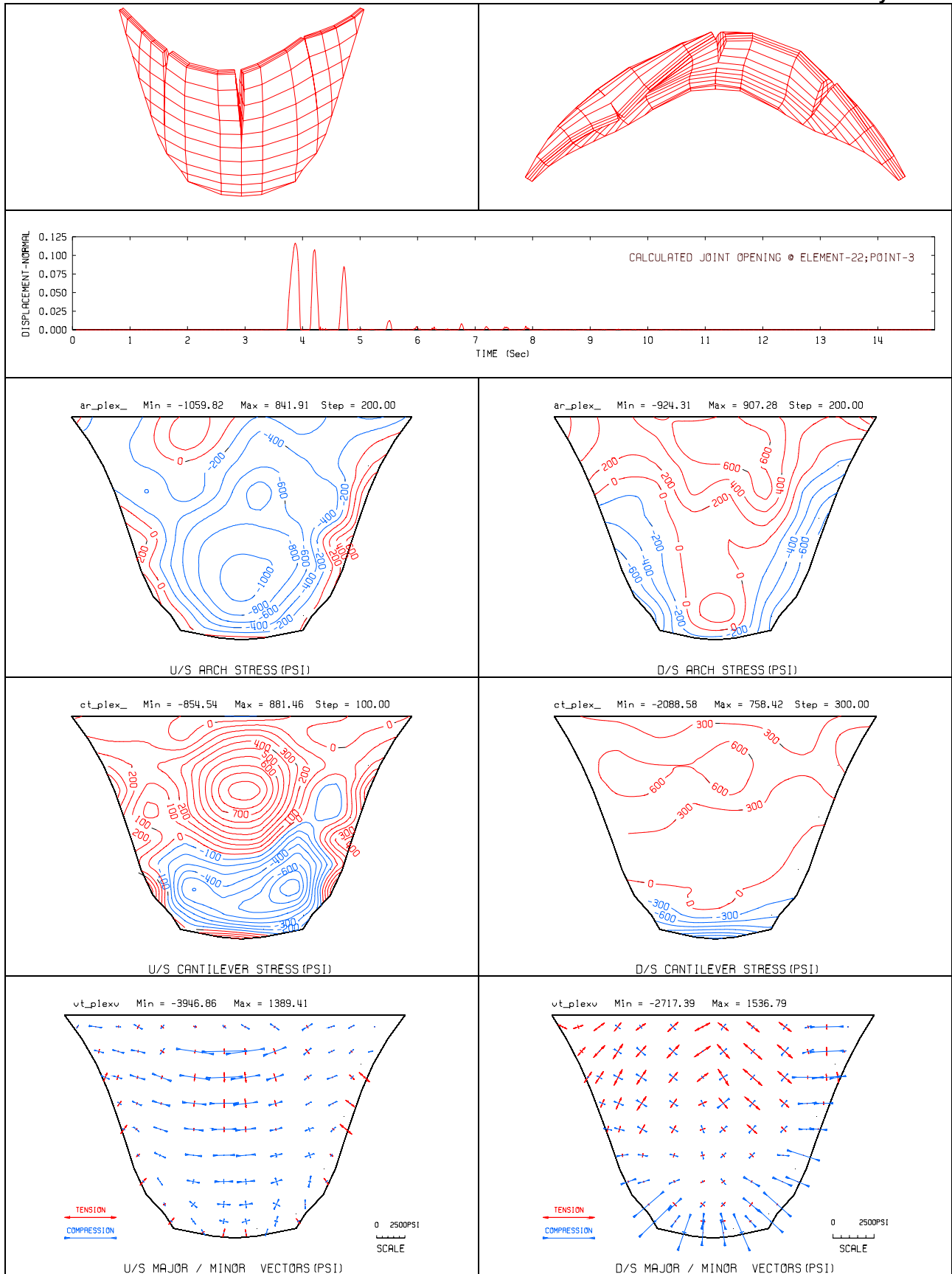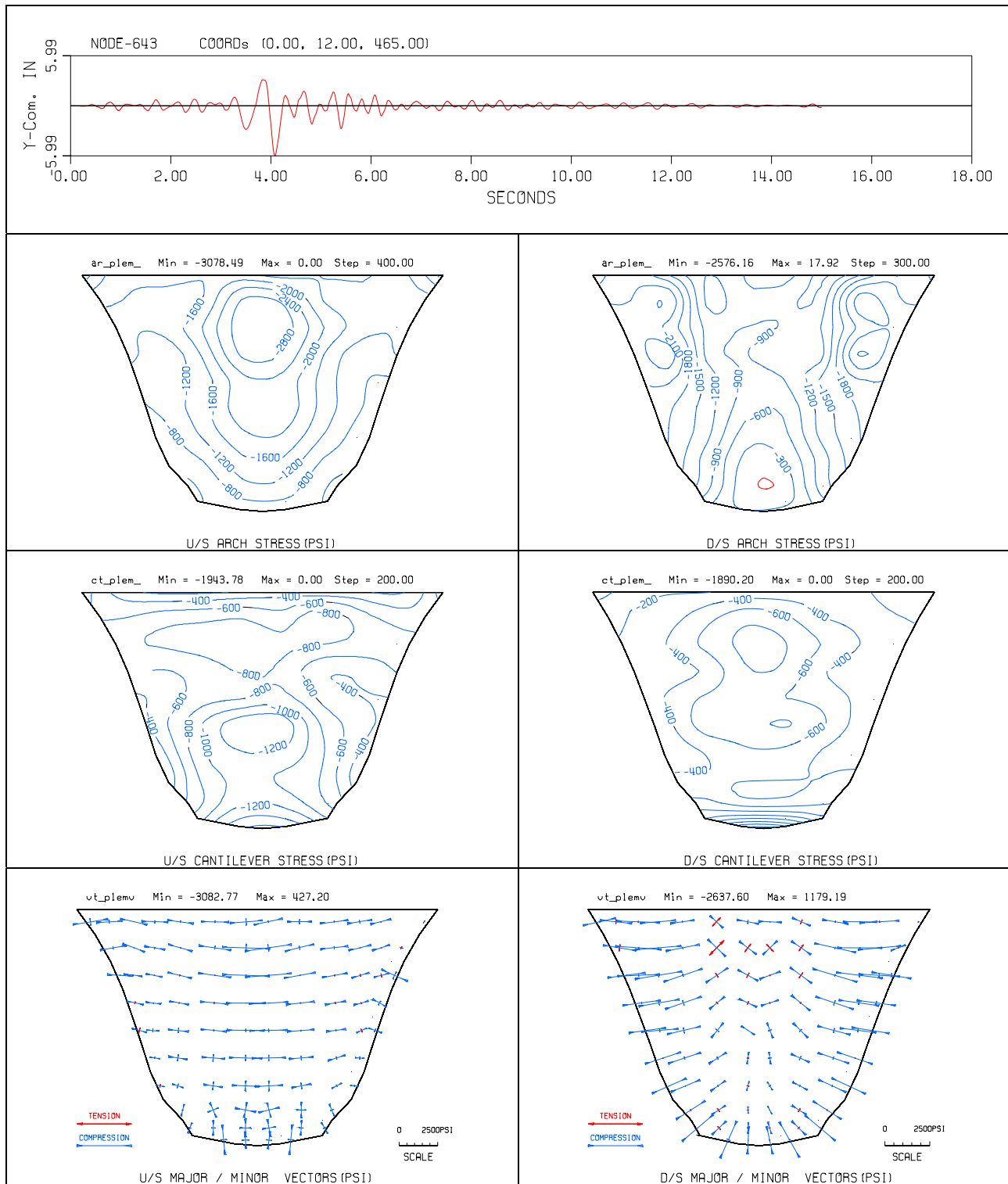
Figure F-12. Deflected shapes, maximum joint opening time history (in units of ft), envelopes of maximum arch & cantilever stresses, & envelopes of principal stress vectors due to PACN record
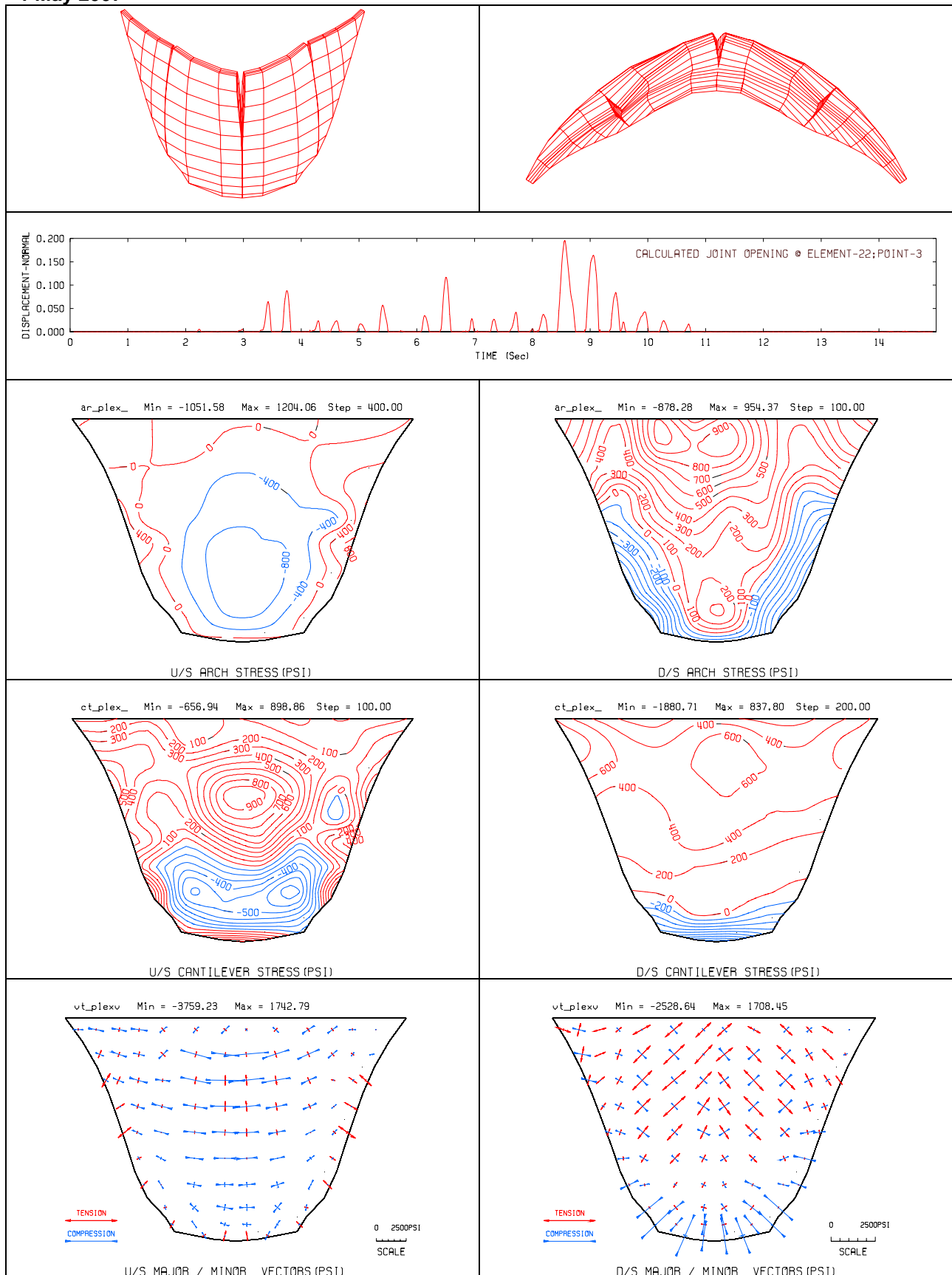
Figure F-13. Deflected shapes, maximum joint opening time history (in units of ft), envelopes of maximum arch & cantilever stresses, & envelopes of principal stress vectors due to PACX record
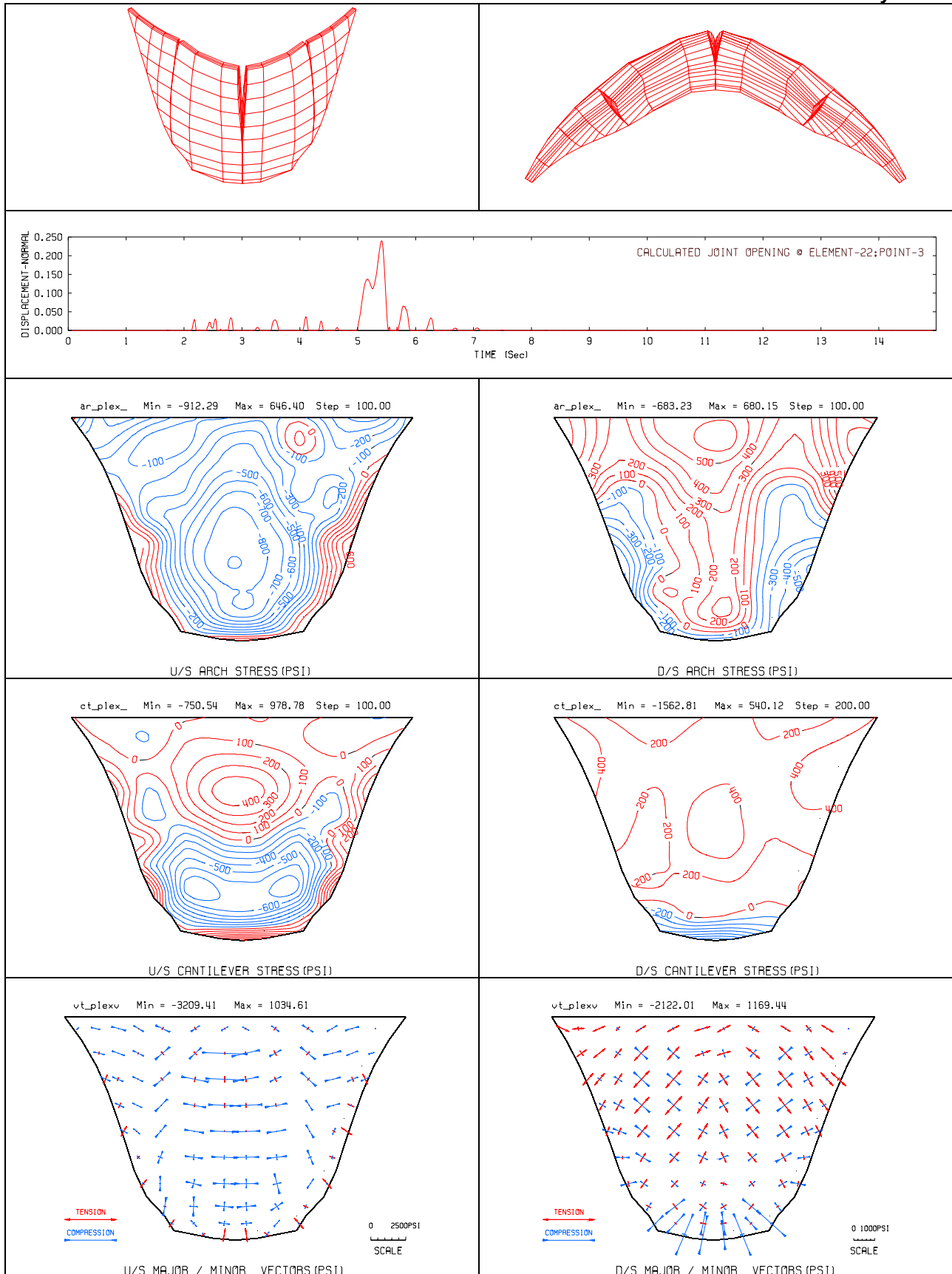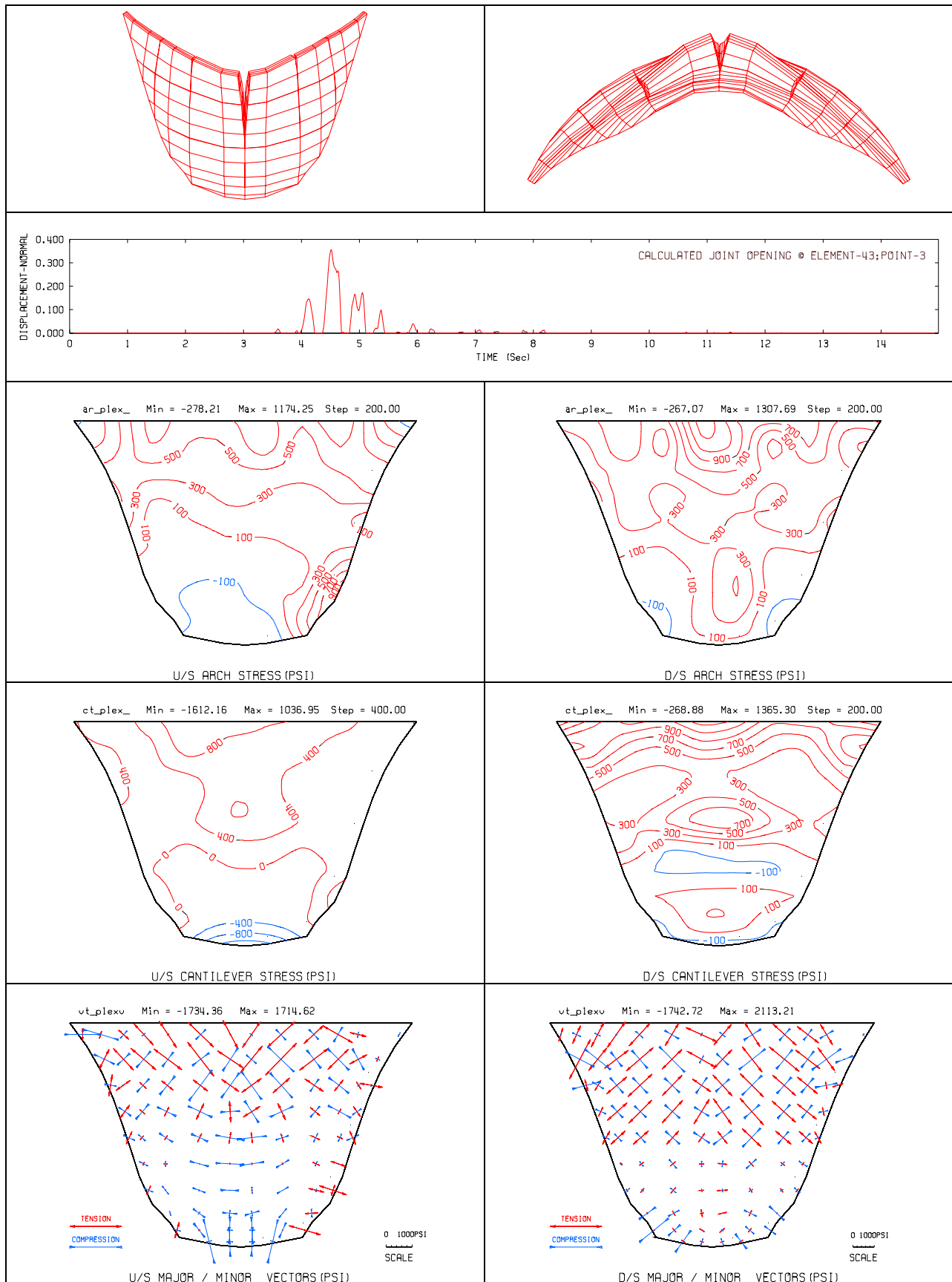
Figure F-14. Deflected shapes, maximum joint opening time history (in units of ft), envelopes of maximum arch and cantilever stresses, & envelopes of principal stress vectors due to U56 record

b. Analysis with Five Contraction Joints (Model 2)

(1) *Description of Model.* The finite-element model with five contraction joints is shown in Figure F-15. The contraction joints were distributed uniformly along the length of the dam. A total of 114 contraction joint elements were employed.

(2) *Results.* Again the analysis began with the application of static loads as the initial conditions, followed by the step-by-step nonlinear time-history dynamic analysis for the selected six earthquake records. The results are summarized in Table F-4 and in Figures F-16 to F-21. Overall, the results for the five-contraction-joint model (Model-2) are similar to those for the three-contraction-joint model (Model-1), except that the amounts of maximum joint openings are 4 to 25 percent smaller. The largest joint opening still occurs for the Gilroy record (GLY), except that at 2.58 inches the Model-2 joint opening is 23% smaller than the 3.36 inches computed for Model-1 (Tables F-3 and F-4). The joint opening reduction for Newhall record (U56) is about 25 percent. The stress magnitudes have increased for some input records and decreased for others showing no obvious tendencies. The changes in stress magnitudes are mostly limited to 0.7 to 1.4 MPa (100 to 200 psi), which are not large. In summary there are no significant differences between the responses of Model-1 and Model-2. However, Model-2 which distributes joint openings to more contraction joints is preferable and will be used in conjunction with the lift joints and peripheral joints in the next section.
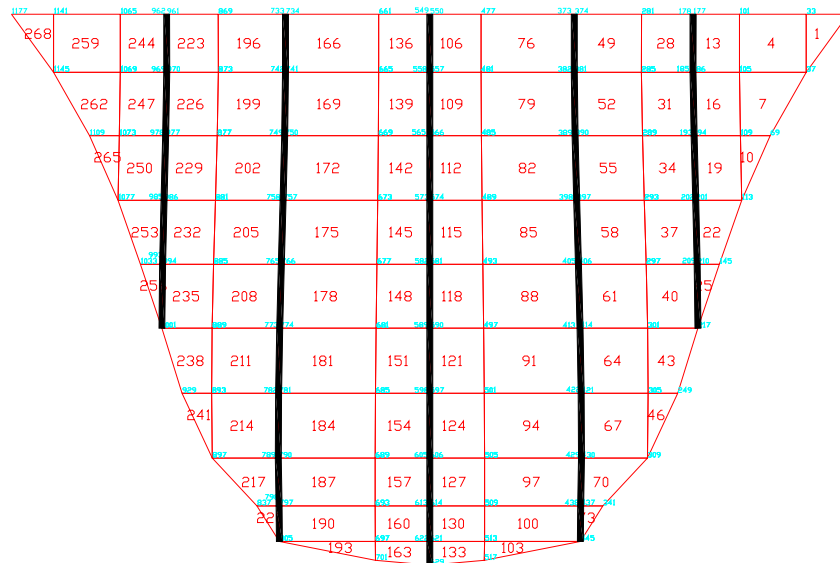
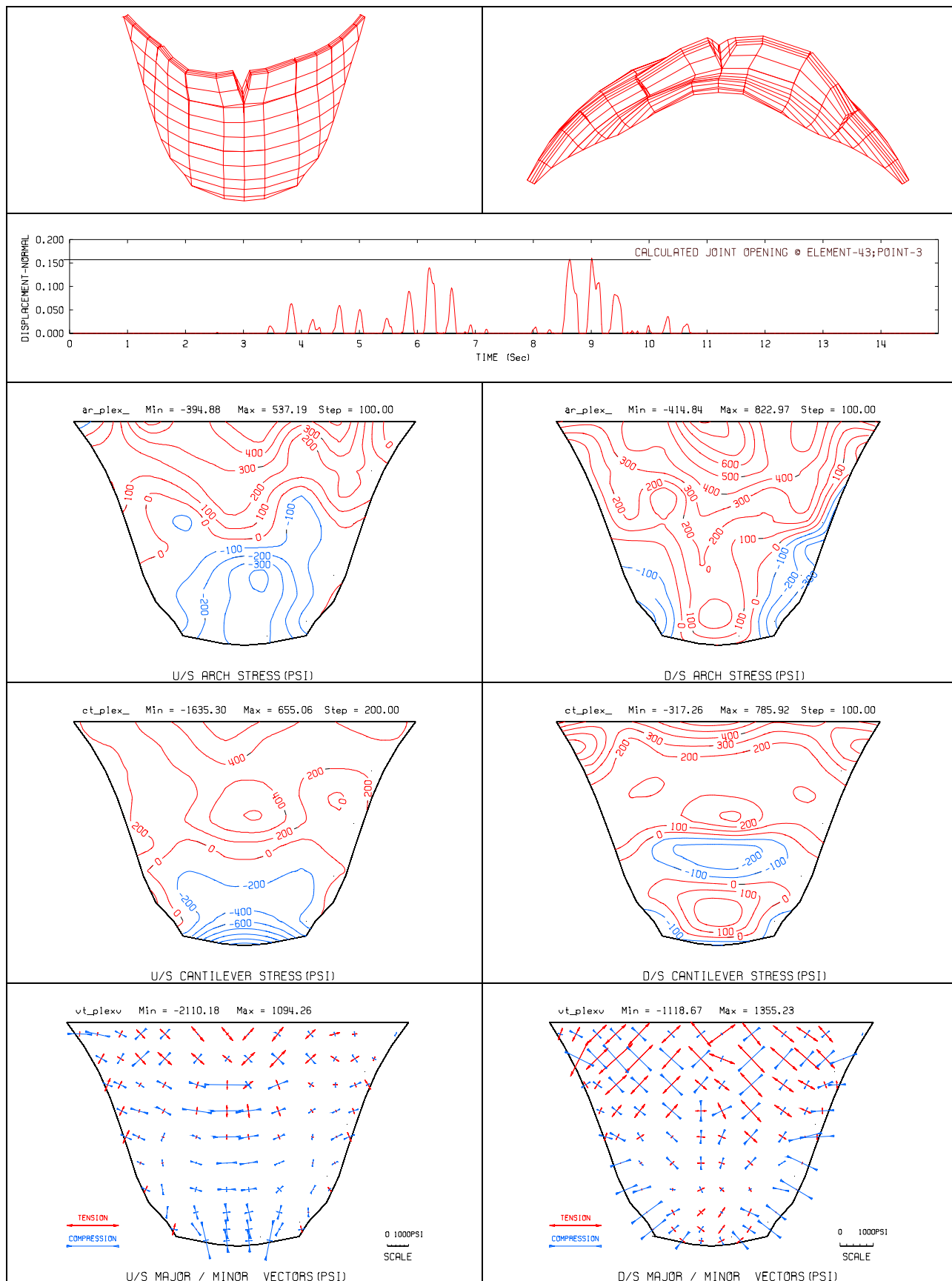**Figure F-15. Finite-element mesh with five contraction joints (Model 2)**
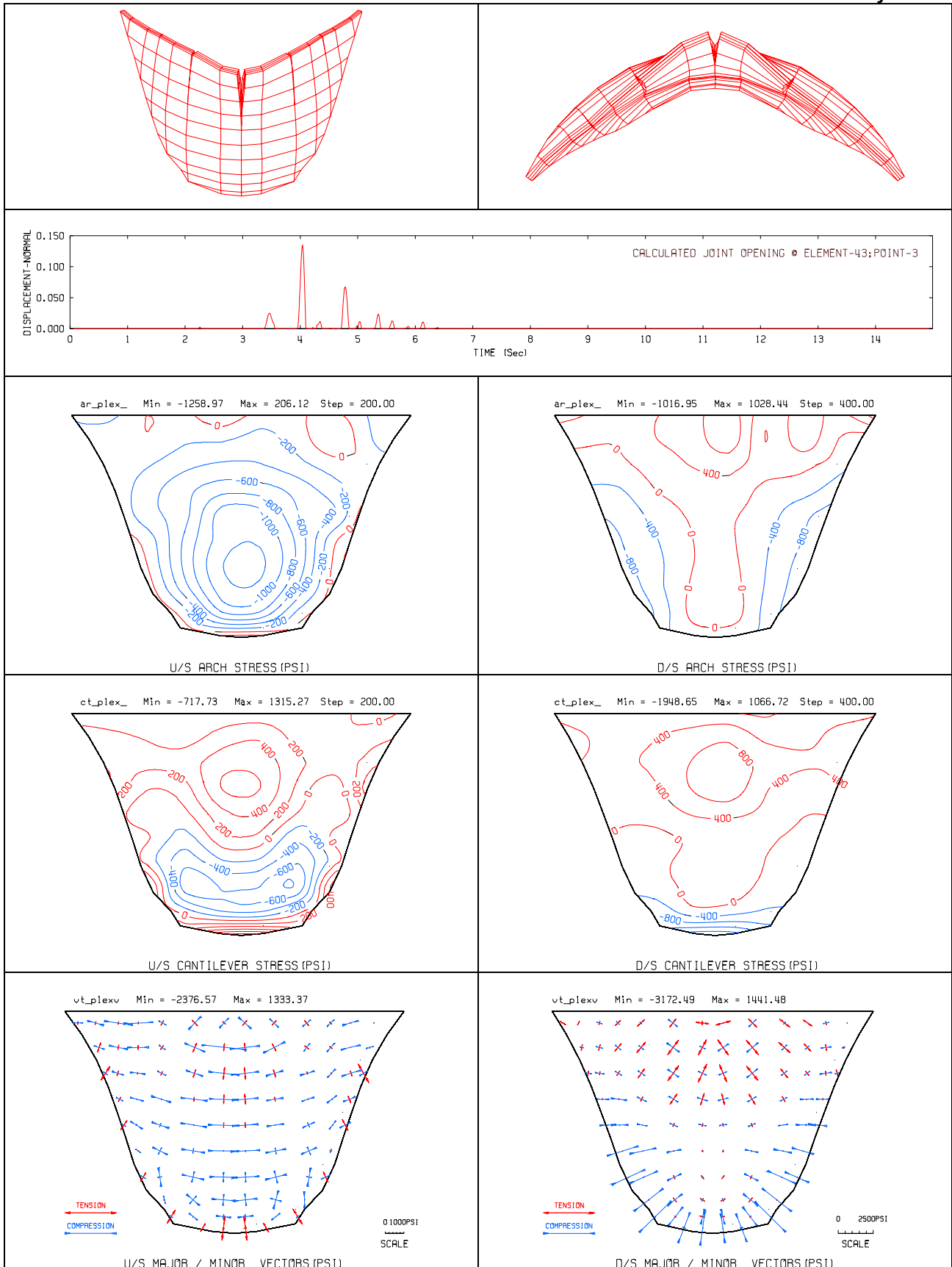
Figure F-16. Deflected shapes, maximum joint opening time history, envelopes of maximum arch and cantilever stresses, and envelopes of principal stress vectors due to CLD record
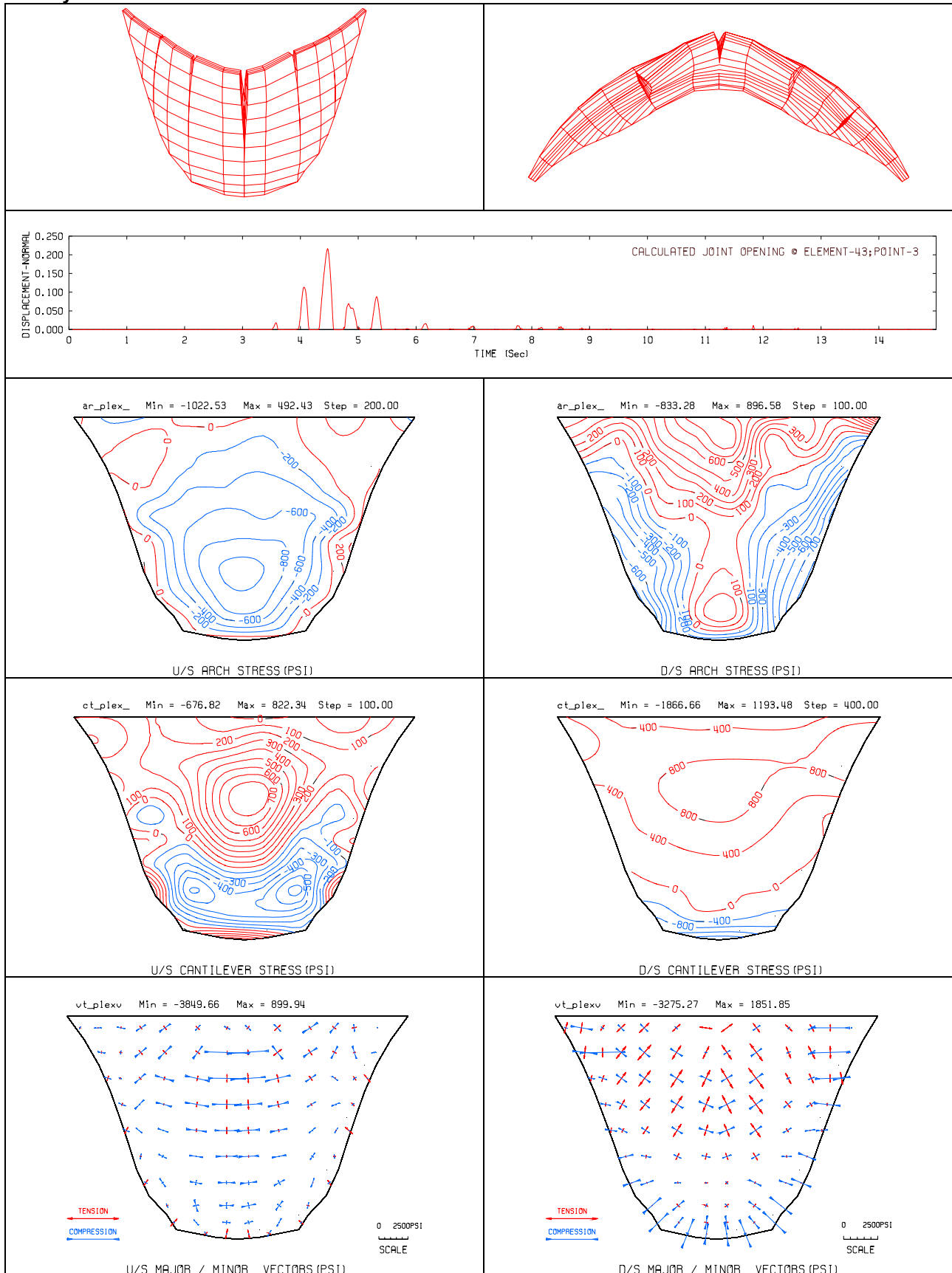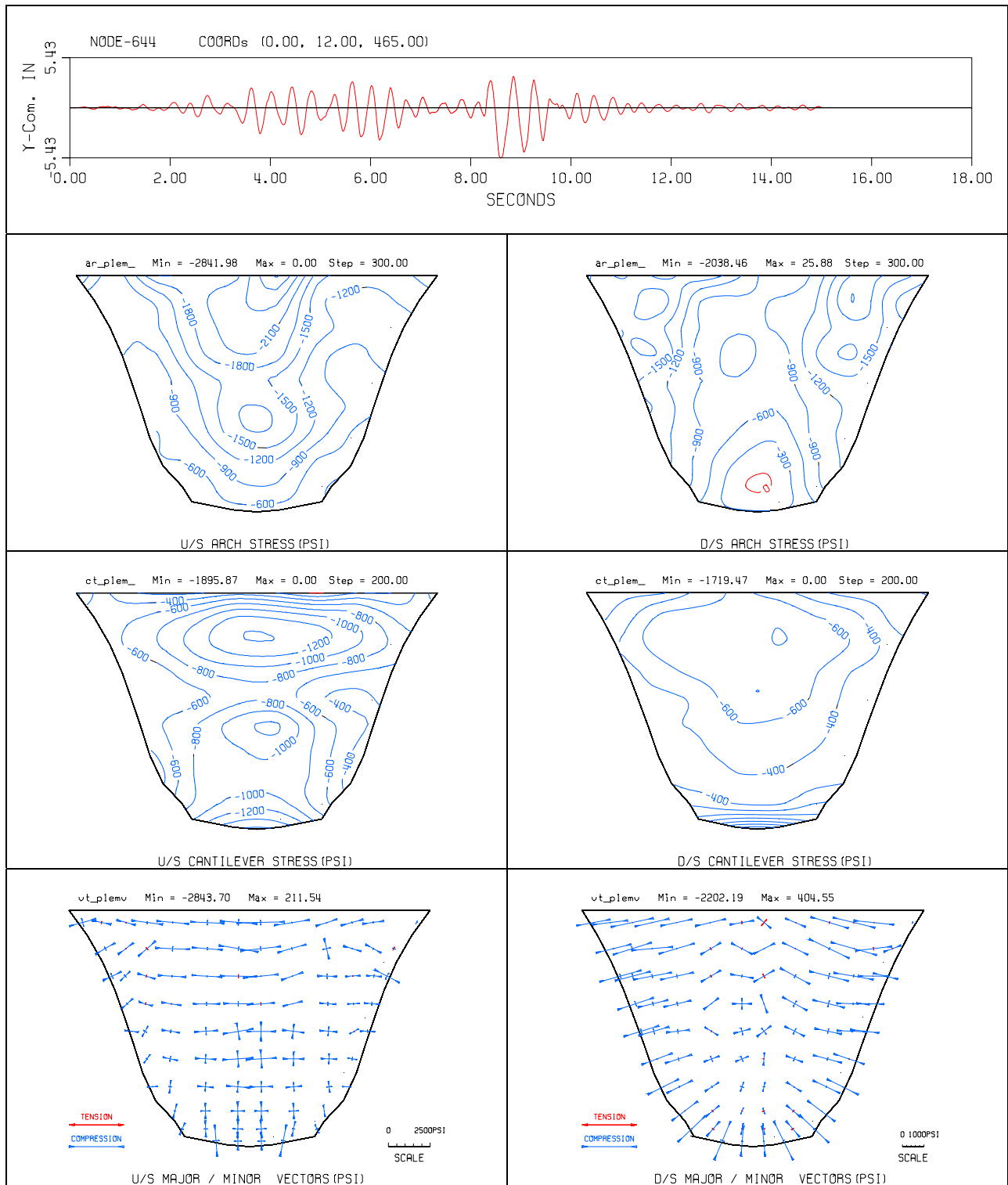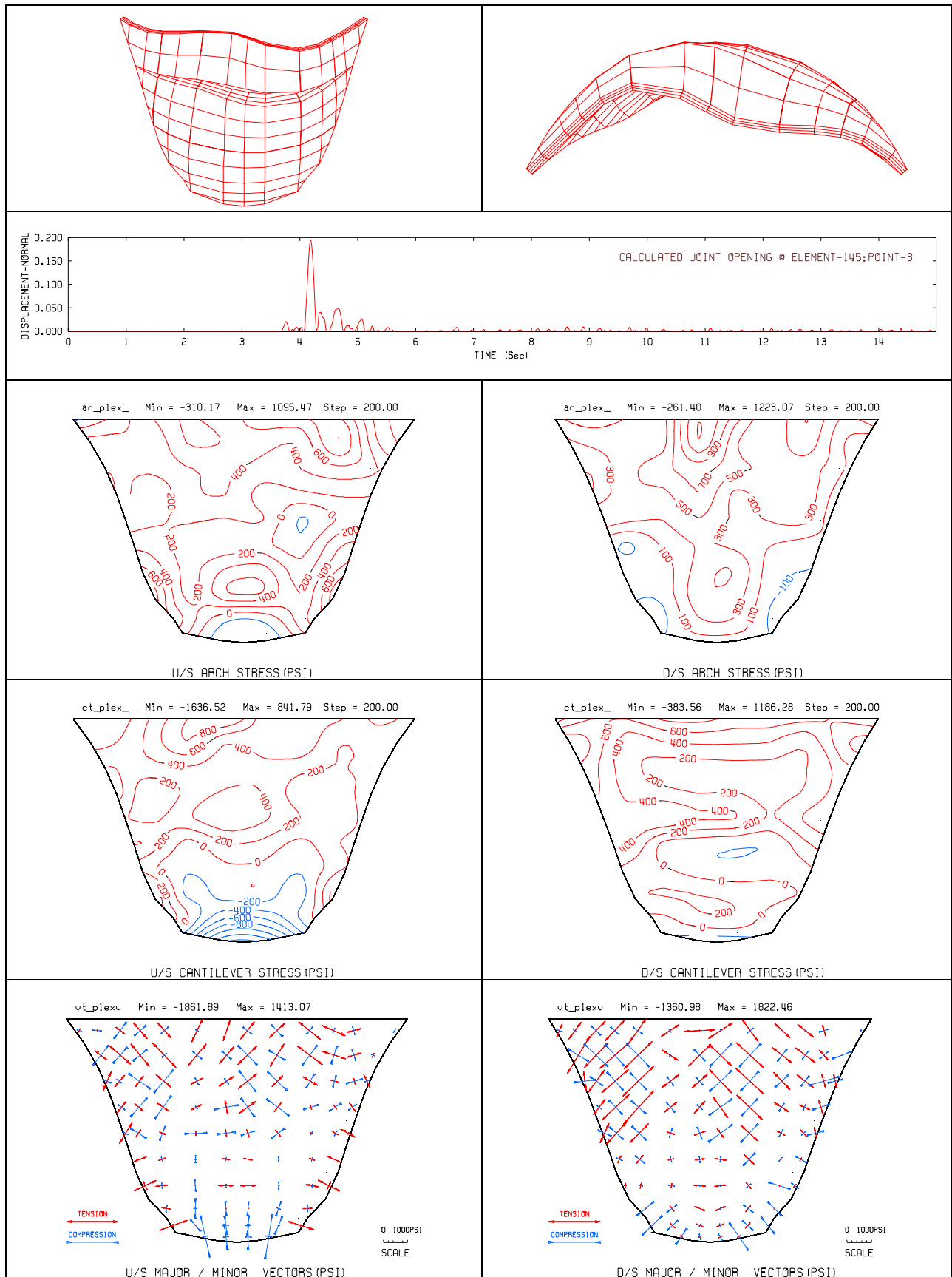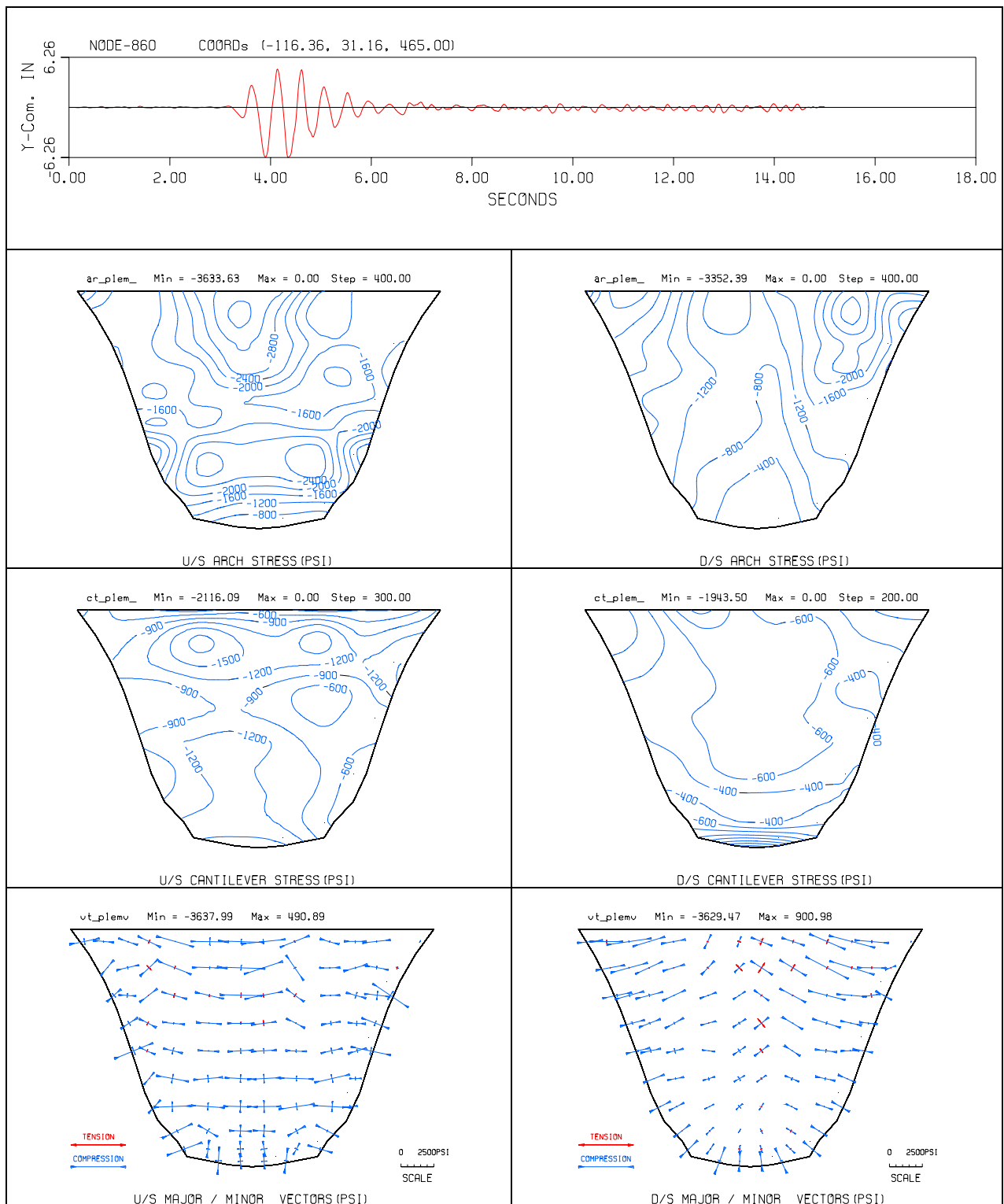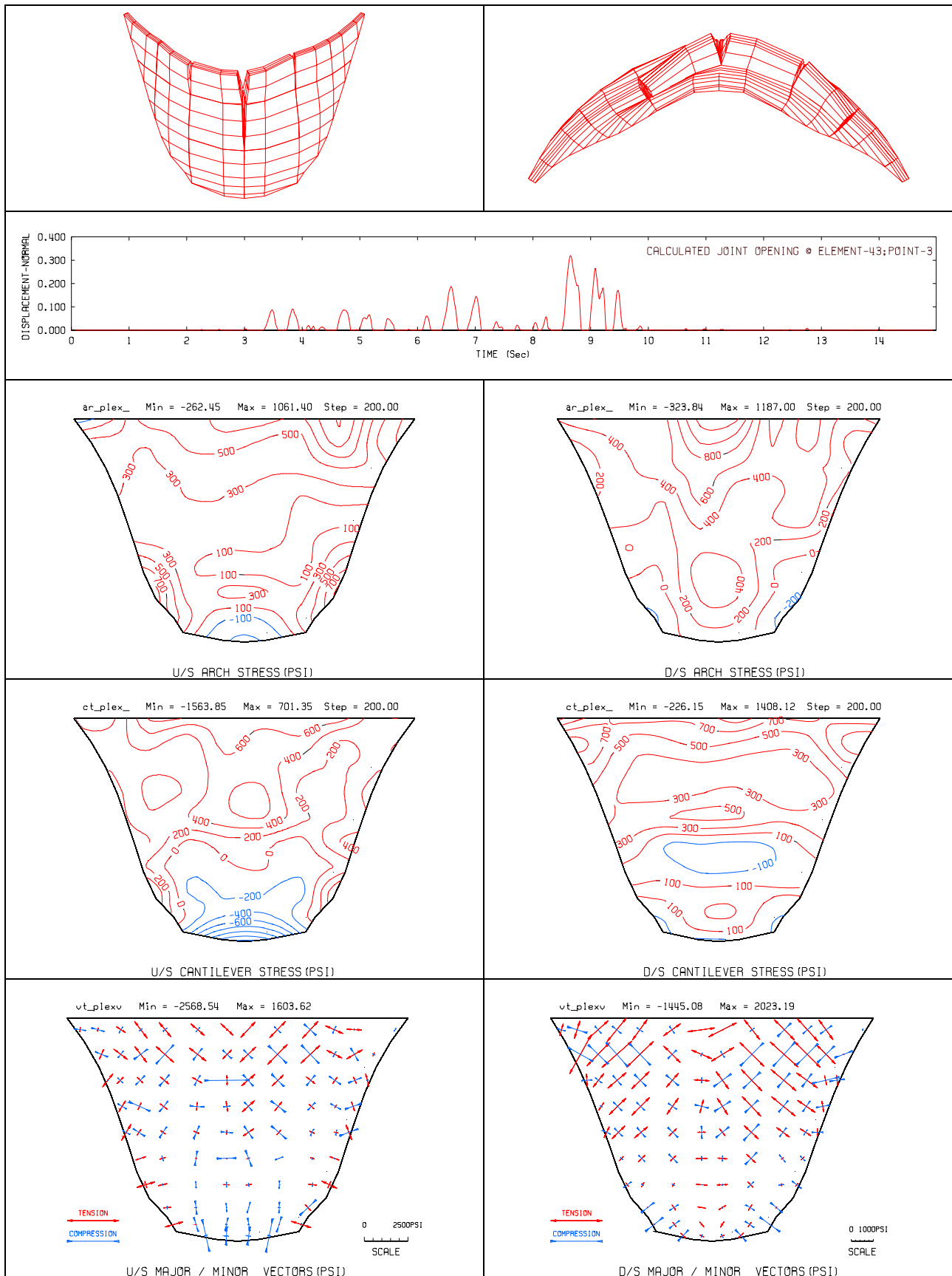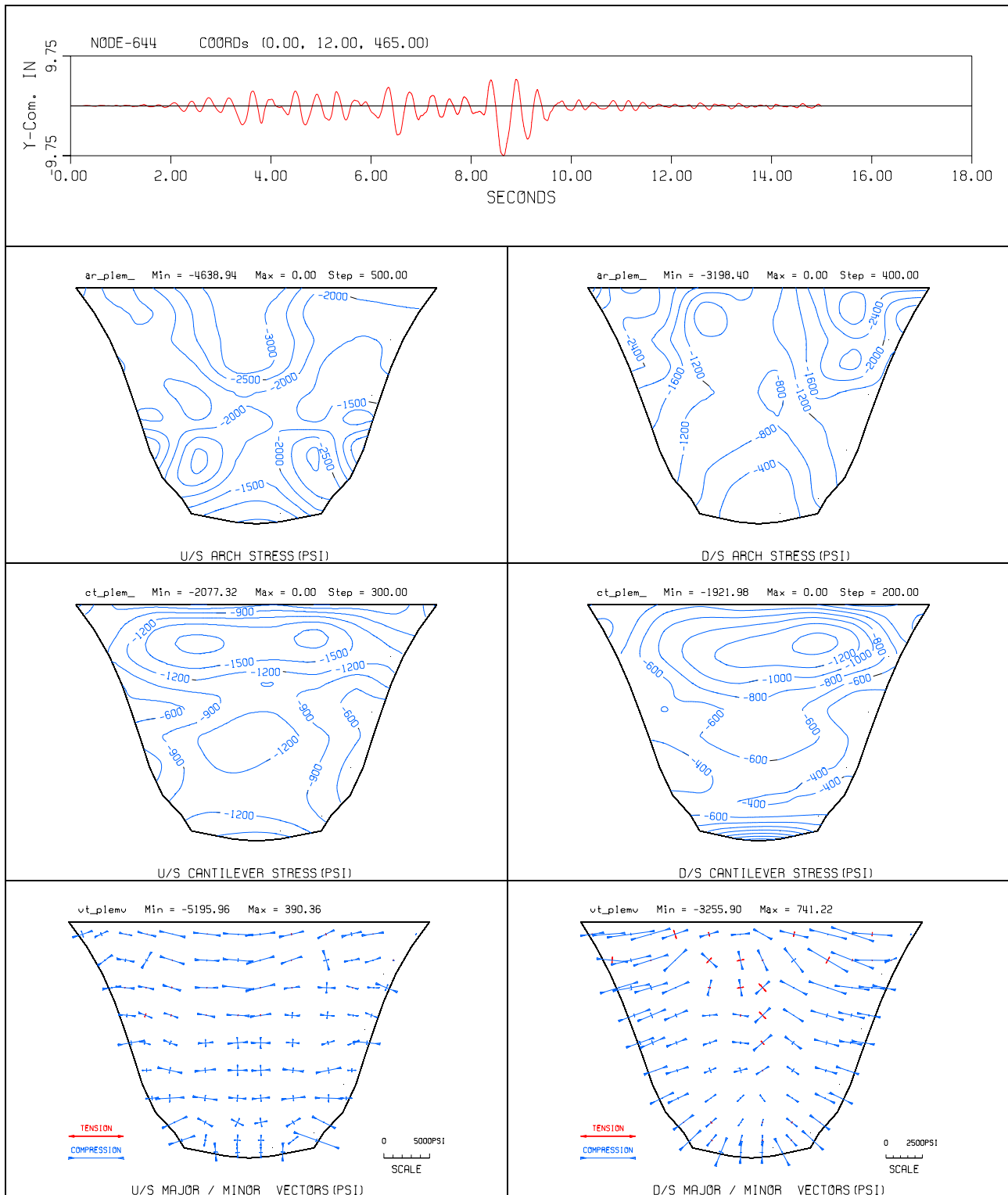
Figure F-17. Deflected shapes, maximum joint opening time history, envelopes of maximum arch and cantilever stresses, and envelopes of principal stress vectors due to GLY record
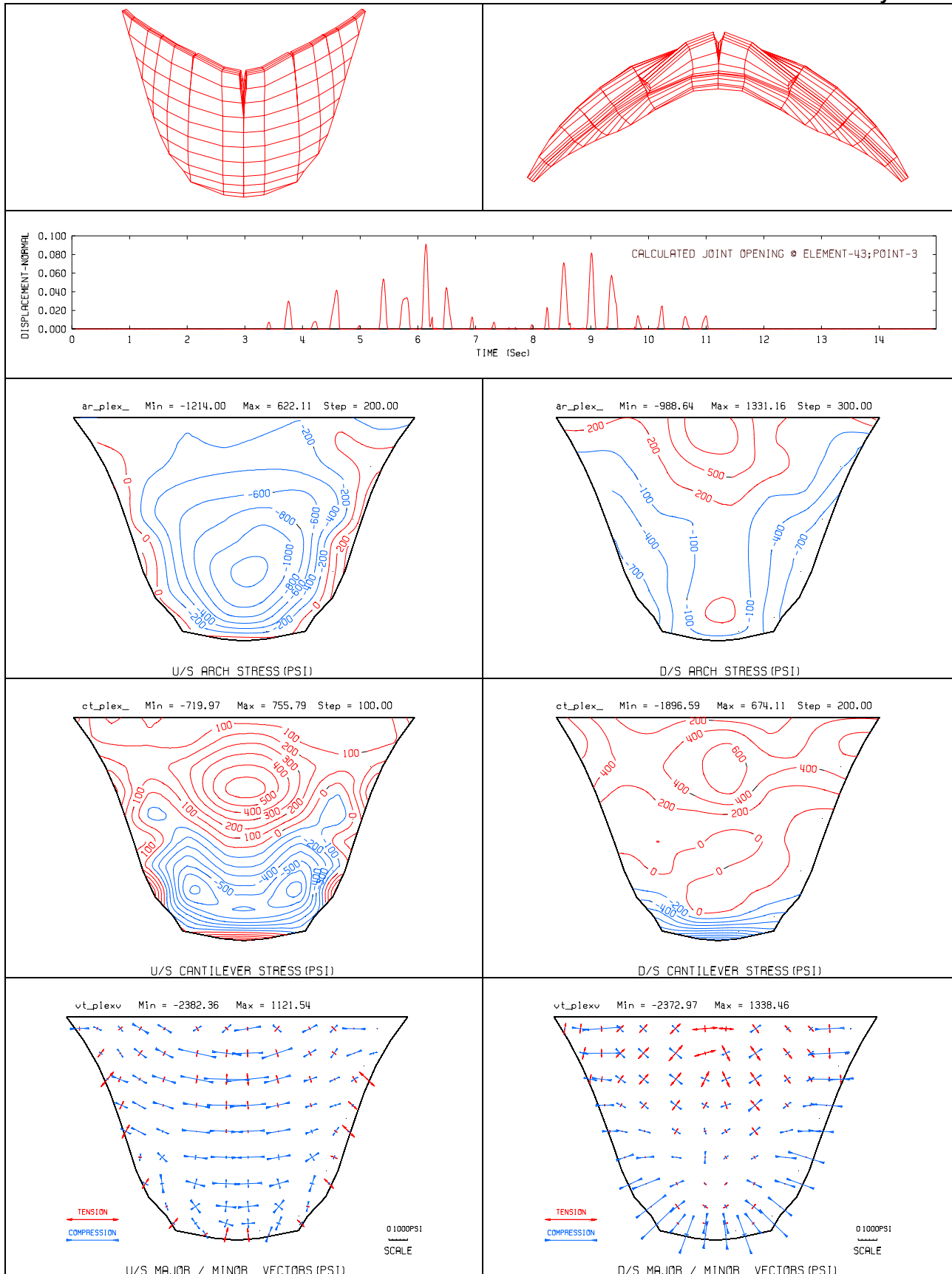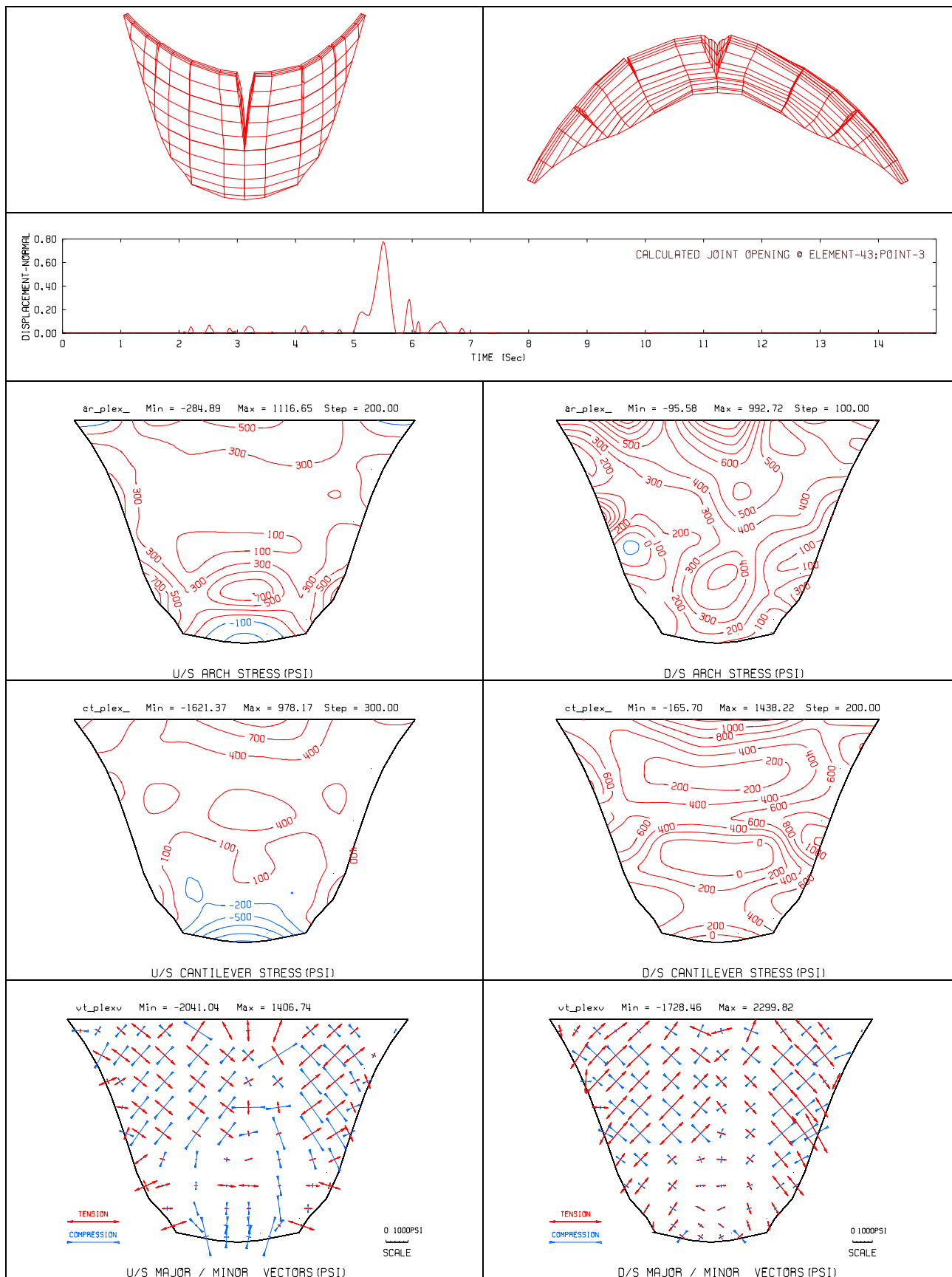
Figure F-18. Deflected shapes, maximum joint opening time history, envelopes of maximum arch and cantilever stresses, and envelopes of principal stress vectors due to PACB record
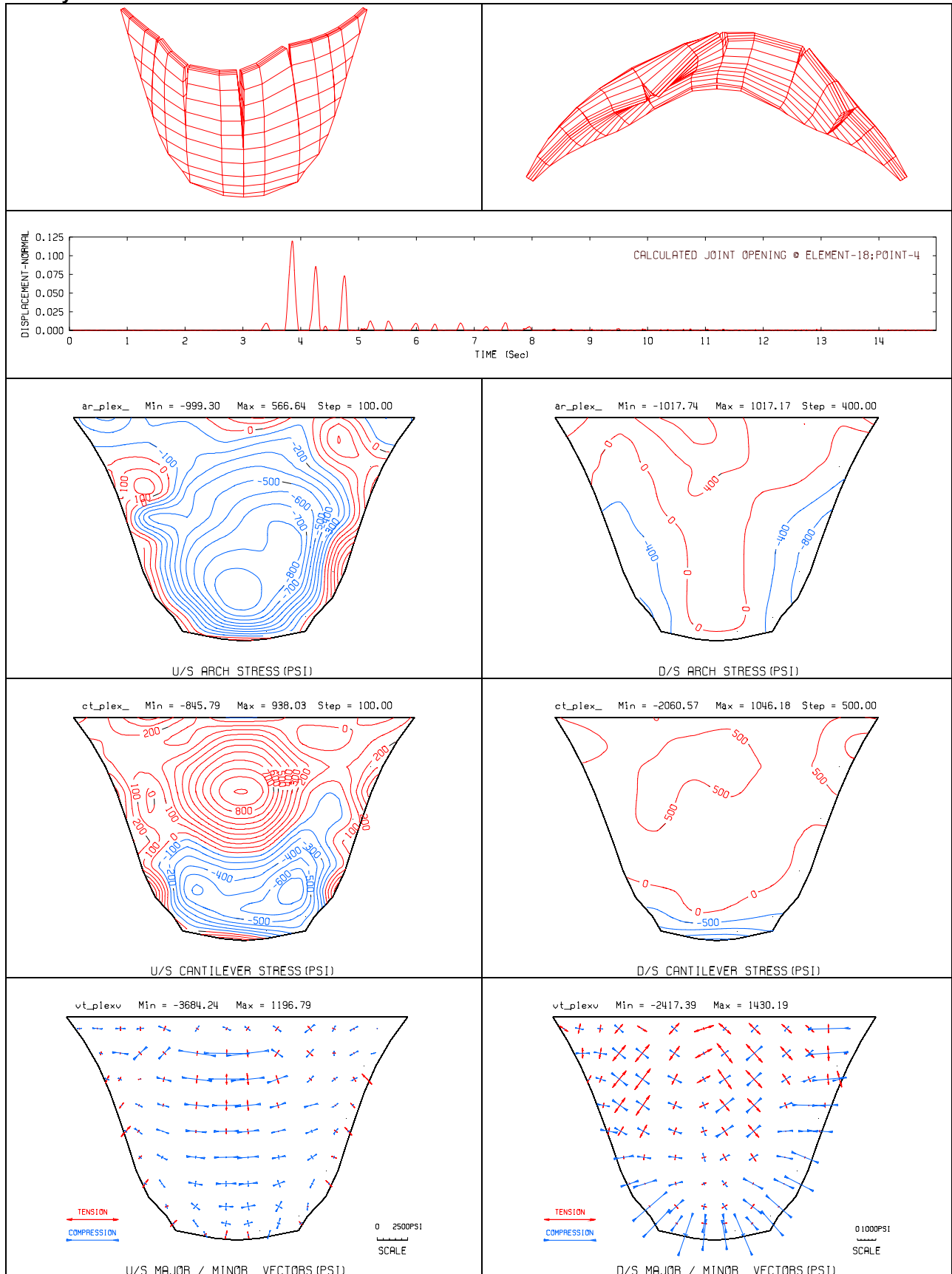
Figure F-19. Deflected shapes, maximum joint opening time history, envelopes of maximum arch and cantilever stresses, and envelopes of principal stress vectors due to PACN record
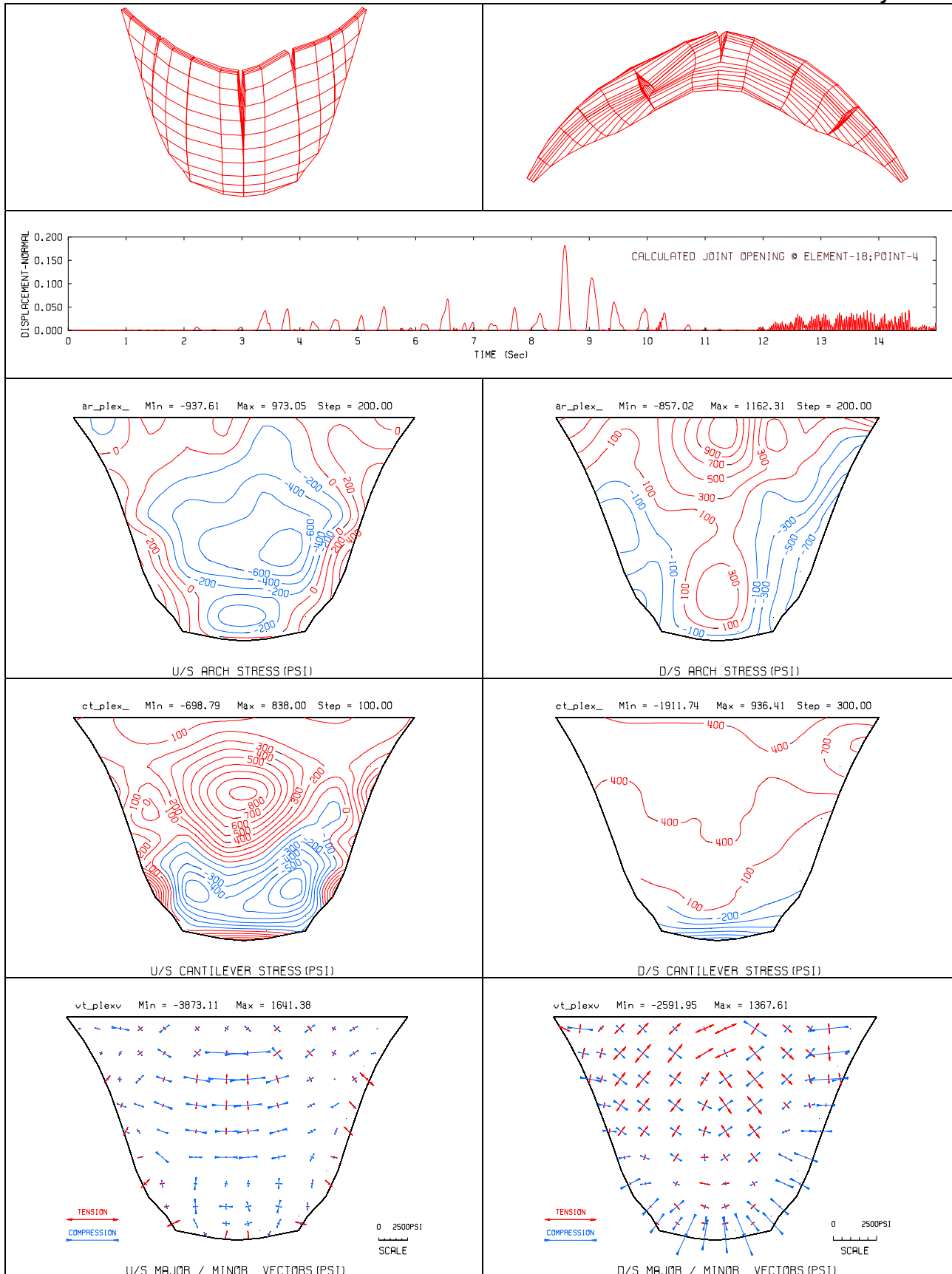
Figure F-20. Deflected shapes, maximum joint opening time history, envelopes of maximum arch and cantilever stresses, and envelopes of principal stress vectors due to PACX record
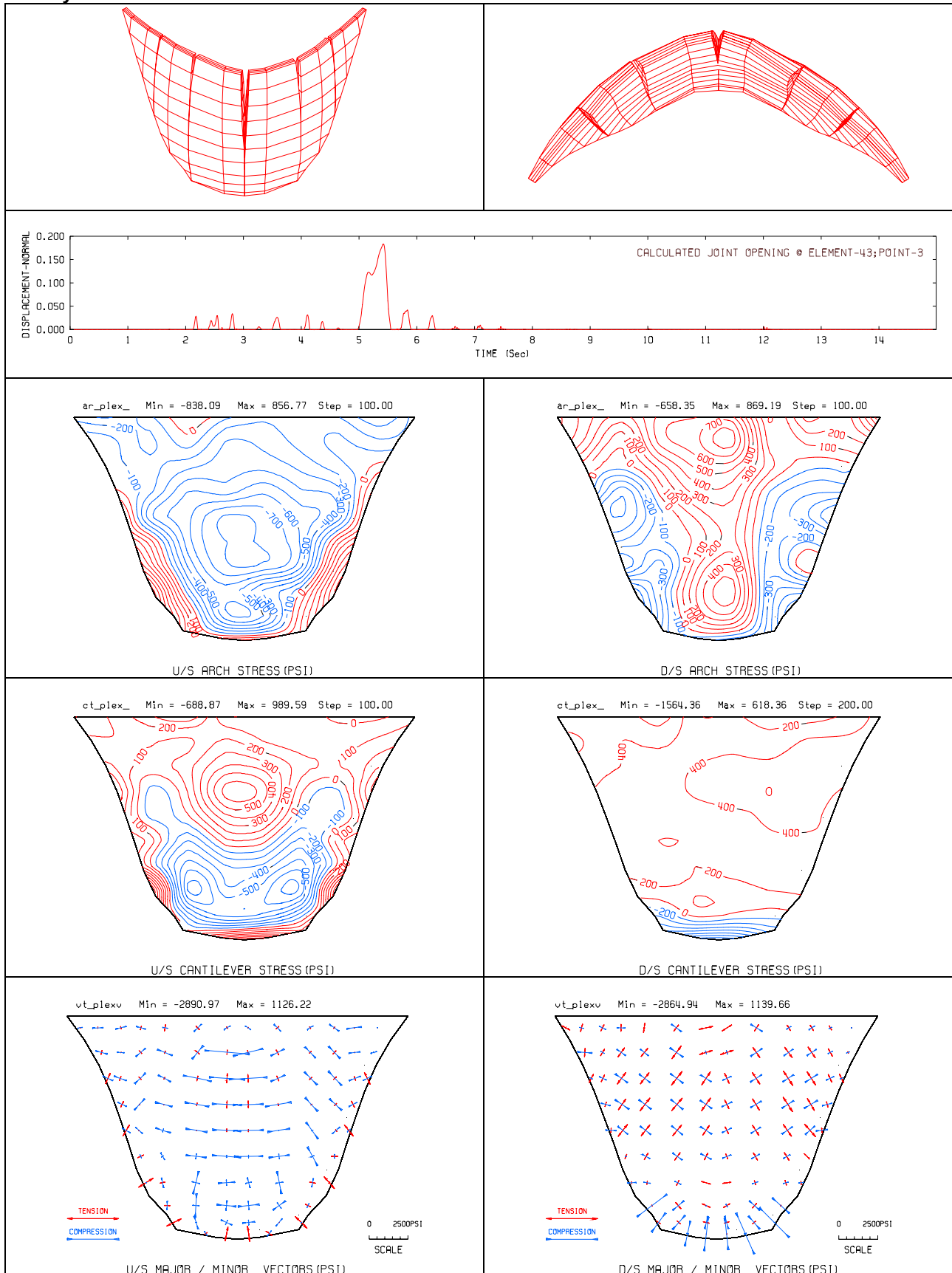
Figure F-21. Deflected shapes, maximum joint opening time history, envelopes of maximum arch and cantilever stresses, and envelopes of principal stress vectors due to U56 record

c. Analysis with Vertical, Horizontal, and Peripheral Joints (Model 3)

(1) *Description of Model.* The results of Model 2 with five contraction joints showed that high tensile stresses still persist within the cantilever blocks isolated by the opened contraction joints and along the dam-foundation contact. Model 3 with five vertical, two horizontal, and the peripheral joints was constructed to study the effects of tensile cracking that may occur at the lift joints and at the dam-foundation contact. As shown in Figure F-22, Model 3 employs the same vertical joints used in Model 2 with two additional horizontal joints at the location of high cantilever stresses and one peripheral joint at the dam-foundation contact. Each of these joints includes three nonlinear elements through the dam thickness and matches the number of solid elements on the faces of the dam. A total of 240 nonlinear joint elements were used.

(2) *Results.* The results for the static plus seismic loads are summarized in Table F-5 and in Figures F-23 to F-28 for the six selected input acceleration time-histories. The maximum dam radial displacements and joint openings listed in Columns 2 and 3 of Table F-5 indicate significant increase in the amount of joint opening, especially for the Newhall record (U56). In addition, Figures F-23 to F-28 show that the joint openings not only are larger for Model 3 but the joints stay open for a longer period. This is because Model 3 is more flexible and vibrates at a longer period than the other two models. Consequently, opening and closing of the joints occur at a slower rate. Another observation is that modeling of the lift lines has also changed mechanism of the nonlinear joint opening. For example, the deflected shape in Figure F-25 exhibits two dislocated blocks at the top of the dam that are isolated by the contraction joint openings on both sides and the bottom lift line. Furthermore, Figure F-26 demonstrates a mechanism where the top and bottom part of the dam are separated through an opened lift line, while the contraction joints apparently remain closed. The largest joint opening reaches 9.5 inches for the Newhall record (U56). Such a large joint opening could affect stability of the dam and will be investigated in the next section. Although stress results indicate that tensile stresses at the contraction joints and lift lines have vanished, they are still persistent within the blocks and have somewhat increased compared to the results for Model 1 and Model 2. The reason for this is the tangential constrain enforced by the joint elements that precludes any joint slippage and thus induces tensile stresses within the blocks. Such constraint is a shortcoming of QDAP program that need to be removed. The results also show the magnitudes of compressive stresses that are usually higher than those computed in the linear analysis. The maximum compressive stresses are approaching the static compressive strength of 27.5 MPa (4,000 psi) but are less than the dynamic compressive strength of 34.5 MPa (5,000 psi) . Nevertheless some minor concrete crushing can be expected to occur as a result of impact during the joint closing. Note that the actual compressive strength of the example dam can be well in excess of 27.5 MPa (4,000 psi).
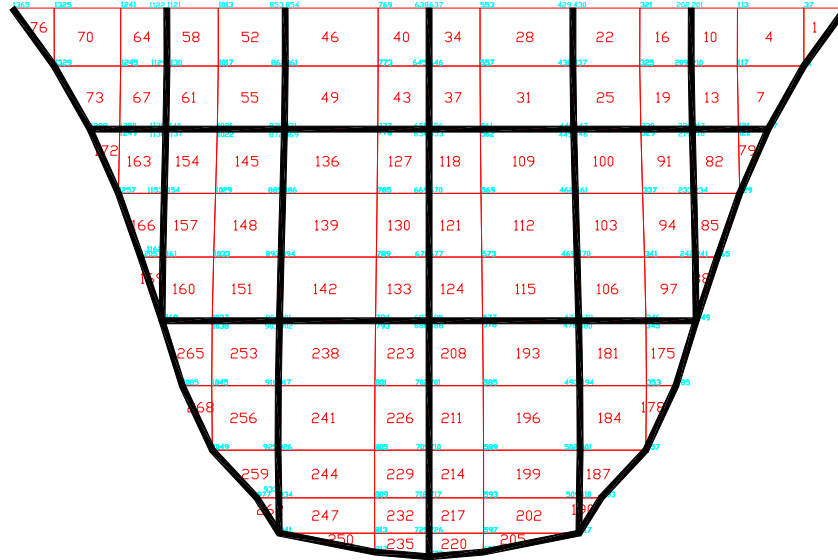
Figure F-22. Finite-element mesh with five vertical, two horizontal, and peripheral joints (Model 3)

Figure F-23. Deflected shapes, maximum joint opening time history, envelopes of maximum arch and cantilever stresses, and envelopes of principal stress vectors due to CLD record

Figure F-23 (continued). Displacement time history, envelopes of minimum arch, cantilever, and principal stresses due to CLD record

Figure F-24. Deflected shapes, maximum joint opening time history, envelopes of maximum arch and cantilever stresses, and envelopes of principal stress vectors due to GLY record
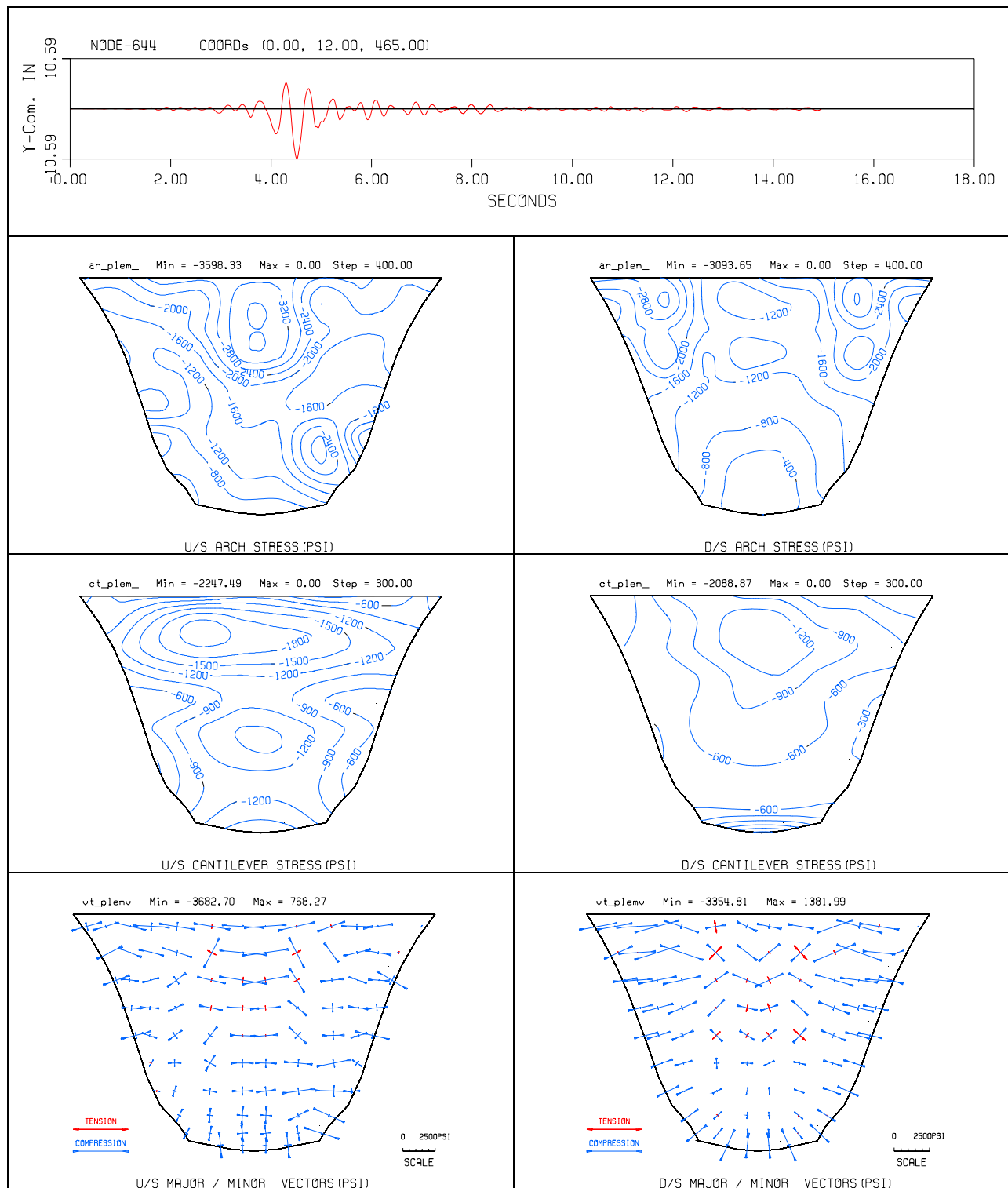
Figure F-24 (continued). Displacement time history, envelopes of minimum arch, cantilever, and principal stresses due to GLY record

Figure F-25. Deflected shapes, maximum joint opening time history, envelopes of maximum arch and cantilever stresses, and envelopes of principal stress vectors due to PACB record

Figure F-25 (continued). Displacement time history, envelopes of minimum arch, cantilever, and principal stresses due to PACB record

Figure F-26. Deflected shapes, maximum joint opening time history, envelopes of maximum arch and cantilever stresses, and envelopes of principal stress vectors due to PACN record

Figure F-26 (continued). Displacement time history, envelopes of minimum arch, cantilever, and principal stresses due to PACN record

Figure F-27. Deflected shapes, maximum joint opening time history, envelopes of maximum arch and cantilever stresses, and envelopes of principal stress vectors due to PACX record

Figure F-27 (continued). Displacement time history, envelopes of minimum arch, cantilever, and principal stresses due to PACX record

Figure F-28. Deflected shapes, maximum joint opening time history, envelopes of maximum arch and cantilever stresses, and envelopes of principal stress vectors due to U56 record
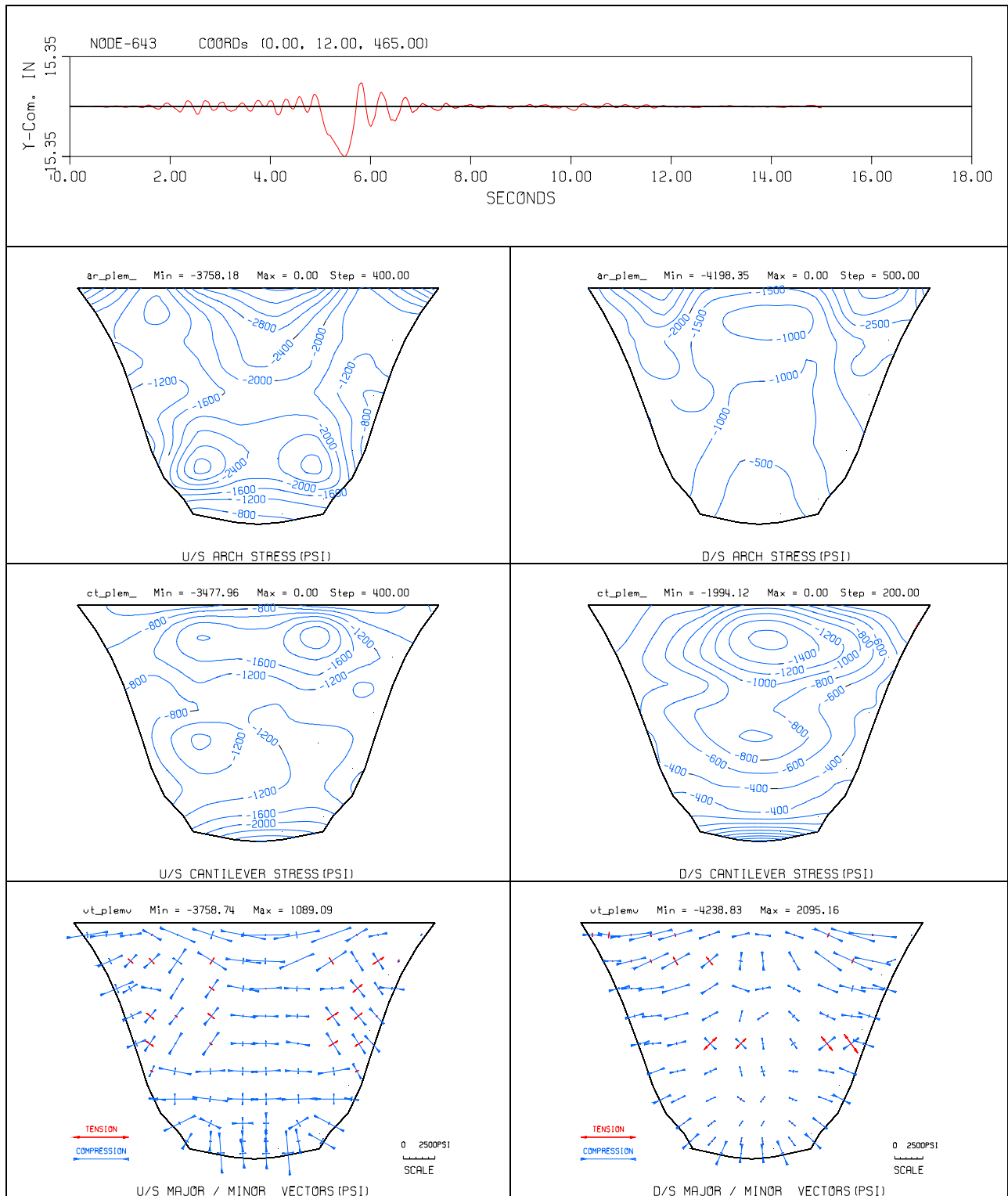
Figure F-28 (continued). Displacement time history, envelopes of minimum arch, cantilever, and principal stresses due to U56 record

F-11. Evaluation of Results

Three finite-element models with three different joint configurations were analyzed using six different acceleration time histories representing a wide range of ground motion characteristics. Model-1 included three vertical contraction joints located at the crown section and at ¼ span points of the dam. Model-2 consisted of five vertical contraction joints uniformly distributed across the length of the dam. Finally Model-3 incorporated five vertical, two horizontal, and the peripheral joints to allow for opening of the contraction joints and cracking/opening along the lift lines and the dam-foundation interface. The results for each model were tabulated and displayed in the form of deflected shapes, time-history of joint openings, stress contours, and the plots of principal stress vectors. Model-1 with three contraction joints indicated large joint opening at the crown section with high tensile arch and cantilever stresses still remaining within the cantilever blocks. Model-2 with five contraction joints was constructed to relieve the high tensile stresses by allowing a higher number of joints to open. The Model-2 results indicated only minor improvement, and high tensile stresses still persisted in the cantilever direction and at the dam-foundation interface. Model-3 was attempted to relief high tensile stresses by allowing two selected lift lines and the dam-foundation interface to open during the ground shaking. The amount of joint opening for Model-3 increased significantly for the Newhall record (U56) containing a one-second acceleration pulse. The significant increase in the amount of joint opening is attributed to the presence of the one-second acceleration pulse and partially free cantilever blocks formed in the upper part of the dam by two opened contraction joints on the sides and the opened lift line at the bottom of the blocks. Despite the significant joint opening, Model-3 still showed high tensile stresses within the cantilever blocks. This is believed to have been caused by the joint elements being constrained against tangential motion at the joint which did not permit joint slippage. The severity of the estimated joint opening is evaluated by comparing the amount of joint opening with the depth of shear keys to determine whether the blocks remain engaged through the shear keys. For this purpose snap shots of the maximum joint openings in the horizontal and vertical directions are shown in Figure F-29. The upper graph in this figure shows that the joint opening on the left side of the upper block (made of elements 28, 31, 34, and 37) exceeds the depth of shear key, but it is much smaller on the right side and bottom of the block. The lower graph in Figure F-29 shows that the amount of contraction joint openings at the time of the maximum lift line opening is much smaller than the depth of the shear keys. Overall, it appears that the upper blocks do not disengage from one another and more likely will remain stable. However, the stability condition should be confirmed by additional analyses that consider slippage across the contraction joints and lift lines which were ignored in this example. Furthermore other configuration of lift line openings should also be investigated.

Calculated joint opening
at the time of 5.51 sec

Joint Open = 8.93"

Joint Open = 0.75"

Shear key Location (6")

Shear key Location (6")

34   28

37   31

Joint Open = 4.83"

Joint Open = 0.45"

Joint Open = 0.40"   Joint Open = 0.20"

MAXIMUM HORIZONTAL JOINT OPENING

Calculated joint opening
at the time of 5.91 sec

Joint Open = 0.98"

Joint Open = 0.01"

Shear key Location (6")

Shear key Location (6")

34   28

37   31

Joint Open = 0.07"

Joint Open = 0.00"

Joint Open = 2.07"   Joint Open = 0.01"

MAXIMUM VERTICAL JOINT OPENING

Figure F-29. Schematic view of estimated joint openings at the time of maximum horizontal joint opening (top) and at the time of maximum vertical joint opening (bottom)

F-12. Conclusions and Recommendations

a. Conclusions. The following conclusions are drawn from this nonlinear analysis example:

(1) It is desirable to perform progressive evaluation of joint opening that starts with a minimum number of contraction joints and progresses by including more joints until realistic results are obtained.

(2) Progressive evaluation of the results necessitates various joint configurations to be studied so that all potential joint-opening mechanisms are captured.

(3) Inclusion of the contraction joints may not completely eliminate tensile stresses, although tensile stresses will be reduced. Allowing joint slippage should further reduce tensile stresses, if such capability is available.

(4) Inclusion of the joints will increase time history displacements and compressive stresses. The resulting displacements and compressive stresses should be evaluated in assessment of the dam safety.

b. Recommendations. Based on the results of this example, the following recommendations are made regarding the nonlinear analysis procedures for arch dams:

(1) Select a suite of six or more earthquake acceleration time histories for the analysis.

(2) Perform linear-elastic time history analyses for all earthquakes input and evaluate the results according to the EM 1110-2-6053 performance criteria. If the linear-elastic performance criteria are not met, continue with nonlinear analyses.

(3) Start the nonlinear analyses with a minimum number of three contraction joints. If dam experiences significant joint openings and large tensile stresses still persist, repeat the analysis with revised number of joints until realistic joint-opening mechanisms are achieved. The revised joint configuration may include vertical, horizontal, and peripheral joints.

(4) Identify and conduct stability analyses for isolated blocks that may get loose and overtop as a result of excessive joint opening and lift line cracking.

(5) Assess the overall safety of the dam with respect to structural stability and its ability to retain the impounded water.

Appendix G

DYNAMIC SOIL-STRUCTURE INTERACTION ANALYSIS OF KENTUCKY LOCK WALL

G-1. Background

Kentucky Lock is located in western Kentucky at Mile 22.4 on the Tennessee River. In order to reduce shipping delays of the Tennessee and Cumberland River systems, a new 33.53-m wide by 365.76-m long (110 ft x 1200 ft) navigation lock is being constructed landward and adjacent to the existing 33.53-m wide by 182.88-m long (110 ft x 600 ft) lock (Figure G-1). The project was authorized in 1996 and construction commenced in 1998. In this example, Culvert Valve Monolith L4 of the lock addition is considered for the soil-structure-interaction (SSI) analysis. Figure G-2 shows general dimensions and geometry of this monolith.
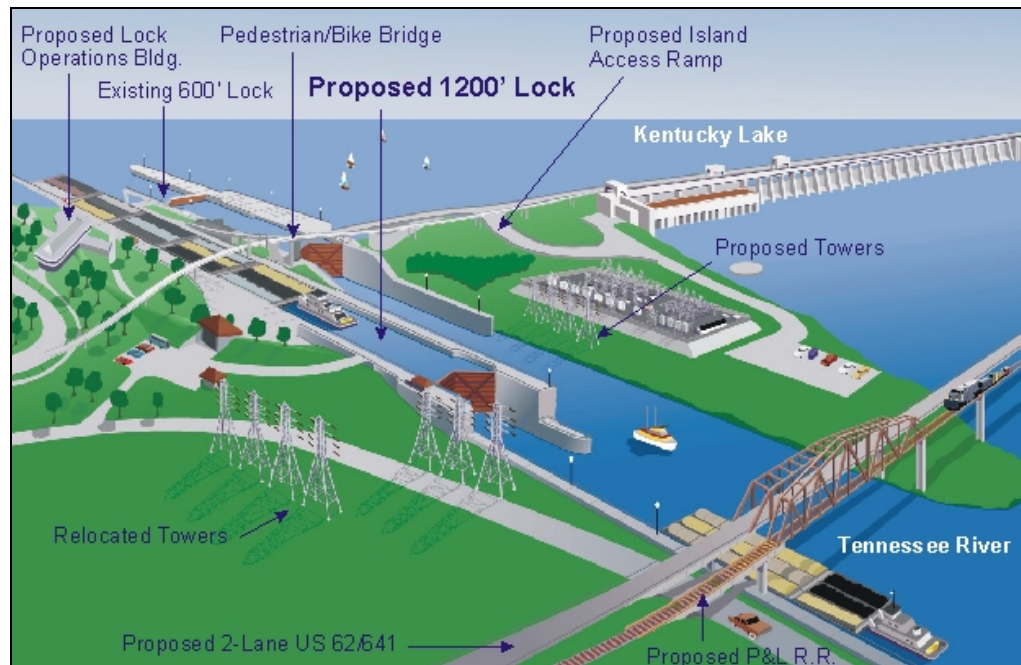
Figure G-1. Kentucky Lock Addition Project

G-2. Purpose and Objectives

The purpose of this example is to demonstrate an approach used to perform dynamic SSI analysis for the proposed Kentucky Lock Addition using time-history analysis. The objectives of the analysis are:

  a. To assess dynamic sliding stability at different sections of the monolith

  b. To compute dynamic backfill soil pressure at the time of peak response

  c. To study nonlinearity of backfill material during dynamic loading

G-3. Scope

The scope of the study included the following:

- *a.* Definition of acceleration time histories for design ground motion
- *b.* Estimation of dynamic properties of backfill material and site rock profiles
- *c.* Development of finite-element model for lock wall-backfill soil system
- *d.* Analysis for dynamic loading
- *e.* Evaluation of response of concrete monolith and backfill soil for earthquake loading
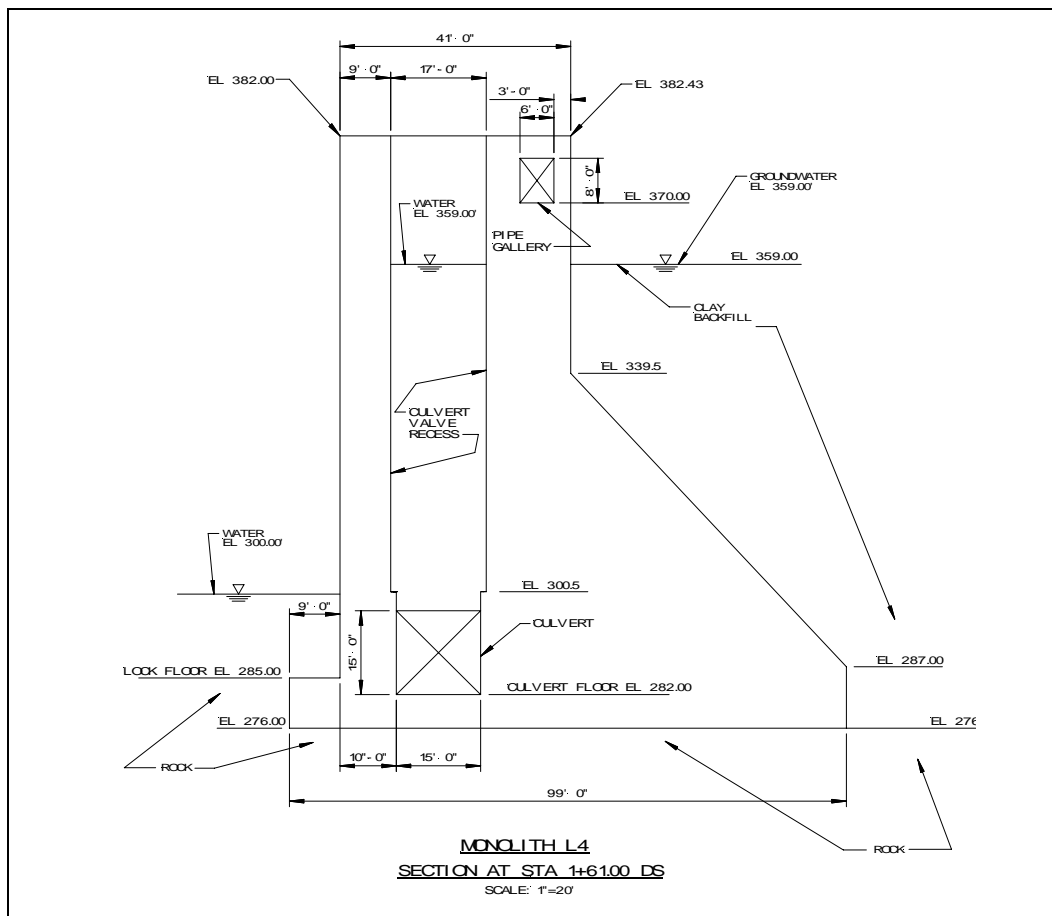
Figure G-2. General dimensions and geometry of Culvert Valve Monolith L4

G-4. Method of Analysis

a. Dynamic SSI analysis can be performed using finite-element method. The soil-structure continuum consisting of the lock monolith, foundation rock and backfill soil is modeled using 2-D plane strain elements. Using this approach, dynamic inertia interaction and wave propagation phenomenon are considered directly.

b. Computer program QFLUSH (Quest Structures 2001), an enhanced version of FLUSH (Lysmer et al. 1975) with pre- and post-processing capabilities, was used to study dynamic SSI analysis of Kentucky Lock monolith. The analyses were performed in the frequency domain for vertically propagating shear and compression waves (from horizontal and vertical excitations). Responses from horizontal and vertical excitations were obtained separately and then combined. The nonlinear soil behavior was approximated by the equivalent linear techniques through iterative procedures. The results for the horizontal and vertical excitations were transformed from the frequency domain back to the time domain. The time-domain results were subsequently combined to obtain the total response for simultaneous horizontal and vertical (shear- and compression- wave) excitations.

G-5. Finite Element Modeling

a. Finite-element Mesh. The Kentucky Culvert Valve Monolith L4 is founded on rock and backfilled by sand on the land side. An idealized stratigraphic profile of the foundation and backfill soil with the lock wall section is shown in Figure G-3. The lock wall, foundation rock, and the backfill soil were modeled by plane-strain 2-D quadrilateral elements with concrete, rock, and soil material properties, respectively. The finite element representation of the lock wall, foundation rock, and the backfill is shown in Figure G-4. The model consisted of 1,693 plane-strain elements. The effect of culvert recess was simulated by smearing the mass and stiffness properties of the region with the recess over a similar region without the recess. This was done by proportioning the mass and stiffness properties according to the volume ratio of the region with and without the recess.

b. Boundary Conditions and Element Size. The model was extended approximately one lock height to the right and one lock height to the left. The bottom boundary was placed at approximately 15.24 m (50 ft) below the lock base. Transmitting boundaries were established at the right and left sides of the model and rigid boundary was assumed at the bottom of the model. Transmitting boundary was used to minimize the horizontal extent of the model and ensure that seismic waves propagating away from the structure are absorbed by the boundary and not reflected back. However, the boundaries were placed far enough from the lock wall so that accurate representations of dynamic interaction effects between the structure and backfill soil and between the structure and foundation rock can be achieved. The element heights were selected using the equation below given in the FLUSH manual such that frequencies up to 30 Hz could be included in the analysis.

$$h_{\max} = \frac{1}{5} \cdot \frac{V_s}{f_{\max}}$$

In this equation V_s is the lowest shear wave velocity reached during iterations and f_{max} is the highest frequency of the analysis. Although there is no restriction of element dimension in horizontal direction in QFLUSH, relatively short elements were used to improve accuracy of analyses.

c. Added Hydrodynamic Mass. The hydrodynamic effects of water on the lock wall were considered by the Westergaard's added mass solution (EM 1110-2-6051). The added mass coefficients were effective only in the direction perpendicular to the lock wall. The water inside the culvert valve recess is fully constrained. The added hydrodynamic mass for the inside water

was therefore taken equal to the mass of water. The added mass for each node was computed according to its tributary area.

G-6. Material Parameters

   a. Basic Material Properties. Uniform properties were assumed for the backfill soil and the foundation rock. It was considered that engineered backfill will be used. The basic material properties for the concrete, foundation rock, and the backfill sill are listed in Tables G-1 to G-3.

Table G-1

Concrete Properties	English Units		Metric Units	
Unit weight (γ_s)	145	pcf	2,322.68	Kg/m^3
Compressive strength	3,000	psi	20.68	MPa
Poisson's ratio (estimated)	0.20		0.20	
Elastic modulus (estimated)	3×10^6	psi	20,684.27	MPa
Shear modulus	1.25×10^6	psi	8,618.45	MPa
Shear wave velocity	6,322	fps	1,926.95	m/s

Table G-2

Rock Properties	English Units		Metric Units	
Unit weight ( )	166.6	pcf	2668.68	Kg/m^3
Peak friction angle ( )	36.7	degrees	36.7	degrees
Cohesion (c)	13.2	psi	91.01	KPa
Unconfined compressive strength	28,296	psi	195.09	MPa
Poisson's ratio	0.3		0.3	
Elastic modulus	5.51×10^6	psi	37,990.11	MPa
Shear modulus	2.119×10^6	psi	1,4610.00	MPa
Shear wave velocity	7,680	fps	2,340.86	m/s

Table G-3

Granular Backfill Properties	English Units		Metric Units	
Saturated unit weight (γ_s)	135	pcf	2,162.49	Kg/m^3
Peak friction angle (ϕ)	32	degrees	32	degrees
Cohesion (c)	0	psf	0	MPa
Poisson's ratio (estimated)	0.30		0.3	
Elastic modulus (estimated)	13.187×10^6	psf	631.40	MPa
Shear modulus	5.072×10^6	psf	242.85	MPa
Shear wave velocity	1,100	fps	335.28	m/s
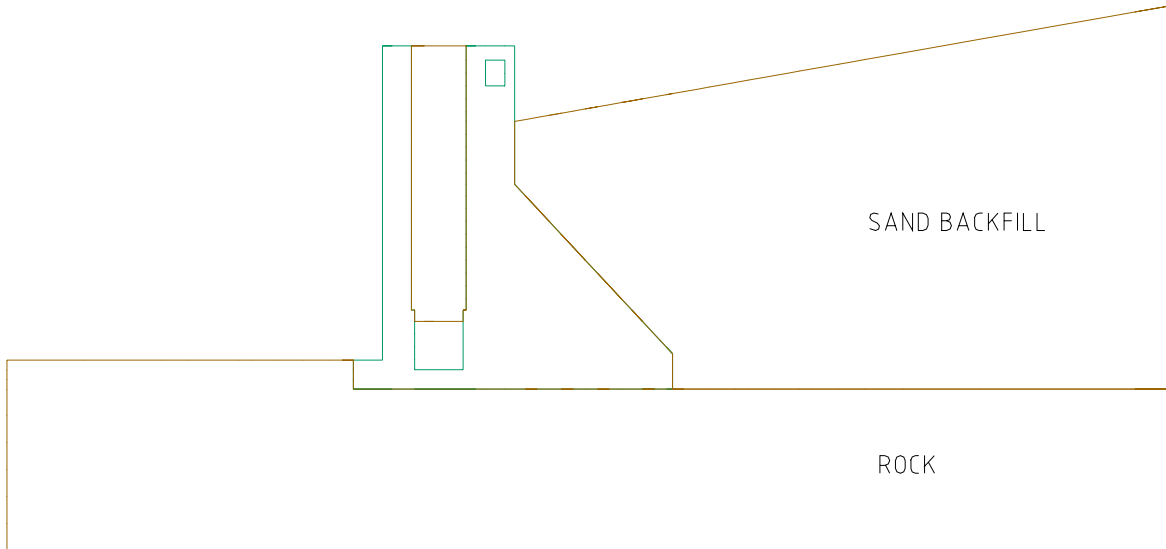
Figure G-3. Idealized stratigraphic profile at the Kentucky lock site
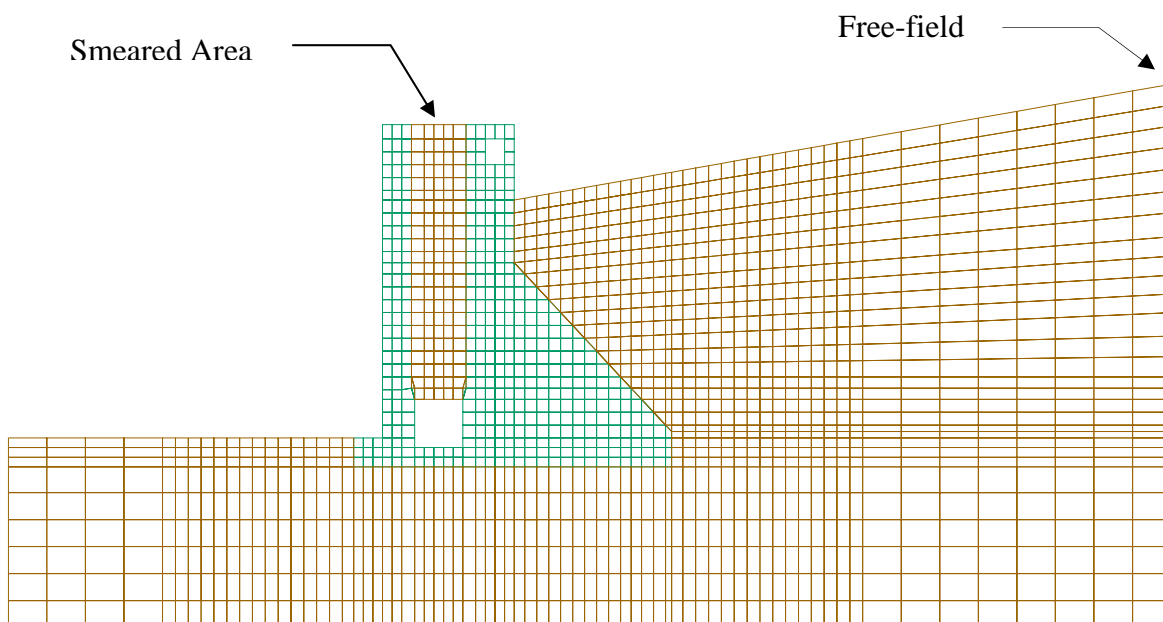
Figure G-4. Finite-element mesh for lock monolith, foundation rock and backfill soil

b. *Strain-dependent Shear Modulus and Damping.* The strain-dependent soil stiffness (shear modulus) and energy absorption (damping) characteristics were obtained from those available in the literature. For SSI analysis, a set of modulus reduction and damping curves based on data for similar soils (sand backfill and rock, Seed and Idriss 1970) were selected and is shown in Figures G-5 and G-6. In these Figures, *G* is the soil shear modulus and G_{max} is the soil shear modulus at low shear strain (strain less than 10^{-4} percent).
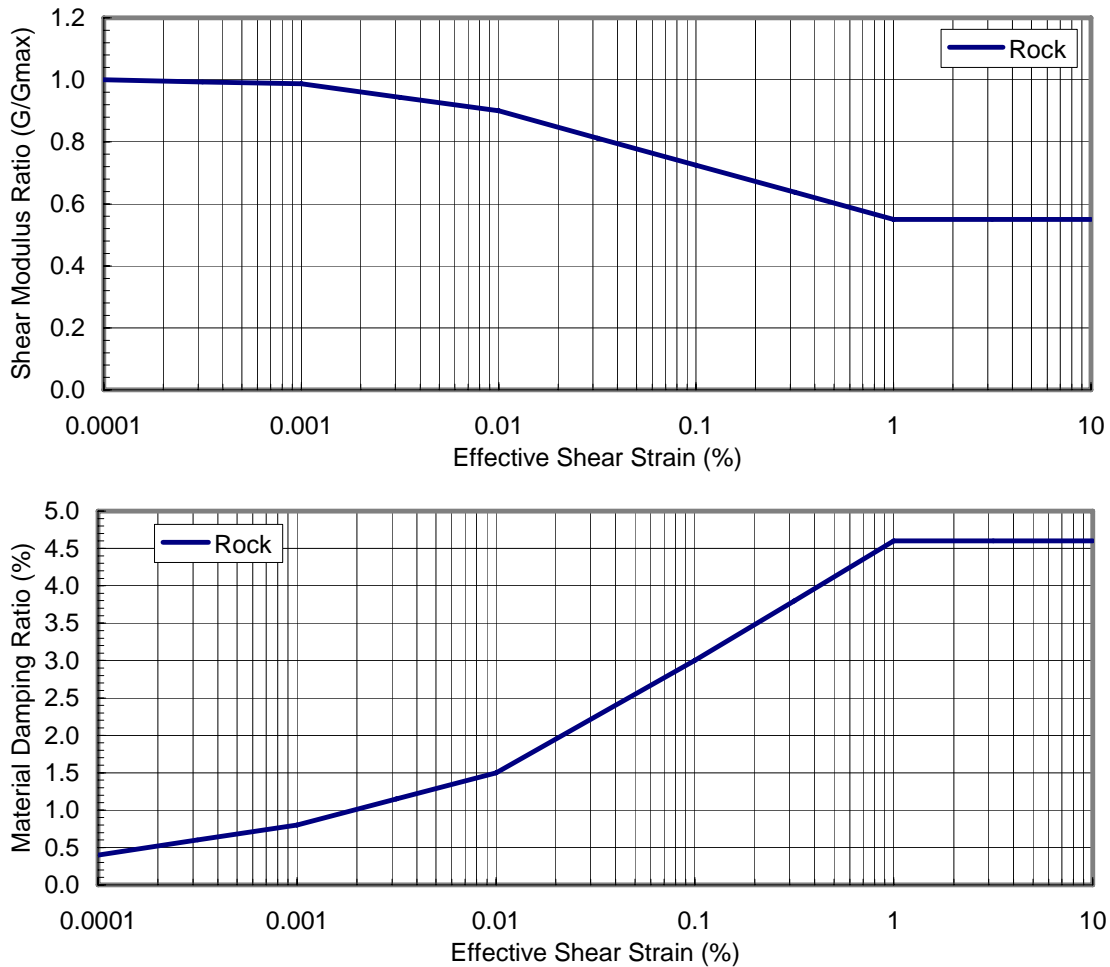
Figure G-5. Strain dependent material properties for rock
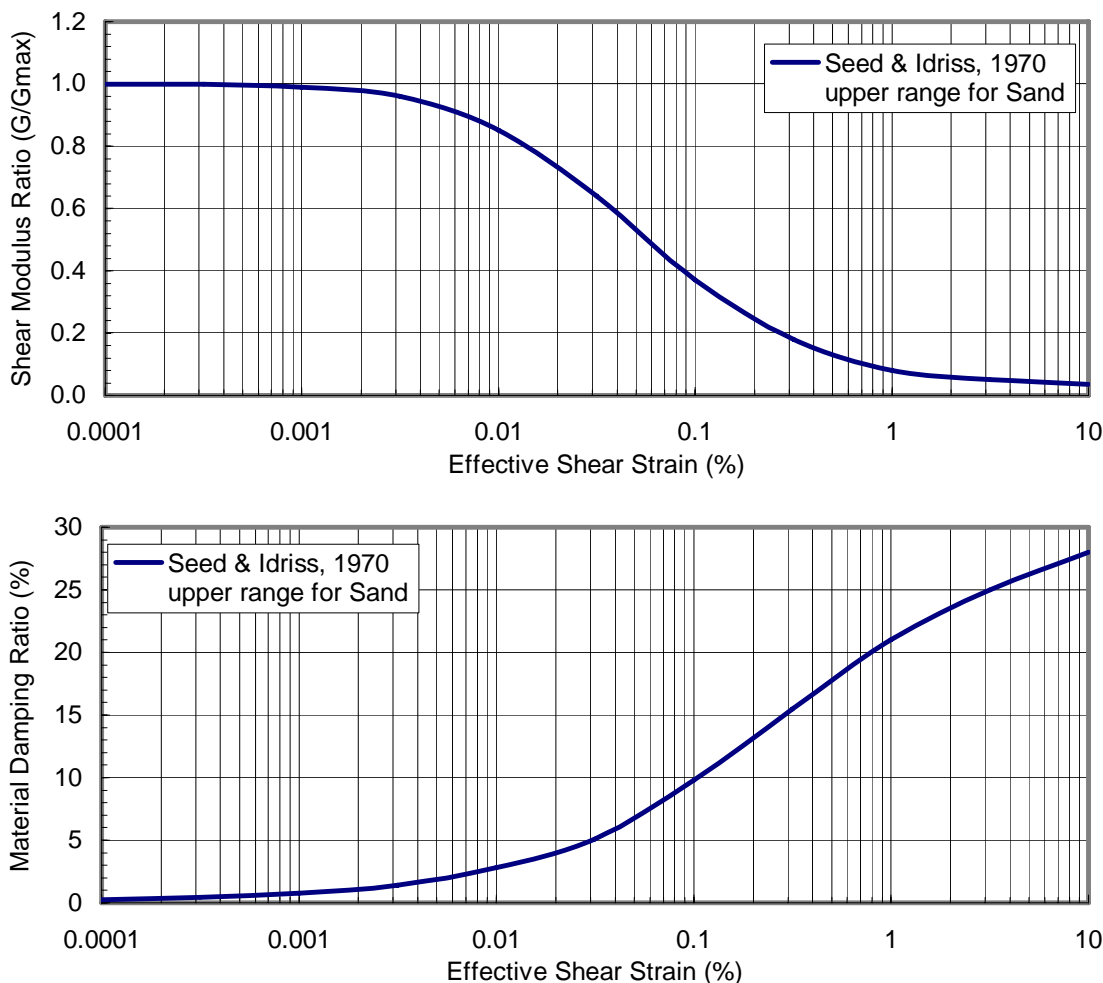
Figure G-6. Strain dependent material properties for sand

G-7. Loading Conditions

a. Static Loads. The static loads for the normal operating condition consisted of the dead weight and normal water pressures. Stress and deformation response due to static load cases were computed using the computer program SAP2000. The SAP2000 results were later converted to the QFLUSH model for superposition with the results of dynamic SSI analysis. The static and dynamic finite-element models, therefore, were identical in terms of geometry, mesh, and element types. The water pool elevation was set at El. 109.42 m (359 ft).

b. Earthquake ground motions. Dynamic SSI analyses for Kentucky lock wall were performed for the MDE level excitations using three input acceleration time histories. The peak ground acceleration for the MDE event was estimated to be 0.25g. The input earthquake acceleration time histories were obtained from a report prepared for the project ("Kentucky Lock Addition – Seismic Design Criteria, February 2001"). The selected earthquake records scaled to a peak ground acceleration of 0.25g for this example included the following:

1. MDE1 - 1989 Loma Prieta Earthquake: Anderson Dam Record, Far Field, M8.1.
2. MDE2 - 1985 Mexico City Earthquake: Papanoa Record, Far Field, M7.1
3. MDE3 – 1987 Superstition Hills Earthquake: Wildlife Record, Near Field, M5.8.

c. These records were selected from a set of 8 time-history records based on their duration of sustained strong motion and time steps. Only records with time steps equal to or less than 0.02 seconds with a Nyquist frequency of 25 Hz and higher were considered appropriate since records with long time steps lack energy in the high frequency range. Anderson and Papanoa records were selected because their "bracketed duration" of strong shaking was the largest. Wildlife record was selected from the near-field records again based on its longest bracketed duration of the strong shaking. A bracketed duration is defined as the time interval between the first and last acceleration peaks that are equal to or greater than 0.05g. The horizontal and vertical components of the selected acceleration records with their respective FFT are displayed in Figures G-7 to G-9.

d. Hydrodynamic force. Hydrodynamic forces were obtained from the inertia forces generated by the added masses attached to the concrete nodal masses. The water pool elevation for earthquake loading was set at 109.42 m (359 ft).

G-8. Presentation and Evaluation of Results

a. Free-Field Site Response. The first step in QFLUSH analysis is computation of the free field motions. In this example this was accomplished by using a column of elements at the right lateral boundary as the soil column, as shown in Figure G-4. Soil profile for the free-field computation consisted of uniform granular soil underlain by uniform rock whose material properties are given in Tables G-2 and G-3 and also in Figures G-5 and G-6. Variations of free-field peak horizontal acceleration with depth were obtained from the free-field site response analysis. They are shown in Figure G-10 for the horizontal and vertical components of each selected earthquake input. The results show that the ground motion changes very little within the foundation rock model. Consequently the ground motions recorded at the ground surface were directly applied at the base of the finite-element model. However, as the ground motion propagates upward, it is modified significantly by the backfill soil. Figure G-10 shows that the horizontal peak ground acceleration at the top of the backfill soil is about 0.63g for Anderson, 0.48g for Papanoa, and 0.56g for the Wildlife record, which has amplified by factors of 2.52, 1.92, and 2.24 over the peak bedrock acceleration. Varying amplification factors for the records are not surprising due to their varied response spectrum characteristics shown in Figure G-11.

b. Nonlinear behavior of Backfill Soil. In the equivalent-linear approach (QFLUSH), the soil behavior is specified as shown in Figure G-6, where the shear modulus and damping ratio vary with the shear strain amplitude. The values of shear modulus and damping ratio are determined by iterations so that they become consistent with the level of strain induced in each soil layer. Figure G-12a compares the initial shear-wave velocity with the final strain-compatible shear-wave velocity as a measure of the level of nonlinear behavior. This figure shows that the shear-wave velocity decreases 40 to 60 percent from the top to bottom of the backfill soil as a result of soil softening. Figures G-12b and c indicates damping ratios as high as 23% for the horizontal and 14% for the vertical component of ground motions are achieved as the soil softens and strain amplitudes increase. Overall the level of nonlinear behavior is considered moderate.

c. Stress Results. The QFLUSH post-processor, QFPOST, provides time-history plots of 2D element stresses, contour plots of maximum and minimum element stresses, and snap shots of element stresses at any user defined time steps. Figure G-13 is an example of stress time histories for four concrete elements located at the toe of the wall. The time-history plots include horizontal, vertical, and shear stresses for all four elements. Using stress time histories for all elements, the post-processor searches for the maximum, minimum, and snap shots at any given time to prepare contour plots such as those shown in Figures G-14 to G-16 for Anderson earthquake record. Figure G-14 represents envelopes of maxim vertical stresses for the concrete, rock, and backfill soil. The positive values indicate tensile stresses and negative values compressive stresses. Note that tensile stresses of 0.275 MPa (40 psi) at the heel of the lock wall are relatively small. Figure G-15 displays a snap shot of horizontal normal stresses at the time of 15.83 seconds which coincides with a peak tensile horizontal stress. Overall the stress magnitudes are moderate. As shown in this figure, the maximum tensile stress of 0.345 MPa (50 psi) occurs at the top of the backfill soil near the lock wall. Figure G-16 is another snap shot showing shear stresses at the time of 15.83 seconds. This figure shows a maximum shear stress of about 0.310 MPa (45 psi).

d. Section Forces and Moments. The stress results can be used to compute section forces and moments to assess sliding and rotational stability of the lock wall. This is facilitated by QFPOST capabilities, which provides time histories of resultant axial forces, shear forces, and moments at user defined sections. Figure G-17 shows three horizontal Sections HS1, HS2, and HS3 that may need to be checked against sliding. For this example time histories of resultant forces and moments at Section HS1 are provided in Figures G-18 to G-20 for all three selected earthquake records. Each figure includes time histories of the normal and shear forces with the moments. The shear forces in these figures represent the shear demands, and the normal forces in conjunction with a friction angle, and cohesion if applicable, can be used to compute the shear resistance for that section.

e. Instantaneous Sliding Factors of Safety. Knowing the shear demands and capacities (i.e. resistance), the instantaneous factor of safety for the section can be computed from the ratio of shear demands to shear capacities and plotted as a time history. In this example a conservative friction angle of 35 degrees with zero cohesion was used. The results show that for Section HS1 the instantaneous factors of safety vary between 3 and 11 during the ground shaking (bottom graphs in Figure G-18 to G-20). The lock wall therefore has ample factor of safety against the sliding. The moment demands can be used similarly and compared with the restoring moment to assess the rotational stability condition.

f. Dynamic Backfill Soil Pressure. Dynamic soil pressure is another parameter of interest that can be obtained from the SSI analysis. In this example two vertical sections VP1 and VP2 were selected for this purpose (Figure G-17). Section VP1 is located at the toe of the wall and VP2 at some distance away so it is less affected by the motion of the wall. The backfill soil pressures (i.e. normal horizontal stresses) along VP1 and VP2 were obtained at several instants of peak responses and are displayed in Figures G-21 to G-23 for all three earthquake ground motions. Note that the smooth pressure distributions on these graphs belong to VP2 and those appearing jagged at lower elevations to VP1. The jagged nature of the pressure distributions for VP1 is attributed to toe motions of the wall. Overall, soil pressures at VP1 and VP2 are similar but the shape of the pressure distribution varies with time and the earthquake ground motion. Pressure distributions for Anderson (Figure G-21) and Wildlife records (Figure G-23) are quite similar, but they differ with those for Papanoa. This observation shows that the dynamic soil pressure changes during the excitation and that it is affected by characteristics of the ground motion. This finding indicates that the simplified dynamic soil pressure should be used with caution.

G-9. Conclusions

An example of the time-history dynamic soil-structure-interaction analysis for a lock gravity wall with backfill soil was illustrated. The procedure was used to analyze the seismic response of the Culvert Valve Monolith L4 of the Kentucky Lock Addition under the MDE loading conditions. Three different earthquake acceleration time histories were used to account for the variability of ground motion characteristics. Modeling aspects of the SSI analysis was discussed and the use of time-history analysis results to access stability condition of the lock wall was described. This was accomplished by computing resultant normal and shear forces along selected sections, and then using them to compute instantaneous factors of safety against the sliding. The resulting instantaneous or time-history of factors of safety indicated ample margin of safety against sliding. The dynamic soil pressures at two vertical sections within the backfill were also retrieved to determine general distribution shapes and dependence on characteristics of the ground motion. The results show that the simplified dynamic soil pressures used in practice differ significantly from those obtained in this example. Therefore, in situations where the backfill soil plays an important role on the seismic response of the structure, the SSI method of analysis is recommended.
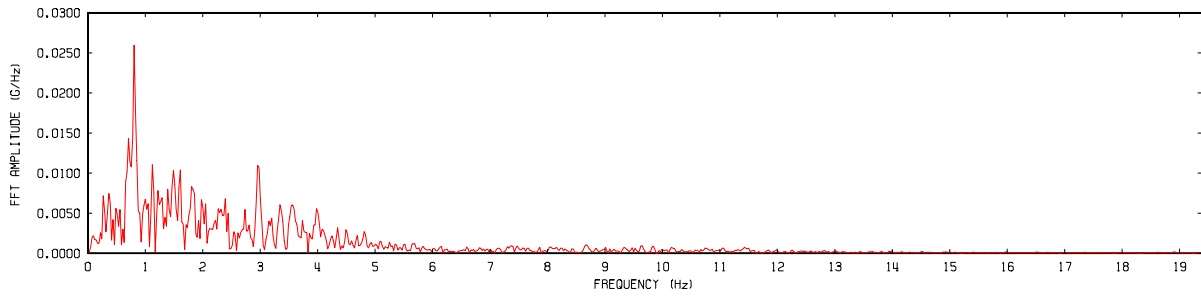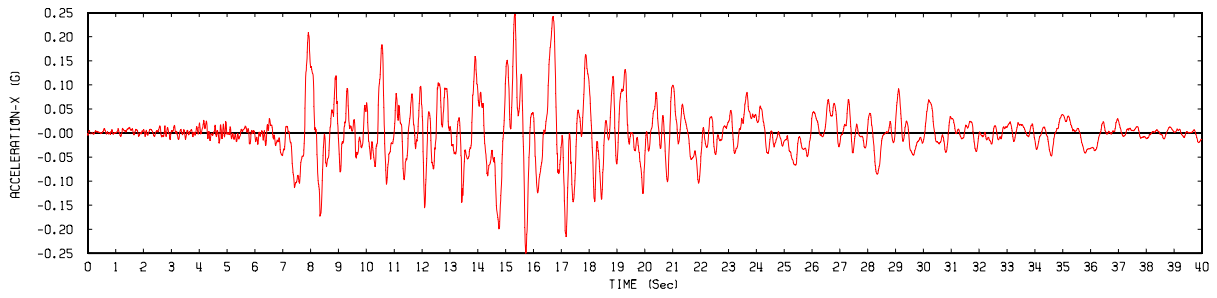
(a) Horizontal component
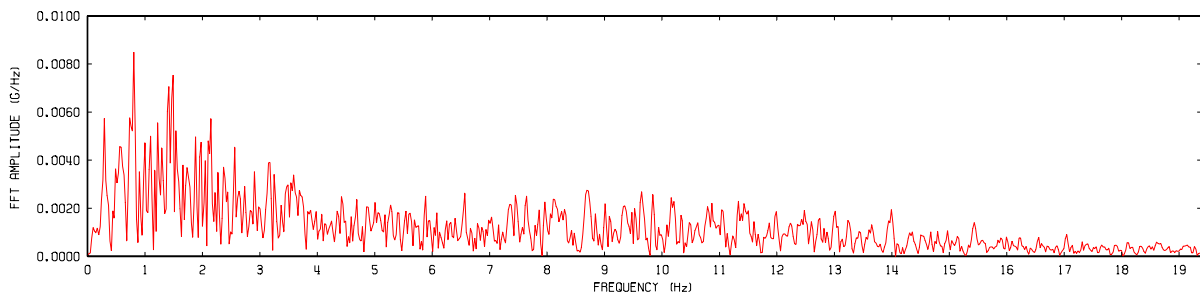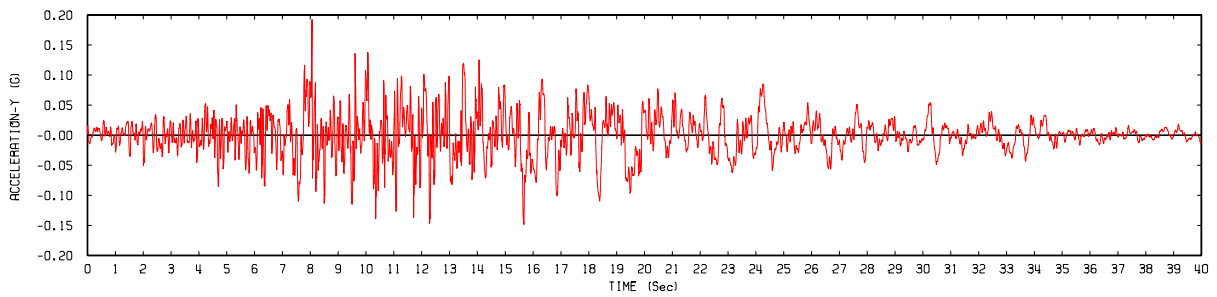
(b) Vertical component

Figure G-7. Time history and FFT of Anderson Dam acceleration record
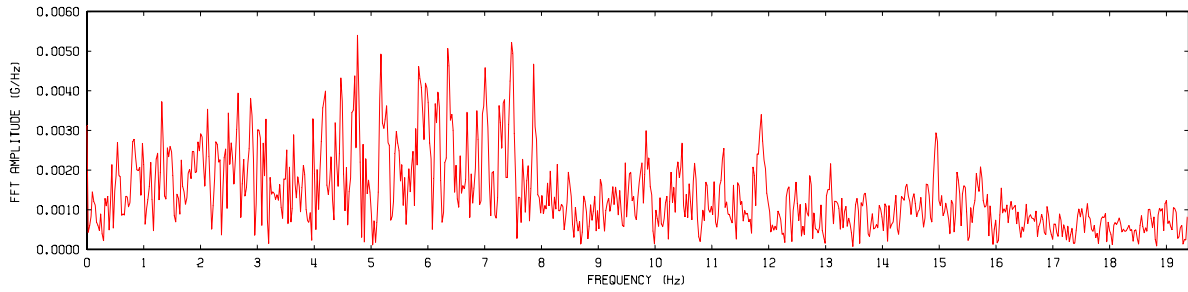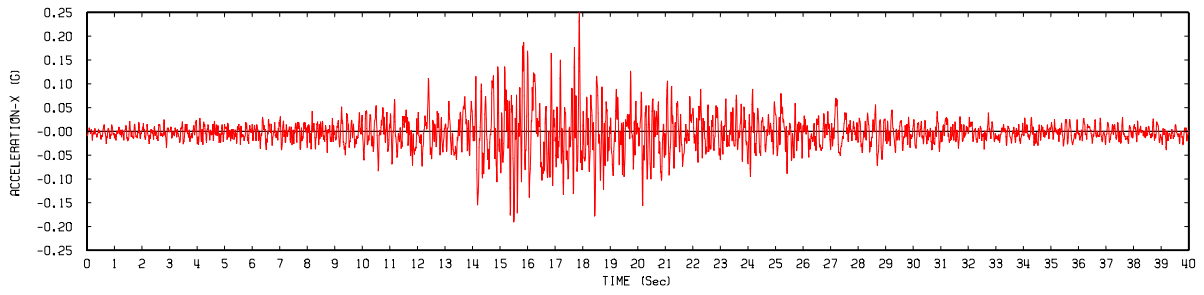
(a) Horizontal component
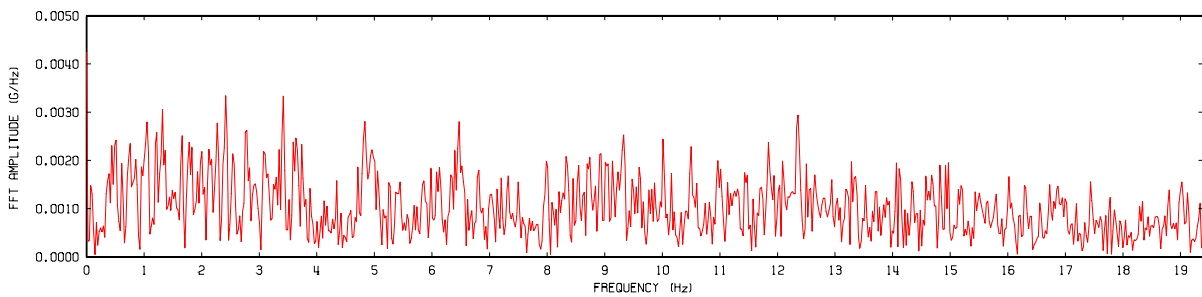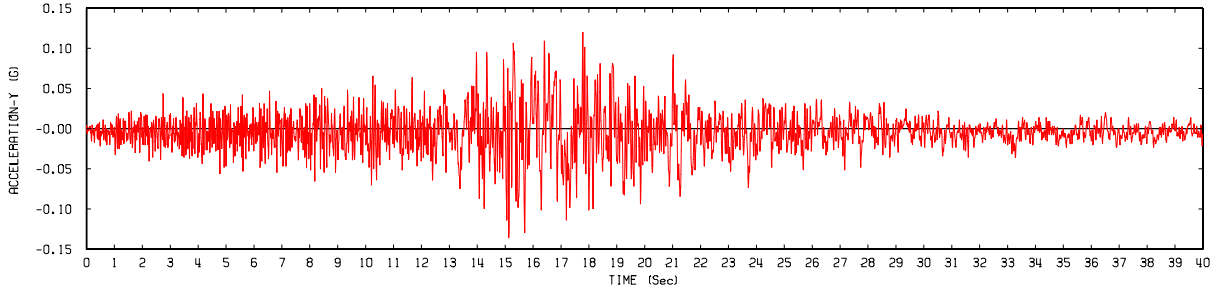
(b) Vertical component

Figure G-8. Time history and FFT of Papanoa acceleration record
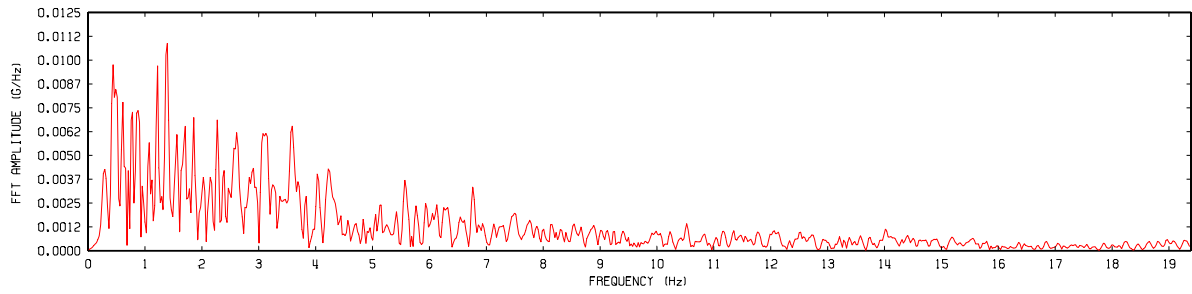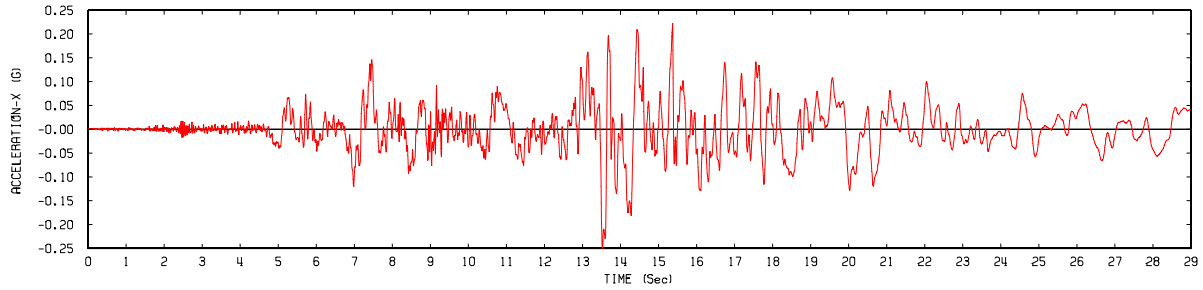
(a) Horizontal component
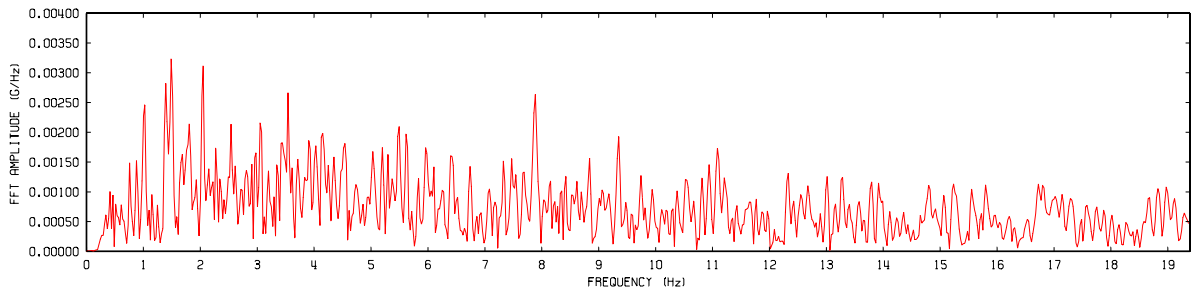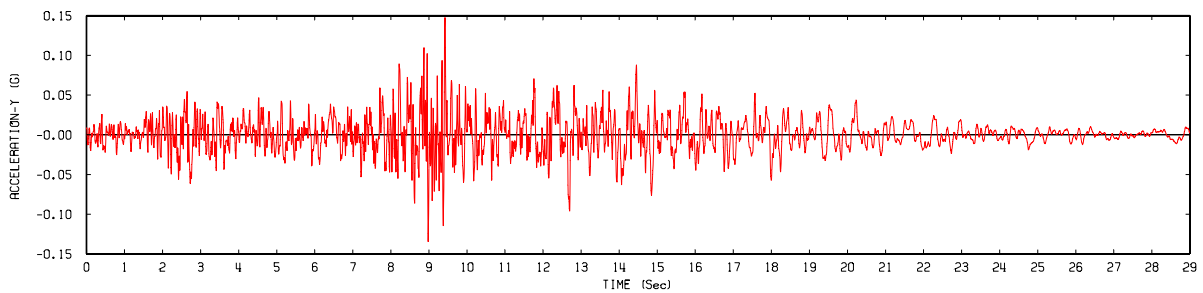
(b) Vertical compoenent

Figure G-9. Time history and FFT of Wildlife acceleration record

(a) Anderson ground motion | (b) Papanoa ground motion | (c) Wildlife ground motion
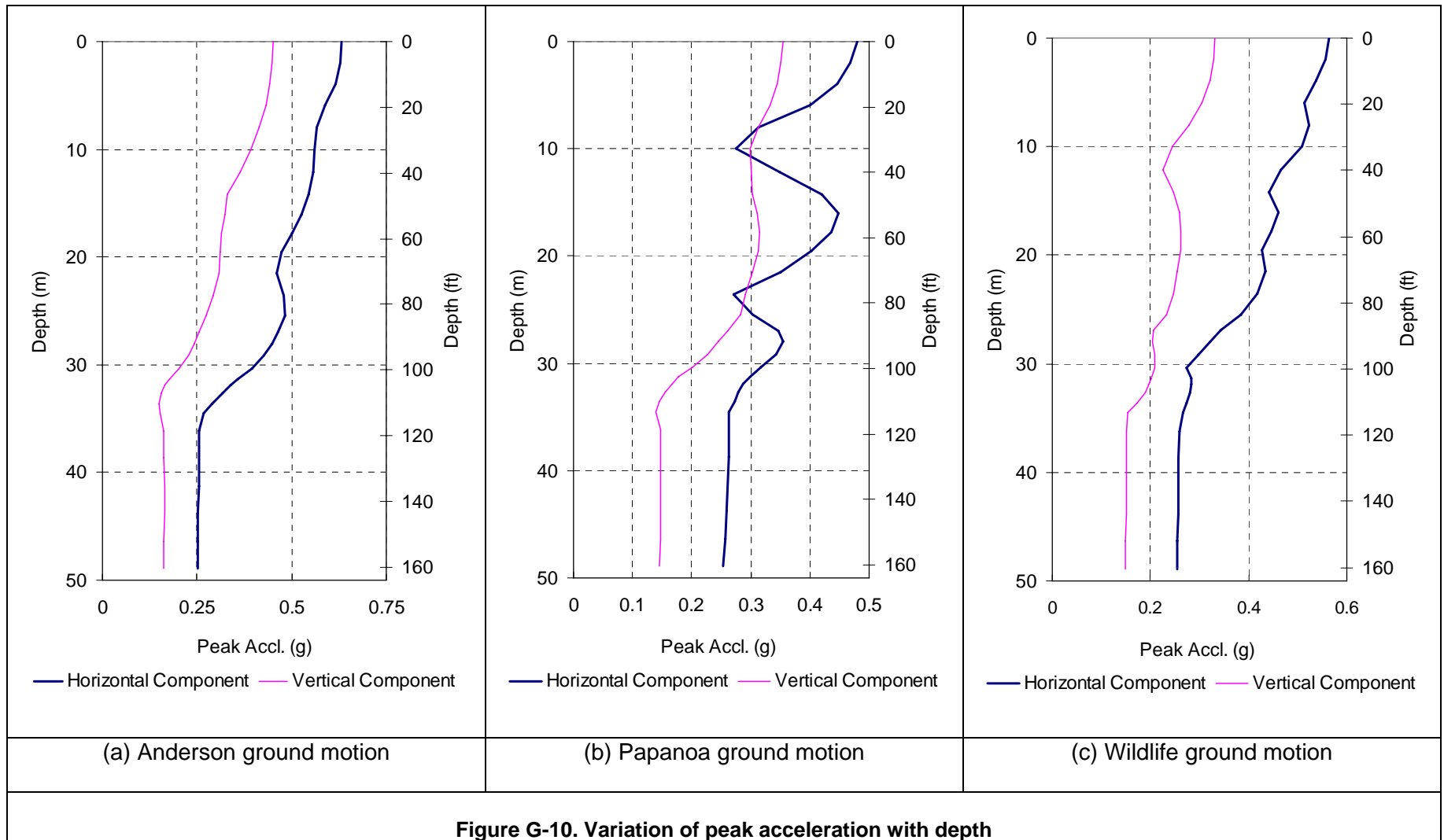
Figure G-10. Variation of peak acceleration with depth
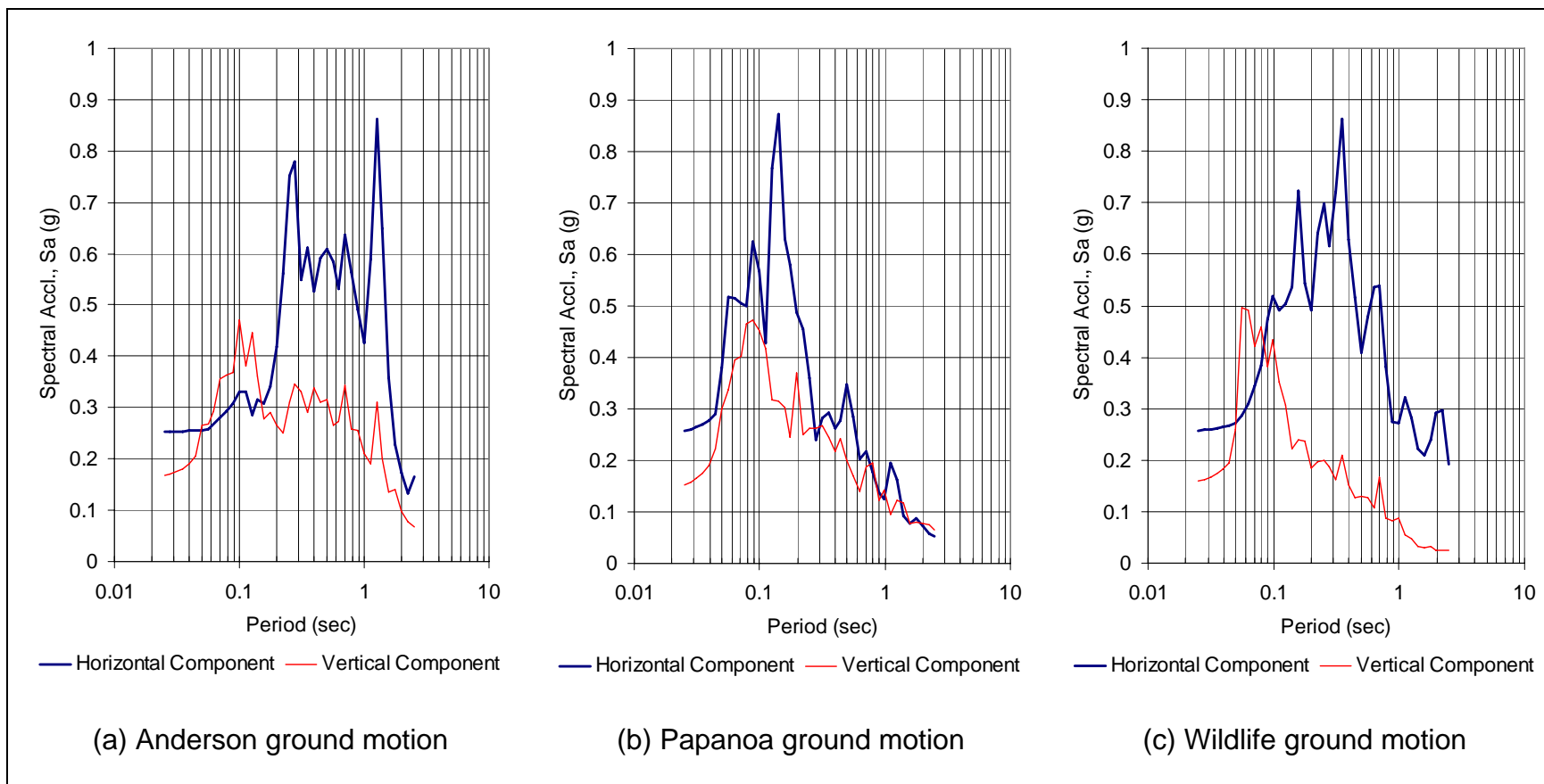
Figure G-11. Rock motion response spectra (5% damping)

(a) Comparison of initial vs. final strain-compatible shear-wave velocity due to horizontal ground motions

(b) Strain-compatible damping ratio profile due to horizontal ground motions

(c) Strain-compatible damping ratio profile due to vertical ground motions
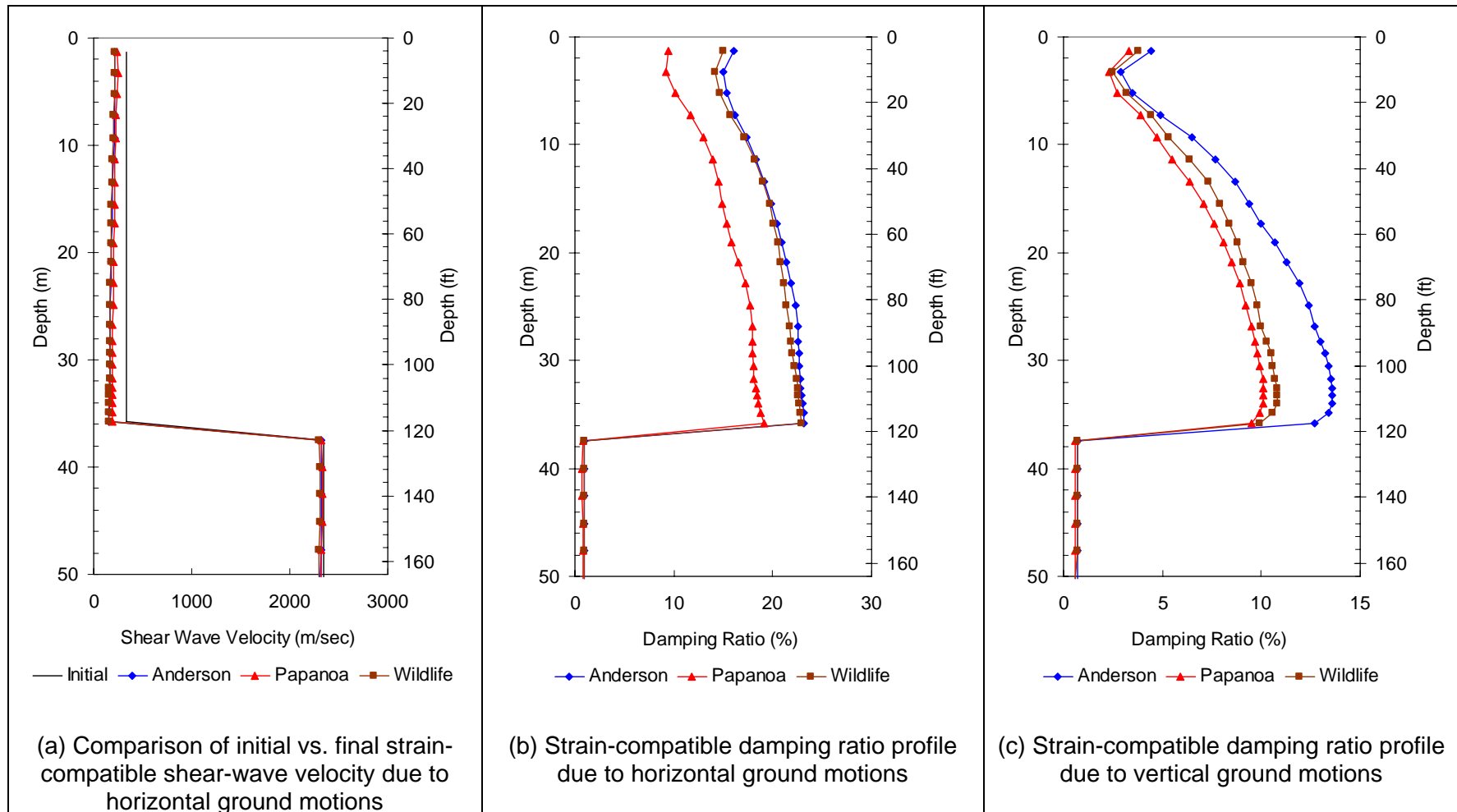
Figure G-12. Final strain-compatible shear-wave velocity and damping ratio profiles
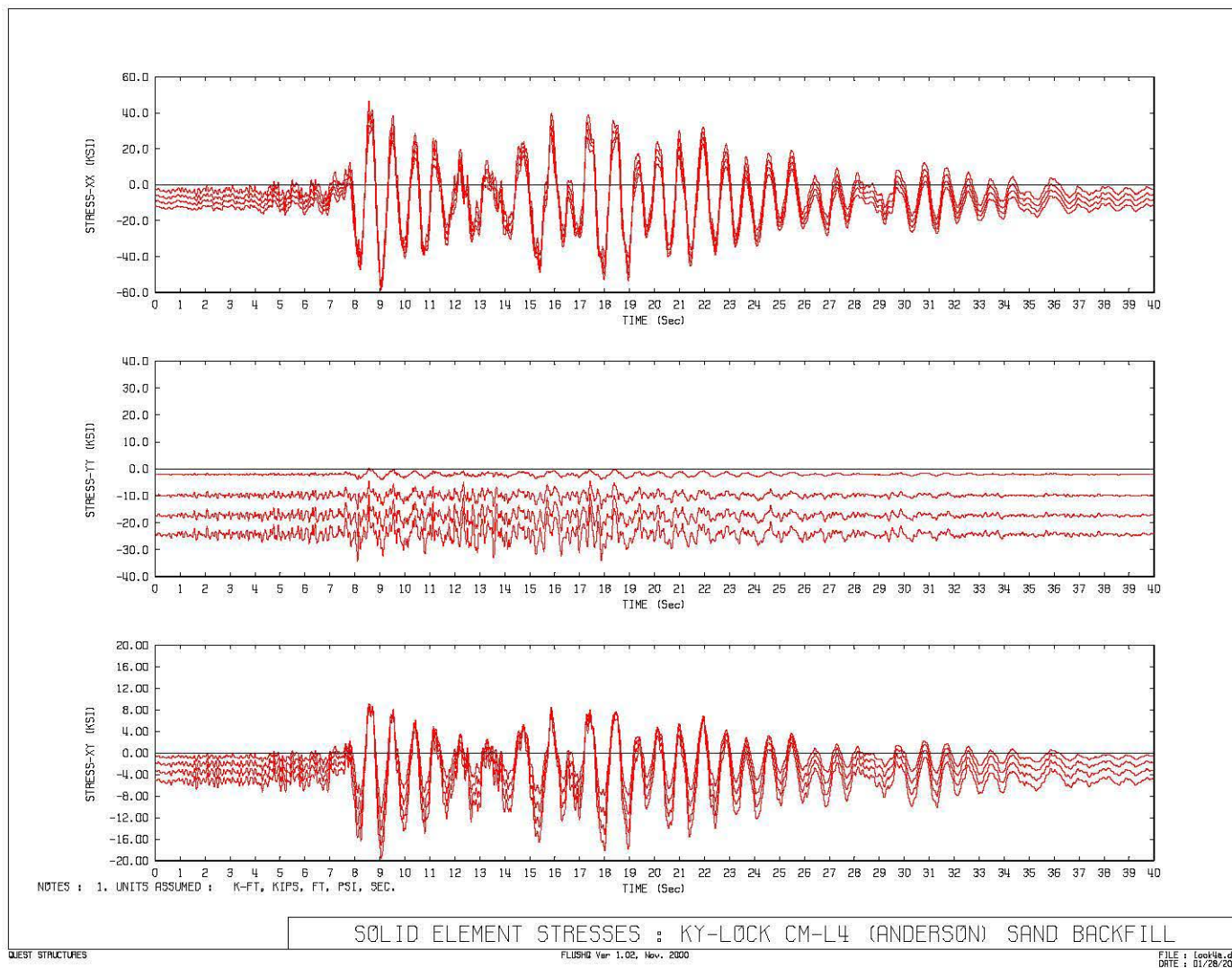
Figure G-13. Time history of horizontal (σ_{xx}), vertical (σ_{yy}), and shear (σ_{xy}) stresses for four elements at the toe of lock wall
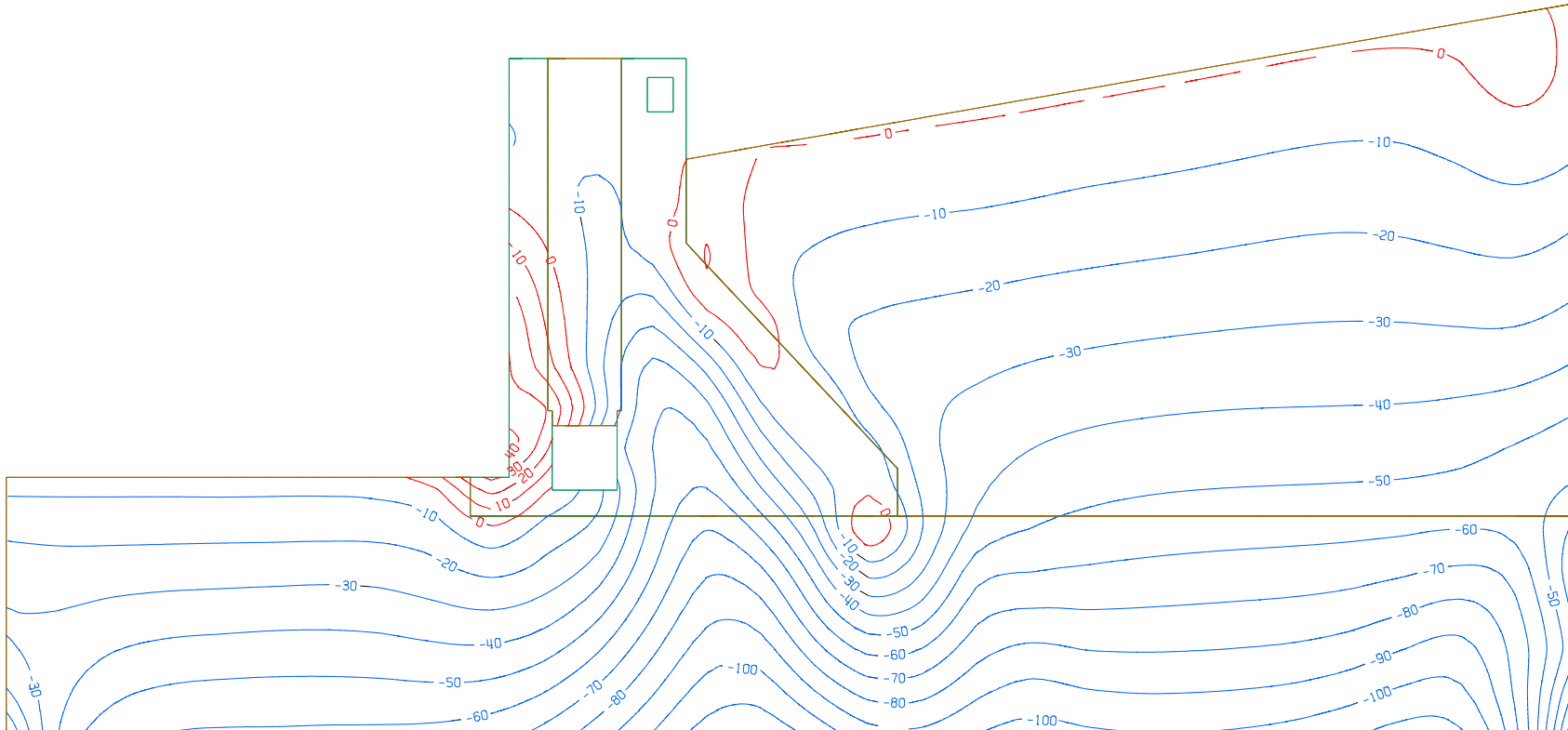
Figure G-14. Maximum vertical stress contours for Anderson earthquake record
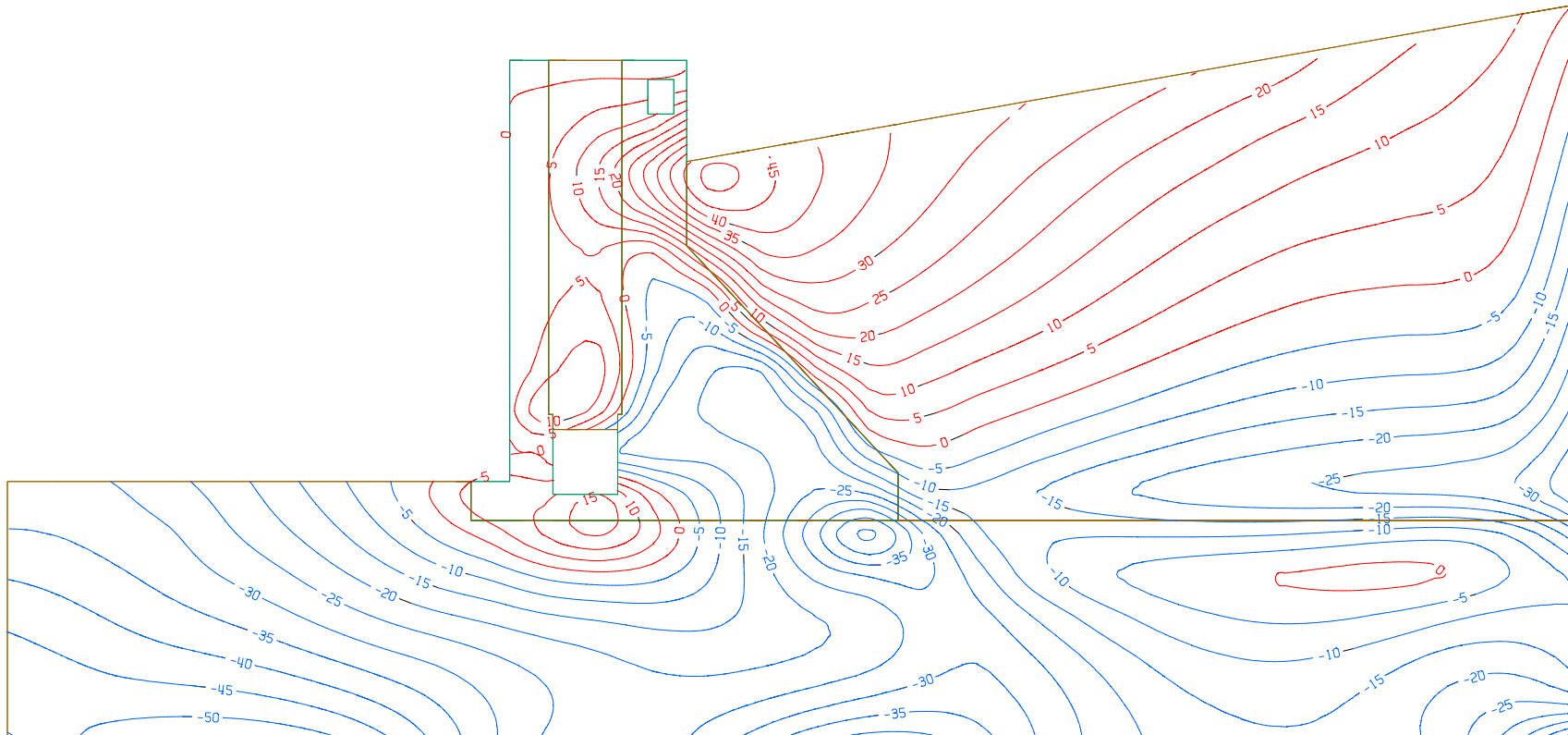
Figure G-15. Snap shot of horizontal stresses at t = 15.83 sec. for Anderson earthquake record
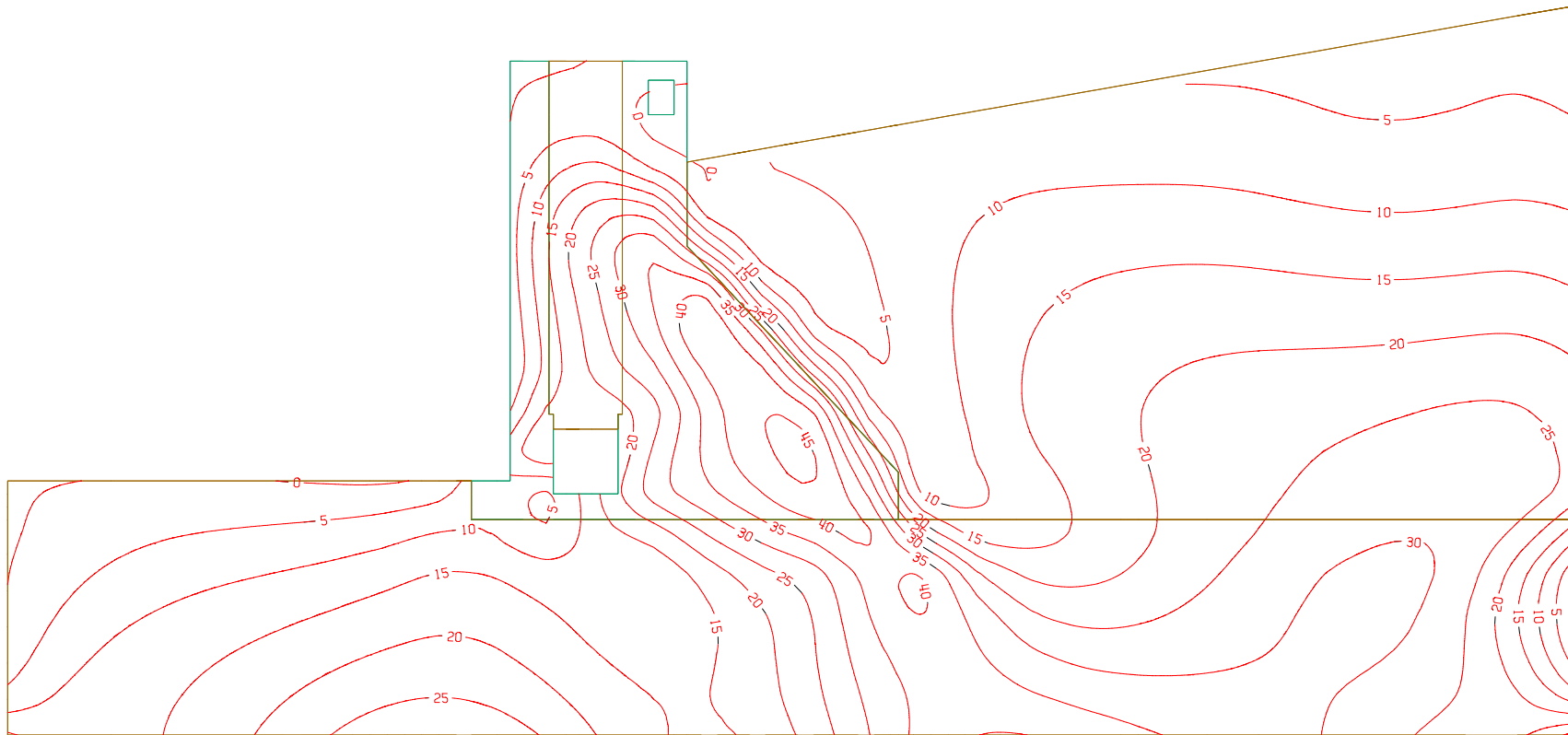
Figure G-16. Snap shot of shear stresses at t = 15.83 sec. for Anderson earthquake record

HS3

VP1

VP2

HS2

HS1
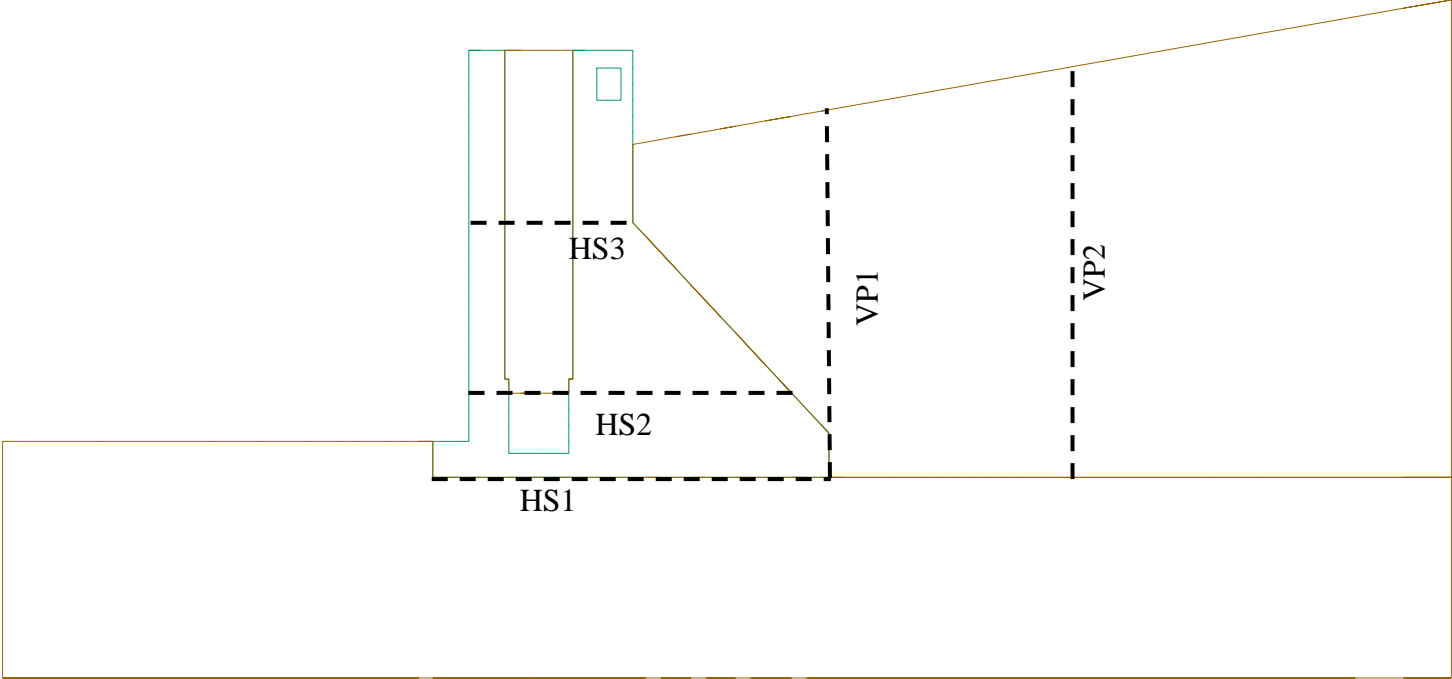
Figure G-17. Horizontal and vertical sections used in the analysis
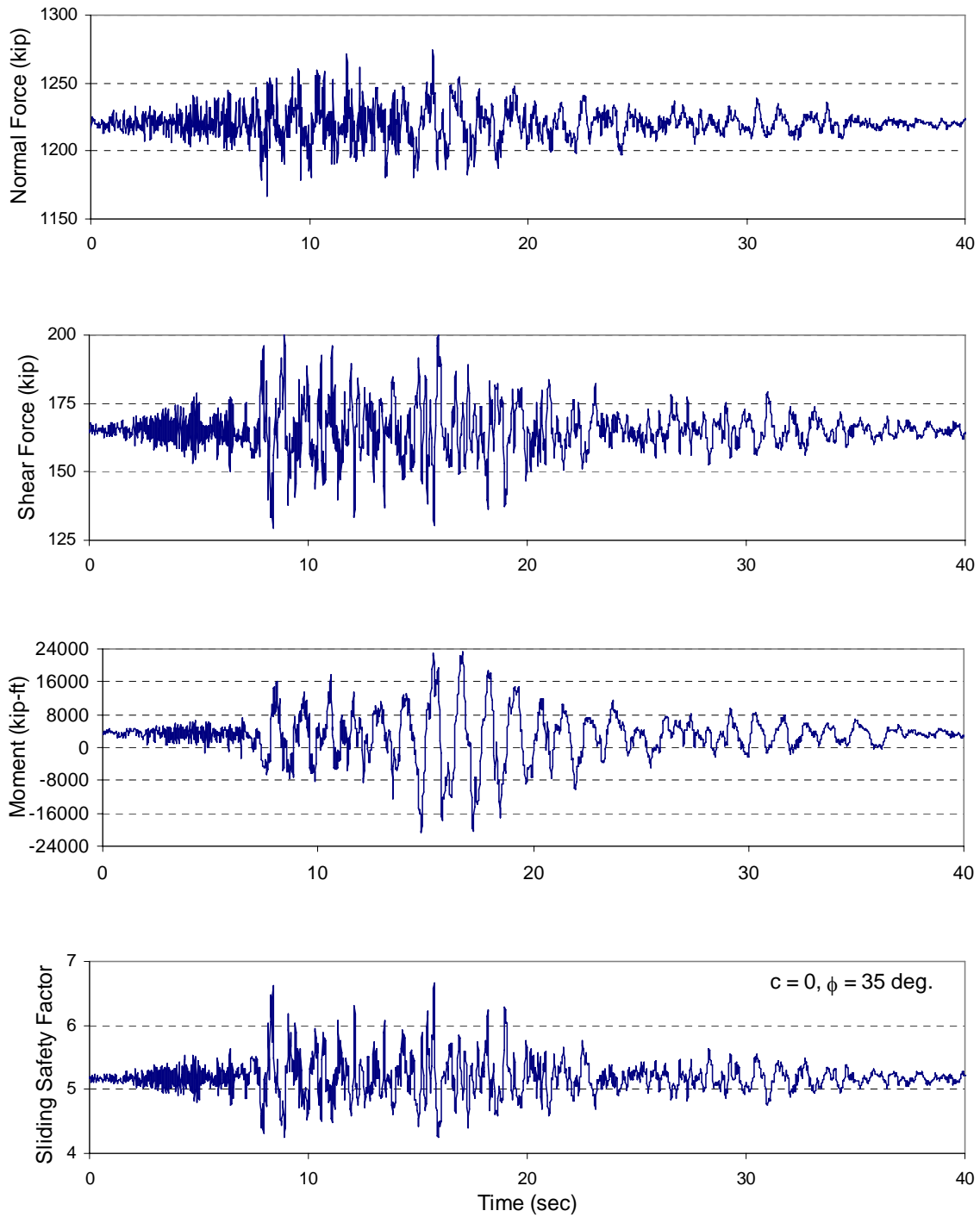
Figure G-18. Time histories of normal force, shear force, moment, and sliding safety factor at Section HS1 for Anderson earthquake record
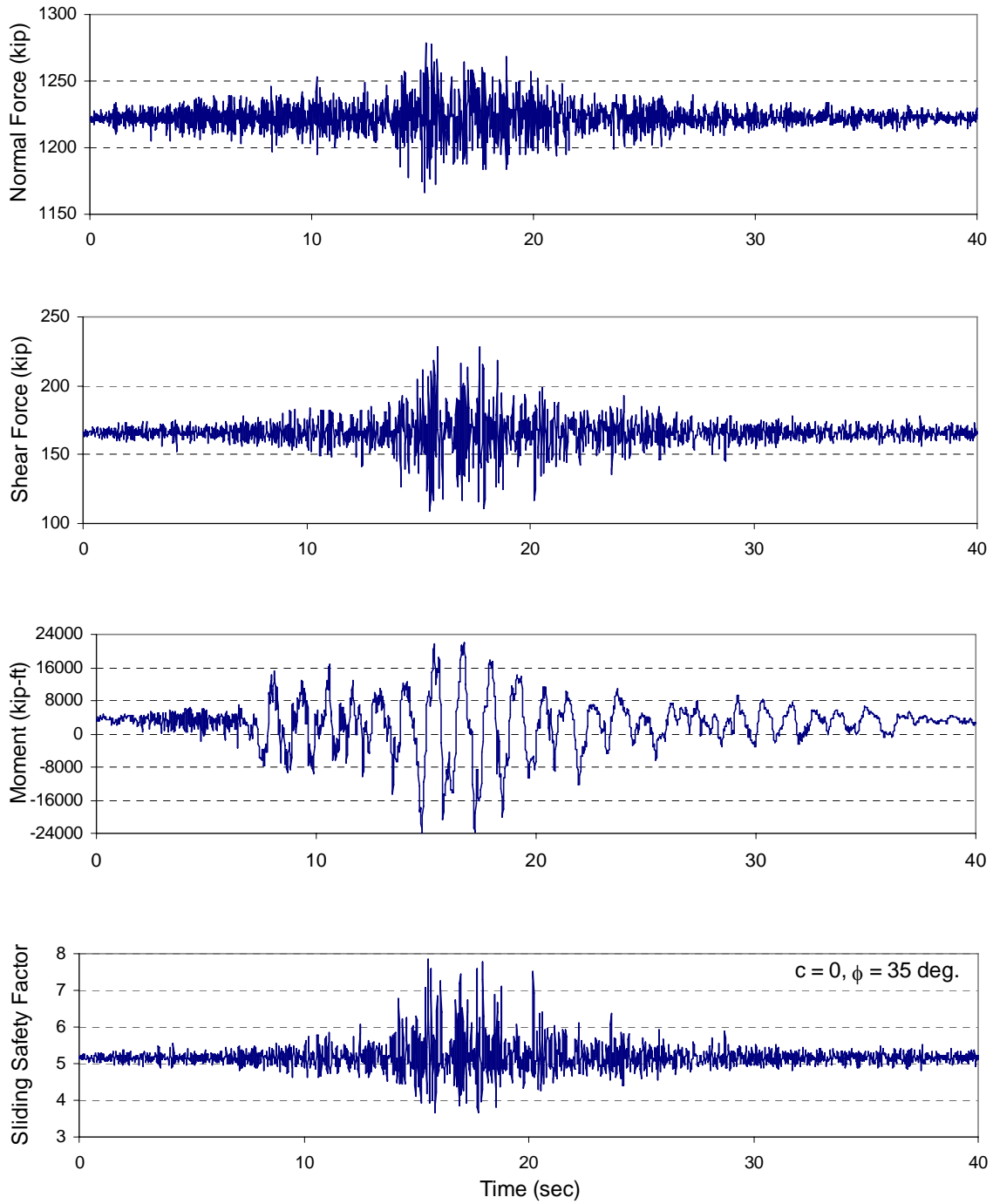
Figure G-19. Time histories of normal force, shear force, moment, and sliding safety factor at Section HS1 for Papanoa earthquake record
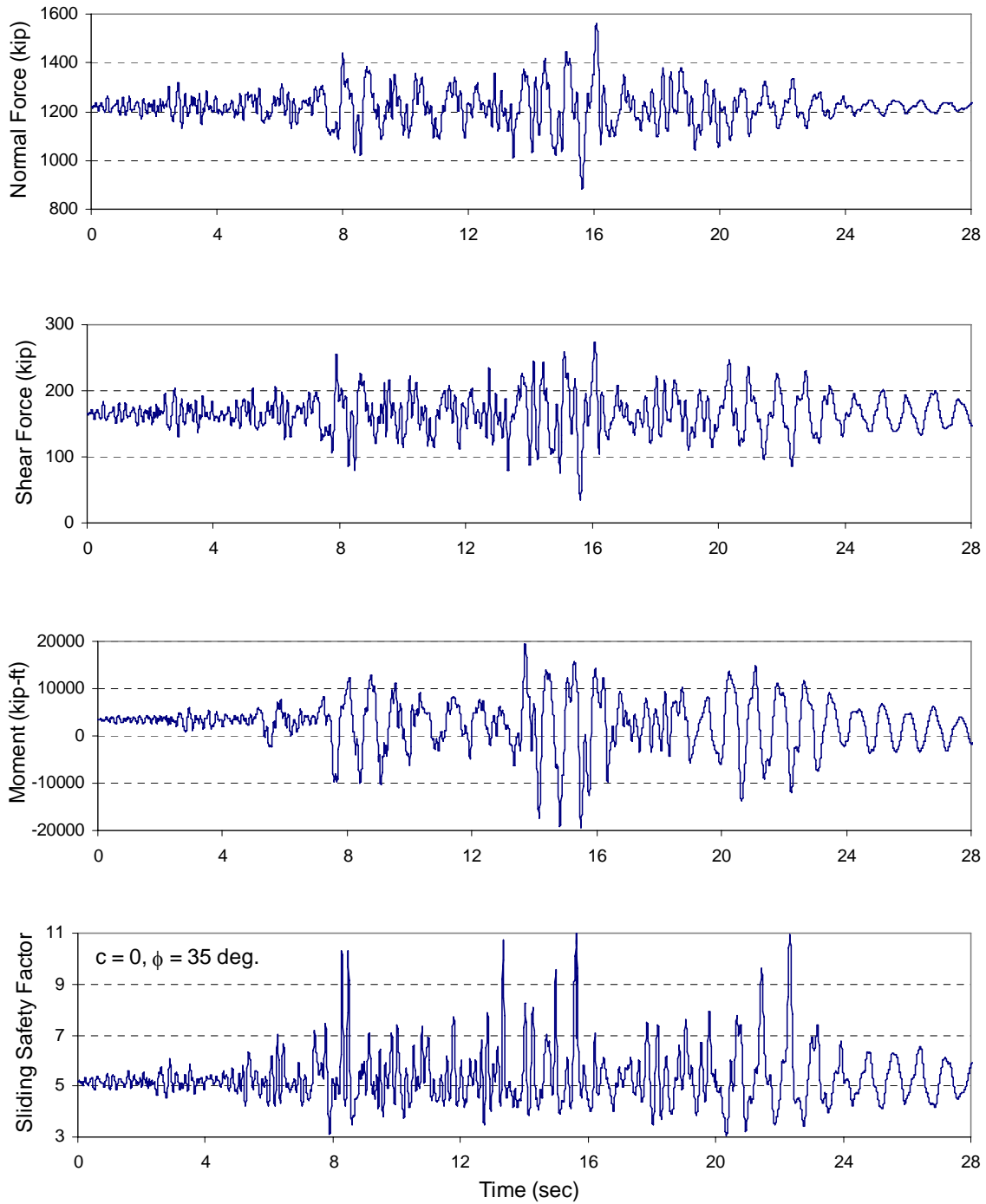
Figure G-20. Time histories of normal force, shear force, moment, and sliding safety factor at Section HS1 for Wildlife earthquake record
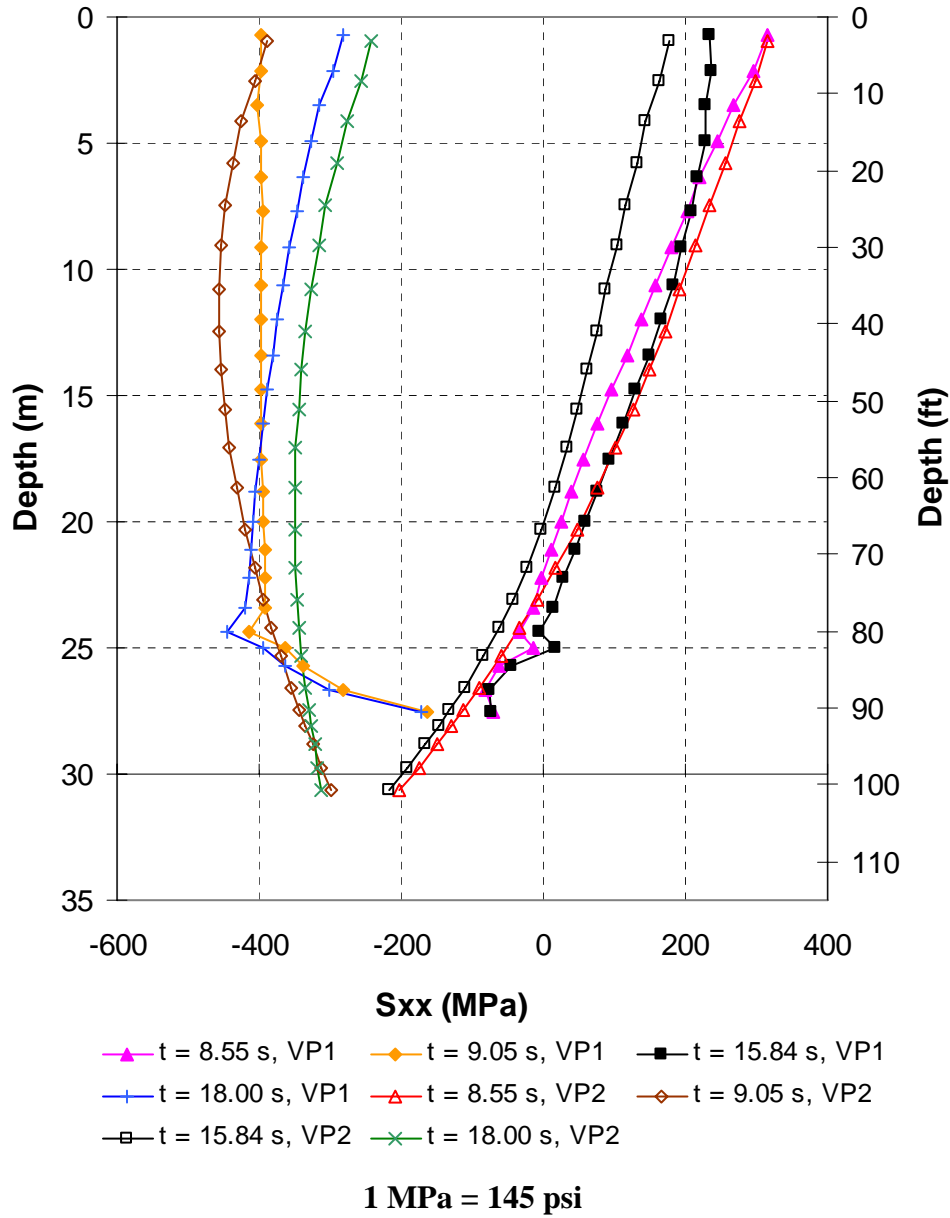
Figure G-21. Dynamic soil pressure profiles (normal stress Sxx) along vertical planes VP1 and VP2
at different instants of peak responses (Anderson ground motion)
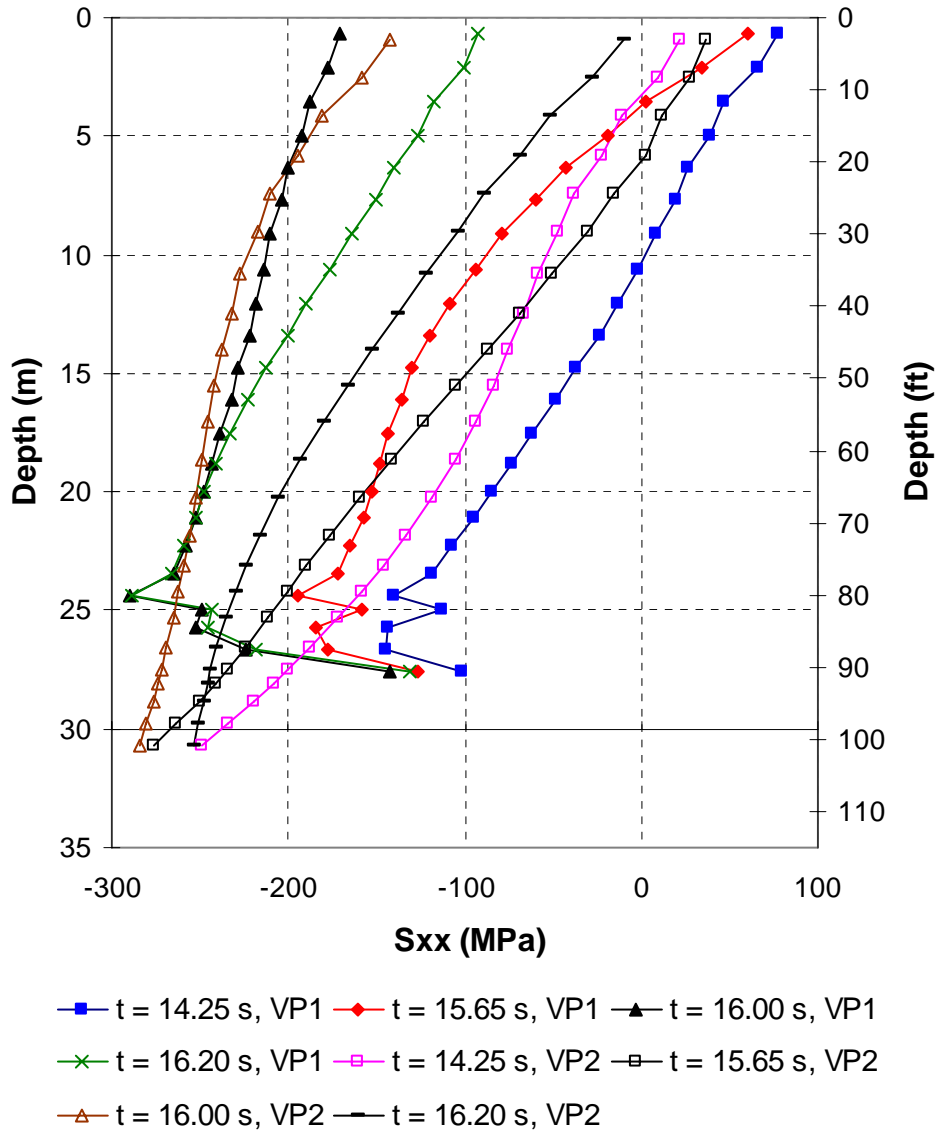
1 MPa = 145 psi

Figure G-22. Dynamic soil pressure profiles (normal stress, Sxx) along vertical planes VP1 and VP2 at different instants of peak responses (Papanoa ground motion)
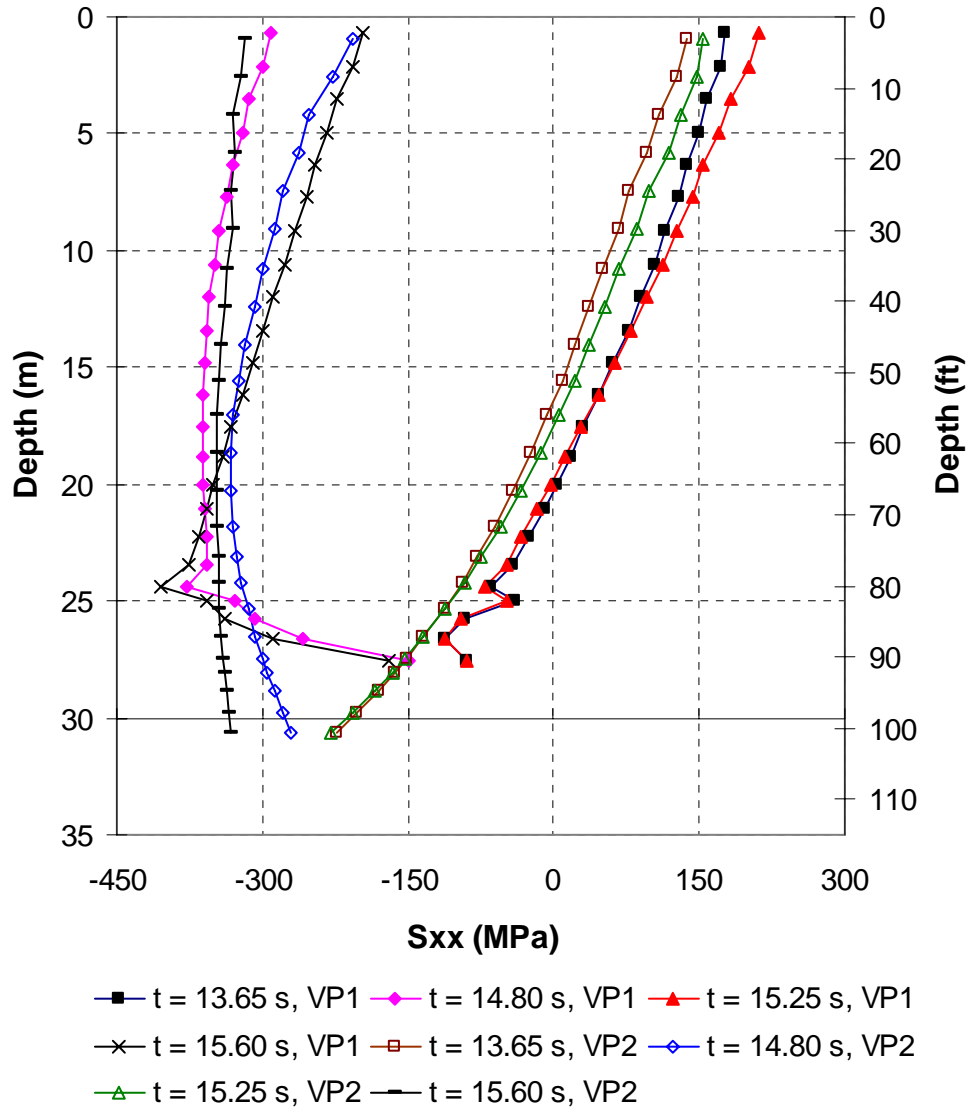
1 MPa = 145 psi

Figure G-23. Dynamic soil pressure profiles (normal stress, Sxx) along vertical planes VP1 and VP2 at different instants of peak responses (Wildlife ground motion)

Appendix H
NONLINEAR TIME HISTORY ANALYSIS OF GRAVITY DAMS

H-1. Introduction

The example problem is a 74 m (243.33 ft) high non-overflow gravity dam section with a crest thickness of 9.75 m (32 ft) and a base thickness of 53.83 m (176.6 ft). On the lower two-third, the dam is sloped at 1/10 on the upstream and at 7/10 on the downstream face. The dam is first analyzed using linear time-history method to illustrate the linear-elastic acceptance criteria discussed in Paragraph 6.4*d*(1), and then evaluated by nonlinear time-history method to assess potential sliding and rocking responses under earthquake shaking.

H-2. Purpose and Objectives

The purpose of this example is to illustrate the application of linear and nonlinear time history methods to earthquake response analysis of gravity dams. The objectives of this study are: 1) to compute displacements and stresses for four sets of earthquake acceleration time histories, 2) to identify main nonlinear mechanisms and potential failure modes, 3) to perform nonlinear analysis with the identified nonlinear mechanisms, and 4) to assess stability condition of the dam.

H-3. Scope

The scope of this example includes the following:

a. Establishment of evaluation earthquake and associated acceleration time histories.

b. Computation of linear earthquake response of the dam including the effects of foundation and impounded water.

c. Evaluation of results of linear time history with the acceptance criteria.

d. Development of nonlinear model with the main nonlinear mechanisms.

e. Evaluation of nonlinear time-history analyses to assess stability of the dam.

H-4. Earthquake Ground Motions

For evaluation of the earthquake response using linear ad nonlinear time-history analyses, the example gravity dam was assumed to be located in the near field of a maximum earthquake event having a moment magnitude M_w of about 6-1/2. Four sets of recorded acceleration time-histories from three earthquakes were selected in accordance with procedures discussed in Chapter 5 of EM 1110-2-6051. These included the Pacoima Dam record from 1971 San Fernando earthquake, the Gilroy Array No. 1 record from 1989 Loma Prieta earthquake, the Newhall record from 1994 Northridge earthquake, and the 1971 Pacoima Dam record modified to match the design response spectra. The design response spectra for the horizontal and vertical components of ground motion are the same as those used in Example D3. The ground motions were scaled such that the sum of ordinates for the response spectra of each natural record would match the sum for the smooth response spectra in the period range of 0.06 to 0.3 sec. The response spectra for the scaled records are compared with the smooth design response spectra in Figure H-1. Time-histories of the horizontal components of the records are

plotted in Figure H-2. This figure clearly demonstrates the pulsive ("fling") type motions contained in the San Fernando and Northridge records.
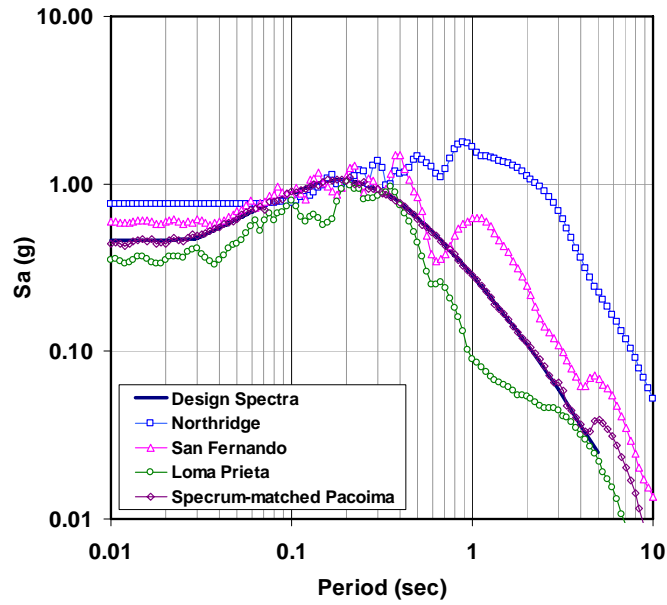
Figure H-1. Comparison of design response spectra with spectra of scaled records
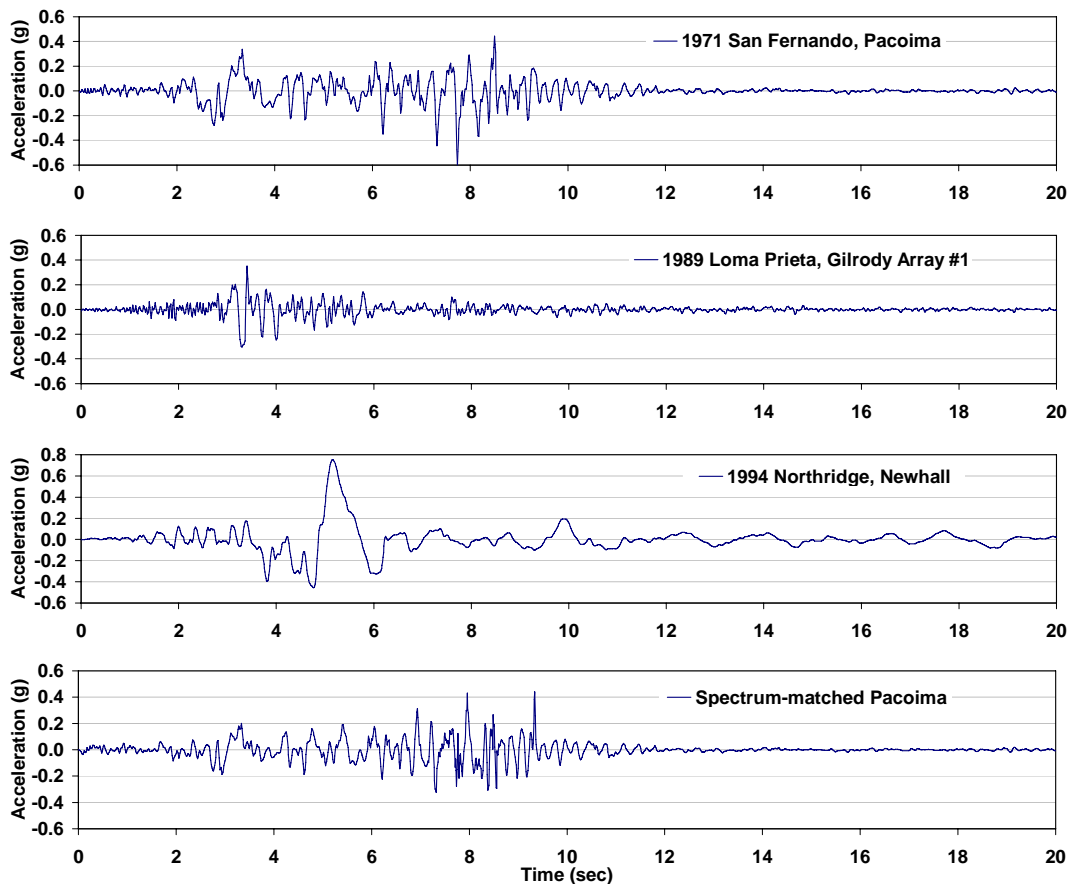
Figure H-2. Horizontal component of earthquake input acceleration time histories

H-5. Linear Elastic Response

a. Finite-element model. The linear-elastic time-history analysis of the example dam was carried out in accordance with Paragraphs 4.3*a*(3) and 6.3*d*(2). The dam and foundation rock were represented by 2D shell elements of unit thickness with concrete and rock properties, respectively. A modulus of elasticity of 282.5 MPa (5.9×10^6 psi), a Poisson's ratio of 0.19, with a unit weight of 2530.9 kg/m^3 (158 pcf) was assumed for the mass concrete. The foundation rock was assumed massless but its modulus and Poisson's ratio were assumed to be respectively 277.7 MPa (5.8×10^6 psi) and 0.19. The inertia forces of the impounded water were represented by added hydrodynamic mass values in accordance with the generalized Westergaard method (see EM 1110-2-6051). The added mass associated with nodal points on the sloped portion of the upstream face consists of horizontal and vertical values. Thus they generate inertia forces in the horizontal and vertical directions. The finite-element model is shown in Figure H-3. A total of 3,417 shell elements were used: 1,493 elements to model the dam, and 1,924 to model the foundation rock. The model included a total number of 3,612 nodal points.
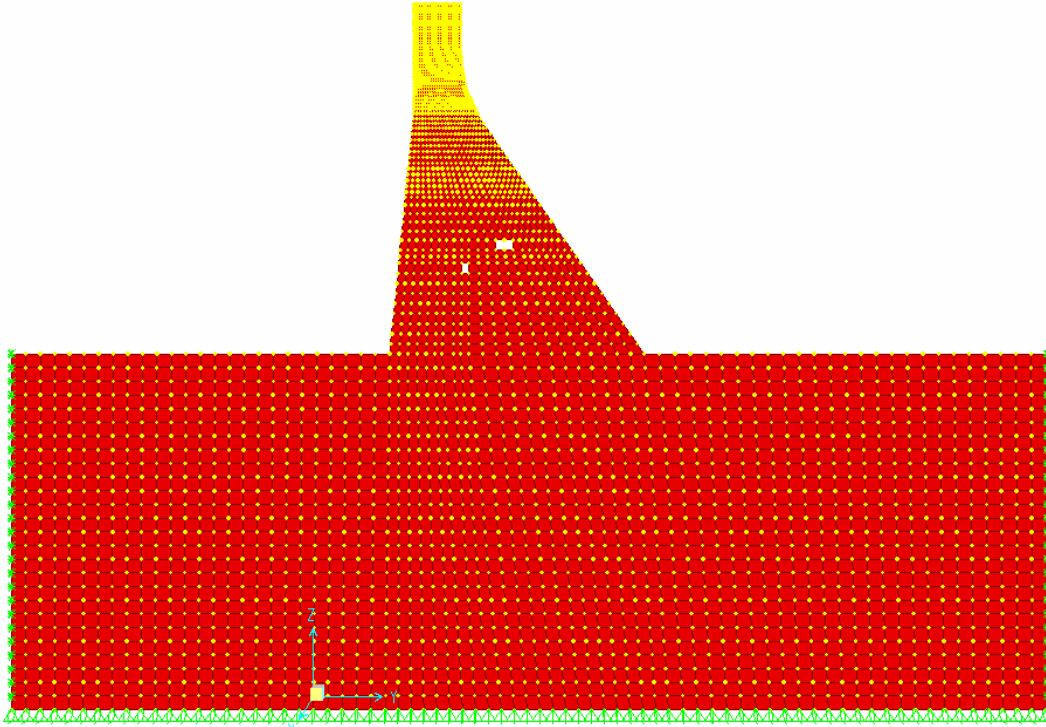
Figure H-3. SAP2000 dam-foundation model

b. Evaluation of Linear Response. The example dam model was analyzed for the combined effects of static plus seismic loads. The static loads included the gravity due to deadweight of the concrete, hydrostatic pressures corresponding to a headwater depth of 73.15 m (240 ft with water level at 3.33 feet below the crest of the dam), and uplift pressures. The earthquake loads consisted of the inertia forces generated by earthquake ground motions described in Paragraph H-4. A linear uplift pressure distribution from 240-ft headwater to zero tailwater was assumed. The uplift pressure was also assumed not to change during the earthquake ground shaking. The results of analyses include envelopes of maximum stresses, time history of stresses, time history of displacements, and time history of reaction forces at the dam-foundation contact. The envelopes of maximum stresses are used to assess severity and extent of overstressed regions. The stress time histories are used to compute cumulative duration of stress excursions for comparison with the acceptance limits. Finally, time histories of reaction forces are used to compute instantaneous factors of safety to assess stability conditions of the dam.

(1) *Envelopes of maximum stresses.* Figure H-4 displays envelopes of maximum vertical stresses for the four earthquake acceleration time histories. The results indicate that high tensile stresses generally develop at the heel and toe of the dam as well as at upper elevations near the change of slopes of the upstream and downstream faces. In terms of the magnitude and spatial extent, high tensile stresses are most severe for the 1971 San Fernando record, where they cover more than 80 percent of the upstream face of the dam. Recognizing that the tensile strength at the dam-rock contact is lower than the tensile strength of the concrete, the cracking is expected to initiate at the heel of the dam and propagate toward the toe. Tensile cracking at the base of the dam causes sliding, but at the same time reduces tensile stresses at locations above the base. This tentative nonlinear behavior will be substantiated by the nonlinear time-history analysis in Paragraph H-6.

(2) *Time history of maximum stresses.* Figure H-5a shows time history plots of maximum stresses at the heel (Element 4001) of the dam and at the downstream change of slope (Element 4767). Also shown on these plots are the static tensile strength of 2.9 MPa (425 psi) and apparent dynamic tensile strength of 5.8 MPa (850 psi) for the concrete. Note that for computation of cumulative duration, the 2.9 MPa (425 psi) corresponds to DCR = 1 and 5.8 MPa (850 psi) to DCR = 2. The results show that stresses at the heel of the dam exceed DCR = 1 and 2. The number of stress cycles exceeding DCR = 2 is 15. This suggests that cracking initiates and propagates from the heel of the dam. The stresses at the top of the dam, even though large, remain below DCR = 2 and may not cause cracking because their magnitudes will be reduce as soon as cracking develops at the base of the dam. This observation will be substantiated by the nonlinear analysis in Paragraph H-6 below.

(3) *Time history of maximum displacements.* Time histories of horizontal displacements at the top of the dam are provided in Figure H-5b for the four earthquake records. At 47.5 mm (1.87 in.), the largest displacement occurs for the San Fernando record, followed with 40.4 mm (1.59 in.) for the spectrum-matched Pacoima, 38.8 mm (1.53 in.) for Northridge, and 35 mm (1.38 in.) for the Loma Prieta records.

(4) *Comparison with acceptance criteria.* The acceptance criteria for the linear time-history evaluation of gravity dams are that the percentage of the overstressed regions and cumulative duration of stress cycles above the tensile strength of the concrete remain below the performance curves given in Paragraph 6.4d(1). As discussed above, the static tensile strength and the apparent dynamic tensile strength of the concrete represent the range of acceptable tensile stress magnitudes. Knowing the static tensile strength of the concrete the surface areas with tensile stresses above demand-capacity ratios of 1, 1.2, 1.4, 1.6, 1.8, and 2 were estimated from the stress contour plots. A plot of the results in Figure H-6 shows that the overstressed areas exceed the acceptance limit for three of the earthquake records; only overstressed areas for the Loma Prieta record fall below the acceptance curve. Figure H-7 compares cumulative duration of stress cycles for Element 4001 at the heel of the dam with the acceptance curve. It is obvious that all cumulative duration for this element exceed the acceptance limits. In addition to Element 4001, the cumulative duration was also computed for four other elements near the heel and toe of the dam, as identified in Figure H-8. The cumulative duration for these elements is compared with the acceptance limits in Figure H-9. The results show that only the cumulative duration for two elements near the heel and one element at the toe exceed the acceptance limits. This suggests that cracking initiates from the heel and toe of the dam but may or may not propagate through the entire base. Thus, a nonlinear time history analysis is needed to evaluate the crack propagation and the effects it may have on sliding of the dam, as discussed in Paragraph H-6.

(5) *Seismic stability condition.* The normal and horizontal forces along the dam-foundation contact were obtained to assess sliding stability condition of the dam. Time histories of vertical (normal) and horizontal (shear) forces were computed by the SAP2000 computer program for the combined effects of gravity, hydrostatic, uplift, and the earthquake loads. The resultant vertical and horizontal reaction forces are displayed in the upper and mid graphs of Figure H-10. Knowing the normal and shear forces and assuming a friction coefficient of unity, the instantaneous sliding factors of safety were computed in accordance with Paragraph 7-3c(1), as shown in bottom graph of Figure H-10. Note that the instantaneous factor of safety at the time of zero represents the static sliding factor of safety, which for this example is 1.2. During the earthquake ground shaking the instantaneous factor of safety oscillates above and below the value of the static factor of safety as the magnitude and direction of inertia force changes. Figure H-10 shows that the instantaneous factor of safety repeatedly falls below unity, an

indication that the dam will slide along its base. The magnitude of sliding displacement however, is estimated using the nonlinear time-history analysis described in Paragraph H-6.
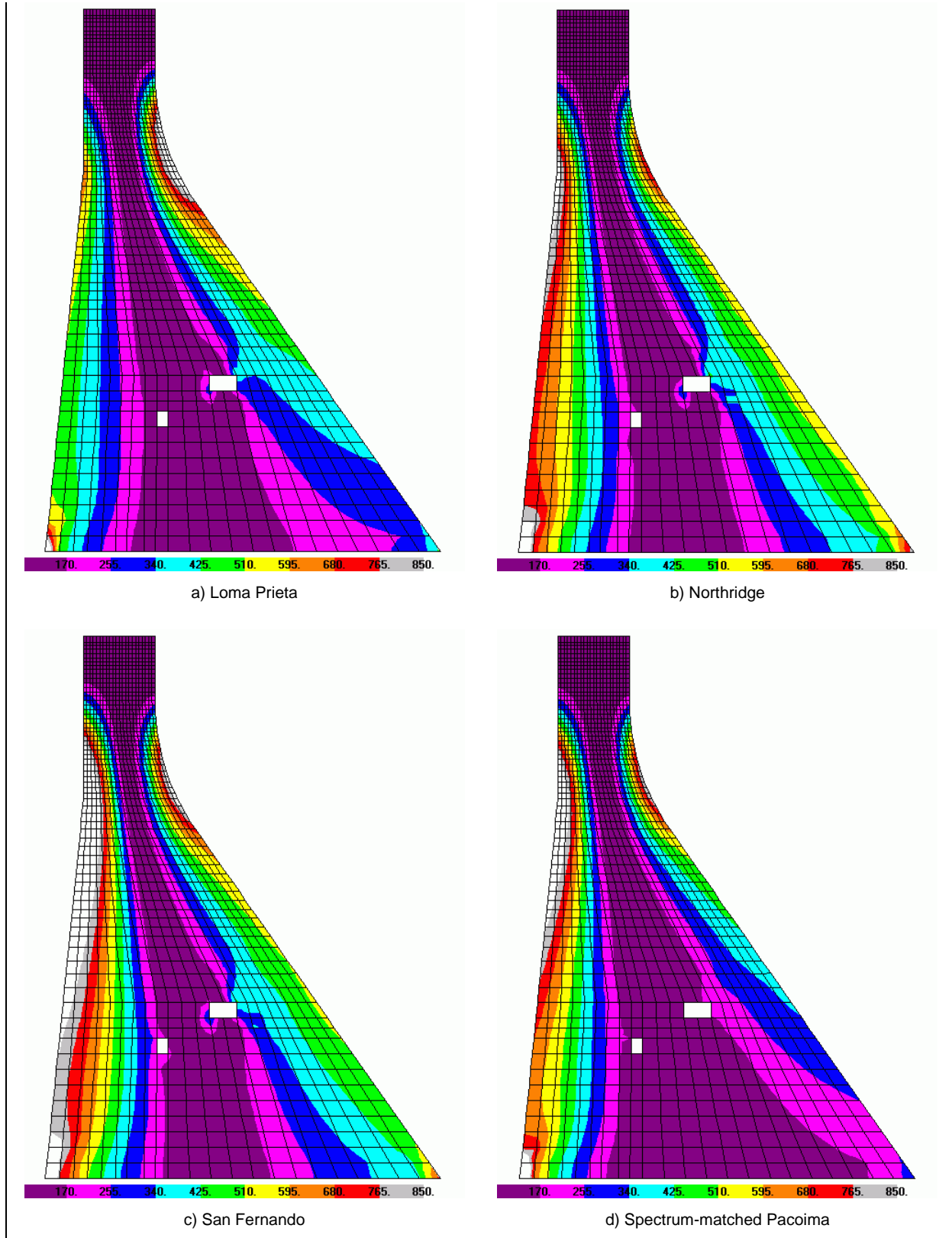
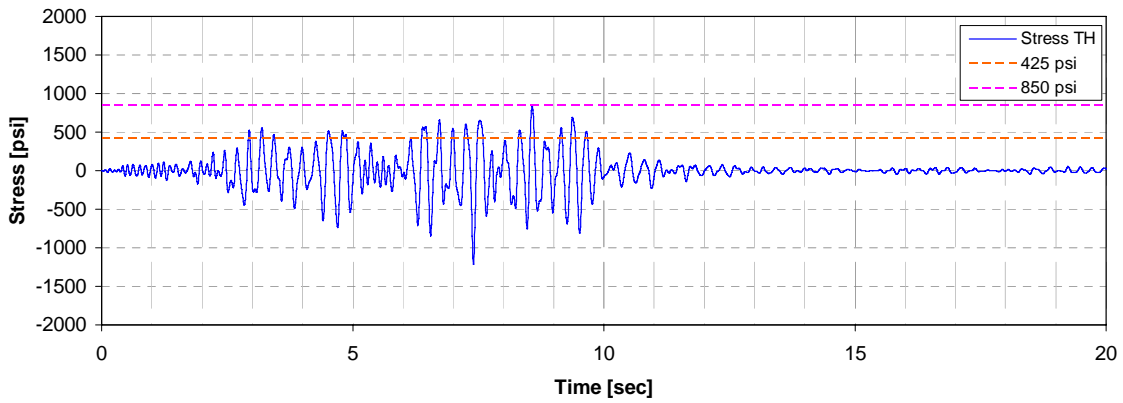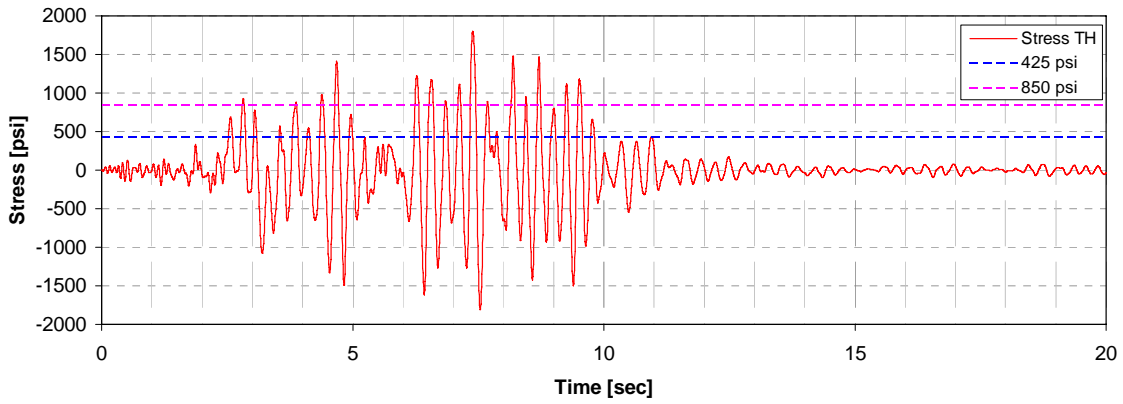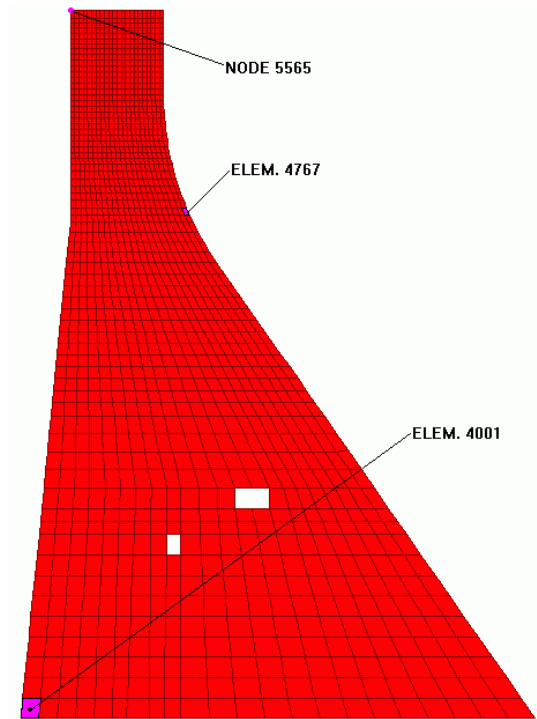**Figure H-4. Envelopes of maximum vertical stresses from linear TH analysis (psi)**

a) Loma Prieta

b) Northridge

c) San Fernando

d) Spectrum-matched Pacoima

Figure H-5a. Time history of maximum vertical stresses at the heel of the dam (Elem. 4001) and at the change of slope on downstream face (Elem. 4767) for San Fernando seismic input
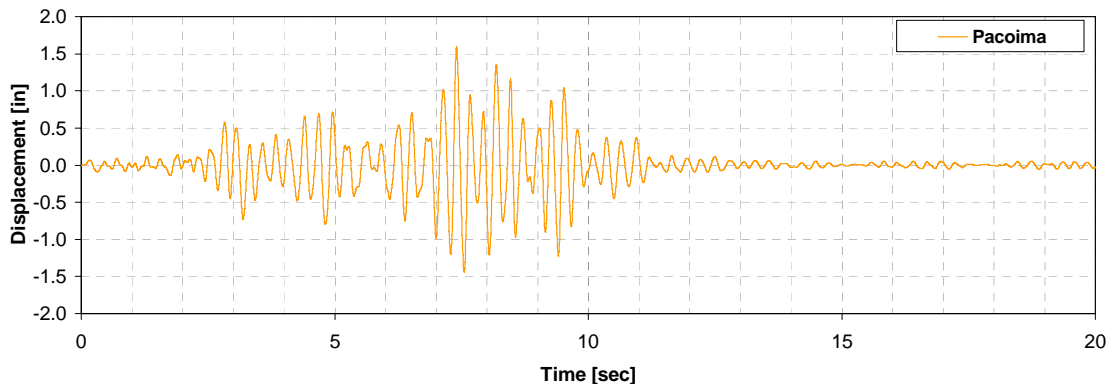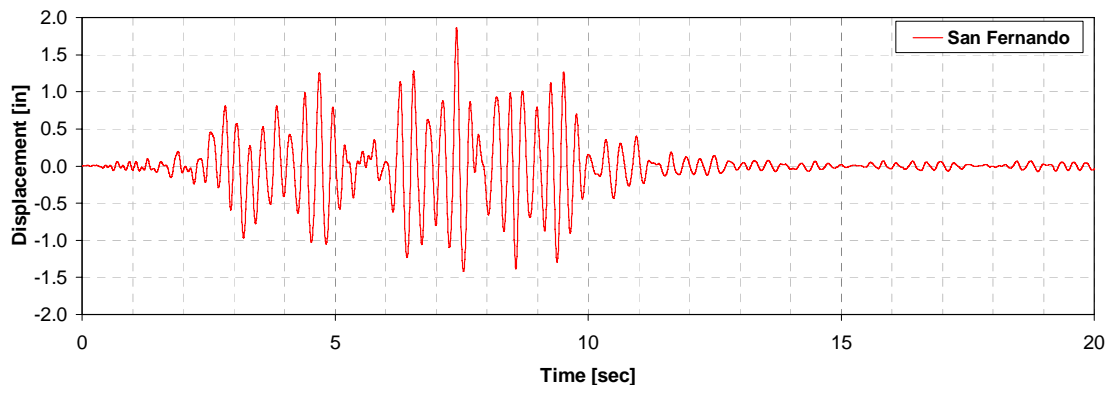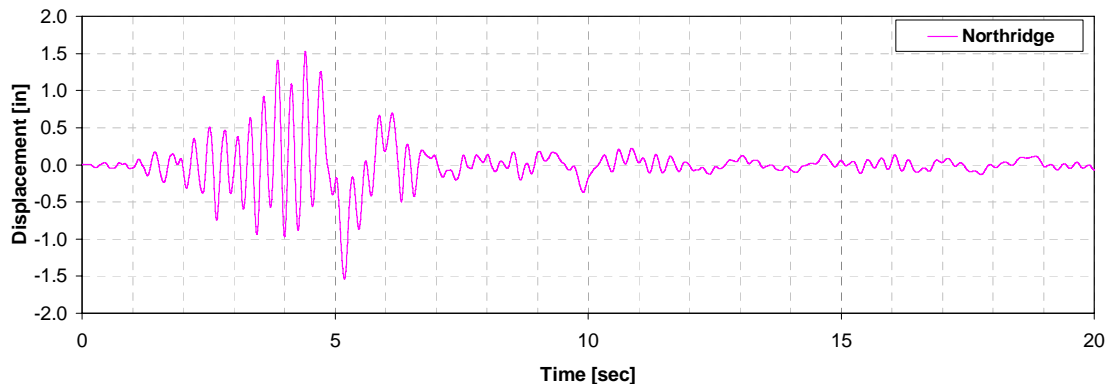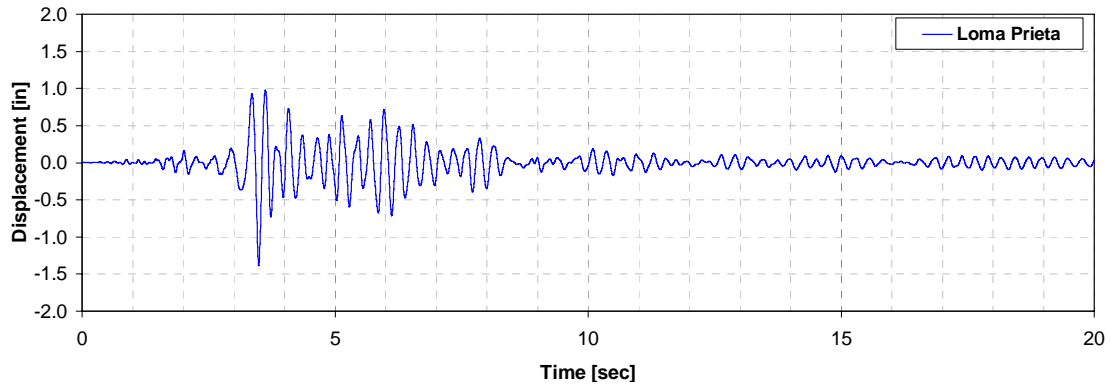
Figure H-5b. Time history of horizontal displacement at top of the dam (Node 5565 in Figure H-5a)
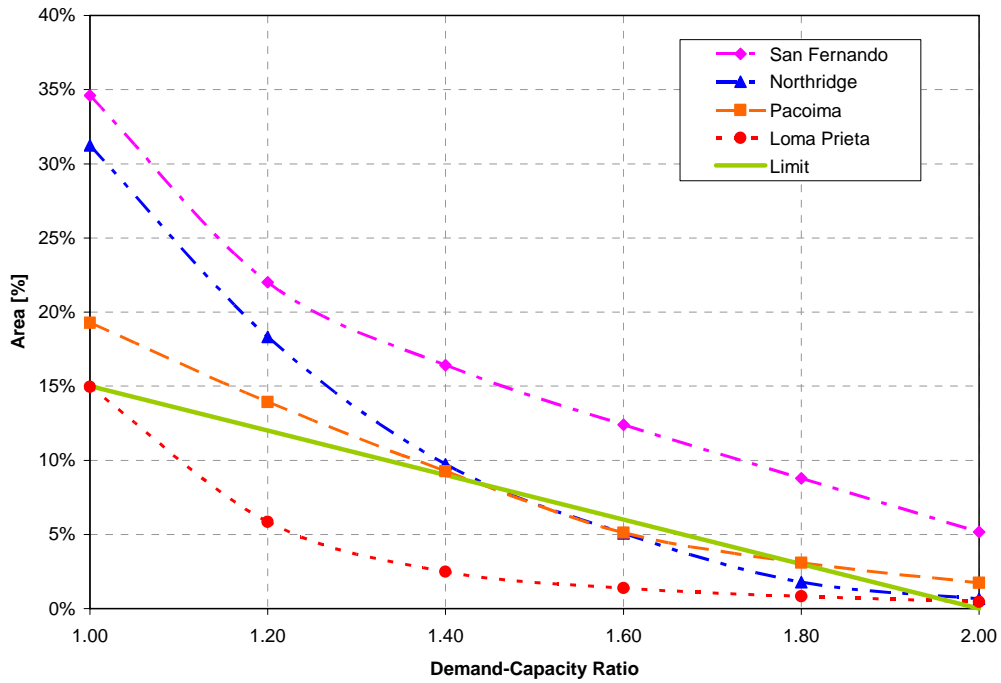
Figure H-6. Comparison of percentage of overstressed areas with acceptance limits
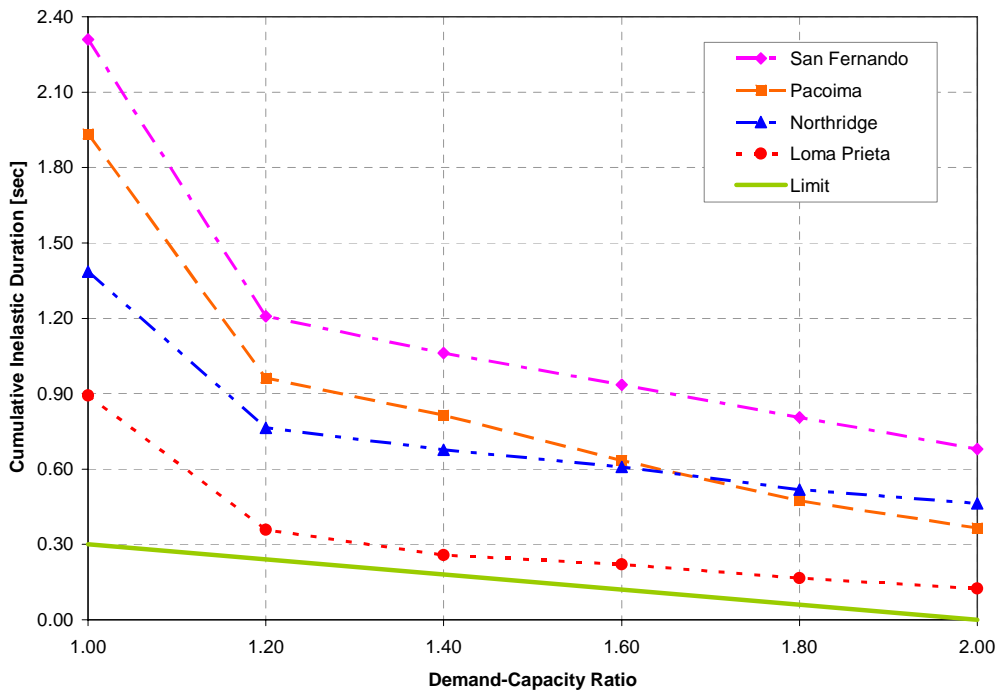
Figure H-7. Comparison of cumulative duration of stress cycles with acceptance limits for stresses at the heel of the dam (Element 4001 in Figure H-8)
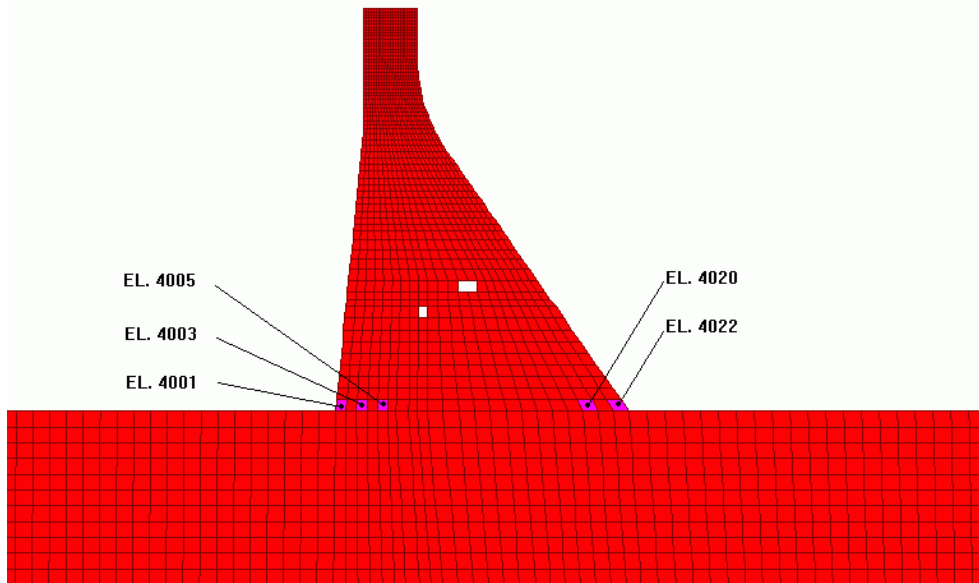
Figure H-8. Elements for which cumulative duration are shown in Figure H-9
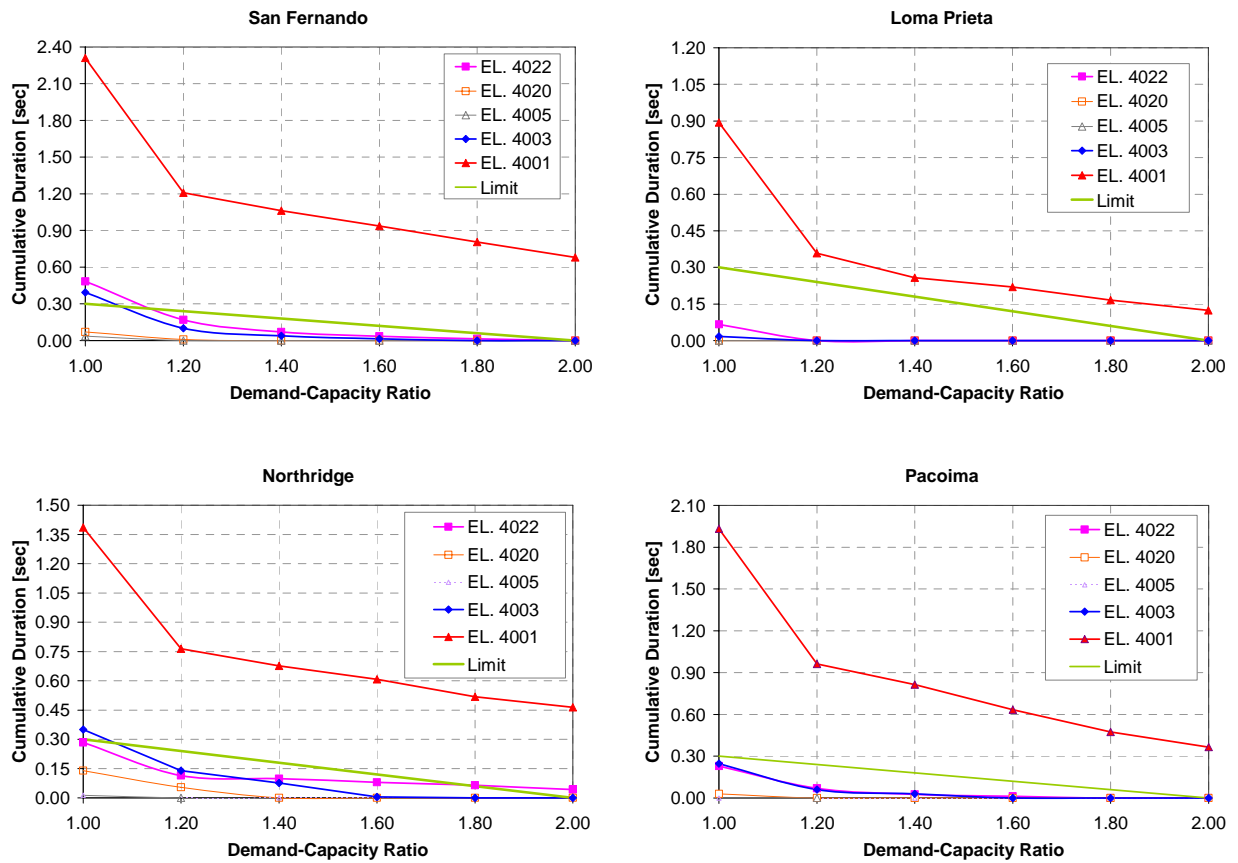
Figure H-9. Comparison of cumulative duration with performance curve for elements shown in Figure H-8
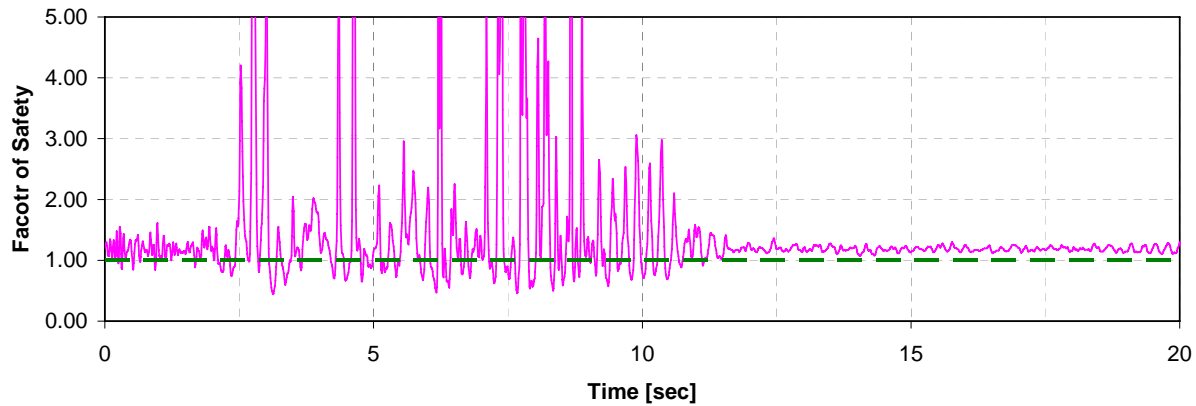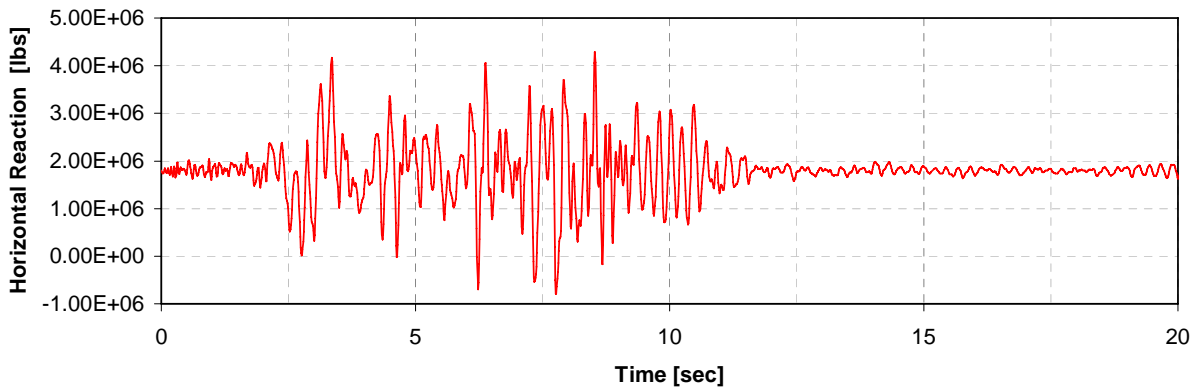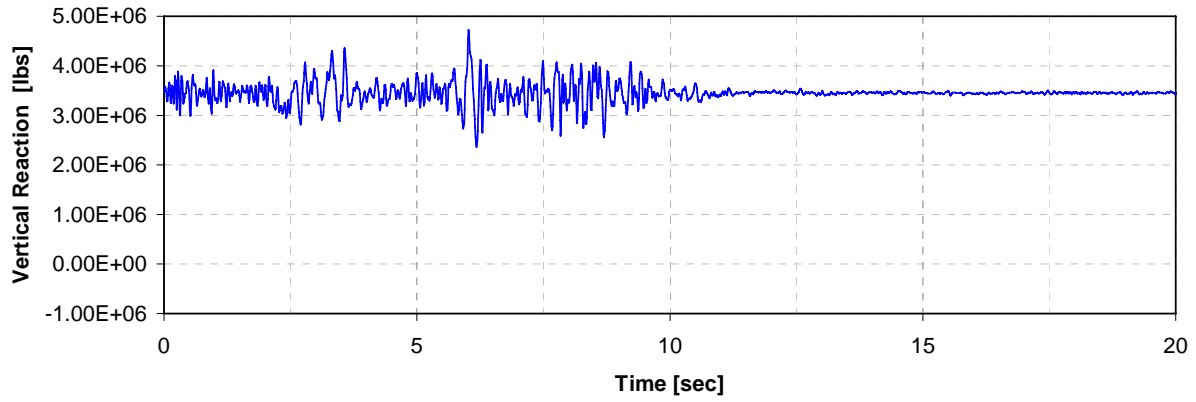
Figure H-10. Time histories of vertical (top graph) and horizontal (middle graph) resultant reaction forces used to compute instantaneous factors of safety (bottom graph). Results shown are for San Fernando record

H-6. Nonlinear Response Analysis

   a. Selection of Nonlinear Analysis Procedure. The results of linear analysis indicate that high tensile stresses develop at the base of the dam, on the upstream face of the dam, and on the downstream face near the change of slope. The magnitudes of stresses are generally higher at the base of the dam than they are at the upper elevations. For this reason and also because tensile strength of the dam-rock contact is expected to be lower than that of the concrete, the nonlinear response in the form of tensile cracking is likely to start at the base. The nonlinear analysis of the dam should therefore be formulated to capture this nonlinear mechanism. In this example, gap-friction elements are introduced at the base of the dam to simulate cracking and the sliding and rocking responses that might follow.

   b. Nonlinear Finite-element Model. Finite-element model for the nonlinear analysis consists of the dam monolith and gap-friction elements. The foundation rock is not included in the model in order to reduce computational efforts. The tensile cracking at the base of the dam is modeled by introducing gap-friction elements between the dam and the rigid foundation. The gap-friction elements are nonlinear elements that can resist bearing and shear parallel to the bearing plane but not tension. The friction forces follow the Coulomb theory and thus are directly proportional to bearing forces in the element. Figure H-11 shows the dam finite-element model with 23 gap-friction elements between the dam and the rigid base. Except for the nonlinear gap-friction elements, the rest of the dam is assumed to remain elastic. Consequently, the dam monolith is represented by linear finite elements as described previously in Paragraph H-5a. The complete finite-element model consists of 1,493 linear shell elements with 23 nonlinear gap-friction elements.
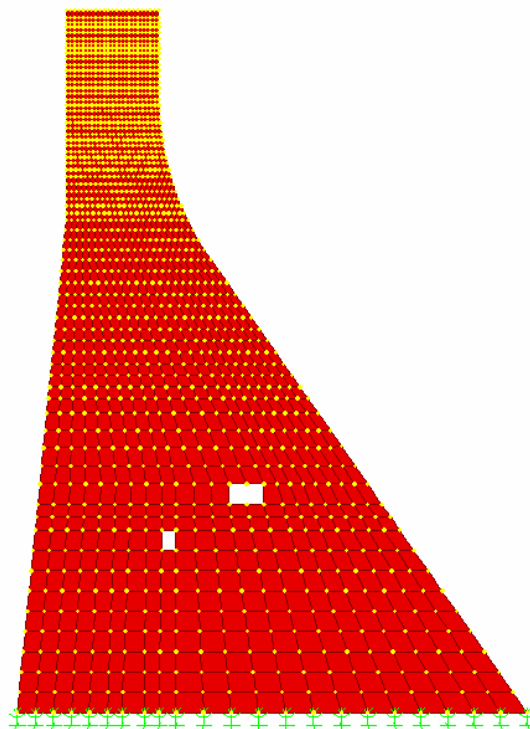

Figure H-11. Dam finite-element model with gap-friction elements

c. Selection of Parameters. The gap-friction elements used in this example have friction properties for shear deformation in the horizontal direction and gap behavior in the axial or vertical direction. The gap properties usually include zero tension resistance but the element can be preloaded so that the element could start with a certain amount of tension resistance. In this example, zero cohesion with a friction angle of 45 degrees were assumed for sliding along the dam-foundation contact surface. Tensile strength of the dam-foundation contact was assumed to be either 1.38 MPa (200 psi) or zero. Using these parameters the following two cases were evaluated:

(1) *Case-I*: No uplift pressure, $f_{interface}$ = 1.38 MPa (200 psi), = 45°

(2) *Case-II*: With uplift pressure, $f_{interface}$ = 0 MPa (0 psi), = 45°

d. Evaluation Loads. The nonlinear dynamic analysis was conducted for the combined action of static and earthquake loads. The static loads included gravity, hydrostatic pressures, and the uplift pressures, all of which were applied as initial loads. The uplift pressures, when applied, were assumed to vary linearly from the headwater to tailwater with no changes during the earthquake ground shaking. A zero tailwater was assumed. The earthquake loads included the same four acceleration time-history records discussed previously in Paragraph H-4.

H-7. Evaluation of Nonlinear Response

a. Case-I. The results for the case with 200 psi interface tensile strength and no uplift pressure are presented in Figures H-12 to H-16. Stress results in Figure H-12 show significant reduction in tensile stresses due to tensile cracking at the base of the dam. Not only tensile stresses at the base of the dam are now limited to 200 psi (i.e. interface tensile strength) but their magnitudes within the body of the dam have also dropped significantly. The maximum tensile stress of 200 psi occurs only at the heel of the dam, while the maximum tensile stresses near the upstream face of the dam are 40 to 80 psi. The stress results confirm the modeling assumption that only tensile cracking at the base of the dam needs to be modeled, because the cracked-base condition tends to relieve high tensile stresses elsewhere. Figure H-13 shows deflected shape at the time of maximum displacement. Thirteen gap-friction elements in the upstream side opened and slid during the earthquake ground shaking. This indicates that cracking starts at the heel of the dam and stops after propagating about half width of the base. Figure H-14 is a plot of gap opening for the gap-friction element at the heel of the dam. This figure indicates that the crack at the base of the dam repeatedly opens and closes during the earthquake excitation. Time histories of sliding displacements for 14 gap-friction elements that indicated opening and sliding are displayed in Figure H-15. This figure shows a permanent sliding displacement of about 0.04 inches at the heel of the dam, which reduces to zero toward the mid section of the base where the cracking stops. The downstream half of the base remains intact with no cracking or sliding. Note that the partial sliding of the upstream half of the base is caused by elastic deformation of the flexible dam monolith due to static and earthquake loads. Figure H-16 shows the horizontal displacement history at the top of the dam, where displacement due to hydrostatic pressure can be noted at the beginning and end of the record.

b. Case-II. The results for the case with uplift pressure and zero tension allowance at the base indicated similar reduction in tensile stresses, except that now tensile stresses at the base of the dam are zero and that the crack propagates through the entire base of the dam. Figure H-17 shows time histories of sliding displacements for all joints across the base of the dam. The sliding displacement varies from joint to joint due to deformations of the flexible dam. The sliding displacements are slightly higher for nodes closer to the heel and reduce as approaching the

toe. For a rigid dam, sliding displacements are the same for all nodes across the base. Figure H-18 displays horizontal displacement history for a crest nodal point, where the permanent displacement at the end of the record is evident. The results show an overall permanent displacement of about 0.8 inches. Although this permanent displacement is relatively small and does not appear alarming, the main concern is the post-earthquake stability condition of the dam under static loads. The post-earthquake static sliding factor of safety for the example dam was found to fall below unity. This is because the uplift forces have increased due to formation of crack at the base of the dam. Therefore the dam should be retrofitted and its shear resistance increased to remedy the situation.

H-8. Conclusions and Recommendations

Linear and nonlinear time-history analyses were used to assess earthquake performance of a typical non-overflow gravity dam section. The linear-elastic time-history analysis was employed to gain insight into the dynamic behavior of the dam, to account for transitory nature of earthquake ground shaking, and to identify potential modes of failure for the subsequent nonlinear time-history analysis. The results of linear-elastic time-history analyses were compared with the EM 1110-2-6051 performance acceptance criteria for gravity dams (see Paragraph 6.4d(1)). This comparison indicated that the example dam would suffer significant cracking along the base and should be assessed on the basis of nonlinear time-history analysis. The results also showed that instantaneous factors of safety obtained from the linear-elastic time-history analysis repeatedly fall below one, an indication that the dam would undergo sliding during the earthquake ground shaking. Subsequent nonlinear time-history analyses were carried out using gap-friction elements to model cracking and sliding along the dam-foundation contact. The nonlinear time-history results indicate that the dam will suffer cracking along its entire base and will undergo sliding with a permanent displacement offset of 0.8 inches in the downstream direction. Although this permanent offset may not be consequential, the post-earthquake static factor of safety for the cracked-base condition falls below one. The dam therefore becomes unstable after the earthquake shaking due to the pore pressure build up beneath the dam. The situation calls for remediation action. It is recommended conceptual remediation schemes be developed and implemented to increase shear resistance of the dam.
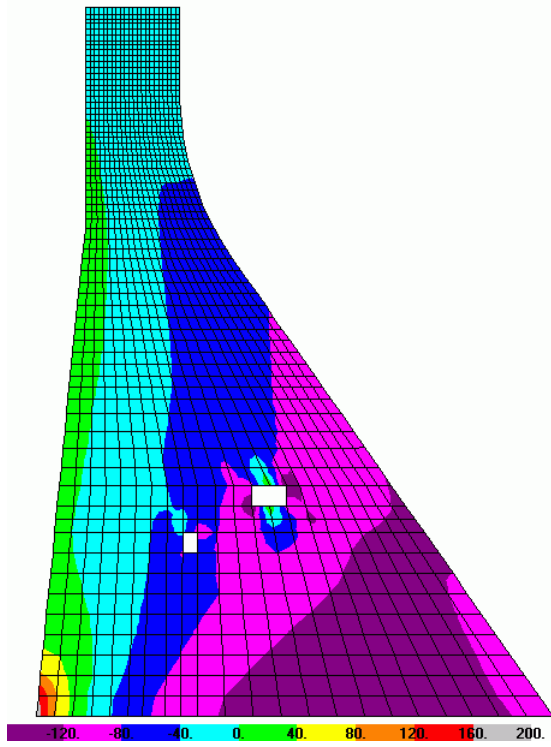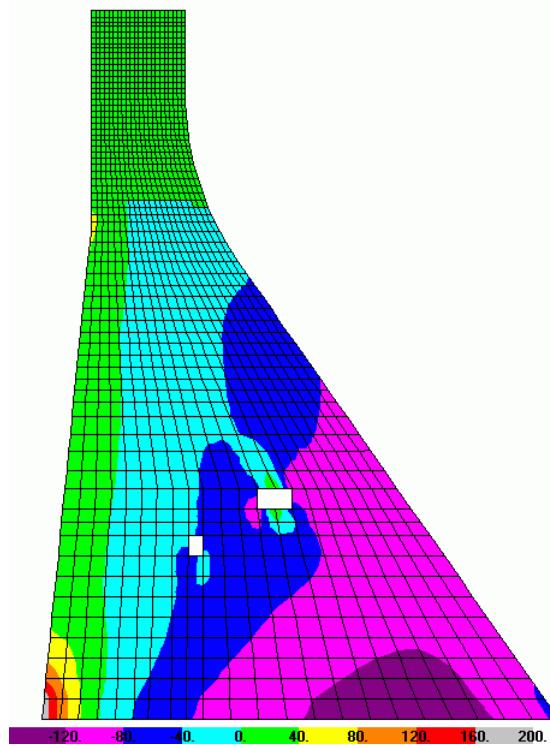
a) Loma Prieta - Nonlinear
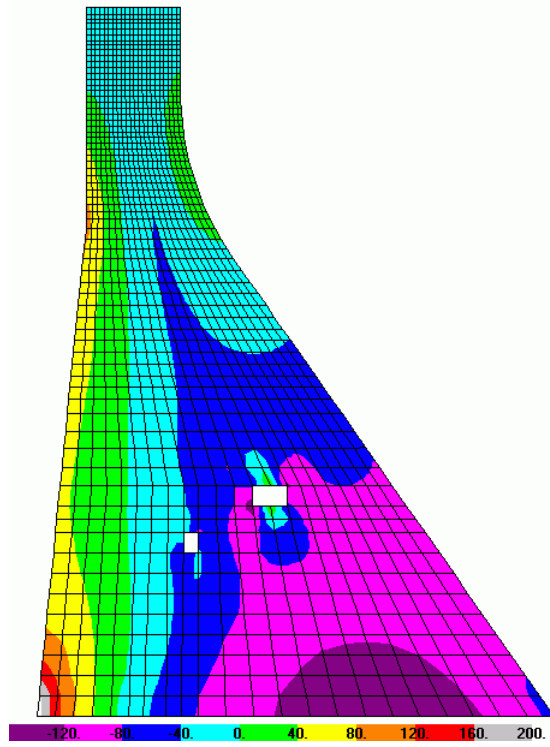
b) Northridge - Nonlinear
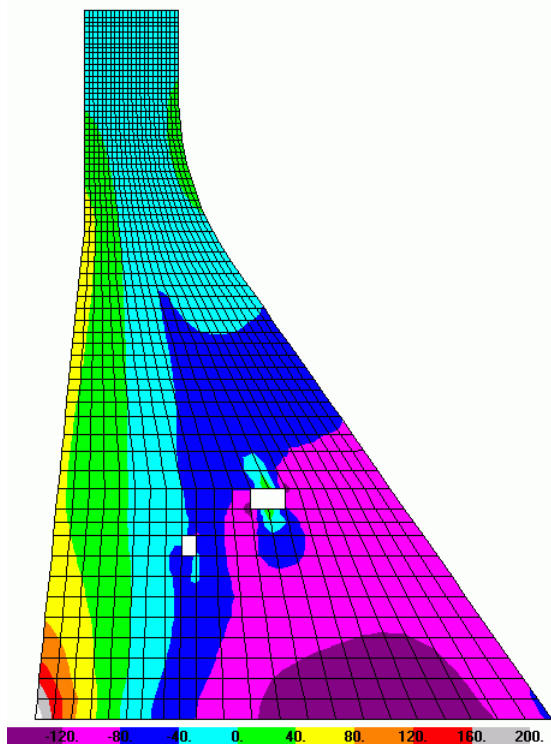
c) San Fernando - Nonlinear

d) Pacoima – Nonlinear

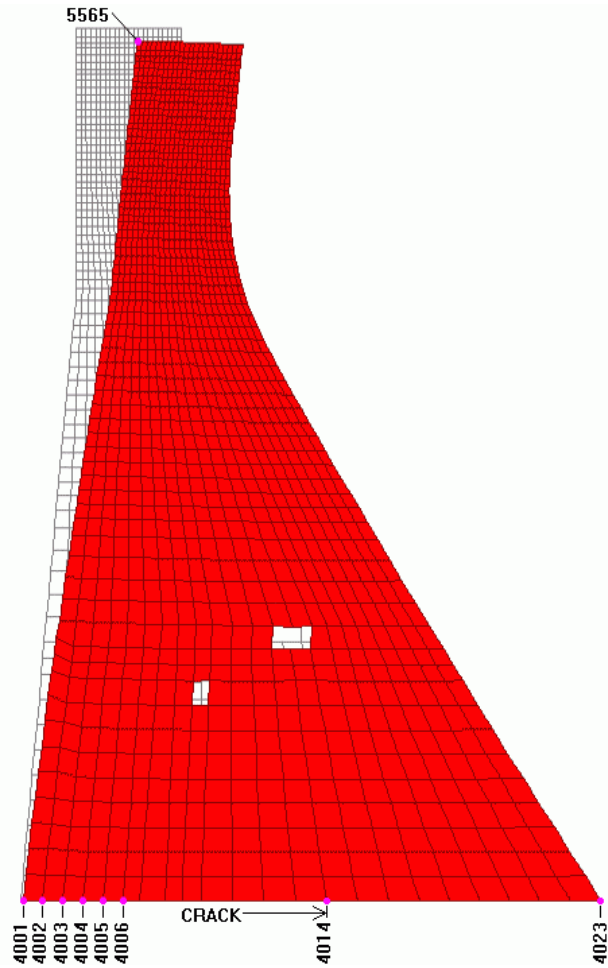**Figure H-12. Envelopes of maximum vertical stresses from nonlinear TH analysis (psi)**

Figure H-13. Deflected shape at the time of maximum displacement. Also shown are 6 gap elements that experienced opening and sliding (San Fernando record)
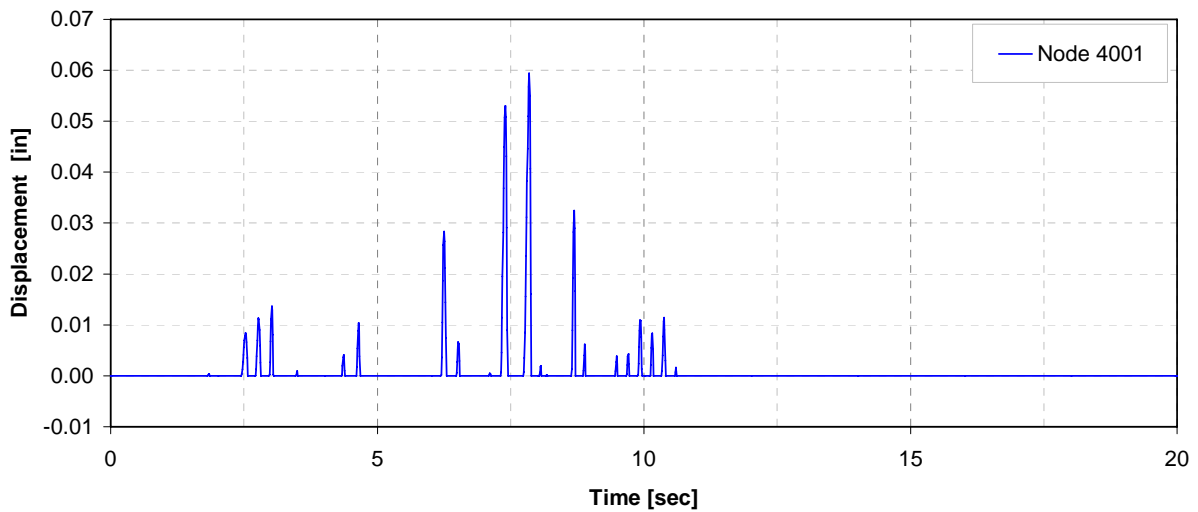

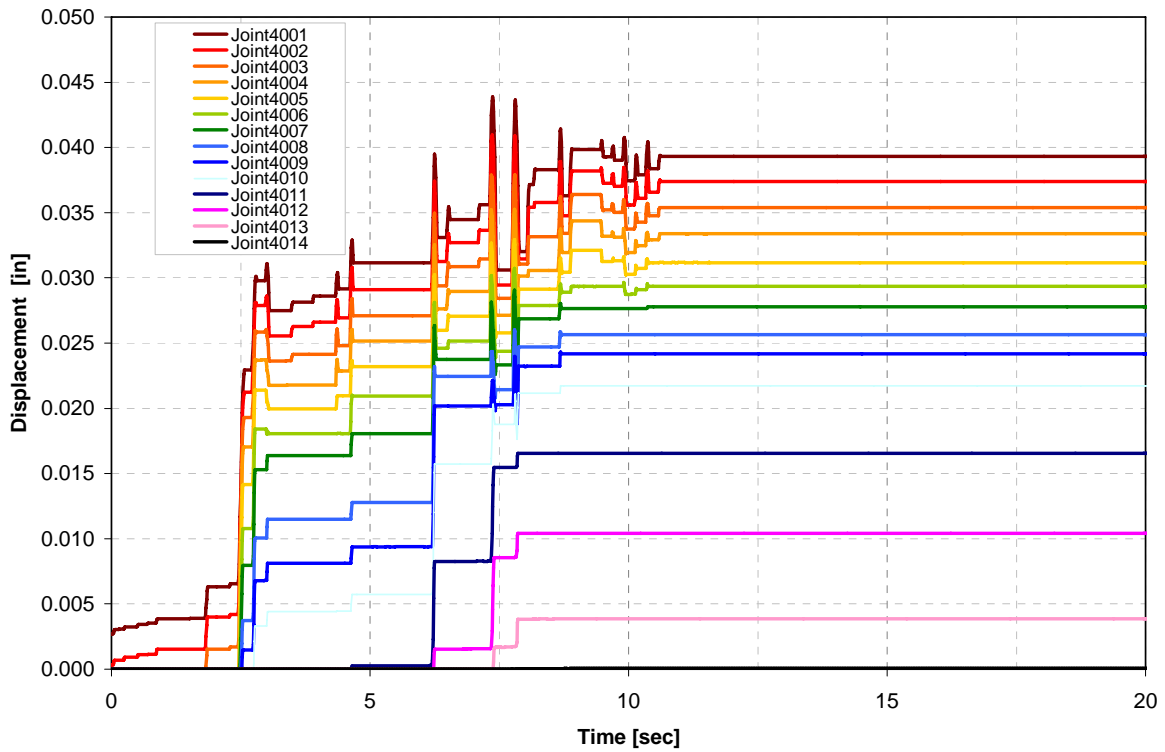**Figure H-14. Gap or crack opening at the heel of the dam (San Fernando record)**

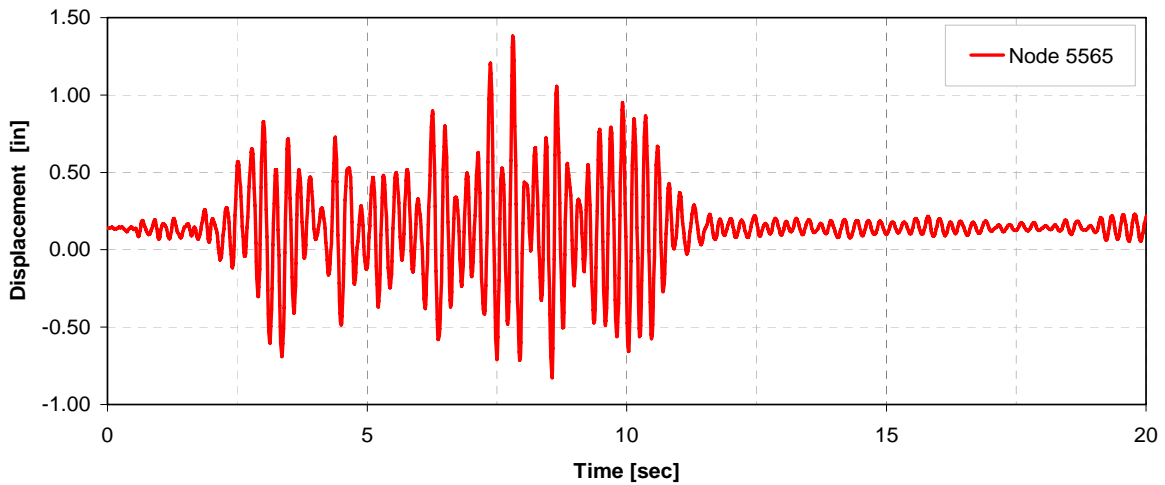**Figure H-15. Horizontal sliding displacements for gap elements located at Nodes 4001 to 4014 (San Fernando record)**

Figure H-16. Time history of horizontal displacement at the top of dam (San Fernando record)
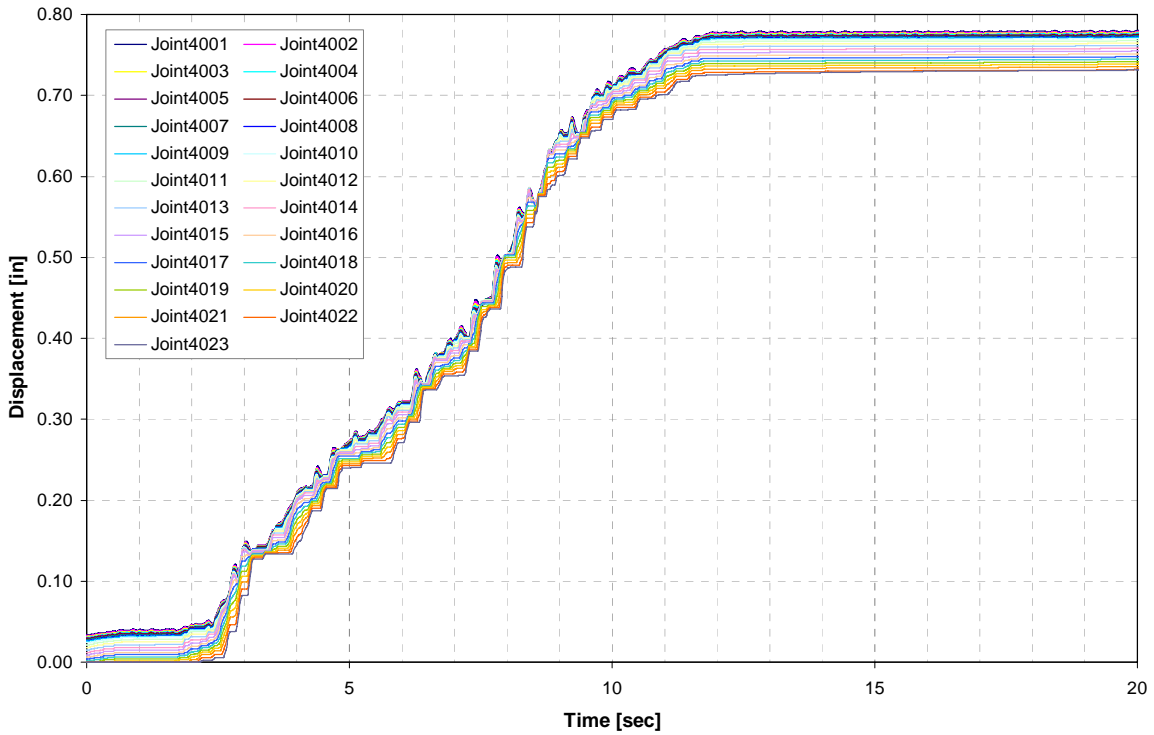
Figure H-17. Time histories of sliding displacements of nodal points at the base of the dam (San Fernando record)
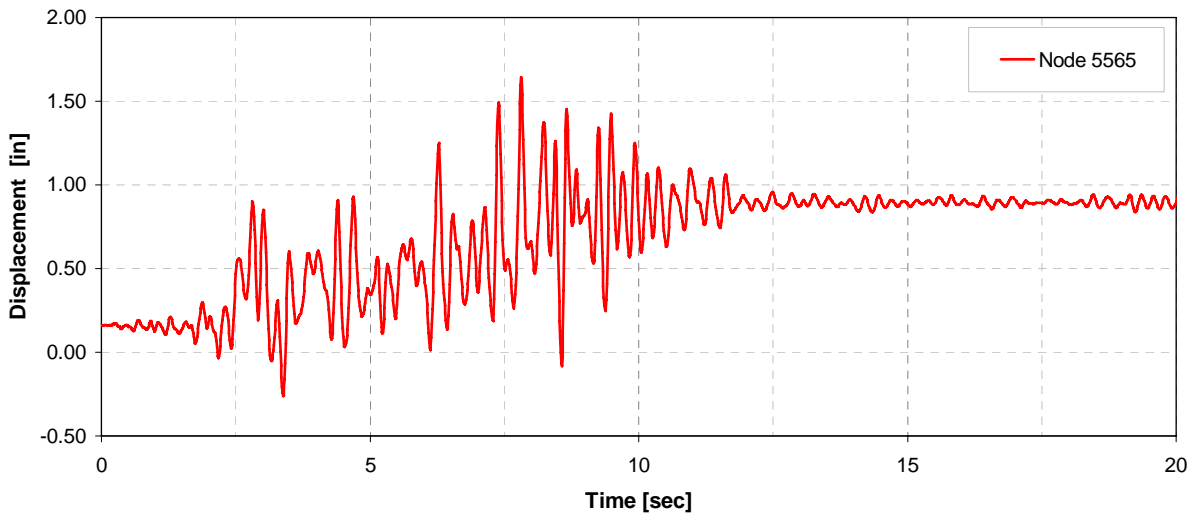

Figure H-18. Time history of horizontal displacement at the top of dam (San Fernando record)